DOCTOR OF PHILOSOPHY

Slate: a study of its thermal chemistry and its potential use in catalysis

Evans, Donna Wyn

Award date:
2001

Awarding institution:
Bangor University

SLATE

A Study of its Thermal Chemistry and its Potential Use in Catalysis

A thesis submitted to the
University of Wales
in candidature for the degree of
Philosophiae Doctor
by

Donna Wyn Evans

University of Wales, Bangor

2001

To David, Mam, Dad, Kerry and Gel.

He first yon mountain's wondrous riches found
First drew its minerals
Blushing from the ground.
He heard the miners'
First exulting shout
Then toil'd near 50 years
To guide its treasures out.

(I. Skidmore, in *Gwynedd*, 1986)

Contents

Acknowledgments

I would like to thank my supervisor, Dr. Peter Holliman, for all the valuable help and guidance he has provided over the course of my studies. Many thanks also go to Mr Hefin Davies and Mr Nigel Edwards, J.W. Greaves & Sons Ltd, Llechwedd Slate Quarry, Blaenau Ffestiniog, for all their enthusiasm for the project and for providing the slate for me to study. Thanks also to Mr Peter Marston, Cynefin Environmental, for his contributions to the project and to Dr Alistair Davies, EA Technology, for his bulk expansion work. I also acknowledge the EPSRC for funding my PhD and J.W. Greaves & Sons Ltd for contributing to the CASE Award.

Many thanks are also due to all the staff at the Department of Chemistry. In particular Mr John Charles for cutting all my slate samples and for fixing my quartz reactor tubes when my slate samples expanded too much; Mr Mike Lewis and Mr John Sambrook for maintaining the working order of the XRD; Mr Dennis Williams for carrying out my GC-MS analysis; Mr Glyn Conley for running my ICP samples; Ms Jane Davies for helping me with the HPLC and Mr Kevin Spencer for teaching me photo-processing. I'm under no illusion that their expertise in various areas has contributed to the success of this project. Many thanks also to Ms Caroline Naylor, Mrs Barbara Kinsella and Ms Jenny Homer for all their help and to Sylwen and Dorothy for making coming to work in the morning easier to bear.

Sincere thanks also goes to Mr Andrew Davies, Biology Dept., for all his training and valuable advise on the SEM. Thanks also to Dr Dave Jenkins, SAFS, for the help he has given me on the mineralogy side of the project.

I would also like to thank Ed Cavanagh for his help and support over the years and to everyone who has made working on the 10th floor a joy (most of the time!). Many thanks to Dr Paddy Murphy's group, past and present, especially Louise, Elinor, Sue, Dafydd and Spencer, and to Kelvin for their friendship and tea-room chats.

Special thanks go to my mum, dad, sister Kerry and nain for being such a great family. Thanks also to Ellen, Sel, Claire and Martin for always being there. Sincere appreciation also goes to Arwyn, Catrin, Sioned, Amanda and Sonja for being good friends and reminding me that there is a life outside chemistry. But most of all thanks to David for loving, supporting and encouraging me every step of the way. Diolch yn fawr i chi gyd!

Abstract

Chapter One, the Introduction, provides a review of the three main areas of the project *i.e.* slate, pyrite and catalysis. Initially a brief overview of the slate industry, past and present, is provided to illustrate the relevance of this study to the slate industry of North Wales. An overview of previous work on the origin, formation and composition of slate is provided in addition to a review of previous work on slate expansion. An overview of the thermal decomposition of pyrite, a common accessory mineral in slate, is also discussed. This section mainly focuses on the work previously carried out on the decay of FeS_2 in oxidising, reducing and inert atmospheres when present in host materials such as coal or gold. Finally an overview of catalyst support materials, hydrogenation catalysts and techniques in catalyst preparation is provided.

Chapter Two, Slate, provides details on the characterisation work carried out on slate from the Llechwedd Slate Quarry, North Wales. Studies have also been undertaken on slate from the Villar del Rey Slate Quarry, Spain. The thermal chemistry of slate is discussed focussing on determining the mechanism behind slate expansion. The investigation undertaken to identify the nature of the expansion gas and the key factors in expansion control *i.e.* heating rate, dwell times and final temperature is discussed.

Chapter Three, Pyrite, investigates the thermal decomposition of pyrite, pyrite in Welsh slate and pyrite in Spanish slate. Experiments have been carried out in nitrogen and in air to provide a mechanistic study of pyrite decay under different atmospheric conditions. A detailed study by SEM of the morphological changes occurring in pyrite after heating is given illustrating the differences in the decay mechanism of pyrite in the various atmospheres. An investigation to determine the differences in the decomposition of FeS_2 within the internal matrix of slate compared to pyrite on its own is also provided. The effect of slate as a host material on the decomposition of FeS_2 is discussed.

Chapter Four, Catalysis, investigates the potential use of expanded slate as a support material for a catalytically active metal. Details on the preparation of copper and

palladium supported metal expanded slate catalysts by following impregnation and electroless plating techniques is provided. The activity of the catalysts towards hydrogenation reactions involving nitrobenzene, maleic acid and cyclohexene is discussed.

Chapter Five, Experimental, provides details of the experimental work carried out and the instruments used in the course of this study to investigate the expansion phenomenon of slate, the thermal decomposition of pyrite and the catalytic properties of expanded slate based catalysts.

Chapter One - Introduction

Chapter One – Introduction

1.0. Area of Study

Slate production has been an important commercial activity in Great Britain for many centuries (Figure 1.1).[1] Regions that have been involved in the working of slate for the production of roofing and building materials include areas in Devon, Cornwall, the Lake District and Scotland. However the leading slate producing regions have traditionally been found in North and Mid-Wales.[2] Slate found in the North Wales area is regarded as being of the highest quality. Indeed North Wales has a global reputation as being a source of the best quality slate in the world.

A slate needs to have a number of physical characteristics to be regarded as a high quality material. Firstly, it is essential that the slate has a regular cleavage in order to ensure that a smooth surface is produced upon splitting.[3] The occurrence of accessory minerals within the slate vein can reduce the ease of splitting, so the composition of the material is an extremely important factor when considering its quality. It is therefore also essential for a good quality slate to have a relatively homogeneous mineral composition, with the presence of accessory minerals kept to a minimum.[3] Slate found in North Wales generally has all of these attributes and therefore generates a material that can be easily split into thin sheets, which is particularly suited for the production of roofing tiles. Indeed, the Welsh slate industry has consistently provided the majority of the roofing slate to the British market ever since its heyday in the late 1800's.[1]

It is evident through archaeological findings in the Gwynedd area that slate has been worked in the region from as early as Roman times.[4] For instance, the early use of slate as a building material can be seen in the ancient Roman fort of Segontium, near Caernarfon in Gwynedd, which is believed to have been founded in the 1st century at around 78 AD. However, the "age of slate" is undoubtedly the 19th century.[5] Around this time, there were a total of 93 slate quarries being worked in Wales alone, ranging in size from small, family run businesses to large enterprises run by rich landowners that provided employment to large proportions of the local communities.[6]

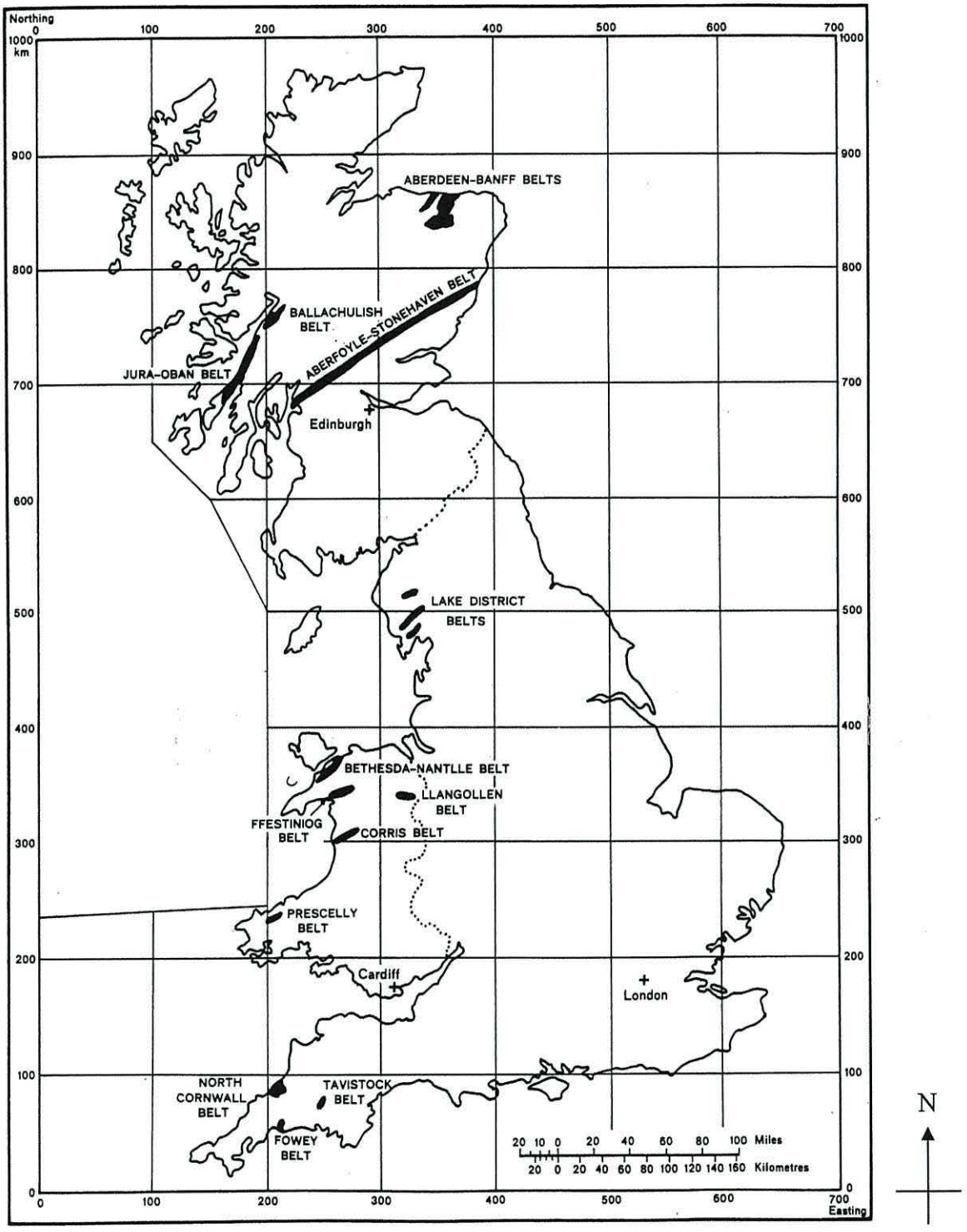

Figure 1.1. Slate producing regions in Great Britain.[1]

This thesis describes studies of slate taken mainly from the Llechwedd Quarry at Blaenau Ffestiniog, North Wales (Figure 1.2).[7] However, in order to obtain a greater understanding of this particular quarry it is necessary to obtain an overview of the Welsh slate industry as a whole. A comprehensive study was undertaken in 1995 for the Department of the Environment (DoE) by Richards, Moorehead and Laing Ltd in order to examine slate waste tips and quarries in Britain.[8] The objective of this study was to provide technical guidance for the rehabilitation of slate workings and waste tips. The environmental impact of removing slate waste was also investigated. The report provided a valuable review of the history of the slate industry by comparing the current UK slate industry with that of the 19th century. For instance at their peak in 1898 North Wales slate quarries generated an annual output in the region of half a million tonnes of roofing slate per year and employed over 16,000 men. The industry has, however, declined considerably since then with the exception of a slight expansion in production during the 1980's. This was ascribed to increased demands for slate from the housing and commercial sectors and the introduction of more modern methods of production such as new, more efficient quarrying techniques and modernised cutting equipment.

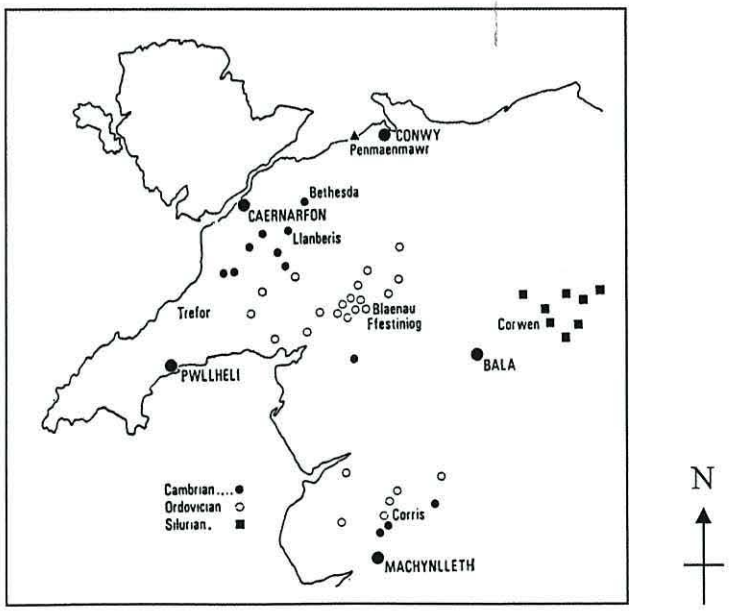

Figure 1.2. Slate quarries of North Wales.[7]

Many smaller quarries in Wales have long since ceased their production and numerous larger sites, such as Dinorwic Slate Quarry near Llanberis, have now also closed. However, slate extraction continues at quarries in North Wales, mainly in Gwynedd, the largest being Penrhyn Quarry at Bethesda (Figure 1.2).[7] Penrhyn Quarry is situated on the Bethesda-Llanberis-Nantlle Cambrian slate belt.[9] This quarry is currently operated by Alfred McAlpine Slate Products Ltd and contributes nearly 50% of the UK roofing slate production.[8] The Ffestiniog slate belt is however being presently worked by the Ffesiniog Slate Quarries group of companies. This group includes the J.W. Greaves & Sons, Welsh Slate Company, which operates the Llechwedd Slate Quarries at Blaenau Ffestiniog. The overall production of slate from the Blaenau Ffestiniog area provided in the region of 35-40% of the total output of roofing slates in Britain in 1995.[8] The DoE report of 1995 clearly shows that Welsh slate still has a major impact on the UK slate industry as a whole and thus provides an important contribution to the Welsh economy through the continuing quarrying of the material in the area. Although less than 550 people (1992 figures) are currently employed in the Welsh slate quarries compared to over 14,000 in 1882, a significant annual production of 26,250 tonnes of roofing slate remains thus reflecting the modern quarrying practices used today.[8]

Although the slate industry is undoubtedly no longer the economic lifeblood of the Snowdonia area, it has clearly left its mark on the surrounding hillsides. Slate quarrying has always produced vast amounts of waste, which have been tipped creating large numbers of artificial slate mountains. Even today the industry still produces large amounts of material which cannot presently be used for any commercial purpose. It has been estimated that approximately 95-98% of all quarried material ends up as waste *i.e.* for every tonne of slate sold an average of 20 tonnes of waste is generated.[8] Indeed it has been estimated that Britain has in the region of 500 million tonnes of waste slate collected in all the tips around the country and around 6 million tonnes is added to this each year.

Waste material is generated in each of the stages involved in the production of commercial slate products such as roofing tiles.[8] This waste is produced from the blasting of the rock face through to the final splitting and dressing of the slate. The first form of waste material usually generated is 'overburden' and 'development'

rock. This material can be made up of a mixture of soil, weathered slate, poorly metamorphosed slate or hard igneous metamorphosed slate all of which need to be removed in order to expose the workable slate vein underneath. Furthermore, blasting and splitting of the slate vein inevitably produces 'quarrying' waste. This waste is made up of irregular shaped pieces ranging in size from tiny shards of material to relatively large boulders. This material can sometimes be of poor quality. However, more often than not, it is unsuitable for further working simply because of its shape and/or size. Careful blasting techniques and the use of modernised sawing machines have ensured that the amount of quarrying waste is minimised resulting in a greater proportion of the quarried material being large workable slate blocks of sufficient quality. Modern practices and machinery ensure that the removal of slate blocks weighing up to 15 tonnes is now conceivable.

Once the large slate blocks have been produced on the quarry site it is then necessary to reduce them to a more manageable size. This process also produces waste through the production of sawn 'off-cuts', which include the irregular shaped ends of the original block. The sawn ends can often be quite large fragments weighing up to 0.5 tonnes. The large blocks are normally cut to size with large circular saws. The introduction of computerised laser-guided systems in modern quarries has resulted in a more accurate cutting operation that reduces the waste produced during this stage. This material again does not signify any lowering of the quality of the slate; it is simply discarded because it has impractical dimensions to undergo further treatment.

The work inside the slate mill also contributes to the total wastage. Here 'trimming' waste and 'mill fines' are continuously generated. Trimming waste is produced when the individual slates, produced upon splitting of the reduced block, requires further trimming down so that slates of standard sizes are produced. These standard sizes have been traditionally named by the Welsh slate industry after female nobility *i.e.* from the largest Queen (>30″ in length), to the most popular countess (20x10″) and down through to ladies (16x8″).[10] Finally, slate processing also produces fine-grained particles or 'sawdust'. All sawing operations are dampened down with water to reduce the amount of air-borne particles. This waste material is normally collected in the form of a clay-like product in settlement ponds or by filter presses. However

when dry this dust can be extremely hazardous to the health of the slate worker since breathing in the fine slate particles is known to cause silicosis.[11]

The waste as a whole is made up of relatively inert material and is therefore usually disposed of through loose-tipping on land around the active slate workings (Figure 1.3). In an attempt to reduce the rate of growth of new waste tips it is now however common practice to deposit the waste into old quarries that are no longer in use.

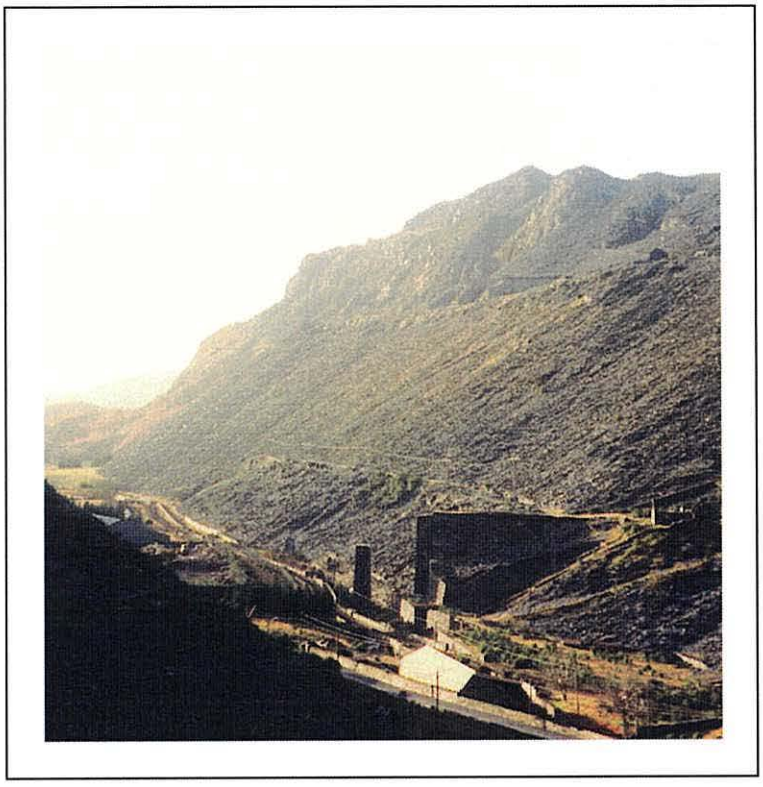

Figure 1.3. Photograph of a slate tip at Blaenau Ffestiniog (1998).

Only a tiny fraction (*ca.* 1%) of the waste material produced during slate extraction is currently utilised in commercial applications.[8] It is mostly used in the crushed form as a bulk fill material in road construction and for the industrial and domestic building industry as foundations and embankments, and in land reclamation schemes. Powdered slate, on the other hand, can be used as an inert filler in various applications from face-powders and lipsticks to paints and bitumastic coatings in undersea pipelines. Reconstituted slate tiles are also often produced from this powdered material by compressing the slate powder with a cement-based compound for increased strength. These 'imitation' slate tiles retain the appearance and texture of

the natural product. However they are generally inexpensive to produce and can therefore be sold at a much lower price than true slate tiles of comparable size.

In recent years the utilisation of slate waste in North Wales has increasingly become an important issue.[12] The injection of government and European funding through projects such as the Slate Valleys Initiative and Objective-1 has shown the timely importance of a study of this kind into the development of Welsh slate and the utilisation of its waste as a commercial product in the expanded form.[13,14] Other potential applications have been identified for using waste slate by first expanding it. Its main use in this expanded form is as a lightweight aggregate in concrete. It can also be heated to form a mineral wool for thermal insulating applications. However, to date the production of these materials from slate does not result in any significant reduction in the total amount of waste produced from slate quarrying.

This thesis reports a study of the heat treatment for slate waste with the aim of producing commercial products. The development of expanded products from slate waste has been achieved by empirical studies of the material (see Section 1.2). However for the first time this thesis reports a detailed study aimed at understanding the fundamental processes that take place to produce a commercially viable product. For this to be achieved it has been necessary to obtain a clear understanding of the mineralogical composition and thermal properties of slate obtained from the Llechwedd Slate Quarry. This thesis then reports an investigation into the expansion process in order to develop a more energy efficient process that can be easily controlled and hence become more economically viable. The effect on one of slate's most problematic accessory mineral *i.e.* pyrite has also been studied with the aim of determining its decomposition mechanism during expansion.

Finally, an investigation into the potential application of expanded slate for catalysis has been carried out. The aim here has been to develop a potential application of expanded slate as a novel support for catalytically active metals. Novel preparation techniques have been developed and the activity of the resultant "catalysts" has been investigated by focussing mainly on expanded slate's potential with regard to hydrogenation reactions.

1.1. Slate

1.1.1. Slate Formation

In the current study an investigation of slate from Llechwedd Slate Quarry, North Wales has been undertaken. Additional slate samples from the Pizarras Villar del Rey slate quarry in Spain have also been studied in order to compare the expansion property of slate from these two regions. However, to help understand the processes involved in the expansion of slate the background formation of the original rock has been reviewed.

The geological processes involved in the formation of slate have been well established and are documented in many geological publications. Pluijim *et al.* reported in a recent publication in Nature that initial work on slate's characterisation took place more than 150 years ago by C. Darwin and H.C. Sorby in 1846 and 1853 respectively.[15] It is believed that this material was one of the first geological features to be analysed on the microscopic scale and even at this early stage a link between the mineralogical composition and the splitting characteristic of slate was evident.

Slate is reported as being classed as a low-grade regionally metamorphosed rock.[3,16] Regional metamorphic rocks are defined as rocks that have been formed when heat and/or pressure within the Earth's crust causes a pre-existing rock to recrystallise.[17] Regional metamorphism typically affects large areas in the crust that correspond to the roots of mountain-chains, these zones are otherwise known as mobile belts.[18] The application of extreme heat and pressure in these areas due to the weight of the overlying rocks result in changes occurring in the composition of the original material. This may have included igneous, sedimentary or even earlier metamorphosed rocks.[16] Although the changes occur at either high temperature or pressure or both, the original rock does not actually melt. These conditions invariably give rise to both structural and chemical changes, typically recrystallisation, in the minerals making up the rocks and thus dramatically alter the physical properties and chemical characteristics of the original rock to form the resulting metamorphosed materials such as slate.

The level of pressure and heat experienced by metamorphosed rocks can vary considerably. Slate is classed the lowest grade of regionally metamorphosed rock.[11] When very little pressure has been exerted on fine-grained sediments, rich in clay minerals and quartz, the sedimentary rock shale is generated.[16] This fine-grained material usually has particle sizes less than 0.1mm in diameter.[19] When shale is subjected to additional pressure it is transformed to slate which is also described as fine-grained. A subsequent increase in the compression and temperature exerted on the slate can then lead to schist being produced which is categorised as a medium-grained rock (grain size 0.1-1mm in diameter).[19] However when subjected to the highest degree of pressures and temperatures schist can be altered to form gneiss, which is a high-grade, coarse-grained metamorphic rock (grain size >1mm in diameter).[16]

Slate is essentially produced by metamorphism of extremely fine-grained clay-like rocks such as shale.[18] These were formed from the clay-like sediments generated from the denudation and erosion of the existing continental margin. Some varieties of slate have also originated from fine-grained volcanic ash. These sediments were then deposited onto a shallow seabed during the Palaeozoic Era about 400 – 600 million years ago (Figure 1.4).[20] Prior to metamorphism, sub-microscopic flakes of the original minerals settle through water so that their crystallographic cleavage directions align themselves parallel to each other and to the bedding plane.[5] After burial metamorphic processes forced the re-orientation of the minerals so that they assumed parallel positions perpendicular to the compressive forces that arose from movements in the Earth's crust during mountain-building processes. This compressional force also resulted in folding of the buried sediment hence changing the direction of the original bedding plane.[18] This geological movement in the turn gave rise to the increased temperatures and pressures required for metamorphic processes to occur within the crust. A diagram illustrating the forces that occur during slate formation is given in Figure 1.5.[21]

STRATIGRAPHY		SLATES IN WALES	OTHER SLATE AREAS
ERA	PERIOD		
CAINOZOIC	TERTIARY & RECENT 60	NO CLEAVAGE HAS BEEN DEVELOPED IN CAINOZOIC OR MESOZOIC ROCKS IN BRITAIN, BUT FISSILE ROCKS, WHICH ARE NOT TRUE SLATES, ARE FOUND IN THE JURASSIC SERIES.	
MESOZOIC	CRETACEOUS 120		
	JURASSIC 145		
	TRIASSIC 170		
PALAEOZOIC	PERMIAN 210		
	CARBONIFEROUS 280		
	DEVONIAN 320		DELABOLE (CORNWALL)
	SILURIAN 350	LLANGOLLEN, CORWEN, GLYN CEIRIOG	LAKE DISTRICT (KIRKBY)
	ORDOVICIAN 400	ABERGYNOLWYN, ABERLLEFENNI, CORRIS, LLANGYNOG FFESTINIOG DISTRICT DYFED	LAKE DISTRICT (GREEN SLATES) LAKE DISTRICT (SKIDDAW SLATE)
	CAMBRIAN 500	ARTHOG, FAIRBOURNE NANTLLE, PENRHYN, DINORWIG	
	PRE-CAMBRIAN	THE PRE-CAMBRIAN ROCKS IN WALES ARE TOO MUCH ALTERED AND CRUMPLED TO YIELD WORKABLE SLATES	CHARNWOOD FOREST (LEICESTERSHIRE) BALLACHULISH, ETC. (SCOTLAND)

Figure 1.4. Stratiography diagram showing the ages of slates from different regions.[20]

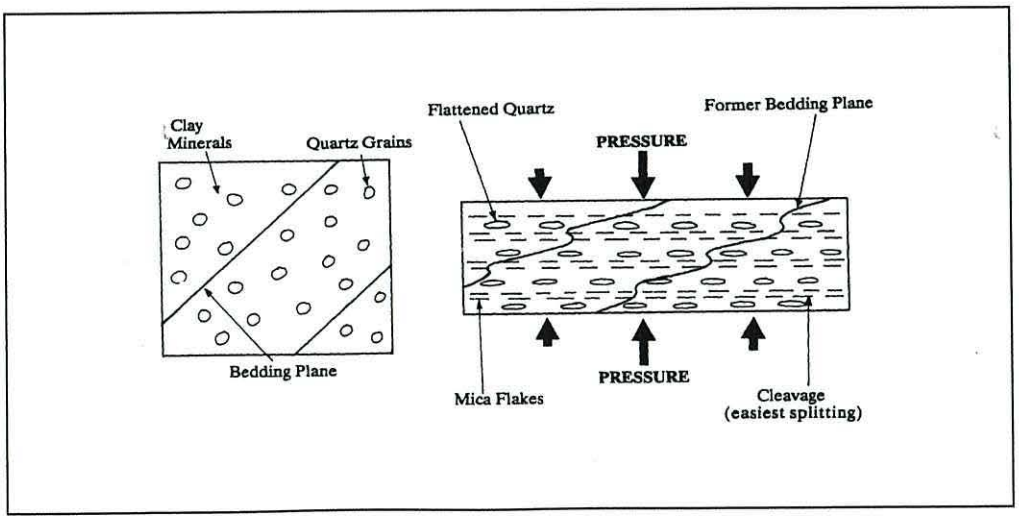

Figure 1.5. (a) Clay minerals orientated parallel to bedding plane. (b) Pressure in Earth's crust resulting in generation of foliated material.[21]

During the Palaeozoic era, especially between Ordovician and Devonian times 500-345 million years ago, areas of Britain were subjected to immense compressional forces. It has been reported that the main area of pressure was focussed on a diagonal line from the Southern Uplands of Scotland down through Ireland and was ultimately responsible for the generation of mountainous areas in Scotland, Cumbria and Wales.[22] This geological event, known as the Caledonian Orogeny, therefore affected the underlying rocks to such a degree that metamorphosed slate beds were created, such as those found in North Wales and in other slate-producing regions in Britain.

Whilst the Caledonian Oregony is a key geological event effecting slate production, slate of varying geological ages can be found in North Wales (Figure 1.2), ranging from the oldest Cambrian deposits (500-570 million years old) found in the Nantlle – Llanberis – Bethesda slate bed to the Ordovician deposits (435-500 million years) that make up the Ffestiniog strata. Younger Silurian (395-435 million years) can also be found in the region around Llangollen.[8] It has been reported that the period of formation affects the quality of the quarried material with the best quality slates arising from older deposits formed during the Lower Palaeozoic era.[23] The Ordovician and Cambrian slates that are currently being worked in the active slate quarries at Blaenau Ffestiniog and Penrhyn, respectively, are some of the oldest therefore most compressed slates available and in turn constitute some of the finest pedigree of slate in the British Isles.

Slate is essentially a silicate bearing rock. Silicates are compounds that are made up of linked Si-O tetrahedra having the basic formula $[SiO_4]^{4-}$.[16,24] Subsequent sharing of the oxygen atoms at the corners of the $[SiO_4]^{4-}$ with adjacent tetrahedra result in the formation of sheet-like structures called phyllosilicates made up of infinite layers with the repeat unit $[Si_4O_{10}]^{4-}$. It has been reported that the most important mineral constituents of slate include the phyllosilicates mica and chlorite, and the tekto-silicate quartz.[3,5,22] Research by Crockett[1] has shown that the general composition of slate from different geological regions is broadly consistent and that the proportion of mica, quartz and chlorite is generally in the region of 38-40 %, 31-45 % and 6-18 % respectively. This general mineralogical composition can also be seen in other materials, such as shales, that have been derived from essentially the

same sedimentary deposits *i.e.* clays/silts. However exposure, as discussed previously, to different geological processes has ensured that each rock type exhibits different physical properties.[5]

Mica forms one of the major constituents of slate.[25] The mica family include minerals that can be characterised by a platy morphology and a perfect basal cleavage that arises due to a layered atomic structure that essentially ensue from the pseudo-hexagonal arrangement of silicon and oxygen atoms.[26] A simplified illustration of the hexagonal silicate framework is given in Figure 1.6.[27] A wide variety of minerals exist within this group which have differing chemical and physical properties. The most common varieties of mica include muscovite, paragonite, glauconite, lepidolite, phlogopite, biotite and zinnwaldite.[28] All have essentially the same basic structure made up of a layer of octahedrally co-ordinated interlayer cations sandwiched between identical layers of $(Si,Al)O_4$ tetrahedra, stacked to produce three-dimensional crystals. The substitution of Al^{3+} for Si^{4+} in the same tetrahedral sites results in an overall negative charge on the Si-Al-O layers; the presence of the inter-layer cations balancing this charge. This arrangement of two adjacent silicate layers bonded together through the interlayer compensating cations is therefore often described as a trimorphic (2:1) composite sheet. Furthermore, the two sheets of linked $(Si,Al)O_4$ tetrahedra have vertices pointing inwards, these vertices are often cross-linked with aluminium or magnesium ions. The resultant electrostatic interaction between the Al-substituted silicate layers and cations effectively increases mica's hardness (H=2.5-4) compared to other structurally similar minerals, such as talc (H=1), where no ionic linkage exists.[29] This characteristic is illustrated in Mohs' scale of hardness, which states that the hardness of a mineral is its resistance to being scratched *i.e.* a mineral with a higher Mohs' number will scratch one that is lower in the scale (Table 1).[16]

Table 1. Mohs' scale of mineral hardness.[16]

Hardness	**1**	**2**	**3**	**4**	**5**
Mineral	Talc $Mg_3Si_4O10(OH)_2$	Gypsum $CaSO_4$	Calcite $CaCO_3$	Fluorite CaF_2	Apatite $Ca_5(PO_4)_3(F,Cl,OH)$
Hardness	**6**	**7**	**8**	**9**	**10**
Mineral	Orthoclase $KAlSi_3O_8$	Quartz SiO_2	Topaz $Al_2SiO_4(F,OH)_2$	Corundum Al_2O_3	Diamond C

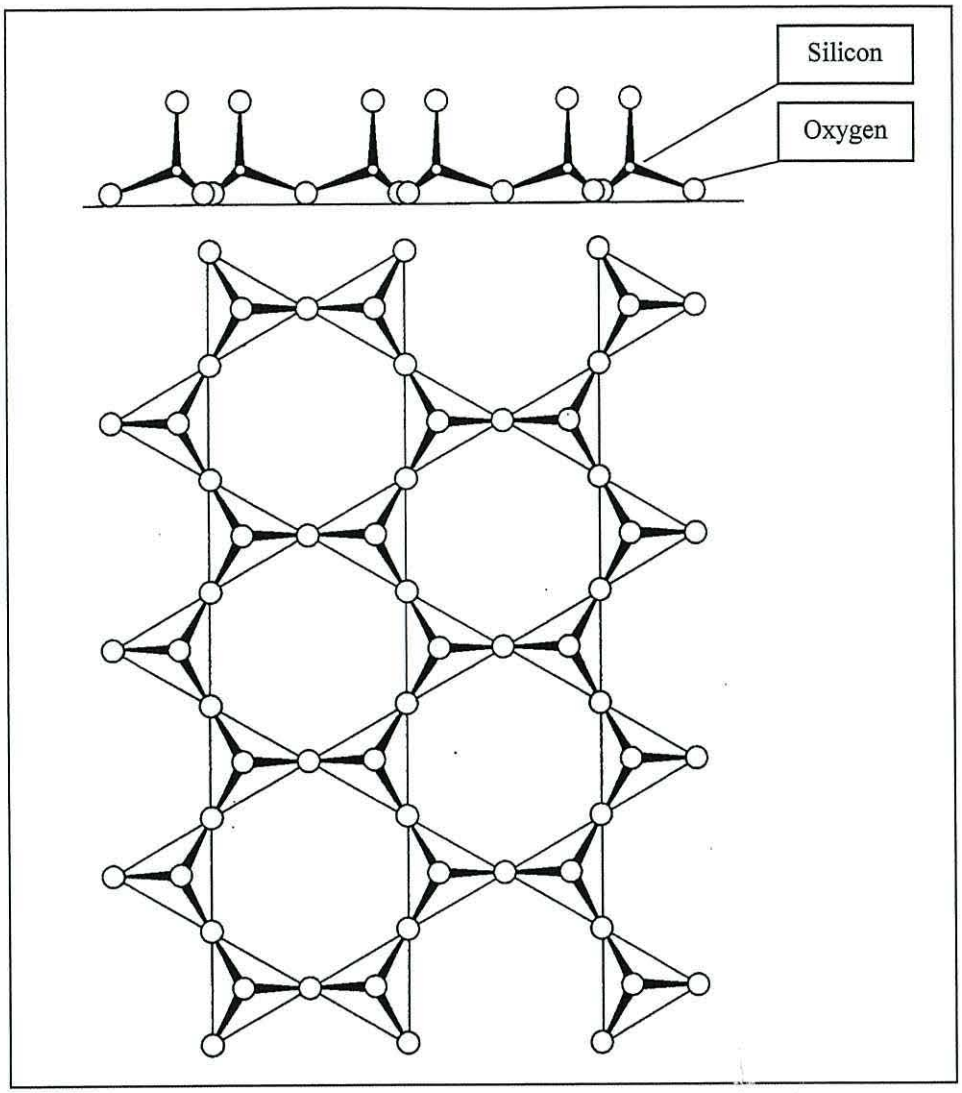

Figure 1.6. Basic structure of a silicate sheet produced when all three oxygen atoms at the bases of the $(SiO_4)^{4-}$ tetrahedra are shared with adjacent tetrahedra. At the top of the diagram a vertical section of the sheet is shown with the shared oxygen atoms slightly offset.[27]

It has been reported that slate contains the mica mineral muscovite.[25] Muscovite, $KAl_2(Si_3Al)O_{10}(OH)_2$ is a hydrous potassium aluminium silicate, which is the most common of all the minerals belonging to the mica family (Figure 1.7).[29] It occurs in a wide variety of geological environments but mostly in low-grade environments from the weathering of feldspars and the recrystallisation as illite (otherwise known as hydrous mica) and other clay minerals.[26] Muscovite is therefore an abundant mineral that is also found in rocks such as phyllites, schists and gneisses produced during low to medium-grade metamorphism[29] thus its presence in slate is unsurprising.

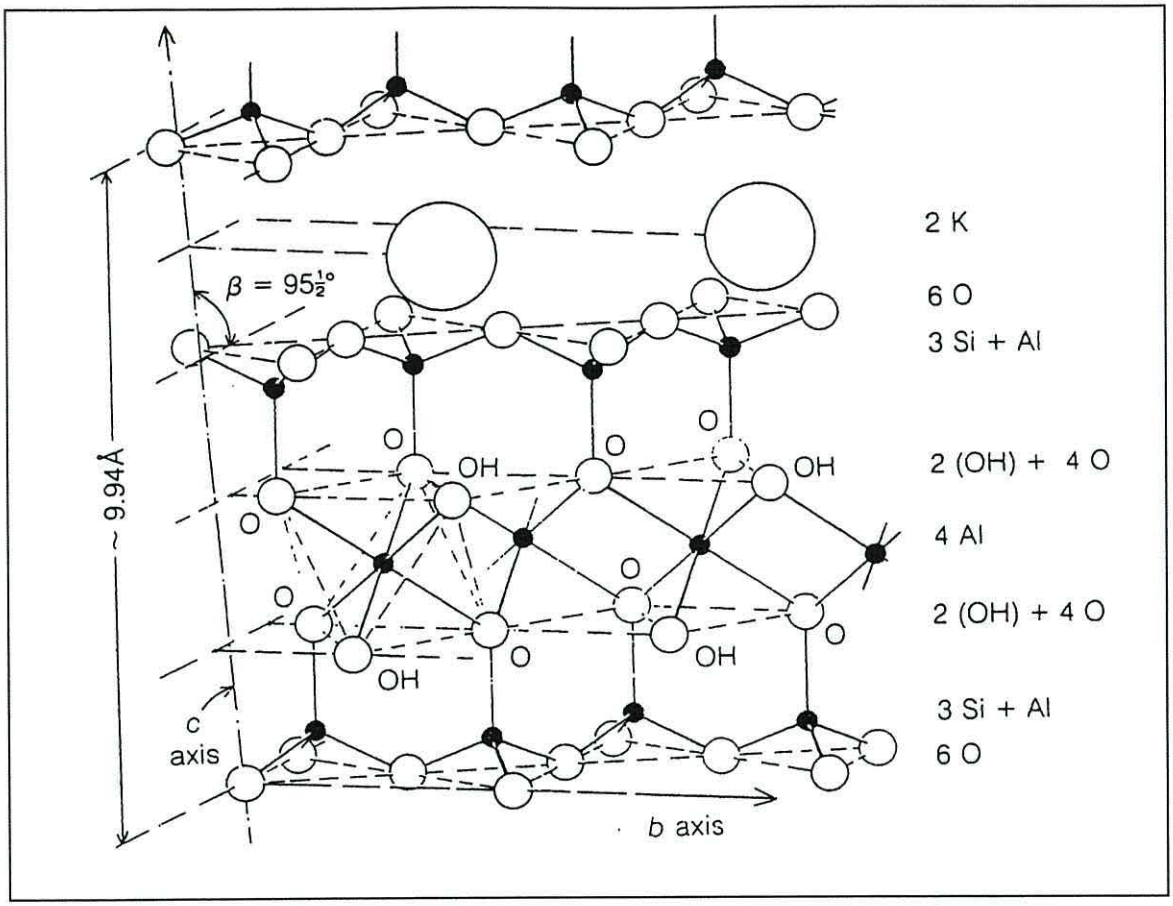

Figure 1.7. Structure of muscovite, $KAl_2(Si_3Al)O_{10}(OH)_2$.[29]

The structure of muscovite follows the general description previously described for the mica family of minerals. However it is specifically composed of pairs of $Si_4O_{10}^{4-}$ sheets where Al^{3+} replaces a quarter of all the tetrahedral Si^{4+}.[30] These sheets are further linked by aluminium ions occupying $\frac{2}{3}$ of the octahedral sites *i.e.* dioctahedral. Hydroxyls are further bound to the cross-linking Al^{3+} to complete its required octahedral co-ordination. Each pair of sheets is separated and electrostatically bonded to the next pair by a layer of positively charged potassium ions in 12-fold co-ordination. Varying atomic substitutions can result in muscovite having a significant range of compositions. Interlayer potassium ions can be replaced by the smaller sodium ions especially if the mineral was formed at elevated temperatures. Furthermore, substitution of Ca^{2+} for K^+ can also occur when Al^{3+} substitution for Si^{4+} lies between 25-50%. This results in a brittle mica being produced as a result of a reduction in the strength of the ionic linkage between the silicate layers. The six co-ordinate aluminium ions can also be partly replaced by Mg^{2+} and Fe^{2+}, and sometimes even by Cr^{3+} or V^{3+}. In addition, the hydroxyl groups within the silicate framework

may be replaced by halide ions, namely fluoride or less often chloride. Replacement of the hydroxide ions by fluoride can effectively reduce the water content of the mica (water content generally 4-5%).[26]

The multitude of possible elemental substitutions within the muscovite/mica structure can make mineral characterisation extremely difficult since excessive substitution can result in a new mineral being named which has the same basic structure. For instance, if the amount of sodium in the mica exceeds the amount of potassium then the mineral is named paragenite not muscovite. Similarly a high silica containing muscovite is often referred to as phengite *i.e.* if the Si:Al ratio is greater than 3:1.[26] Slate is often said to contain sericite mica or white mica,[3,31,32] which is in fact a form of muscovite that is extremely fine grained. Sericite is not structurally different to muscovite but can however often have a higher Si, Mg and H_2O content.[26]

Muscovite crystallises in a monoclinic system producing in general colourless six-sided tabular platelets *i.e.* it is pseudo – hexagonal (Figure 1.8).[33] Varieties of muscovite with pale green, grey or brown colouring can also be found.[29] It can be cleaved in one direction only, along the {001} plane. This cleavage produces thin sheets that are flexible and elastic in nature. In addition the increased mechanical strength of the cleaved sheets has ensured muscovite's economic importance in both industrial and technical applications. For instance, it displays good electrical and thermal insulating properties which are enhanced due to the near transparency and the relatively low iron content of the sheet material.[26] Almost 90% of all the sheet muscovite obtained from the leading producers in India and the USA is used in condensers and as insulating material between commutator segments and as insulators in heating elements.[29] Furthermore, as a result of its high resistance to heat and its ability to form strong, thin colourless sheets, muscovite has been used as an alternative to glass in stove and furnace doors.[34] In fact the name muscovite was derived from Muscovy, a region in Russia where it is believed that muscovite was firstly used as an alternative window 'glass' material.

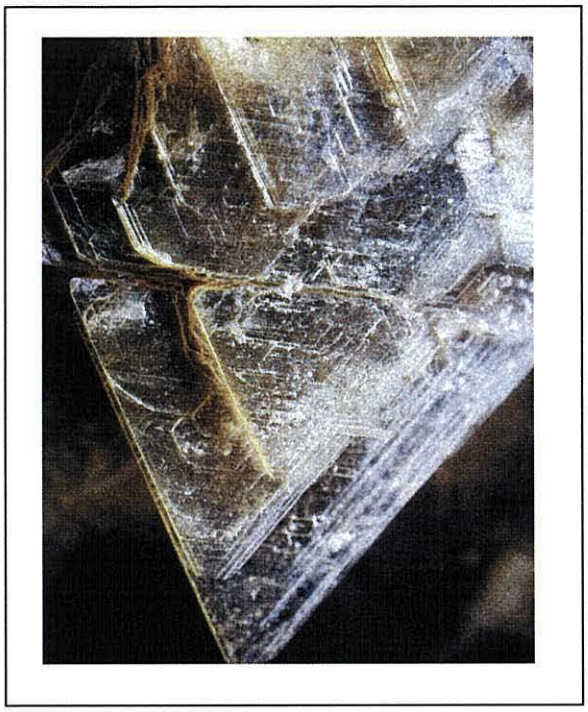

Figure 1.8. Picture of a muscovite crystal.[33]

Chlorite is also an important component of slate. The term chlorite in fact refers to an extensive group of minerals, which result from a high degree of atomic substitutions that can take place within the layered structure of this mineralogical family. Chlorite is a common mineral that can be found in abundance in low to medium grade metamorphic rocks, especially in those rocks that have been metamorphosed at temperatures up to *ca.* 400°C and pressures of a few kilobars.[26]

The typical stoichiometry of chlorite, $[(Mg,Fe,Al)_6(Si,Al)_4O_{10}(OH)_8]$ a hydrous magnesium iron aluminium silicate, is very similar to that of the mica family since it is mainly made up of layers of $Si_4O_{10}^{4-}$ (Figure 1.9).[29] However, although the composition of chlorite is closely related to that of mica *i.e.* triphormic (2:1), a significant difference is that no alkali elements are present within its structure. By comparison, the inter-layer potassium ions which are present in muscovite are commonly replaced by medium sized cations; Fe^{2+}, Mg^{2+} or even Al^{3+} in octahedral co-ordination between two OH^- layers in chlorite.[28] Alternatively, chlorite's structure can be described as being essentially made up of negatively charged tetrahedral layers with positively charged interlayer octahedral sheets resulting in a 2:1 build-up of the respective layers.[35] This mineral can therefore includes talc-like

$[Mg_5Al(Si,Al)_8O_{20}(OH)_4]$ layers with brucite-like $[Mg_5Al(OH)_{12}]$ layers in between, replacing the alkali elements present in mica.[36]

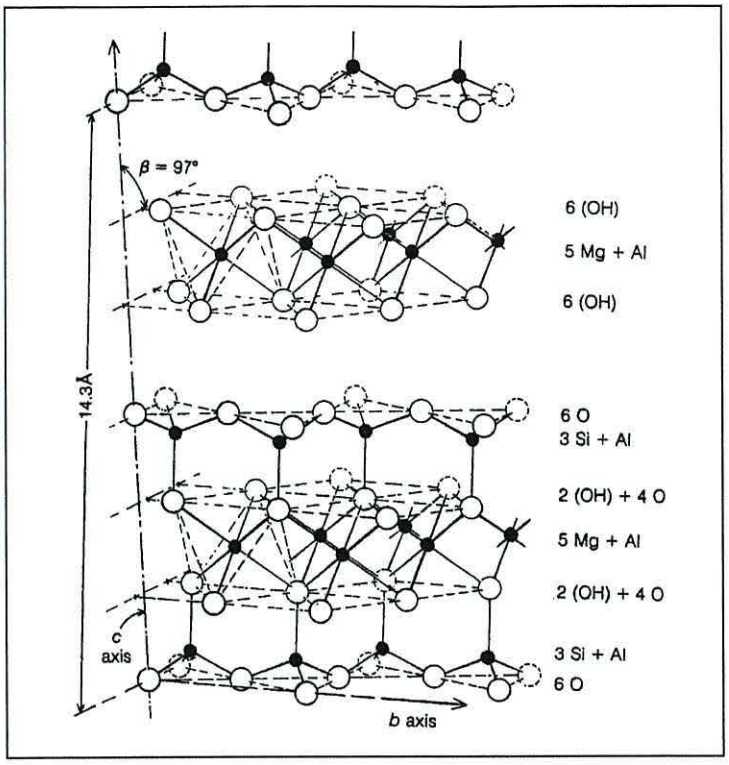

Figure 1.9. Structure of chlorite, $[(Mg,Fe,Al)_6(Si,Al)_4O_{10}(OH)_8]$, consisting of interlayered layers of brucite-type $[Mg_5Al(OH)_{12}]$ and talc-like $[Mg_5Al(Si,Al)_8O_{20}(OH)_4]$ layers.[29]

The most commonly occurring chlorites are clinochlore; a Mg-rich chlorite with the chemical formula $[(Mg,Fe)_5Al(Si_3Al)O_{10}(OH)_8]$, and chamosite $[(Fe,Mg)_5Al(Si_3Al)O_{10}(OH,O)_8]$ which is rich in Fe^{2+}.[29] However, Fe^{2+} and Mg^{2+} are often interchangeable in nature; as a result categorising mineral types in the chlorite family can be extremely difficult. This is particularly evident in chlorites occurring in slate since as it has been reported that variable concentrations of Fe and Mg can occur even within different microstructural domains within the same slate.[26] Chlorite can also contain trace amounts of chromium, nickel and manganese as replacement cations for iron and magnesium.[28]

In the same way as muscovite, chlorite crystallises in a monoclinic system as pseudo-hexagonally shaped platelets (Figure 1.10).[33] Chlorite is commonly green in colour due to Fe^{3+} however rare varieties with high manganese or chromium content can

have an orange-brown and violet coloration respectively. It also has perfect cleavage along the {001} plane producing strong and flexible platelets. However unlike muscovite, these cleaved flakes are not elastic and do not have thermal and electrical insulating properties that are as effective as muscovite. As a result, chlorite is not currently used in any major industrial applications.[29]

Figure 1.10. Picture of a chlorite crystal.[33]

Quartz (SiO_2) also exists as a lesser component in slate. It belongs to the silica group of minerals and is one of the most abundant minerals found in the Earth's crust since it is very stable over a wide range of geological conditions.[29] Quartz, together with feldspar, make-up >60% of the minerals in the surface of the Earth.[37] Quartz can therefore commonly be found as a major constituent in all kinds of rock *i.e.* in igneous, sedimentary and metamorphic rocks.[16] Furthermore, it can also occur as an accessory mineral and as a secondary mineral in veins running through other rocks *e.g.* slate.[26]

The stability of quartz can be related to its very structure being made up of a three-dimensional network, where every $[SiO_4]^{4-}$ tetrahedron shares all its corners with other tetrahedra *i.e.* every silicon atom is bound to 4 oxygen atoms and every oxygen is linked to 2 silicon atoms (Figure 1.11). Thus a neutral compound with an overall silicon:oxygen ratio of 1:2 is produced *i.e* SiO_2.[29] Furthermore, the relatively high Si-

O bond energy (466 $kJmol^{-1}$) and SiO_2 enthalpy of formation, $\Delta_f H$ equal to –910.94 $kJmol^{-1}$ gives rise to a very stable material that is particularly inert even at relatively high temperatures.[38]

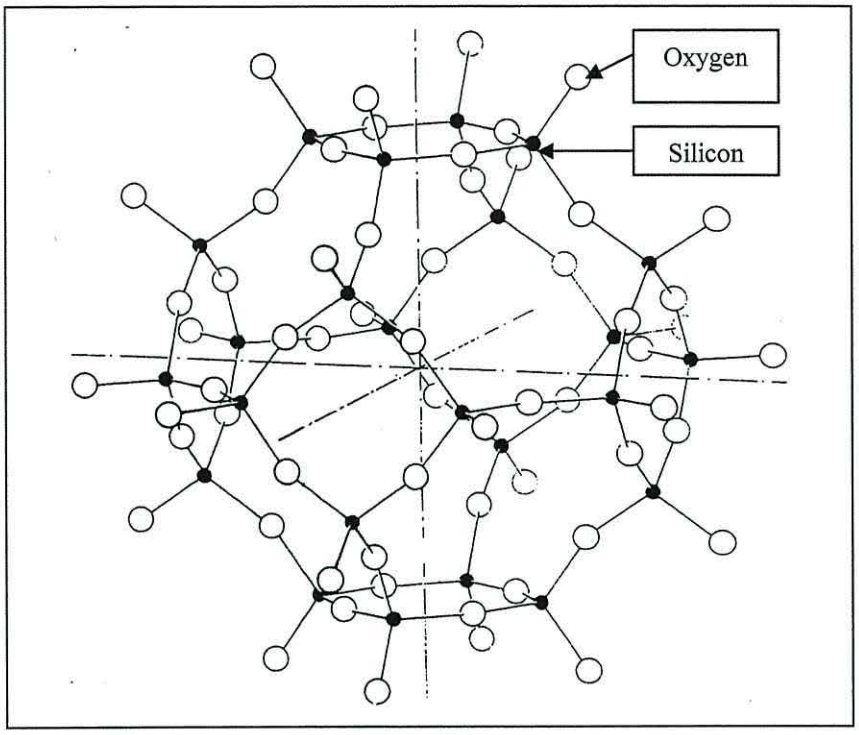

Figure 1.11. The structure of quartz.[39]

The pattern of linkage between the tetrahedra in the three-dimensional framework can vary, essentially producing three silica polymorphs. At atmospheric pressure quartz, metastable tridymite and metastable cristobalite can be found.[26] Quartz is the low-temperature phase and is stable up to 867°C, tridymite is stable between 867 and 1470°C whereas cristobalite occurs from 1470°C up to its melting temperature at 1713°C.[33] Low- and high-temperature modifications of each of the three silica phases also exist, denoted by the prefixes α and β respectively. For instance a transformation between the α and β phases takes place for quartz at 573°C.[27] At this temperature the symmetry of quartz changes from trigonal to hexagonal with increasing temperature. The crystal structure of the low temperature α-quartz is indeed very similar to that of the high temperature β-quartz however the SiO_4^{4-} tetrahedra of α-quartz are more irregularly arranged with a slight rotation having occurred from their ideal positions. The α-β inversion involves only small atomic movements since the Si-O bond is not broken and therefore occurs rapidly when the transition temperature is reached.

These processes are invariably reversible and thus upon cooling the structure inevitably reverts back to the most thermally stable polymorph. As a result of the temperature and pressure conditions of the low-grade metamorphic processes, which gave rise to the formation of slate, it is evident that the stable silica polymorph present in rocks of this kind should be quartz. However subsequent thermal treatment of the material will inevitably result in transformations within the structure taking place.

In nature, high temperature β-quartz is generally found to crystallise forming hexagonal prisms, terminated by rhombohedra which, if perfectly formed, give the appearance of a hexagonal dipyramid.[39] However the crystals are more often than not twinned or distorted, often due to irregularities occurring in the rate of crystal growth.[16] By comparison quartz exists in slate as detrital granules *i.e.* granules that remain from the original sedimentary deposits prior to metamorphism and remain relatively unchanged in the metamorphosed rock.[16,40] Quartz is therefore structurally very different to both muscovite and chlorite. It does not have a well-developed cleavage and normally exists in a very pure state *i.e.* very few atomic substitutions or impurities occur within its structure.[26] Indeed quartz is normally composed of 100% SiO_2, although on occasion substitution of the tetrahedral Si^{4+} with Al^{3+} can result in trace amounts of other ions such as Li^+ or Na^+ also being present to complete the overall neutrality of the compound. The stability of quartz is further illustrated by its high resistance to chemical weathering and in its insolublity in all acids except for HF.[29] Furthermore, due to the lack of cleavage and a hardness of 7 it is also relatively unaffected by physical weathering processes.[26] The presence of quartz in slate may therefore contribute to slate's durability as a building material.

However, in addition to the major constituent minerals in slate *i.e.* muscovite, chlorite and quartz, other micaceous and rock forming minerals such as illite (hydrous mica) $[(K,H_3O)(Al,Mg,Fe)_2(Si,Al)_4O_{10}((OH)_2,H_2O)]$ and feldspar $[(K,Na,Ca)AlSi_3O_8]$ have also been reported as being present.[5] The feldspar group of minerals in particular signify the most abundant mineral class in the Earth's crust and therefore often represent the original mineral from which many aluminosilicate minerals, such as muscovite and chlorite, have been evolved.[26] By comparison, illite is closely related to muscovite, although it generally has lower K^+ and higher Si^{4+} content. It can be found in many argillaceous (fine grained) sediments such as shale.[16] Studies carried

out by Crockett have also shown that haematite (Fe_2O_3) and rutile (TiO_2) can also represent around 3-6 wt.% and 1-1.5 wt.% of the overall slate composition respectively.[1] This observation was further supported by an investigation carried out by Gutt *et al.* for the Building Research Establishment (BRE) in 1974.[3] These minerals can however be regarded as minor minerals within slate and consequently do not generally play an important role in the physical and chemical properties associated with it when used as a traditional building material *i.e.* these minerals have been incorporated into the structure during slate formation but do not contribute to the splitting property of the final rock. Haematite, when present in metamorphic rocks, is generally formed from the recrystallisation of iron containing minerals[31] such as magnetite (Fe_3O_4) and siderite ($FeCO_3$); its presence in slate is often due to the inclusion of these minerals in sediments prior to metamorphism.[26] By comparison, rutile is often formed in clay and shale sediments and as a result of its relatively high thermal stability (melting point 1825°C) can often be found thereafter in the sediments' metamorphosed equivalents *i.e.* in slate.[26] A variety of accessory minerals can also be present within slate. These can often give rise to changes in the physical characteristics of the material and can potentially reduce the quality of the slate if present in a high concentration. Pyrite (FeS_2) and calcite ($CaCO_3$) are the accessory minerals most commonly identified in slate.[3,5,32] The occurrence of ilmenite ($FeTiO_3$), gypsum ($CaSO_4.H_2O$) and epidote ($Ca_2(Al,Fe)_3Si_3O_{12}(OH)$) has also been reported.[3,32] Watson, on the other hand, reports dolomite ($CaMg(CO_3)_2$) as an accessory mineral.[5] These minerals are normally regarded as being unaltered fragments of the original rock from which the slate was initially formed and generally remain as trace impurities within the metamorphosed rock.[31] Furthermore, organic minerals like graphite can also be found, which result from the crystallisation of ancient carbonaceous material. Substantial amounts of these accessory minerals can however have a detrimental effect on the quality of the quarried slate; particularly minerals such as calcite and pyrite which can be extremely vulnerable to weathering processes. These minerals are susceptible to dissolution in mildly acidic rain-water (CO_2 decreases pKa to 5.6)[41] and pyrite can be oxidised in air thus generating areas of weakness within the slate where a reaction has taken place. The presence of pyrite, in particular, can cause significant problems to the quality of marketable slate products and will consequently be discussed in more detail in Section 1.3.

In summary, although the basic composition of all slates is essentially the same *i.e.* made up of varying amounts of mica, quartz and chlorite, the multitude of other minerals that can also be potentially found in the material can result in a complex overall mineralogical composition. Consequently, the composition and thermal chemistry of slate can differ from area to area and even vary to some degree within the same quarry or vein.

1.1.2. Properties and Characteristics of Slate

The most important physical properties of slate are its cleavage, chemical inertness and hydrophobicity. It is these properties in particular that have made it such a commercial success, especially as a roofing material. Indeed, the term slate is derived from the French verb 'esclater' meaning to split.[21] As discussed previously, this fissility is believed to be directly attributed to its mineralogical make-up *i.e.* to the presence of muscovite and chlorite.[22]

The layered structure and fine-grained nature of this material ensures that slate has very low porosity and consequently is extremely impermeable to water. The low water absorbing property of slate has been clearly demonstrated in a report by O'Niell for the Quarry Manager's Journal in 1959.[23] The author reported here that immersion of completely dry slate from the Ffestiniog bed only resulted in a 0.016% increase in weight after 24 hours. Consequently, slate is immune from frost damage and thus practically everlasting. The inertness of slate has been clearly demonstrated by the 250 year old roofing slates of the St. Asaph Cathedral in North Wales which have recently been found to be sufficiently well preserved to be reused.[11]

The physical properties observed in the major mineral component of slate *i.e.* muscovite, are indicative of those that have been determined in slate. Slate has also been found to be a good thermal insulator.[25] Indeed, it has been shown that slate has comparable thermal conductivity to materials traditionally used as furnace linings such as terracotta and firebrick *i.e.* 0.0032Cal/cm/sec compared with 0.0040 and 0.0030 Cal/cm/sec respectively.[11] Furthermore, its laminae have inherent compressional strength (failure stress *ca.* 53 N/mm^2)[42] and exhibit considerable

elasticity. It has been reported that Llechwedd slates (12 x 0.6ins) are able to bend up to 1 inch when subjected to a load of 166lbs.[11]

As previously mentioned the presence of impurities within the rock, such as calcite or pyrite, can often result in the deterioration of the slate sample through weathering processes giving rise to the dissolution and oxidation of these minerals respectively. However, the presence of finely distributed accessory minerals within the matrix of the slate can influence the appearance of the in-hand sample. It is apparent that the colour of slate varies considerably; from black, to grey, to blue and to green. It is even possible to have shades of purple to red.[31] The colour can also give an indication to slates original chemical composition and to the physical changes that have occurred during metamorphism.[31] Black and dark grey slates, such as those found in Spain, indicate the presence of traces of decomposed organic matter such as graphite. These dark slates can also indicate finely divided pyrite. Ferrous iron in chlorite generally give a green tint, whereas ferric iron in the form of hematite can give rise to a red coloration.[31] This variation in colour can therefore provide valuable information on the composition of the material.

1.2. Expanding Materials

On the whole, upon heating to increasing temperatures (>1000°C) aluminosilicate minerals and rocks sinter and then melt to form a fused material upon cooling.[43] This is apparent in the ceramics industry which utilises clay minerals, such as illite and kaolinite [$Al_2Si_2O_5(OH)_4$], in the production of pottery and china. When heated these materials generally undergo significant transformations. The dehydration of the free-water adsorbed onto the surface of the clay initially occurs at a temperature between 50-120°C. The clay structure then becomes unstable at 120-600°C leading to the loss of the "water" held between the layers and the formation of a more amorphous substance between 600-900°C. Finally at temperatures above 900°C recrystallization of the clay normally takes place with the loss of crystalline water, held in the structure as hydroxyl groups, occurring above 1000°C. In most clays this loss of water generally signifies a reduction in volume. In the manufacture of ceramics the most important transformations are therefore those that occur between 600 and 1000°C. It

is at this temperature zone that new minerals are formed, not only as a result of the decomposition of the clay minerals themselves but also due to the interaction of the clay with additives such as sand, quartz or feldspar in the furnace during firing. A more rigid, glass-like substance is normally produced as a result of the changes in the physical states of the heated material *i.e.* fusion and loss of structure producing an amorphous material.

However, in contrast to the processes that occurs during the production of ceramics, when slate is subjected to high temperature it has an ability to expand to several times its original volume.[5] Other natural materials such as some shales and even some clays also have this property and can exhibit some degree of expansion when heated to relatively high temperatures. These three material types can have similar chemical compositions and physical properties. The exposure of these original sediments to fundamentally different geological conditions over varying lengths of time has however ensured the formation of essentially different rocks.

Clay is the softer of the three substances.[34] It is defined as being a material consisting of particles less than 2μm e.s.d. (equivalent spherical diameter) and has the ability to absorb water thus producing a material with apparent high plasticity when wet. Indeed two types of clays exist, namely swelling and non-swelling clays.[43] This swelling characteristic however refers to the change in volume that can take place due to the amount of water molecules or polar ions that can be absorbed into their structure and does not reflect any increase in volume that might occur when heated. Swelling clays normally consist of minerals from the smectite group *e.g.* montmorillonite, whereas non-swelling clays largely include kaolinite, feldspars and mica-like minerals such as illite and chlorite, which has an analogous structure and composition with the high-temperature chlorite phases in metamorphic rocks. On the other hand, as discussed earlier, shale and slate are reportedly products derived from clay sediments.[16] Consequently, shale and slate are much harder materials compared to clay and retain their shape when wet. However, shale is distinguishable from slate since it is generally softer and its fissility lies parallel to the bedding plane in contrast to slate where the cleavage plane is often independent of the original bedding. Indeed, the major phases present in expandable clay are reportedly kaolinite and/or montmorillonite compared to illite and chlorite in shale, and muscovite and chlorite in

slate.[44] However irrespective of the compositional differences that may occur, the essential minerals composing clay, shale and slate are all characterised by a layered arrangement resulting in a lamellar macroscopic structure. This sheet structure clearly has an important impact on the expansion characteristic seen in these three types of material.

Lightweight aggregates for use in concrete have traditionally been made from natural materials such as pumice and volcanic cinders.[45] These so-called natural lightweight aggregates have been used to produce lightweight concrete dating back to the early Greeks and Romans.[46] Natural lightweight aggregates can therefore be defined as substances that are naturally found in the Earth that require only limited processing such as crushing, washing and grading.[47] One of the first artificial lightweight aggregates was developed from cinders obtained as a by-product from the railways industry during the steam locomotive era.[45] The use of this material however died with the introduction of diesel engines around 1930.[46] Materials that are currently classed as raw material for the synthesis of lightweight aggregate include colliery waste and pulverised fuel-ash from coal-fired power stations.[47] These waste materials and industrial by-products are generally crushed and pelletised prior to being heated to temperatures from 50 to 400°C. Substantial expansion is not normally observed during heating. The porosity required for the production of suitable aggregates from these materials is usually generated through the loss of carbon during firing due to the presence of carbonaceous compounds in coal and as a result of the packing nature of the crushed particulates giving rise to tiny voids within the material.[47] A significant disadvantage of this process is the associated air pollution problems that can occur resulting from incomplete carbon combustion, which can release CO gas during the firing stage.

Interest in the use of expanded clay, shale and slate has mainly come from the lightweight aggregate industry. It is reported that normal aggregates generally have an uncompacted bulk density of 1000-1700kg/m^2.[48] By comparison, a lightweight aggregate is defined by having a density in the region 300-1000 kg/m^2. The density of expanded clay and shale generally falls between 380 and 720 kg/m^2 whereas expanded slate is normally slightly denser but remains within the lightweight aggregate threshold at *ca.* 560-860 kg/m^2. Studies have therefore been carried out in

an attempt to gain a basic understanding of the processes taking place within each rock type to produce the expanded material. Research has mainly been undertaken in the USA, however a few important studies in the UK have also been reported. This research dates back to the beginning of the 20th century and has provided valuable information on the general processes that occur. Currently, slate forms a small proportion of the total current production of lightweight aggregate. This is clearly illustrated in the United States where in the 1970's five slate aggregate plants were in production compared to 70 lightweight shale and clay establishments.[45] Moreover, according to the Expanded Shale, Clay and Slate Institute (ESCSI) only two expanded slate plants are now active namely, Carolina Staylite Company and the Solite Corporation.[49]

In the early 1900's, S.J. Hayde established the first commercial heating process for the production of lightweight aggregate from natural argillaceous (fine-grained) material in Kansas City, USA.[46] He invented a process based on a rotary kiln with the specific aim of producing an expanded material from shale. This product was found to have adequate strength and was of sufficient quality for use as a lightweight aggregate to be applied in reinforced concrete structures. Hayde subsequently patented the process in 1929,[50] hence the product "Haydite" was conceived. An example of the early use of haydite was in the construction of liberty ships in World Wars I and II. This lightweight aggregate was used in concrete to reinforce the hulls of the war ships. The product is now however referred to as Buildex and the company is currently one of America's leading producers of expanded shale, producing annually more than 750,000 cubic yards of expanded product in plants located in both Kansas and Missouri, USA. The raw material is quarried specifically for the production of the lightweight aggregate. The shale is introduced to the rotary kiln and heated to 2000K over 1 hour to produce the expanded material. The density of the shale decreases upon heating and all organic compounds are reportedly lost during the process. Hayde however gives very little information on the composition of the shale samples that undergo heat treatment or any details on the mechanism behind the expansion process. It is however reported that the resultant material becomes vitrified whilst numerous microscopic, isolated voids are observed within the internal matrix of the expanded material. Furthermore, since Buildex (Haydite) was manufactured at

high temperatures it has also been found to be fire resistant and extremely stable to further heating.

The heat treatment of slate to produce a material suitable for use in concrete is believed to date to workers in Russia in 1931.[5] Thereafter, the first report focussing on the expansion of slate in Britain was carried out by E.H. Coleman in the 1930's at the Building Research Station. This work led from a patent being obtained in 1933 that provides details of an improved method for obtaining cellular products from laminated rocks such as slate.[51] Slate samples for this study were mainly obtained from Welsh quarries situated in Gwynedd.[52] The report aimed to identify the sources of suitable slate for the production of an expanded material and to investigate its suitability for use in concrete. He determined that not all slates expanded to the same extent and that those obtained from Ordovician and Silurian formations expanded best (3-7 times). At that time an expansion of less than 2.5 times did not provide a material that was considered to be a sufficiently light for aggregate use. It was also found that a rapid heating rate was needed to ensure that the maximum expansion was obtained. Coleman therefore had successfully undertaken one of the first empirical studies into slate expansion. However little information on the characterisation of the slate either before or after heating was reported. Furthermore, it was apparent that although he believed that the expansion was related to the formation of gases from slate's constituent minerals no attempt was made to identify this expansion gas in order to fully explain the process that was observed.

Following this British study, J.E. Conley[53] carried out an investigation in 1942 on the possible use of waste slate as a source of raw material for lightweight aggregates in the United States. Conley stated that all the slates he tested expanded to some degree when heated under the appropriate conditions and that this expansion took place normal to the cleavage plane. Furthermore, those samples that expanded to 3-7 times their original volume were again shown to be the most suitable for use in concrete. Conley believed that an important characteristic of expanding slates was that they fused at relatively low temperatures prior to the release of gases, such as CO_2, which caused expansion. He believed that this fusion was facilitated by the presence of lime (CaO), magnesia (MgO) and iron oxides, in particular ferric oxides such as Fe_2O_3. The presence of Fe_2O_3 was noted as being of particular importance due to its ability to

supply oxygen to react with carbonaceous compounds that may be present in the slate in order to produce the necessary expanding gases such as CO or CO_2. Furthermore he believed that the reduction of Fe^{3+} to Fe^{2+} produced a compound which was believed to act as a fluxing agent which effectively reduced the fusion temperature of the sample. It was also suggested that the addition of fluxing agents (ferrous oxides or lime) during firing could produce more effective bloating in slate samples which were found to have a high Al_2O_3 or SiO_2 content since it was believed that these slates tended to have higher melting temperatures. Conley showed that the addition of combustible compounds into the furnace during firing aided in the bloating of expandable materials. Furthermore, the potential environmental implications of such additives incorporated into the furnace would undoubtedly prove to be a significant drawback if such a system was necessary in a commercial process.

In parallel to Conley's work an extensive investigation was undertaken in 1948 by Cservenyak *et al.*[54] to evaluate the expansion characteristics of slates, shales and clays obtained from areas in Virginia and Pennsylvania, USA. In general, the slates under investigation were all found to have a common mineralogical composition of quartz, sericite mica, chlorite, pyrite and dolomite in addition to some carbonaceous compounds. Secondary minerals including biotite, haematite and microline were also reported as being present in some of the samples. Minerals reported to be present in both the clay and slate samples analysed in this study were limited to quartz and sericite mica with different clay samples also containing various amounts of kaolinite, haematite, pyrite, tourmaline or rutile. Cservenyak utilised a small gas-fired rotary kiln to heat the samples to temperatures between 1100 and 1350°C in order to produce his expanded material. However, not all of the clay samples investigated expanded upon heating. For those samples that did expand, a similar degree of expansion was observed for all three types of materials, a volume increase generally in the region of 2-2.5 times their original volume was noted. However the greatest expansion was achieved by a slate sample in which a 3-fold increase in volume was observed. A visible inspection by Cservenyak of the resultant material showed that a product with a smooth, sealed surface containing fine to medium sized pores within its interior was generally achieved. Furthermore, with regards to the non-bloating clays it was found that some degree of expansion could result from the addition of agents such as sulfur or carbon (as charcoal). The greatest volume increase was found

to occur when fuel oil was added, especially when NaOH, Na_2SiO_3 or Fe_2O_3 were also incorporated into the mixture. In this case, a volume increase of up to four times could be achieved. The study therefore concluded, in agreement with Conley's findings, that the essential requirement for attaining expansion was that softening of the samples to a pyroplastic state coincided with the release of expanding gases. These gases were believed to result from the degradation of compounds such as carbonates, sulfates, sulfites and carbonaceous materials present within the original samples. Furthermore it was believed that materials deficient in the gas-forming constituents could be made to bloat through the incorporation of admixtures such as sulfur, carbon, sulfates, carbonates and hydrocarbons into the furnace during heating. However, in the context of developing a modern, commercial process to produce expanded slate, the necessity to add such compounds has significant pollution implications due to the inevitable release of harmful gases such as SO_2 during the heating process. Cservenyak *et al.* also stated that enhancement of the expansion for those samples containing the necessary gas-forming compounds but which were deficient in so-called fluxing elements could be achieved through the addition of iron, lime or alkali compounds again in agreement with Conley. The report however did not attempt to provide any explanation on why some materials bloat and others remain unexpanded even when heated to temperatures as high as 1300°C. This inconsistency was evident within clay samples in particular. It is therefore apparent from this paper that a more complex expansion mechanism is involved and that other factors independent to composition can also influence the extent of bloating.

Ehlers[55] also undertook an investigation in a further attempt to determine the composition of the gases responsible for the volume increase observed in expanding materials, mainly clay. The clay samples were identified as containing mainly illite, kaolinite and quartz. In agreement with previous studies, Ehlers concluded that the thermal decomposition of accessory minerals such as carbonate minerals, namely calcite ($CaCO_3$) and ankerite [$Ca(Fe,Mg)(CO_3)_2$], were responsible for the expansion phenomena since they were the only minerals found in each sample that were believed to be capable of evolving a gas when heated *e.g.* releasing CO_2. It was reported that a calcite content in the region of 0.796% would effectively correspond to a 0.412% CO_2 content in the original samples. Consequently he believed that the release of carbon dioxide could sufficiently account for the observed expansion. By

comparison, an investigation by Baudet in 1971 suggested that the presence of other minerals for instance pyrite and some ferrous oxides may contribute to the expansion process.[56] Baudet stated that pyrite (FeS_2) can react with oxygen releasing sulfur dioxide whereas it is possible that ferrous oxides react with water vapour producing ferric oxides and hydrogen gas. A series of reactions (Equations 1-5) have been provided by Baudet thus illustrating the different routes of producing gaseous compounds that he believed could be responsible for the expansion mechanism in materials such as slate. The formation of sulfur, sulfur dioxide or even hydrogen as a direct result of the decomposition of accessory minerals within the matrix of the expandable materials were therefore thought to be responsible for the expansion process.

$$FeS_2 \rightarrow FeS + S(g) \quad [1]$$

$$FeS_2 + O_2 \rightarrow FeS + SO_2(g) \quad [2]$$

$$2FeS_2 + 5\tfrac{1}{2}O_2 \rightarrow Fe_2O_3 + 4SO_2(g) \quad [3]$$

$$S + O_2 \rightarrow SO_2(g) \quad [4]$$

$$2FeO + H_2O(g) \rightarrow Fe_2O_3 + H_2(g) \quad [5]$$

It is therefore clear that most of the early work on expanded slate/clay/shale was carried out in the United States. This work led to a number of patents being obtained most of which claim to describe improved methods for the commercial production of expanded material from clays and shale. These patents generally date from the 1940's through to the late 1950's.[57,58,59,60]

After the initial interest by workers in expanded slate during the post World War II era little development occurred in the British industry until the early 1960's.[5] Indeed, expanded slate aggregate was not produced in the UK until 1966. This product was sold under the name of "Solite" and was manufactured at a plant located in a disused slate quarry at Bwlchgwyn near Wrexham, North Wales. "Solite" was produced from the waste slate tipped at the site during the active years of the quarry. This waste material was subsequently crushed and screened before being introduced into a rotary kiln to be heated. The plant reportedly employed around thirty men at its peak in 1969[61] and an annual production of 150,000 tonnes was recorded as being achieved in 1972.[5] However, the company faced significant environmental problems since the

process involving the crushing of waste slate generated large amounts of dust that polluted the surrounding district. It was reported that atmospheric pollution at Bwlchgwyn was six to seven times higher than the national average of industrialised areas of the UK.[62] The local community therefore generated immense pressure against the plant throughout its years of operation. However, irrespective of the obvious advantages and commercial success of the final product the opposition from the public resulted in the eventual closure of the Solite company in July 1973.[63]

Renewed interest in slate expansion was however observed later in the 1970's resulting from the Building Research Establishment commissioning further studies in order to investigate the thermal properties of various slates from Wales with the aim of ascertaining possible uses for this, the major industrial by-product and waste material in the area.[3,32] A number of slate samples were collected from the majority of the slate quarries in North Wales. These samples were generally heated to temperatures between 1150°C and 1200°C. Coleman[52] first published his finding on the initial development work in the 1930's. However Nixon found that this early work was highly relevant and therefore formed a good basis for his more current investigation. According to Nixon and Coleman[32] most of the Welsh slates expanded to several times their original volume. However, significant differences were observed in the expansion properties of slate from different areas. The oldest formations developed from the Cambrian era (600-500 million years old), such as the old Caernarfonshire slates of the Penrhyn quarry at Bethesda and Dinorwic quarry in Llanberis, expanded least *i.e* generally expanded from 1.1 to 2.5 times their original thickness. This expansion was in agreement with that previously found by Cservenyak *et al.*[54] By comparison, the younger Ordovician (500-450 million years old) and Silurian slates (400-450 million years old), such as those from Blaenau Ffestiniog and Llangollen respectively, expanded to a much greater extent. Indeed the slates from the Ffestiniog slate belt were found to consistently expand to between 4-5.5 times their original thickness. Furthermore, two types of expansion were noticed within the Silurian and Ordovician slates, each producing a material with a slightly different structure. The Silurian slates of Llangollen were reported to expand producing a material that appeared to have a glass-like outer shell surrounding an internal matrix of relatively large isolated pores.

By comparison, the Ordovician slates of Blaenau Ffestiniog produced a highly vitreous material containing a greater number of smaller sized pores and a less glassy surface. It was reported however that this expansion resulted from the decomposition of slate's constituent minerals. In agreement with previous studies, Nixon *et al.* believed that the simultaneous action of two processes caused the expansion mechanism *i.e.* as slate is heated to very high temperatures it is softened and its outer surface becomes fused effectively leading to the formation of a pyroplastic exterior that increases the resistance to gas transport to the outer boundary layer. It was believed that the evolved gases were trapped within the structure and the expansive pressure generated effectively opened up the laminated structure of the slate perpendicular to the plane of weakness *i.e.* cleavage plane. For the first time water vapour was implicated as having a role in the expansion process. In addition, Nixon and Coleman reported that the mineralogical composition of slate was not the only factor affecting the expansion process; the compactness of the rock, grain size and angle between the bedding and the cleavage plane was also believed to effect the expanding characteristics of slates from different areas. No data was given in this paper to support the supposition that the release of H_2O directly related to expansion. This hypothesis arose due to the fact that both muscovite and chlorite, which were found to be abundant in slate, contained a degree of water within their structure.[27] No thermal analysis or characterisation of the expanded slates was undertaken in the course of their investigation. The present study therefore aims to address this and to provide proof to identify the expansion gas.

Research into slate expansion apparently died down after the 1970's. However, a recent paper by Boateng *et al.*[44] in 1997 shows that interest in expanding materials is ongoing. Boateng and co-workers aimed to provide a model for the pyroprocess kinetics involved in the production of expanded shale aggregate in high temperature zones of a rotary kiln. A mathematical model was therefore formulated, which Boateng and co-workers believed could also be applied to the expansion of slate and clay. It was reported that the model was able to predict the temperature distribution within a shale particle as well as the density changes that occur during expansion. It was also believed that heterogeneous gas-solid chemical reactions in association with a mass transport phenomenon were responsible for the process. Three general steps were reported to be involved. The first step involved a chemical reaction that

resulted in the generation of a gas. The authors did not attempt to identify the nature of this gas in this study and therefore appear to have accepted Ehlers[55] conclusion that the decomposition of carbonate minerals resulting in the evolution of CO_2 was most likely to account for the expansion in shale, slate and clay. The second and third stages involved the diffusion of the gaseous product through the core and outer boundary of the heated particle respectively. These final stages were believed to be dependent on the heating rate since it had been demonstrated that slowly heating a sample resulted in an unexpanded product, clearly illustrating the consequence of allowing adequate time for the gases to escape the outer boundary layer. However, according to Boateng *et al.*, for the gas to be trapped it was vital that a pyroplastic exterior be attained. In accordance with Nixon and Coleman, it was believed that this physical state inevitably increased the resistance to gas transport to the outer boundary. The vesicular nature of the expanded material was thus believed to show that a much faster rate of gas evolution was taking place compared to the rate of diffusion through the slate particles. Furthermore, it was reported that the thermal diffusivity of shale decreased with increasing temperature and was directly related to the heat capacity and the thermal conductivity of the material during the heating process. As the thermal diffusivity of the material decreases, its thermal conductivity was also lowered which in turn led to the initial fusion of the periphery of the particle hence the formation of the pyroplastic exterior. Boateng and co-workers reported that, if heating was continued beyond this stage, pore collapse was initiated and sticking and agglomeration of the expanded product took place giving rise to a less expanded product unsuitable for use as a lightweight aggregate.

It is therefore evident that at present, the most important application for expanded slate is as a lightweight aggregate in concrete. It has been shown to have a relatively low density but has a comparatively high mechanical strength.[47,48] One of the major commercial advantages of producing lightweight aggregate from expanded slate is that very little additional processing costs are involved in obtaining the raw material since it can be easily recovered from either slate waste tips or during the normal workings involved in generating the slates for roofing purposes *etc.* General crushing and screening to remove small fractions is normally all that is required to prepare the slate prior to heat treatment. However, uses for this expanded slate are not just limited to the construction industry alone. Recent developments have been made

utilising expanded slate as a filter medium in the water purification process.[64] Potential applications can also be found in the field of hydroponics for horticultural purposes. Analogous materials are currently being produced from natural clay.[65] This light expanded clay aggregate (LECA) is reported as being produced by heating 'pure', natural clay at 1150-1200°C for 3 hours. It has been shown to provide an ideal moisture, food and air balance to plants. Furthermore, the aggregates can carry nutrients down to the plant roots more effectively since solutions can pass more freely over the aggregate surface and can reduce the risk of root-rot since spaces between the aggregate "pebbles" allows access to oxygen to the plant's roots.

Indeed, the renewed interest in expanded slate production in North Wales has clearly been demonstrated by patents obtained by J.W. Greaves and Sons Ltd[66] and Kyffin[67] in 1988 and 1996 respectively. It is evident that an expanded material can be produced from slate on a large commercial scale both in Britain and in the USA.[5] However to ensure the success of future developments the pollution problems experienced in the past, in both the crushing and heating/expansion stages, must be taken into consideration and overcome. It is also vitally important that the process itself can be controlled to ensure the homogeneity of the final product and that the energy efficiency of the process is optimised. The location of the expanded slate site and its proximity to a source of waste material is also a key factor in establishing the commercial viability of this process. Fundamental knowledge relating to the expansion of slate is limited and contradictory information has previously been documented thus providing an unclear picture of the actual expansion mechanism. This thesis therefore aims to provide an investigation into slate expansion by providing a mechanistic study of the expansion process to gain a better understanding on the nature of the expansion gas. The reviewed literature also shows a lack of information on the expanded product itself, so detailed analysis and characterisation of expanded slate has been undertaken. A potentially novel application for this inert, thermally stable solid will be explored in the course of this study. This work will focus on the development of expanded slate as a support material for a new heterogeneous catalyst. It is clear that finding a novel application for this material would be extremely beneficial to both the slate industry and to the environment, since less waste slate would inevitably be produced. The information gained in this present study will therefore potentially be of great benefit to the development of new

commercial processes utilising slate waste in North Wales and other slate-producing regions.

1.3. Pyrite

One of the most common accessory minerals found in association with slate is pyrite (FeS_2).[39] In slate, pyrite tends to appear as cubic crystals within narrow veins parallel with the slate's cleavage plane and can therefore not only be found within the interior of the cleaved slate but also on the surface after splitting has taken place. Indeed pyrite can occur in a variety of geological situations and its occurrence is not just limited to metamorphic formations as in the case of slate. It can also be found as an accessory mineral in igneous and sedimentary rocks.[26] In addition to pyrite a variety of other iron sulfide minerals exist in nature.[68] For example, marcasite can be found having the same chemical composition as pyrite but existing as orthorhombic FeS_2 rather than cubic. Other iron sulfide systems also exist that become increasingly deficient in iron, these minerals include a range of pyrrhotite minerals ($Fe_{1-x}S$) where x reportedly varies from 0.125 (Fe_7S_8) to 0.0 thus forming stoichiometric FeS which is known as troilite.[69] A mineral that is deficient in sulfur also exists, this is known as mackinawite (FeS_{1-x}). In this case the metal to sulfur ratio is greater than unity since x normally takes values between 1.04 and 1.07.[68] These minerals are commonly precipitated in anaerobic environments. Furthermore, pyrite can be found together with other sulfide containing minerals such as galena (PbS), arsenopyrite (FeAsS), sphalerite (ZnS) and chalcopyrite ($CuFeS_2$) in ore deposits.

Pyrite (FeS_2) however is considered to be the most common sulfide mineral at the Earth's surface.[17] It naturally crystallises with cubic symmetry, belongs to the space group *Pa*3 (205) and has a lattice constant a = 5.417Å.[29] The iron atoms are located at the corners and face centres of the cube and are present in the II+ oxidation state. The sulfur atoms exist in pairs as $[S_2]^-$ ions at the mid-points of the cube edges and at the cube's body centre (Figure 1.12).[24] The crystal structure is consequently made up of distorted octahedra, where each ferrous ion is surrounded by six sulfur atoms at a distance of 2.26Å.[26] The centre point of the sulfur pairs can therefore be regarded as being cubic close packed with an iron atom occupying the centre of each of the

resulting octahedral holes. Cubic crystals of pyrite are typically formed but octahedral or pyritohedral (pentagonal dodecahedral) shaped crystals can also be found.[33] These can often be found as twinned crystals in nature. The predominantly pale, brass-yellow colouration with greenish-black streaking and metallic lustre of pyrite gives rise to its nickname "Fool's Gold".[30,70]

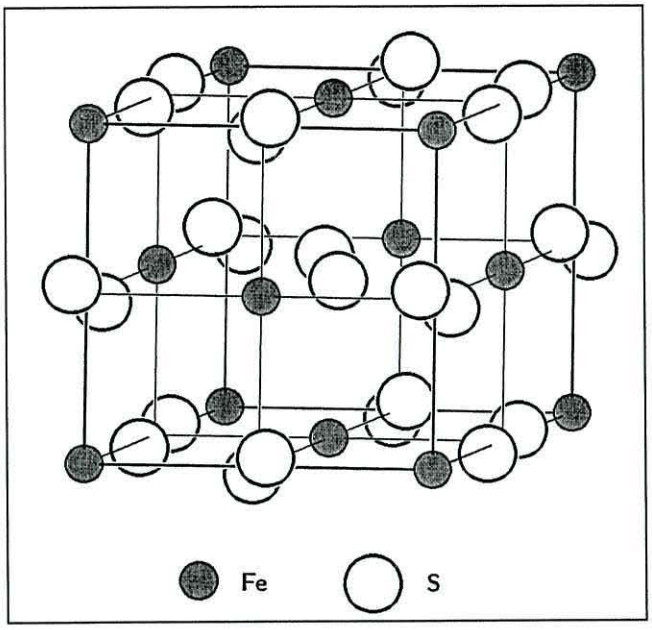

Figure 1.12. Structure of pyrite.[24]

Literature on the usage of pyrite in a medicinal capacity exists as early as *ca.*75 AD,[71,72] Though evidence from these writings suggests that references to pyrite's healing powers can be further traced back to Theophrastus at around 315 BC.[73] During this period of Greek history it was believed that pyrite had powers for stopping "blood decay" and was therefore often worn as an amulet to guard against such an affliction. Indeed pyrite's link to ancient Greece is clearly evident since its name is derived from the Greek word '*pyr*' meaning fire, since as it is broken sparks are often discharged.[30] Furthermore it is known that pyrite was used as a source of vitriol and sulfuric acid as far back as the Middle Ages and during the early days of modern chemistry.[74] Further research into the understanding of the basic chemistry of pyrite came about during the 19th century and beginning of the 20th century at a time when there was great interest in iron and iron containing compounds. A comprehensive review by Mellor has been written documenting the history of pyrite. Mellor also provides an extensive review of the information gained on pyrite's

chemical and physical properties thus illustrating the importance of iron sulfide chemistry even to workers of this early period.[75]

Nowadays, pyrite ore still has some economic importance. Extensive studies into the sulfur–iron system therefore still has great significance in the area of mineralogy and metallurgy, in addition to its importance in the coal-fired power station sector. Pyrite is principally mined due to its presence in ores containing other more commercially valuable metals such as copper or gold. It is important in the copper extraction industry since it often exists in association with the main copper containing ore chalcopyrite ($CuFeS_2$).[76] Its importance in the gold industry relies on the fact that gold can often be present as tiny grains in pyrite, especially in some commercial Precambrian deposits. Nevertheless, pyrite itself is still occasionally mined as a source of sulfur so that it can be subsequently used in the production of sulfuric acid and sulfate compounds.[29] It is also applied to the formulation of some paints and polishes.[30]

1.3.1. Thermal Decomposition of Pyrite

The decomposition of this mineral is of particular relevance to this present study since it is vital that a fundamental understanding of its thermal chemistry is gained in order to fully understand the properties of slate, the processes that occur during its expansion and the nature of the expansion gas. A study to gain a comprehensive understanding of pyrite's decomposition within slate's internal matrix and exterior surface during heating has therefore been provided. Furthermore the potential environmental issues that may arise due to pyrite's decomposition during the firing of slate have also been taken into consideration when developing a commercial slate expansion process.

Previous research into pyrite decomposition has mainly been carried out due to the occurrence of pyrite in coal and gold deposits. It is an undesirable mineral for these industries since the thermal processes involved in the use of coal as fuel and in the generation of pure gold can result in pyrite decomposition and possible release of sulfur volatiles (particularly SO_2 gas) leading to pollution problems such as acid

rain.[77] However this review will initially focus on the decay of pyrite through natural weathering processes. The effect of heat on pyrite alone will then be discussed followed by a discussion of previous work with respect to pyrite associated with coal. It is evident that extensive research has been undertaken in this area and that the decomposition of pyrite in both reducing and oxidising environments has been investigated. Finally, previous studies on the thermal chemistry and of this mineral in gold ore will be reviewed in order to ascertain what information previous workers have gained on the decomposition mechanism of pyrite in different host materials. In the course of this review it has become evident that no literature exists on the thermal decomposition of pyrite in slate.

Pyrite decay through weathering processes is caused by its oxidation in air produces a rust-like material made up of iron oxides.[78] This is a particular problem when using unexpanded slate for building purposes such as a roofing material.[79] The aesthetic appearance of the slate product can be affected due to discoloration caused by the brown, rust-like stains of the newly formed iron oxide minerals. Furthermore a break down of the slate structure by the generation of sites more susceptible to the effects of physical weathering can also arise from the presence of pyrite in slate. Previous work analysing weathered roofing slate from the Llechwedd Slate Quarries, Blaenau Ffestiniog, North Wales clearly shows an increased concentration of iron and sulfur around the areas of greatest slate destruction.[80] This suggests that the weathering problems can be closely linked to the presence of iron sulfide minerals in the slate since these minerals can naturally undergo reactions either with oxygen from the atmosphere or rainwater forming iron oxides and sulfur.[81] Unfortunately because the slates in this study had already undergone substantial weathering, pyrite in this case could not be conclusively identified as the mineral phase responsible for the observed decomposition problems. It has been reported that a wide range of iron sulfides can be found in nature, made up of a varying amount of the component elements *e.g.* from pyrite (FeS_2) to pyrrhotite ($Fe_{1-x}S$) to troilite (FeS).[81] However, research on Llechwedd slates provided in this thesis shows that the main sulfide species present is indeed pyrite. Its presence in the slate therefore undoubtedly plays an important role in weathering processes that result in the destruction of slate samples.

The presence of pyrite also has implications for the use of slate in the expanded form as lightweight aggregate since the presence of sulfur and sulfate ions can seriously affect the integrity of concrete products.[48] It has previously been shown that the weathering of sulfide minerals found in aggregate material bound by cement can release $[SO_4]^{2-}$ ions from the oxidation of $[S_2]^{-}$ ions causing serious damage to the final concrete product and resulting in its eventual failure.[82] Concrete degradation has been reported to arise from chemical reactions taking place between sulfates and the calcium silicates commonly present in cement.[48] The reaction products that are normally associated with sulfate attack are gypsum ($CaSO_4.2H_2O$) and ettringite ($3CaO.Al_2O_3.3CaSO_4.31H_2O$). The formation of these compounds effectively result in the breakdown of the concrete structure. Furthermore, bloating of the concrete can also occur which often gives rise to surface cracking which consequently reduces the integral strength of the material. In addition, discoloration or staining can again ensue from the generation of iron oxides, as seen in slate roofing tiles.

Research on the oxidation of pyrite has been carried out by Casanova *et al.*[83] Their studies aimed to obtain a greater understanding of the effects that iron sulfides have on concrete products. This work has also focused on the oxidation of other iron-sulfur minerals, in particular pyrrhotite ($Fe_{1-x}S$), since together these two materials form a major proportion of the iron sulfide minerals present in natural rock. Here pyrite and pyrrhotite oxidation processes involving a sequence of different reactions were studied. It was believed that sulfide degradation by-products, such as haematite (Fe_2O_3), geothite (FeOOH) and ferrihydrite ($Fe(OH)_3$), were normally produced. These oxidation products often gave rise to concrete degradation since they generally had a greater molar volume compared to their precursors and could therefore result in bloating causing surface cracking. However, the rate of sulfide oxidation through natural weathering was found to be slow and was also found to be dependent on the alkalinity, oxygen availability and sulfide grain size within the aggregate.[82] This is relevant because if expanded slate is to be further developed as a lightweight aggregate material for concrete blocks, it is important to know the fate of any iron sulfide mineral present in the original slate before and after it is expanded. Under extreme conditions the presence of pyrite could potentially affect the commercial viability of expanded slate as a lightweight aggregate.

The thermal decomposition of coal-derived pyrite has recently been studied by Yperman *et al.*[77] These workers have focussed on the thermal chemistry of pyrite in a reducing atmosphere using temperature programmed reduction (TPR) experiments with hydrogen gas along with thermal gravimetric analysis (TGA) in an argon atmosphere to temperatures up to 1000°C. The TPR studies in hydrogen show a two stage reduction of FeS_2: first to FeS and H_2S at 590°C and then to Fe and H_2S at around 800°C, as shown in equations [6] and [7]. By comparison the TGA study under an inert atmosphere (argon) showed a single peak at 600°C corresponding to the formation of troilite (FeS). In addition, following this TGA study in argon, it has been suggested that an intermediate product, pyrrhotite ($Fe_{1-x}S$), be initially formed before the formation of FeS as seen in equation [8]. In fact, the reported weight loss calculations corresponded well to the removal of a single sulfur atom for every FeS_2 molecule indicating that complete sulfur liberation was not achieved in this case even though a final temperature of 1000°C was reached. This is in accordance with previous work carried out by Schoenlaub whereby a weight loss in the region of 23.5 to 24.8% was determined when pyrite was heated to 1000°C in neutral or reducing gases (nitrogen and carbon monoxide).[84] This earlier study showed that the main weight loss occurred between 550 and 800°C with the maximum rate of weight loss taking place at 600 to 660°C.

Yperman and co-workers also reported that the initial conversion of pyrite to troilite takes place at a slightly higher temperature in argon than in a hydrogen atmosphere *i.e.* 600°C compared to 585°C.[77] These workers reported that this variance in decomposition temperature was due to an increased reactivity of sulfur towards hydrogen thus commencing pyrite decay at a lower temperature. A similar trend had also previously been observed by Maa and co-workers.[85] Studies carried out investigating inhibition isotherms between sulfide minerals in coal and hydrogen sulfide gas within a temperature range of 600 and 870°C showed that sulfur removal was greater under a hydrogen atmosphere than in an inert N_2 atmosphere. Indeed, Maa *et al.* found that conversion of the pyritic sulfide to FeS was complete at *ca.* 600°C in hydrogen compared to 740°C in nitrogen.

$$FeS_2\,(s) + H_2\,(g) \overset{590^\circ C}{\rightleftharpoons} FeS\,(s) + H_2S\,(g) \qquad [6]$$

$$FeS\,(s) + H_2\,(g) \overset{800^\circ C}{\rightleftharpoons} Fe\,(s) + H_2S\,(g) \qquad [7]$$

$$2FeS_2\,(s) \rightleftharpoons [Fe_{1-x}S] \rightleftharpoons 2FeS\,(s) + S_2\,(g) \qquad [8]$$

Particle size has also been reported as having a strong influence on the decomposition of pyrite in a reducing environment.[86] Montano *et al.* reported that the maximum reduction temperature tended to decrease as pyrite particles became smaller.[86] This trend has also been seen by Yperman *et al.* where it was attributed to the fact that smaller grains had an increased relative external surface area and were therefore more accessible to attack by hydrogen atoms.[77] However, heating in hydrogen can give rise to additional chemical reactions that can effect the extent of desulfurization. It has been reported that small amounts of hydrogen sulfide can promote the reverse reaction whereby FeS and FeS_2 are reproduced *i.e.* the reaction equilibrium of equations [6] and [7] shift in favour of the formation of the starting compounds. This reverse reaction had previously been recorded by Zielke *et al.* where it had been found that 0.5% H_2S was sufficient to initiate its reaction with Fe to regenerate FeS.[87]

Work on the reduction of pyrite in a hydrogen atmosphere has also been carried out by Lambert and co-workers.[88] These workers investigated the kinetics and mechanism of the pyrite-pyrrhotite conversion under various atmospheric conditions, namely under H_2, in inert atmospheres (Ar and He) and *in vacuo*. A TGA investigation of pyrite was conducted over a temperature range of around 400 to 700°C and pressures between 0.2Pa and 7.0MPa. These workers suggested a two-stage consecutive process where sulfur vapour desorption from the crystal surface was believed to be the rate-controlling step. It was believed that pyrite initially decomposed through the loss of sulfur atoms to pyrrhotite (FeS_x, $1.00<x<1.23$), where its composition in equilibrium with pyrite was dependent on temperature. The value of x was found to increase with increasing reaction temperature *i.e.* the FeS_x formed at higher temperatures was inclined to be richer in sulfur. The pyrrhotite was then found to

undergo further reduction to troilite (stoichiometric FeS) in hydrogen and inert atmospheres. However eventual reduction to iron was only believed to occur for those samples heated in hydrogen. Furthermore, it was believed that the compound whose composition lies between that of troilite and pyrrhotite, which was in equilibrium with pyrite, was indeed present as a solid solution of sulfur in troilite. Lambert *et al.* proposed a mechanistic picture describing the processes that occur during pyrite decomposition, which they stated could be applied to the reduction of pyrite to pyrrhotite both in hydrogen and inert atmospheres. The first step involved the release of sulfur atoms from the pyrite lattice. These atoms were believed to be adsorbed onto the outermost surface of the pyrite particles where they could react with H_2 to be subsequently abstracted as gaseous H_2S. By comparison, if in an inert atmosphere Lambert *et al.* believed that these same sulfur atoms combined with other adsorbed sulfur atoms, instead of H_2, and thus desorbed from the pyrite surface as gaseous S_2 and not H_2S. In both cases, once sufficient sulfur was removed from the pyrite lattice, Lambert and co-workers reported that the outermost pyrite layer converted to the pyrrhotite structure *i.e.* FeS_x formed as a result of the loss of S from FeS_2. It was suggested that upon formation of this new pyrrhotite outer layer, further loss of sulfur from the internal pyrite surface firstly required adsorption of the lost sulfur onto the boundary between the distinct pyrite layer and the newly formed pyrrhotite interface. Subsequently, it was reported that diffusion of the sulfur atoms through the outer pyrrhotite layer was required so that reaction with either hydrogen or other sulfur atoms, depending on atmosphere, could take place. The authors however reported that this apparent sulfur diffusion through the pyrrhotite layer could be misleading. The rate of inward diffusion of iron atoms towards the pyrite core from the outermost layers was believed to be more significant than the rate of outward migration of sulfur. Lambert therefore believed that the iron atoms moved inwardly in order to assist the sulfur atoms moving into the outer FeS_x layer. As a result, the lowering of the concentration of iron atoms in the outer layer was believed to promote the eventual release of sulfur atoms into the flowing gas stream. As a consequence of this sulfur liberation from the outer FeS_x layer, a decrease in the sulfur concentration was observed. A third layer was reportedly formed, as a result of this further sulfur liberation, consisting of troilite (FeS) as a new exterior surface. The interface between this new FeS layer and the pyrrhotite layer also apparently travelled inwards towards the pyrite core as more sulfur was lost. A macroporous external structure

was reportedly produced due to the formation of troilite, as seen in Figure 1.13. Lambert believed that this porosity accounted for the apparent increase in the specific surface area of the particle. It was suggested that upon arrival in this outermost FeS layer the sulfur atoms were able to diffuse to the external surface and combine with either H_2 or other S atoms if heated in a reducing or inert atmosphere respectively. The resulting gases, H_2S or S_2, were then believed to undergo desorption from the surface and disperse away from the particle through the pores. Lambert and co-workers thus concluded that the sulfur desorption as H_2S or S_2 was the rate-controlling step governing the decomposition of pyrite in the presence of both hydrogen (temperature > 500°C) and inert atmospheres. This may provide a possible explanation for the increased rate observed by Yperman[77] and Maa[85] for pyrite decomposition in a hydrogen atmosphere compared to an inert atmosphere of either argon or nitrogen respectively.

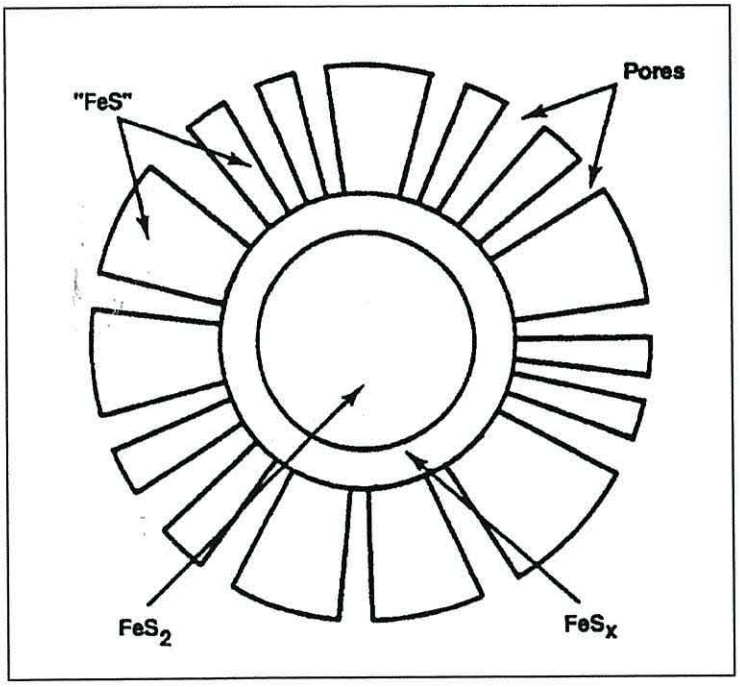

Figure 1.13. Diagram showing decomposition of pyrite.[88]

In summary experimental evidence suggests that the extent and rate of pyrite decomposition under reducing or inert conditions is favoured by reaction in a hydrogen environment rather than in an inert atmosphere such as nitrogen. However, it has also been reported that heating pyrite in hydrogen results in the formation of

H_2S and this may in turn give rise to the reverse reactions to regenerate FeS and FeS_2. One aim of this present study into the thermal decomposition of pyrite is the removal of all traces of pyritic minerals from within the slate samples as they are heated. It is therefore clear that to reduce the risk of reverse reaction occurring, heating pyrite in an inert atmosphere rather than H_2 is preferable.

At present the commercial processes involved in the development of an expanded material from slate, shale or clay for use as lightweight aggregates has typically been carried out in air. It is therefore essential to review the literature on the thermal chemistry of pyrite in various oxidising environments since a range of O_2 concentrations can occur within a commercial furnace *i.e.* an O_2 concentration gradient can occur due to oxygen being used up in combustion. Schoenlaub,[84] in addition to his work on the decay of pyrite in nitrogen and carbon monoxide, focussed on the thermal decomposition of pyrite in oxidising gases such as oxygen, air and carbon dioxide. Schoenlaub stated that a two-stage process was believed to take place during oxidation. These workers used thermal differential analysis (DTA) and thermal gravimetric analysis (TGA) to follow the oxidation processes and found two distinct stages of reaction. The first showed a sharp peak between 445 and 520°C corresponding to a weight loss of 24% (similar weight loss as in a reducing environment) thus believed to be due to the initial loss of sulfur through the formation of FeS and SO_2 *via* equation [9]. The second stage following equation [10], at between 620 and 660°C resulted in further weight loss and was attributed to the oxidation of FeS to Fe_2O_3 with additional SO_2 released. This study also showed that a rapid heating rate and lower oxygen partial pressure tended to increase the temperature at which decomposition occurred and thus showed that pyrite oxidation was dependent not only on the oxygen concentration but also on the length of time of exposure to the oxidising environment.

$$FeS_2\,(s) + O_2\,(g) \xrightarrow{445\text{-}520^\circ C} FeS\,(s) + SO_2\,(g) \qquad [9]$$

$$2FeS\,(s) + 3^1/_2O_2\,(g) \xrightarrow{620\text{-}660^\circ C} Fe_2O_3\,(s) + 2SO_2(g) \qquad [10]$$

A study by Groves *et al.* has been carried out investigating the effect of atmospheric oxygen content on pyrite decomposition.[89] These studies compared the decomposition

of pyrite pellets (mean pellet size approx. 27x5mm) heated to 1100°C in a tube-furnace in atmospheres of decreasing oxygen content *i.e.* in air, 2% oxygen in nitrogen, and in nitrogen. These workers showed that the final material produced was greatly dependent on the partial pressure of oxygen in the furnace. XRD analysis of pyrite samples heated in air to 1000°C showed some evidence for the presence of small amounts of magnetite. However further heating resulted in only haematite and trace amount of pyrrhotite being detected. They summarised that the magnetite present at lower temperatures had therefore been subsequently oxidised to haematite. On the other hand, samples heated to 1100°C in a 2% O_2 in nitrogen environment showed only trace amounts of haematite and pyrrhotite whereas magnetite was found to be the major phase. Indeed haematite had been detected at lower temperatures, in the 2% O_2 tests, with its maximum intensity being observed at around 900°C yet as the temperature increased the amount of haematite formed decreased steadily while the amount of magnetite formed increased. A similar trend was also observed for samples in a nitrogen atmosphere. However the workers ascribed this to residual traces of oxygen in the nitrogen source which meant that a truly inert environment had not been obtained. In this case complete pyrite decomposition to pyrrhotite was achieved by 700°C. However small amounts of haematite were also detected at this temperature. Under these relatively inert conditions the pyrrhotite remained stable to further decomposition until around 1000°C at which point the magnetite intensity was found to increase significantly resulting in the final composition of the samples heated to 1100°C consisting again of magnetite as the major phase, with traces of haematite and residual pyrrhotite. Groves and co-workers therefore concluded that a reduction in the O_2 partial pressure favoured the formation of magnetite rather than haematite and that pyrrhotite showed greater stability over a wider temperature range as the O_2 concentration became lower. This has implications when considering the decomposition of pyrite during slate expansion since different areas in a commercial furnace can have varying O_2 concentrations. The complete loss of sulfur from pyrite in the low oxygen zones could therefore be slower and require higher temperatures according to Groves' findings.

Musić and co-workers have also investigated the thermal chemistry of pyrite in an air atmosphere.[90] Using X-ray powder diffraction (XRPD) and ^{57}Fe Mössbauer spectroscopy, they reported the presence of haematite (Fe_2O_3) and pyrrhotite ($Fe_{1-x}S$)

after heating pyrite at 600°C for 2 hours. For the same sample after a further 2 hours at 950°C only haematite was found. By comparison, a sample of pyrite heated for 6 hours at 600°C resulted in pure haematite showing the importance of the dwell time of each experiment. Furthermore no decomposition occurred when pyrite was heated to only 300°C for 2 hours. These findings are in agreement with Schoenlaub's TGA/DTA work illustrating that a minimum decomposition temperature in the region of 400-500°C is required to ensure the initiation of pyrite oxidation. An insufficient temperature even though a considerable dwell time had been incurred evidently did not compensate for not reaching this minimum temperature range. However no evidence of magnetite was reported reflecting the high oxygen content of the atmosphere.

Following the study by Musić *et al.*, in 1994 Smart *et al.* reported a mechanistic study of pyrite decomposition in a furnace firing pulverised coal.[91] Using XRPD and electron microprobe studies, these workers found pyrite to decompose to pyrrhotite followed by oxidation to haematite in agreement with Musić and co-workers. However, in agreement with *Groves et al.* this study also found evidence for magnetite (Fe_3O_4) indicating incomplete oxidation of Fe^{2+} due to the presence of Fe^{3+} in Fe_3O_4. The sulfur though had seemingly been completely removed. Indeed it was suggested that the decomposition of pyrite, in this case, initially produced pyrrhotite, which then underwent oxidation to form magnetite which was then subjected to further oxidation resulting finally in haematite *via* the reaction sequence given in equation [11]. It is therefore evident that Smart and co-workers believed that a three-step process occurred during pyrite oxidation in contrast to the two-step pyrite-haematite conversion by Musić and co-workers.

$$\begin{array}{ccc} 3\,FeS_2 & \longrightarrow & 3FeS + 3\,S \\ & & \downarrow 7\,O_2 \\ {}^{3}/_{2}\,Fe_2O_3 & \xleftarrow{{}^{1}/_{2}\,O_2} & Fe_3O_4 + 6\,SO_2 \end{array} \qquad [11]$$

The thermal chemistry of pyrite in coal has also been studied with respect to pyrite's decomposition in different types of furnaces, namely in fluidised bed reactors rather than in traditional fixed bed or rotary kilns. Fluidised bed reactors are generally made

up of a bed of fine solid powder.[92] A gas is passed through this bed and at a critical velocity the bed appears to "boil" whereby the particles move continuously. When this state is attained the reactor bed is said to be fluidised. Work by Monteiro[93] showed that the rate of pyrite decomposition in these reactors was sensitive to temperature, particle size and gas velocity. Indeed, Yperman[77] also reported on the relationship between particle size and pyrite decomposition (in reducing atmosphere) and showed that smaller particles decomposed at lower temperatures. Monteiro however believed that the controlling step was essentially heat transfer through the pyrite particle. Consequently, according to Monteiro's findings the transfer of heat through large particles would be slow compared to small particles thus resulting in a reduced rate of pyrite decomposition. Monteiro therefore believed that the dependence of pyrite decay on heat transfer was consistent with the shrinking core model of decomposition.

The importance of pyrite decomposition is also apparent when considering the gold extraction industry. Gold can be found in a variety of sulfide minerals. It is often found in pyrite as fine particles completely enclosed within the mineral grains or as coarser particles located in surface irregularities and fractures.[94] A process exists at present extracting gold from pyritic concentrates. The pyrite is normally roasted in air so that the gold becomes accessible to a cyanide leaching solution. Research by Gibbs *et al.* has again focussed on the pyrolysis of pyrite again in fluidised-bed reactors.[95,96] These workers aimed to study and enhance a process for the abstraction of gold so that less atmospheric pollution (SO_2 gas) was produced during pyrite roasting. Heating the pyrite was found to produce porous particles made up of non-stoichiometric iron sulfides (pyrrhotite), but sulfur vapour was released instead of SO_2 when the process was carried out in the absence of air.[95] This newer process was therefore believed to have a much lesser environmental impact since the sulfur could be recovered and used in other industrial processes. The studies by Gibbs *et al.* were carried out at temperatures between 594 and 643°C in a nitrogen environment. Initial decomposition of the pyrite particles was believed to commence at the surface and then progress inwards thus forming an outer layer of porous pyrrhotite.[95] The kinetics of the pyrite decomposition were therefore initially believed to follow the shrinking core model, which would normally have assumed a negligible sulfur partial pressure in the fluidised-bed. They stated that the standard shrinking core model could

normally be used to describe the reaction of a single solid particle with the surrounding gas by dividing the reaction process into five sequential steps.[97] For pyrite decomposition following this shrinking core model Gibbs *et al.* proposed that the following steps would be involved in the process:[95]

1. Heat transfer through the gas film to the particle surface.
2. Heat transfer from the particle surface through the outer pyrrhotite layer to the reaction interface.
3. Chemical reaction at the surface of the unreacted core, which absorbs heat and forms sulfur vapour and porous pyrrhotite.
4. Diffusion of product sulfur through the pyrrhotite layer to the particle surface.
5. Mass transfer of sulfur from the particle surface and through the gas film to the bulk fluid.

However, contrary to their earlier beliefs, Gibbs and co-workers concluded that the overall rate of decomposition in a fluidised-bed was actually dependent on the vapour pressure of sulfur over the pyrite and therefore did not conform to the conventional model.[95] Furthermore, once complete conversion of pyrite to pyrrhotite had taken place further desulfurization of $Fe_{1-x}S$ was observed if a sufficiently low sulfur partial pressure was present. The rate of pyrite decomposition was therefore believed to be controlled by the rate at which the sulfur vapour was removed from the system and not solely by the rate of heat transfer through the particle. This was in agreement with the proposed mechanism discussed earlier by Lambert and co-workers.[88]

It has therefore been seen that pyrite decomposition in inert, reducing or oxidising atmospheres, invariably results in the release of sulfur containing gases. The sulfur vapour released during pyrite decomposition in inert gases can potentially contain a mixture of molecules from S_1 to S_8.[98] This inference is also supported by the work carried out by Pelovski *et al.* where it was shown that a mixture of sulfur molecules ($S_2 - S_8$) was produced when pyrite concentrate was heated to temperatures below 600°C in an inert atmosphere.[99] However at temperatures above 600°C, S_2 was generally found to be the dominant species. As discussed previously, in hydrogen H_2S gas is reportedly produced, and this is believed to affect the extent of pyrite

desulfurization in this environment.[77] Interestingly, Hausen reported for the first time the possibility of reverse reactions occurring between pyrite and pyrrhotite in the presence of SO_2.[100] This work is important since it shows that the composition of the surrounding environment may potentially have a significant impact on the thermal oxidation of pyritic minerals. Hausen stated that XRPD and DTA showed that above 350°C pyrrhotite and SO_2 reacted to produce pyrite and magnetite but that pyrite still decomposed to pyrrhotite and sulfur above 520°C regardless of the presence of SO_2. This is a significant result for this project as it is hoped that any iron sulfide present in the original slate as it expands will be oxidised to iron oxide.

Obtaining a clear picture of the thermal chemistry and mechanism involved in the decomposition of pyrite in various atmospheres is of particular relevance to the expansion of slate in a commercial furnace. The potential polluting effect of pyrite releasing gaseous SO_2, S_2 or even H_2S into the atmosphere must be taken into account. The presence of sulfur or sulfur containing compounds in the final expanded product also has significant implications in catalyst development work in this thesis since sulfur can act as a poison for many metallic catalysts such as iron, copper and platinum group metals.[92] Most metals react with sulfur compounds and H_2S gas forming the corresponding metal sulfides as a result of the sulfur lone electron pairs forming strong bonds with the metal surface. Consequently, access for the reactants to the catalytic surface is denied due to the poison (sulfur) being more strongly adsorbed to the surface. The activity of the catalyst could therefore be significantly impaired if pyritic minerals remain in the expanded product after heating.

1.4. Catalysis

The area of catalysis forms a formidable field of research. It is a subject that forms a fundamentally important role in many of today's academic investigations. In the past this research often relied on empirical methods to determine the suitability of a potential catalyst for a particular reaction system. Reactions involving the addition or removal of hydrogen are believed to be some of the simplest catalysed reactions available since the activity of the catalyst can generally be easily followed by monitoring changes in hydrogen pressure or temperature of the reaction system.[101] In

the course of testing the activity of a potentially novel catalytic system, hydrogenation and dehydrogenation reactions are therefore often studied since they effectively produce products that are easily distinguishable from the original reactants. Extensive research has been documented on the activity of different metals towards these kinds of reactions. However this review will be limited to four metals that have been shown to be particularly suited to reactions involving hydrogen *i.e.* Ni, Cu, Zn and Pd. The nature of the support material also forms an important area of research. This review will focus on the four main supports utilised in industrial catalyst manufacturing *i.e.* silica, alumina, carbon and zeolites. The method of catalyst preparation is also of fundamental importance to this study since the production of an active catalyst from expanded slate is highly dependent on the success of metal deposition on the catalyst support. A review of the main established methods of catalyst preparation will therefore be given. Finally, a relevant and novel catalyst preparation method (electroless plating) will also be reviewed. All these areas are relevant to the development of expanded slate as a catalyst support for use in hydrogenation reactions; the subject of this thesis.

The area of catalysis has been of great scientific interest since Berzelius first defined it in 1836.[102] He defined catalysis by the following statement;

" I shall therefore call it the catalytic power of substances and the decomposition by means of this power catalysis, just as we use the word analysis to denote the separation of the component part of bodies by means of ordinary chemical forces. Catalytic power actually means that substances are able to awake affinities which are asleep at this temperature by their mere presence and not by their own affinity."

The word catalysis in fact originates from two Greek words, the prefix *cata-* meaning down, and the verb *lysine* meaning to split or break.[92] Therefore by Berzelius' definition a catalyst breaks down the normal forces that inhibit the reacting molecules. However the accepted definition of a catalyst today is a substance that increases the rate at which a chemical system approaches equilibrium without itself being consumed in the process (Figure 1.14).[102]

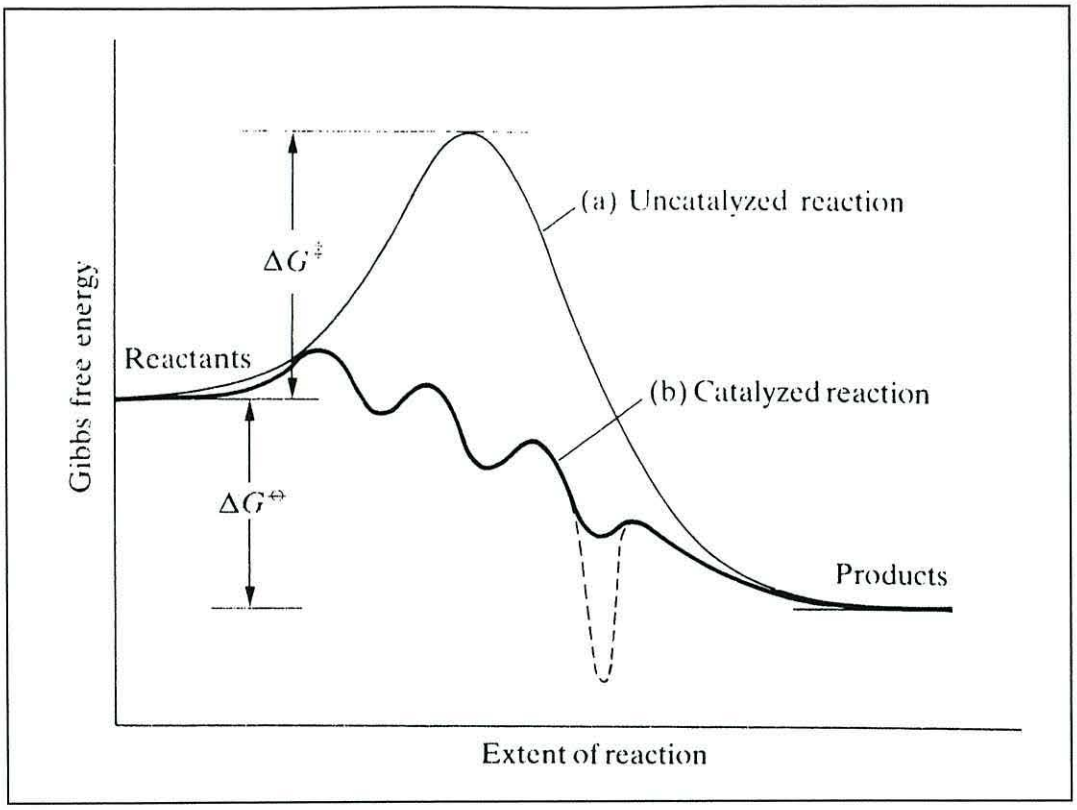

Figure 1.14. Energy diagram.[102]

It is reported that the use of catalysts in recent years has enhanced the production of nearly 70% of the products obtained from chemical and oil-processing.[101] Furthermore, Wells reports that over 90% of processes utilising new technologies are now aided by catalysts, illustrating the growing importance of catalysis to modern industry.[103] It is therefore evident that catalysis plays a significant role in manufacturing processes that effect our daily lives. Catalysts impact processes ranging from the production of the food we eat to the medicines we take, from the manufacture of the fabrics we wear to the building materials that we use, not to mention aiding the production of fuels that warm our homes and run our cars.[104] To ensure the effectiveness of these modern chemical processes it is essential that a good catalyst be utilised. The main requirements of a good catalyst are selectivity, high activity and long-term stability.[105] The selectivity of a catalyst refers to its ability to form the required product *i.e.* the ability to transform the reactants along one specific pathway only.[106] It is vital that a high proportion of the desired product is obtained with the minimum amount of side products. This property therefore has a significant economic impact on industries utilising catalysts to enhance their productivity as it

reduces separation problems. On the other hand, the activity of a catalyst reflects its ability to convert the feedstock (reactants) to products. Finally the long-term stability or life of a catalyst is also an important consideration of a good catalyst since "downtime" in a commercial process can present a significant cost to a company. The catalyst life therefore reflects the time for which a sufficient level of activity and/or selectivity can be maintained.

There are two main types of industrial catalysts, namely homogeneous and heterogeneous.[102] A homogeneous catalyst exists in the same phase as the reactants and/or products, normally in the liquid state, and no phase boundary exists between them. By comparison, in heterogeneously catalysed reactions a phase boundary exists between the catalyst and reactants/product *e.g.* solid-liquid, solid-gas or liquid-gas phases. However, in general a heterogeneous catalyst exists in the solid phase and catalyses the conversion of reactant to product in the liquid or gaseous phases. Heterogeneous catalysis is therefore primarily concerned with the physical and chemical properties of a solid catalyst. In general, industrial heterogeneous catalysts have a high surface area to ensure high catalytic activity since the greater the amount of surface area accessible to the reactants the more active sites there are present.[92] Furthermore for catalysis to occur there must be a chemical interaction between the catalyst and the reactant to produce the required product surface (Figure 1.15).[104] This is an important factor in the development of expanded slate for catalytic purposes since the hydrophobic nature of expanded slate produces a material that does not form strong interactions with substances in aqueous solutions or , as our results suggest, in solvent systems either. However in order to conform to Berzelius' definition, any reactant/catalyst interaction must not change the overall chemical nature of the catalyst since the catalyst invariably needs to be reused in subsequent reaction cycles. The reactants must therefore be compatible with the catalyst to ensure that the reaction only takes place at the surface and does not penetrate into the interior of the solid.

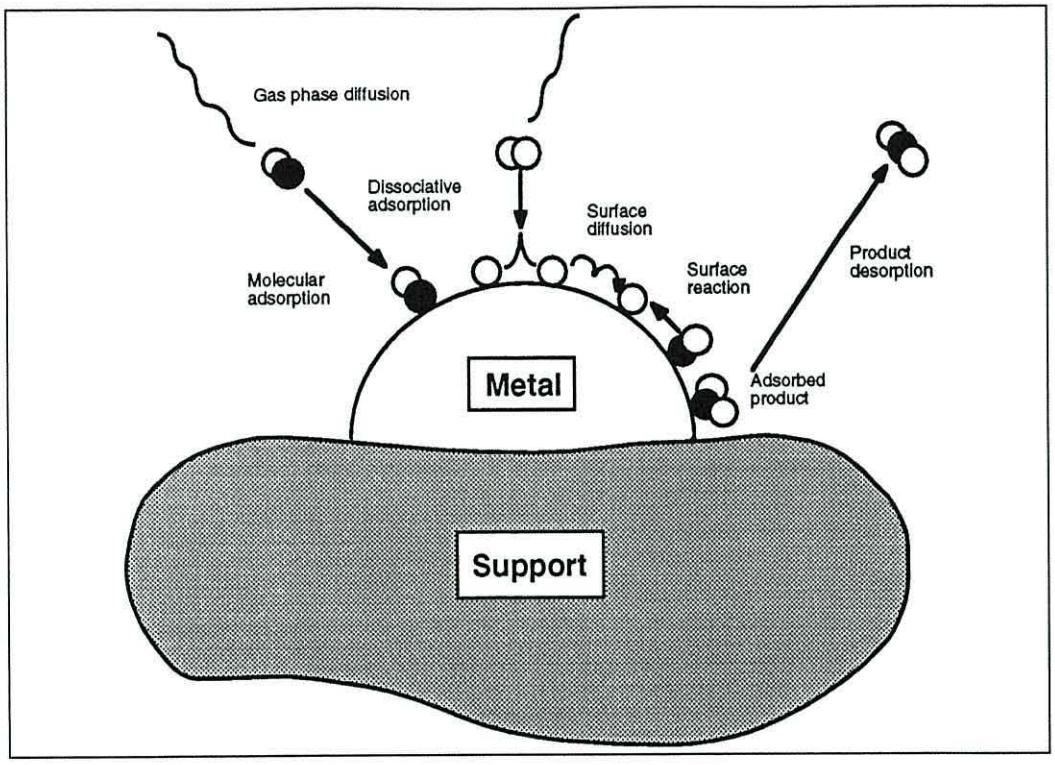

Figure 1.15. Diagram of a typical heterogeneous catalytic cycle.[104]

Metals such as iron, nickel, copper, zinc, palladium and platinum have been shown to have excellent catalytic properties when it comes to reactions involving hydrogen *i.e.* in hydrogenation and dehydrogenation reactions.[92] Catalytic activity of different metals is highly dependant on the strength of chemisorption of reactants on the catalyst surface.[38] A balance is required between adsorption and desorption since although good adsorption is necessary for heterogeneous catalysis to occur, this adsorption must not be so strong that the reactants remain on the surface blocking the active catalytic sites. Hydrogen gas readily adsorbs onto the surfaces of metals, such as Fe, Ni, Cu, Zn, Pd and Pt, and therefore constitutes one of the main reasons why these metals are particularly suited for reactions involving this gas. Iron based catalysts are widely used in the industrial dehydrogenation of hydrocarbons,[107] such as ethylbenzene.[105] However, it is the noble metals from groups 8-10 such as palladium and platinum that exhibit the greatest activity towards hydrogenation reactions in the liquid phase *e.g.* hydrogenation of nitrobenzene to aniline.[101] These metals also show good catalytic activity towards dehydrogenation reactions. The activity of different metals towards this kind of reaction has been illustrated by the volcano diagram representing the decomposition of formic acid (HCOOH) to CO and H_2O (Figure 1.16).[101] In this case the reaction temperature for a set rate of formic acid

decomposition is taken as a measure of catalyst activity, this has then been plotted against the heat of formate formation per metal equivalent.

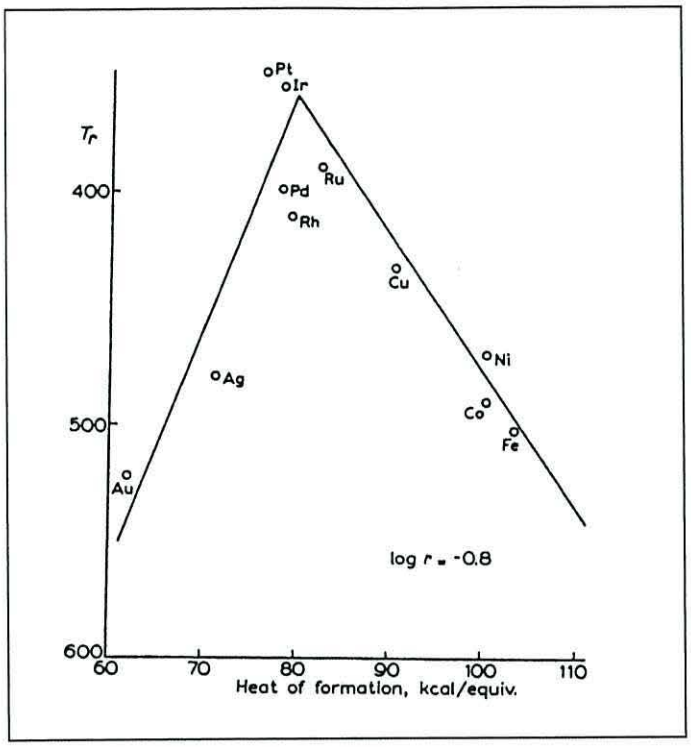

Figure 1.16. Volcano diagram illustrating the most active metals for the decomposition of formic acid.[101]

Sometimes the high surface area of a pure metal or alloy acts as the catalyst *i.e.* an unsupported catalyst. Raney nickel is one of the first examples of a commercially successful unsupported catalyst. It was developed by Murray Raney and was extensively researched by Adkins and co-workers in the 1920's.[108] Raney nickel is an alloy made up of nickel and aluminium and it is often used for the hydrogenation of organic molecules.[101,109] The Raney nickel catalyst is activated through the addition of sodium hydroxide. The sodium hydroxide removes some of the aluminium, leaving a highly porous nickel with an increased surface area. Nickel is essentially the active ingredient however the aluminium species within the alloy is also believed to promote the activity of the final catalyst. Raney nickel is a highly active catalyst towards reactions such as the hydrogenation of nitrobenzene[105] and glucose.[110]

Zeolites are also an example of a solid that can act as an unsupported catalyst. In this case a metal oxide rather than a metal or alloy acts as the catalytic species. They are a class of aluminosilicate minerals, with the general formula $M_w(AlO_2)_x(SiO_2)_y.zH_2O$.[24] Their basic structure is based on a rigid anionic framework with large regular channels and cavities. It is this network, which gives rise to the massive internal surface area achieved by zeolitic catalysts.[111] The openings to these channels vary from one zeolite to another but are generally of molecular dimensions *i.e.* in the region between 3-10 angstroms in diameter. Zeolites can therefore adsorb molecules that are small enough to enter through the channels. It is this shape-selectivity and the presence of catalytic sites within the cavities, which make zeolites such efficient shape-selective catalysts. Zeolites are naturally occurring minerals but can also be produced synthetically *e.g.* ZSM-5 (zeolite Socony Mobil, named after the company that first developed it).[92,112] Zeolite catalysts have been used in a range of industrially important processes, these range from the production of ethylbenzene, styrene and xylenes to the dehydration of isopropanol.[113,114,115] Both acidic and basic zeolites can be manufactured. An example of acid zeolites being applied in catalysis is in the production of ethylbenzene from benzene and ethene for use in polystyrene production.[114] The acid sites within the zeolite arise from the loss of loosely bound protons attached to oxygen atoms that bridge the Al and Si atoms. The use of basic zeolites in catalysis has also been reported. They have been found to be effective in the hydrogenation of carbon monoxide and unsaturated hydrocarbons, such as ethene.[115] The basicity of these zeolites generally arise from the negative charge generated by the oxygen in the Al-O-Si system. However it can also be generated due to the presence of hydroxyls, encaged oxide clusters, supported metals or reducing centres within the zeolite. Dehydrogenation of saturated hydrocarbons or alcohols such as the conversion of 2-propanol to acetone are also reportedly catalysed by basic zeolites. As previously mentioned, bulk iron-oxide catalyst have also been used for the dehydrogenation of hydrocarbons.[107] However, problems have been documented regarding the use of metal oxide catalysts in industrial dehydrogenation processes.[107] Mechanical degradation of the unsupported dehydrogenation catalysts have been reported resulting from structural transformations of the iron oxide phase under reaction conditions.[116] Recent work, using a material available as a commercial preshaped support body which has the proper physico-chemical properties *e.g.* thermal and chemical stability, has therefore been undertaken in an attempt to

overcome these problems. Boot and co-workers carried out an investigation into the utilisation of a support material such as zirconia (ZrO_2) for improved iron oxide dehydrogenation activity towards 1-butene.[117,118] Homogeneously distributed, well-dispersed iron oxide/zirconia catalysts were reportedly produced.[117] The workers however found that the catalyst deactivated during operation.[118] This deactivation was believed to result from carbon deposition in the small pores of the zirconia support.

In general, the use of a solid material acting as a support for a catalytically active species have been shown to be extremely successful in numerous industrial catalytic processes. Support materials and their applications in catalysed chemical processes have therefore been extensively studied and reviewed.[92,101,105] Many different types of support can therefore be found for catalytic materials. However, the most common types of support material include alumina, silica, zeolite and carbon.[112] The support acts as a vehicle for the active phase and any promoters (*i.e.* a substance that allows the active phase to function to its maximum capacity) that may be present.[92] The primary criteria for a support material is that it is stable under the condition of use.[101] In addition, the support itself is generally required to be catalytically inactive and thermally stable. It is also normally essential that the support provides a large surface area over which a good distribution of the active phase can be achieved. For example silica and γ-alumina supports are reportedly available with surface areas up to 500-600 m^2g^{-1}.[101] By comparison carbon supports can have surface areas reaching 1000-1200 m^2g^{-1}.

The use of nickel catalysts in industrial hydrogenation reactions can be seen in the production of solid or semi-solid fats from food oils *e.g.* in the hydrogenation of oleic acid to stearic acid.[119] It has been reported that nickel supported on alumina (Al_2O_3) or silica (SiO_2) catalysts with a surface area ranging from 200 to 323m^2g^{-1} have been produced.[120] It is believed that the relatively high nickel surface area is achieved on supported catalysts of this type due to the metal particles being distributed homogeneously over the support surface, essentially existing as small islands on the support.[121] This alumina or silica support material was generally calcined at relatively high temperatures prior to dosing with the active phase precursor in order to ensure that the final catalyst had greater thermal stability.[105]

Supported copper catalysts are also widely used in a variety of industrial processes, such as in oxidation reactions, alkane dehydrogenation and in the hydrogenation of aldehydes and ketones.[122] One of the most industrially important application of a supported copper catalyst can be seen in the synthesis of methanol from synthesis gas *i.e.* carbon dioxide and hydrogen.[123] Development of the highly active copper oxide/zinc oxide/alumina catalyst was carried out by ICI in the mid 60's.[105] The alumina acts as a high surface area support for the catalytically active copper crystallites whereas the zinc oxide is required to neutralise acidic sites on the alumina support. It is also believed that smaller copper crystallites are produced on the surface when zinc oxide is present. The catalytic activity of supported copper on γ-alumina catalysts towards isopropanol dehydrogenation has been studied by Pepe, Rossi and Jacono.[124] A series of catalysts were prepared with known surface concentrations of Cu(II), Cu(I) and Cu(0). As a result of their investigation Pepe and co-workers proposed that the surface active species responsible for the dehydrogenation was in fact Cu(0).

The catalytic activity of zinc oxide has been demonstrated further by Levec *et al.* in its use in the gas-phase dehydrogenation of methanol to formaldehyde.[125] Levec and co-workers reported that ZnO supported on silica (surface area ranging from 4-143 m^2g^{-1}) possessed long-term stability and produced better product yields compared to reactions catalysed by supported metal zeolite catalysts in their study. In addition, the incorporation of iron oxide was believed to increase the selectivity of the ZnO/SiO_2 catalysts towards HCHO formation. By comparison, the zeolites (Na- and Cu-ZMS-5) investigated showed promising selectivity but lacked activity even though their surface area was generally much higher than that observed for the silica supported catalysts *i.e.* zeolite surface area reportedly 248-308m^2g^{-1}. The poor performance of the zeolites was believed to be a consequence of "coking" reactions forming carbon on the zeolite surface thus reducing the number of active catalytic sites that consequently reduced the lifetime of the catalyst. Supported metal zeolites such as Cu-ZSM-5 have also been demonstrated to aid the decomposition of nitrogen oxides.[126] The adsorption-desorption properties of the ion-exchanged zeolites Cu-ZSM-5 and Co-ZSM-5 in the catalytic decomposition and reduction of NOx has been studied by Zhang and co-workers.[127] These workers found that these ion-exchanged zeolites reversibly and irreversibly adsorbed the largest amount of gaseous NO

compared to other cation-exchanged zeolites that were investigated. They believed that great potential was shown by these supported metal zeolite catalysts for the removal of NO_x gases, which in turn could aid the reduction of gases that contribute to the formation of acid rain and air pollution.

The application of palladium catalysts supported on alumina or silica has also been widely documented due to their catalytic activity towards the hydrogenation of unsaturated hydrocarbons.[128] Palladium is reportedly unique in its ability to hydrogenate alkynes with almost complete selectivity and high activity.[92] Recent work by Jackson and Casey investigating the hydrogenation of propyne demonstrated that Pd/SiO_2 catalysts showed 100% selectivity to propene.[129] This high selectivity has been related to palladium's ability to dissolve hydrogen atoms thus ensuring a low hydrogen concentration on the surface.[92,101] It has been hypothesised that reaction may therefore take place due to dissolved hydrogen atoms emerging from beneath the palladium surface to react with the hydrocarbon species adsorbed onto the catalyst.[101] Palladium's activity was thus believed to have been enhanced due to the hydrocarbon being attacked from below. An earlier study by Shimazu and Kita[130] on the catalytic hydrogenation of buta-1,3-diene by a series of metal catalysts again illustrates the effectiveness of Pd on an Al_2O_3 support for this type of reaction. These workers believed that the hydrogenation of butenes occurred *via* a two step process and found that the rate of the first step, involving the formation of a "half-hydrogenated" species *i.e.* formation of a vinyl radical, followed the order of Pd > Pt > Rh > Ru. However, it was believed that the second step involved the ionisation of adsorbed hydrogen and that the rate followed a different order *i.e.* Pt > Pd >Rh >Ru.

It has been reported that activated carbon also acts as a support for catalytically active metals, especially for the noble metals.[101] This support is generally produced by heating naturally-occurring cellulosic or carbonaceous material such as peat, coconut-shell, wood or coal in a vacuum or inert atmosphere at relatively high temperatures (800-1000°C). This carbon-based material can often be obtained as a waste by-product from other processes *e.g.* as the carbonaceous waste collected from coal-fired power stations. All volatile matter is reportedly expelled during the heating process and thereafter activation is carried out by exposing the material to a high-temperature steam-treatment.[119] One of the most common supported carbon catalysts used in

organic chemistry is platinum-black. The hydrogenation of 1,5-cyclooctadiene over Pt-black has been extensively studied.[131,132] However perhaps the classic example of the activity of Pt-black is its use in catalysing the reaction between hydrogen and oxygen gases to generate water.[133] The catalytic properties of noble metals, namely Ru-graphitized carbon black, towards CO hydrogenation has also been studied. Ruiz and co-workers[134] found that the activity of the Ru-black catalysts declined as the Ru particle size decreased. Furthermore, selectivity towards alkane or alkene formation was found to change as the Ru dispersion on the surface of the support increased *i.e.* a decrease in the alkane:alkene ratio was observed.

Alternative high surface area aluminosilicate or clay supports can also be used in catalytic processes. These include clay catalysts such as Pd supported hydrotalcite for the selective hydrogenation of phenol in cyclohexanone production.[135] Recent work on the application of pumice, a naturally occurring aluminosilicate, has also been reported.[136,137] Natural pumice is a light, porous rock containing many hollows and cavities which often join to form elongated channels throughout its structure.[16] It has a composition similar to rhyolite *i.e.* an igneous rock containing minerals such as feldspar and ferromagnesians generated from lava produced during volcanic eruptions. In addition to these major mineral phases, pumice also contains a significant amount of "glass" (amorphous silica). Liotta and co-workers have investigated the suitability of this material as a support for a catalytically active metal, namely palladium.[136] The performance of the catalysts were tested by following their activity towards the selective hydrogenation of 1,3-cyclooctadiene in the liquid phase.[137] It is reported that at constant hydrogen pressure (1atm) the reaction followed zero order kinetics. Pd/pumice catalysts with low metal dispersion (<20%), in comparison to Pd/silica catalysts, were generally found to exhibit higher catalytic activity. Furthermore, Liotta *et al.* found that pumice supported catalysts doped with alkali metal ions showed almost 100% selectivity towards the formation of cyclooctene.

In addition to high surface area solids, low-area materials ($\sim 1 m^2 g^{-1}$) are also utilised in catalysis.[92] These supports basically consist of α-alumina or mullite[92,101] (an aluminosilicate of general composition $3Al_2O_3.2SiO_2$).[26] They are generally non-porous materials that can maintain their strength and stability at high temperatures.

These supports are often referred to as monoliths and are often applied to the treatment of vehicle exhaust gases where they act as a support for an alloy catalyst generally made up of Pd, Pt and Rh.[106]

Catalysts therefore clearly impact a wide range of industrial processes in addition to forming an important element in numerous research projects. It is evident that solid, heterogeneous catalysts play a fundamental role in most of today's chemical industries. They have been shown to have numerous advantages over homogeneous catalysts in that they are normally stable at high temperatures, have good mechanical strength and are easily separated from the products.[106] However, the lifetime of a heterogeneous catalyst can be reduced by factors such as poisoning of the active sites by impurities such as sulfur; or by sintering and mechanical breakdown of the solid which can arise after prolonged exposure to high temperatures.[107] The use of support materials has been reported to improve the mechanical strength of some heterogeneous catalysts in addition to providing an increased surface area for the deposition of active metals.[92] This has enabled more efficient catalysts to be produced for commercial processes involving, for example, hydrogenation reactions. The development of novel support materials in catalysis therefore provides a valuable avenue of research. Furthermore, it is apparent that the utilisation of waste materials, such as expanded waste slate, provides an interesting alternative to the materials that are currently available. Development of slate waste as a catalyst support would undoubtedly provide a positive impact on the environment where waste of this kind is normally tipped.

1.4.1. Catalyst Preparation

Numerous preparative techniques exist to produce heterogeneous catalysts.[105] An early method that is still used to produce unsupported catalysts is fusion. In this case the main components of the catalyst are fused together at high temperatures *e.g.* magnetite with potash, lime and alumina for ammonia synthesis catalyst;[106] the Raney method which involves alloying two metals, one of which is leachable in acid or alkali *e.g.* Al^{3+} leached in alkali from Ni-Al alloy producing a porous Raney nickel catalyst;[108] physical mixing, where dry powders of the individual components are

mixed together and then calcined at high temperature *e.g.* mixtures of Fe_2O_3 and Sb_2O_3 used in propene oxidation; and wash-coating involved in the large scale industrial preparation of car catalysts.[106]

Wet chemical methods can also be used and these are more appropriate to the production of supported catalysts. The first method to be described is the precipitation (or co-precipitation) method. This technique involves the active phase and the support being made *in situ*. The process involves the rapid mixing of concentrated solutions of metal salts.[105] A finely divided precipitate is normally produced. The precipitate is initially filtered and washed and then undergoes drying and heating stages in order to ensure decomposition of the original amorphous hydroxides/carbonates to the corresponding oxide species. One of the main advantages of the precipitation method is therefore the formation of these small particles that usually results in high surface area catalysts. Alumina based catalysts are often produced by this method.[125,138,139] It is also widely used to produce precipitated mixed hydroxides or carbonates.[112] An example of an industrial precipitated catalyst is ICI's copper/zinc/alumina catalyst, as discussed earlier in Section 1.4.[140] In this case nitrates of copper, zinc and aluminium are mixed together. Sodium carbonate is then added to the mixture resulting in co-precipitation taking place due to the sudden change in pH. A gel is subsequently produced, which is then washed to remove Na^+ ions and finally dried and calcined to produce the final catalyst made up of copper oxide, zinc oxide and alumina as the support phase (ICI series 52).[92] This catalyst has been successfully used in methanol synthesis since 1966. Methanol synthesis was indeed one of the first large-scale processes to utilise catalysts of the precipitated kind, a process utilising zinc oxide and chromia was initially developed in the 1920's however attempts to improve the efficiency of the process eventually led to the development of the current more effective copper containing catalyst.[105] The importance of methanol synthesis is clear since methanol is currently used as a solvent in numerous industrial processes, as a starting material in the production of other organic compounds such as formaldehyde and as a freezing point suppressant in gasoline lines or window washing liquids.[140] Whilst, precipitated catalysts have therefore been successfully employed in industrial applications for many years, a significant disadvantage in their use can be directly related to their very characteristic of being finely divided, high surface area precipitates. This property

can give rise to problems in the final manufacturing stages since the precipitate may be so fine that it often blocks filters thus generating significant efficiency and continuity problems in the overall process. [105]

Whilst many of the most industrially important supported metal catalysts are produced *via* the precipitation or co-precipitation technique, an alternative process that is often employed is the impregnation technique.[105] Examples of impregnated catalysts include copper and palladium supported catalysts used in the hydrogenation of various organic molecules, such as alkenes,[130] alkynes,[129] alcohols,[141] aldehydes and ketones.[122] Indeed the majority of commercial natural gas catalysts, such as nickel supported on alumina for the steam reforming of hydrocarbons, are currently formed by the impregnation technique.[105] In the case of impregnation the active phase is adsorbed onto the surface of a preformed support. The support is often made from a porous oxide that has a high surface area such as γ-alumina or silica.[112] The impregnation procedure is generally separated into four main stages; (i) the initial production of the catalyst precursor phase, usually an aqueous solution of the corresponding metal nitrate, (ii) contact between the aqueous precursor with the support material for a certain period of time resulting in adsorption of the active phase onto the surface, (iii) drying stage and (iv) heating or calcination to convert the soluble metal salt to the corresponding insoluble oxide, which is commonly the required active phase. Furthermore a fifth reduction stage may sometimes be required instead of, or as well as, calcination in order to reduce the oxide formed upon calcination to an active metallic species. Adsorption of the catalyst precursor onto the support is normally carried out by simply pouring the solution onto the solid *i.e.* wet impregnation. The excess water is then removed through evaporation thus leaving behind microcrystals of the precursor material on the surface of the support.[92] Alumina and silica catalysts can also be prepared by following this method.[138] Alternatively, an incipient-wetness method can be followed where the precursor can be sprayed or added to the dry, powdered support until sufficient solution is taken up to ensure adequate metal loading without exceeding the pore volume of the support.[142] It is normally clear when sufficient solution has been added since the powder becomes slightly tacky or paste-like. It has been reported that a more controllable process can be achieved by following the incipient-wetness method when the interactions between the active precursor and the support are relatively weak.[138] It is

also believed that the metal content of the final catalyst can be controlled more effectively by this method since varying the concentration of the active precursor in solution can lead to more catalyst precursor being adsorbed if a concentrated precursor solution is utilised or conversely less precursor from a weak solution. Variations in the precursor concentration can also affect the particle size of the adsorbed active material since an increased metal loading tended to produce larger particles compared to those obtained from relatively weak metal salt solutions (Figure 1.17).[92]

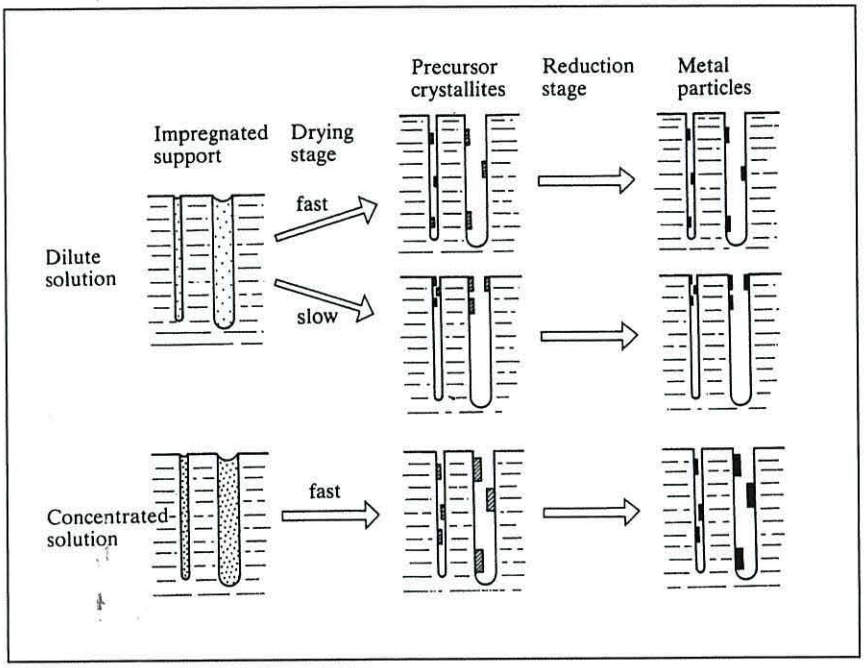

Figure 1.17. Diagram illustrating step involved in preparation of impregnated supported metal catalyst: pores of support initially impregnated with dilute or concentrated metal salt solution.[92]

Both types of impregnation methods inevitably require a drying stage. In general, slow drying of the impregnated support results in the adsorbed material migrating towards the external surface of any pores present. This movement is generally seen where weak interactions exist between the salt and the support. In some cases, the drying process can effect weakly adsorbed catalyst precursor by resulting in the redistribution of the impregnated species on the surface of the support. Consequently, a non-homogeneous dispersion of the active phase can be produced in the final catalyst.[138] It has been reported that a more even distribution of the active metal

remaining within the interstices of the pore system can be achieved if the support undergoes a relatively rapid drying stage (Figure 1.17).[92] This high dispersion of the active species is generally believed to be an essential requirement in the production of a industrially successful catalyst.[112] Perego and Villa report that a greater utilisation of the active species on the surface of the support in this way effectively increases the surface area of the available active sites thus giving rise to increased overall activity.

The final stage in the preparation of impregnated supported metal catalysts is the conversion of the precursor to the active state. This invariably involves the calcination of the solid in air in order to form the metal oxide from the original metal salt adsorbed onto the surface. Reduction of this oxide to the metallic state may be further required to form the final catalyst. Noble metal oxides such as palladium oxide can be reduced relatively easily under H_2 at temperatures around 200-300°C to produce the catalytically active species *i.e.* Pd^0. In this case no further reduction stages are required to produce the active catalyst. This factor can be advantageous to industrial processes since additional costs involved in producing the active phase during a separate operation would not be incurred. The conversion could therefore normally be carried out at the beginning of the catalytic process. By comparison, base metals, such as nickel oxide, require harsher reducing conditions, typically *ca.* 400°C, and therefore potentially reflect a greater cost to the overall process utilising this type of catalyst.[104]

It has previously been mentioned that interaction between the catalyst precursor in solution and the support is essential to ensure impregnation (incipient wetness method requires very weak interactions only). Three main types of interaction have been documented *i.e.* specific adsorption, ion exchange and adsorption-precipitation.[105] When significantly stronger interactions occur between the catalytic component and the support surface compared to those between the solid surface and the solvent molecules, normally water, "specific adsorption" is said to occur. This generally results in the formation of a 'shell' catalyst where the active metal is concentrated on the outer layer of a support pellet thus providing an excellent catalyst for reactions that are limited by pore diffusion. By comparison, when metal ions from the impregnating solution exchange with ions present in the support surface a second, stronger type of interaction occurs, namely ion-exchange. This generally occurs in

high surface area solids such as silica and zeolites. It has been reported that when the bulk of the support is made up of an oxide of an electronegative element such as silicon then dissociation of the hydroxyls can result in the formation of protons giving rise to a support that is acidic in nature. Conversely, an electropositive element is reported to produce a basic support material since OH^- ions are generally released upon dissociation of the surface hydroxyl species (Equation 12).[92] The formation of these cations and anions therefore allow for substitutions to take place *e.g.* the exchange of protons from acidic supports with cations such as Pd(II) or hydrated Ni(II).[104] A good metal distribution can generally be achieved when this type of interaction occurs since essentially an atom to atom deposition can be obtained over the whole surface of the solid.[105] The strongest type of interaction occurs when reaction and precipitation takes place within the pore system *i.e.* adsorption-precipitation.[104] This can be observed in the case of residual sodium on the surface of alumina increasing the pH so that metal hydroxides are precipitated onto the surface of the support. When this occurs a uniform distribution of metal on the surface can prove extremely difficult to obtain.[105]

$$MO^- + H^+ \rightleftharpoons M\text{-}OH \rightleftharpoons M^+ + OH^- \qquad [12]$$

A significant disadvantage of the impregnation procedure is that the amount of active material incorporated on to a support is much more limited than the amount available through the precipitation technique. It is therefore often necessary to carry out multiple impregnation/drying/calcination cycles in order to sequentially increase the metal loading on the support.[105] By comparison, impregnation provides a significant advantage to catalyst preparation since the active phase and the support material are usually prepared separately to each other thus simplifying the overall manufacturing process. In this way the support can essentially be tailor-made to suit the catalyst user's needs, for example it can be made more thermally stable prior to the addition of the active phase. This is of vital importance to the production of catalysts used in high temperature processes since the support material can ideally be made to withstand exposure to this high temperature environment thus increasing the lifetime of the working catalyst. For instance, the production of metal/zeolite catalysts is also facilitated by separation of the support and active phase during the initial stages of manufacture.[105]

A major advantage of impregnated catalysts is their reported greater in-service mechanical strength and durability compared to precipitated catalysts.[105] This increased strength of an impregnated catalyst has been illustrated in the case of nickel as a catalyst for the steam reforming of hydrocarbons. The reported success of commercial natural gas catalysts that are produced *via* the impregnation technique has been ascribed to the fact that a sufficiently high nickel surface area can be obtained with the added bonus of having a catalyst which has an in-service strength around 30% greater than the corresponding precipitated catalyst with comparable nickel surface area. Furthermore, although it has been reported to be possible to prepare precipitated catalysts with a higher concentration of active sites there was evidence that an optimum loading existed, beyond which a further increase in metal content did not affect the activity of the catalyst. This phenomenon has been observed for both impregnated and precipitated nickel catalysts, where their optimum metal contents were in fact 15% and 20% respectively. It is therefore evident that the inherent strength found in the impregnated nickel catalyst provides a greater benefit to the overall process since the most effective metal contents are similar for both catalyst types. In addition, as long as the precipitation method is carried out correctly, impregnated catalysts generally have excellent metal dispersion with no loss of metal into the support matrix *i.e.* the active material is located on the accessible, external surface. This factor is clearly an important consideration for the production of catalysts based on the expensive platinum-group metals since any metal incorporated within the support phases would essentially be inactive. The increased cost incurred would therefore hinder the overall manufacturing process since no significant benefit would be achieved through increased catalyst activity.

The precipitation and impregnation techniques therefore represent some of the most important industrial processes for catalyst preparation. An alternative technique for the deposition of metals onto the surface of a suitable substrate is electroless plating. This has more recently been applied to catalyst manufacture. Electroless plating is a method that relies on the presence of a chemical reducing agent rather than an electric current to reduce a metal from its ionic state in solution to its metallic form deposited onto the surface of the substrate.[143,144] Electroless plating, initially known as 'electrodeless plating', was discovered by Brenner and Riddell in 1947.[145] They came

upon this discovery by accident whilst carrying out an investigation into the effect the addition of different chemicals had on nickel plating baths. It was observed that upon addition of sodium hypophosphite to one such bath a cathode efficiency of greater than 100% was recorded. This led to their belief that a chemical reduction was taking place (Equation 13).[144]

$$M^{n+} + ne^- \rightarrow M^0 \qquad [13]$$

However, the reaction was found to only take place on a catalytic surface and that once initial deposition has occurred it was reported that the metal deposited must itself be catalytic to ensure that the reaction continued. A restriction on the metals available to be plated electrolessly has therefore been reported since not all exhibit the necessary catalytic properties. Therefore in additional to the traditional nickel electroless plating[146,147,148,149] other metals that can be used in this processes reportedly include palladium, platinum, copper, gold, silver and alloys containing a mixture of these metals.[143,150,151] Electroless plating can therefore also be referred to as autocatalytic plating, which has been defined as:[143]

"*deposition of a metallic coating by a controlled chemical reduction that is catalysed by the metal or alloy being deposited*" (ASTM B 374).

Electroless plating is generally associated with the electrochemical industry.[144] It is a technique that is currently used in the generation of thin films for the production of electronic parts, computer parts and printed circuit boards. It can also be applied to the production of components in the automotive, aircraft and oil industry. It has traditionally been a technique that can deposit an uniform distribution of an active metal onto a support thus generating materials that have better physical and chemical properties than those generated by traditional electroplating techniques. This technique has further advantages over more conventional plating methods, for example additional apparatus such as power supplies, electric contacts and electrical measuring devices are not needed.[143] Electroless deposition has been found to take place wherever the solution had free access to the surface. It is believed that autocatalytic plating, as for electroplating, can theoretically produce a coating of unlimited thickness since it is reported that deposition generally proceeds linearly

with respect to time.[144] It is reported that this factor generally results in a coating without excessive build-up at edges and protrusions. Furthermore, deposition control is believed to be easily achieved by varying the concentration of the metal in solution. Deposition has also been successfully carried out on non-conducting (non-catalytic) surfaces but only if appropriate pre-treatment had been undertaken prior to the electroless plating procedure.[143] Nevertheless, a significant disadvantage of electroless plating is that chemical reducing agents agents, such as hypophosphite, formaldehyde, hydrazine, borohydrides and amine boranes, are generally a much more expensive source of electrons than an electric current. This is a factor that must be carefully evaluated when considering electroless plating as a viable method of depositing a metal onto the surface of a substrate.

In recent years extensive work has been carried out in Taiwanese laboratories investigating the properties of novel catalysts prepared by an electroless plating technique. The main workers in this area are reportedly Chang, Saleque and co-workers.[152,153,154] Their initial work focussed on the development of novel copper catalysts supported on alumina.[155,156,157,158] A series of catalysts were produced and their activity tested with regards to the dehydrogenation of isopropanol and cyclohexanol.[152] It was recorded that the surface area of the copper catalysts increased with loadings up to 15wt.% Cu, above this a reduction in the copper surface area was observed. This loading value also corresponded to the highest activity and selectivity observed for the electroless plated catalysts in both reactions. Chang and co-workers therefore believed that the dehydrogenation activity and selectivity were dependent on the number of exposed copper sites. A further study by these workers investigating the effect of catalyst acidity on the activity of the electroless plated copper catalysts has also been carried out.[153] The acidity of electroless plated catalysts were generally found to be higher than the precipitated catalysts, which were prepared as a comparison. The acidity of the catalysts were found to decrease up to *ca.* 15-18wt.% Cu, after which an increase in copper loading did not appear to affect the acidity of the samples. The number of exposed alumina acid sites was believed to be directly related to the Cu loading since high copper content was found to effectively reduce the efficiency of the acid sites thus reducing the dehydration ability of the electroless plated catalysts. The selectivity of electroless Cu/alumina catalysts was also investigated.[152] Chang and Saleque reported that the selectivity to cyclohexanone,

from the dehydrogenation of cyclohexanol, increased as copper loading increased to a certain limit. For the catalysts prepared by electroless plating this selectivity remained almost constant thereafter. By comparison, for catalysts prepared by impregnation a reduction in the selectivity was observed after this limit was reached. Precipitated catalysts however were reported to show very poor activity.

Chang and Saleque reported that, in their opinion, catalysts prepared by the electroless plating technique are generally better catalysts for use in dehydrogenation experiments than those prepared by either impregnation or precipitation methods. The application of electroless plating in catalyst preparation is evidently a relatively new concept. However the recent work by Chang and co-workers clearly show the potential in this process. The utilisation of electroless plating in catalysis will therefore be further studied in this thesis for the development of expanded slate as a catalyst support in hydrogenation reactions.

Chapter Two – Slate

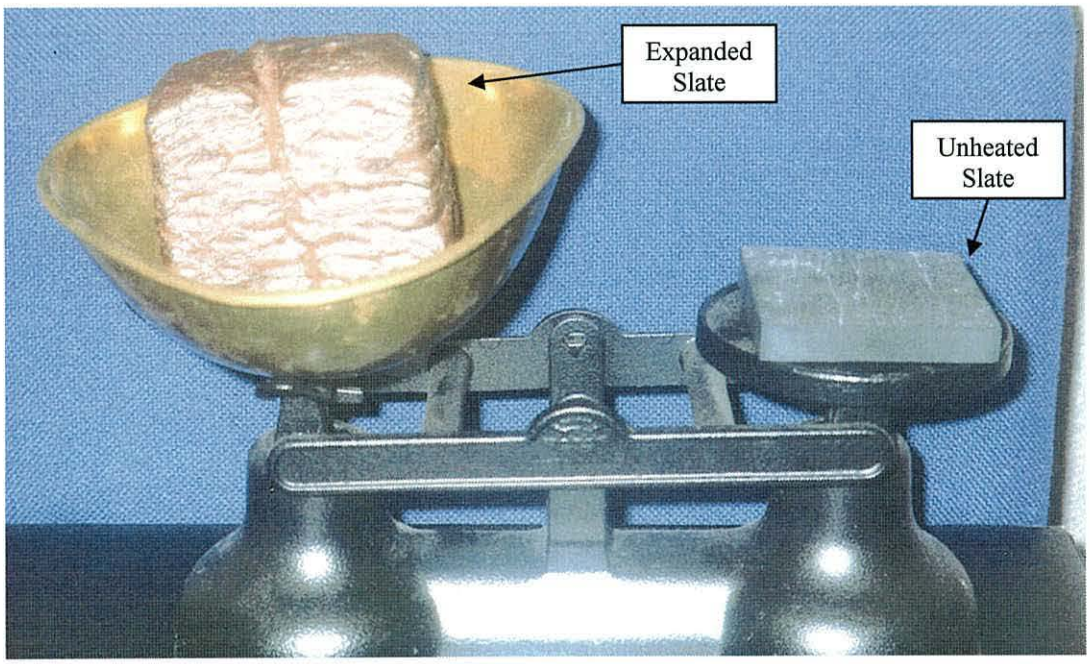

Chapter Two - Slate

As discussed in the Introduction, slate is an abundant rock in areas of North Wales but particularly in Gwynedd. Its extraction and development has formed an integral part in Welsh history and its reputation as being a strong, hard-wearing, weather resistant building material containing relatively few impurities remains just as high today. One unusual property of slate is its ability to expand when heated to temperatures above 1273K. In this thesis expanded slate will therefore be studied in detail so that a fundamental understanding of the mechanism arising during the heating of slate is established for the first time. In order to gain this understanding untreated slate was firstly analysed using XRD, IR, XRF, SEM, EDS and DTA to determine the major components of the rock and to establish whether any accessory minerals are present in the samples. Previous workers have reported that accessory minerals such as pyrite (FeS_2) and calcite ($CaCO_3$) play a key role in the expansion of slate.[53,54,55] This study therefore intends to determine the significance, if any, of such minerals by identifying the nature of the expansion gas. This study also includes experiments that follow the decomposition of slate's constituent minerals as the material is heated towards the expansion temperature to provide information on the mechanism involved in expansion. Detailed characterisation of the treated slate samples has been undertaken by XRD to determine the composition of the heated samples. Subsequent studies have concentrated on controlling expansion and determining the optimum heating parameters for producing a homogeneously expanded product.

Previous workers have shown that the degree of expansion exhibited by slate can vary from region to region.[32] This study has mainly concentrated on investigating the thermal chemistry of slate from the Blaenau Ffestiniog area in Gwynedd, North Wales. This quarry has five working slate veins as illustrated in Figure 2.1. Slate samples from each of the 5 Llechwedd veins were therefore studied (Table 2.1). In addition, Spanish slate provided by Villar del Rey slate quarry situated in the Badajoz region of Spain has also been studied to form a comparison between slate from different areas.

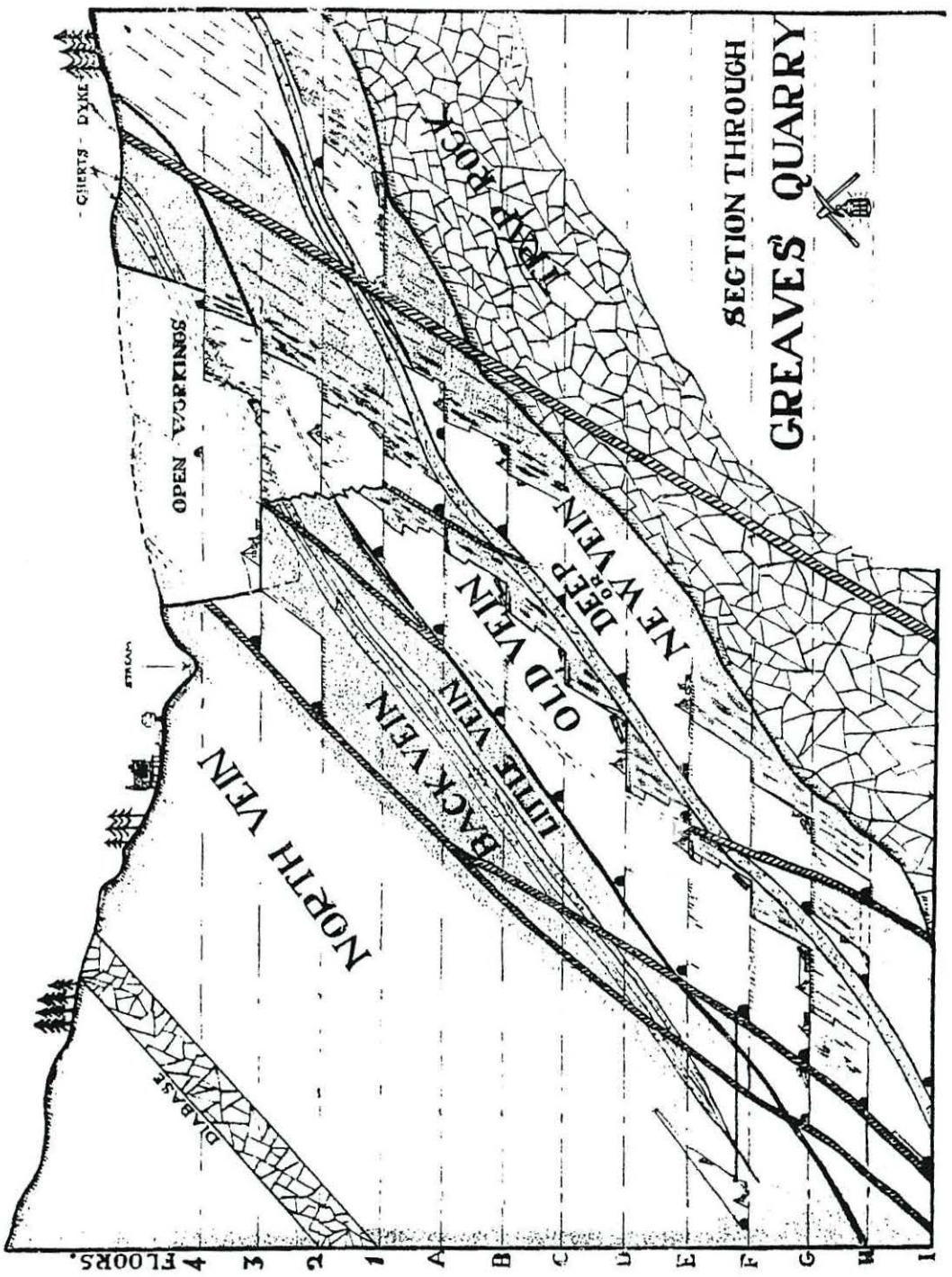

Figure 2.1. Diagram illustrating the five slate veins at Llechwedd Slate Quarry, Blaenau Ffestiniog.

Table 2.1. Summary of slate samples from five slate veins of Llechwedd Slate Quarry, North Wales and slate from Villar del Rey, Spain.

Label	Source
Back (B)	Back Vein (Llygaid Coch), Bôn, Llechwedd
Narrow (NAR)	Narrow (Little) Vein, Llechwedd
New (N)	New Vein (deep), Llechwedd
North (NOR)	North Vein, Maenofferen, Llechwedd
Old (O)	Old Vein, Llechwedd
Spanish (S)	Spanish Slate, Villar del Rey, Badajoz

2.1. Analysis of Slate

2.1.1. Mineralogical Determination

X-ray powder diffraction analysis of slate from the Old, New, Narrow, Back and North Veins of Llechwedd Slate Quarry was carried out using powdered samples to ensure random crystal orientation. Analysis of samples from the various slate veins typically produced diffraction patterns containing a series of relatively narrow, clearly defined peaks with high signal to noise ratio (Figure 2.2 and 2.3). This is consistent with an high degree of crystallinity within the sample, a relatively large crystal size and a multiphase structure.

Samples analysed from the five veins produced very similar diffraction patterns overall. Intense peaks were present at similar diffraction angles in each case with only slight variations in the intensity of the peaks from vein to vein (Figure 2.3). The differences in peak intensities indicate that some variations do exist in the concentrations of the minerals making up the slate from the different veins (see Table 2.2). The major phases found in all the slate samples analysed corresponded to be quartz, muscovite and chlorite. The mineralogical composition of the slate veins from Blaenau Ffestiniog, North Wales

was therefore found to be in accordance with that found in the literature.[25] Analysis of Spanish slate produced a diffraction pattern that correlated well with those produced by the Welsh slate samples *i.e.* quartz, muscovite and chlorite were again found to be the major phases. This arises from an apparent similarity in the composition of the slate from the two countries. By comparison, slate from Ireland was found to generate a completely different XRD pattern. In this case only quartz was found to be the major mineral present with very weak peaks corresponding to muscovite (Figure 2.4). No chlorite peaks could be found. Although the sample obtained from Ireland was named a "slate" it is evident from the XRD that its composition clearly does not reflect that of slate from Wales or Spain. As a consequence Irish slate was not studied further in the course of this project.

Table 2.2. The d-spacings (angstroms) of the major peaks corresponding to the chlorite, muscovite and quartz phases from the XRDA of slate samples from six different veins. (Relative intensities are given in parentheses).

Old	New	Narrow	Back	North	**Inference**
					Major Chlorite planes
14.21(14)	14.23(8)	14.23(10)	14.30(12)	14.05(20)	{001}
7.08(61)	7.09(31)	7.09(58)	7.10(61)	7.04(100)	{002}
3.53(44)	3.36(84)	3.54(35)	3.54(39)	3.52(70)	{004}
					Major Muscovite planes
10.05(29)	10.09(23)	10.05(27)	10.01(34)	9.96(33)	{001}
5.01(14)	5.02(12)	5.02(14)	5.02(17)	4.99(16)	{002}
3.34(100)	3.35(100)	3.35(100)	3.35(100)	3.34(93)	{003}
					Major Quartz peaks
4.26(18)	4.27(20)	4.27(17)	4.27(24)	4.25(20)	
3.34(100)	3.35(100)	3.35(100)	3.35(100)	3.34(93)	

It was more difficult to conclusively determine the minor phases present in slate by XRPD due to the effects of low signal to noise ratio resulting in weak intensity peaks being difficult to resolve from the baseline. However it is believed that some evidence

for trace amounts of ilmenorutile ($(Ti,Nb,Ta,Fe)O_2$), ilmenite ($FeTiO_3$), and feldspar-rubidium aluminium silicate ($RbAlSi_3O_8$) exists.

Characterisation of powdered slate by X-ray diffraction does not provide any information on the orientation of the minerals making up slate. Two further samples were therefore prepared from each vein from Llechwedd, one cut parallel to the slatey cleavage and the other made from 2-3 tablets cut perpendicular to the cleavage and glued together. The surfaces parallel and perpendicular to the cleavage were then cut to the appropriate height for the XRD instrument (<5mm) and polished to ensure that a new perfectly flat surface could by analysed.

The results obtained from the slate tablets cut parallel to the cleavage showed, by comparison to the diffraction pattern of slate powder, that the peaks corresponding to muscovite and chlorite have much higher intensities compared to those of quartz (Figure 2.5). This illustrates that both muscovite and chlorite are preferentially orientated parallel to the cleavage plane. As discussed in Chapter One, these minerals have a planar Al-substituted silicate framework which gives rise to the characteristic layered structure of slate. By comparison, quartz is evident in the diffraction patterns of both parallel and perpendicular cut samples. It is therefore clear that quartz in effect does not have a preferred orientation.

There is also some evidence, in the XRD patterns of both the samples parallel and those perpendicular to the cleavage, for rutile (TiO_2) and ferisilicate (SiFe) as well as the other minerals stated above. However no trace of calcite or pyrite could be found in the diffraction patterns of any of slate samples. This is in agreement with previous work by Jenkins analysing slate from the Blaenau Ffestiniog area which also showed no evidence for the presence of either calcite or pyrite.[159] The decomposition of these minerals has been reported as being responsible for the expansion,[53] their absence therefore suggests that they do not play a significant role in the expansion mechanism of slate.

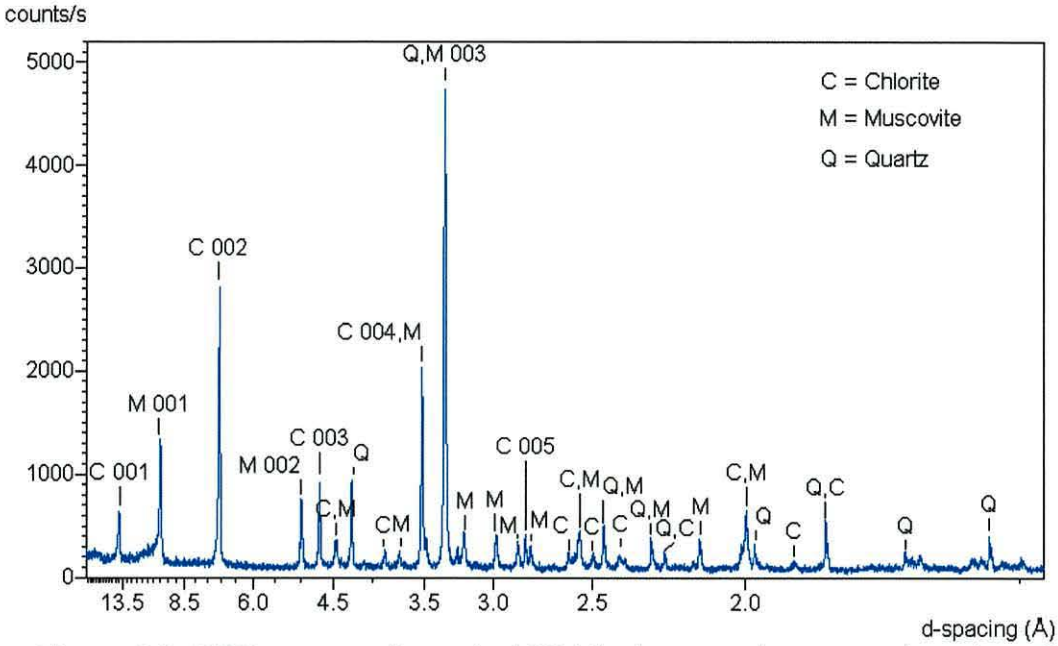

Figure 2.2. XRD pattern of a typical Welsh slate sample annotated to show the major phases; quartz (Q), muscovite (M) and chlorite (C).

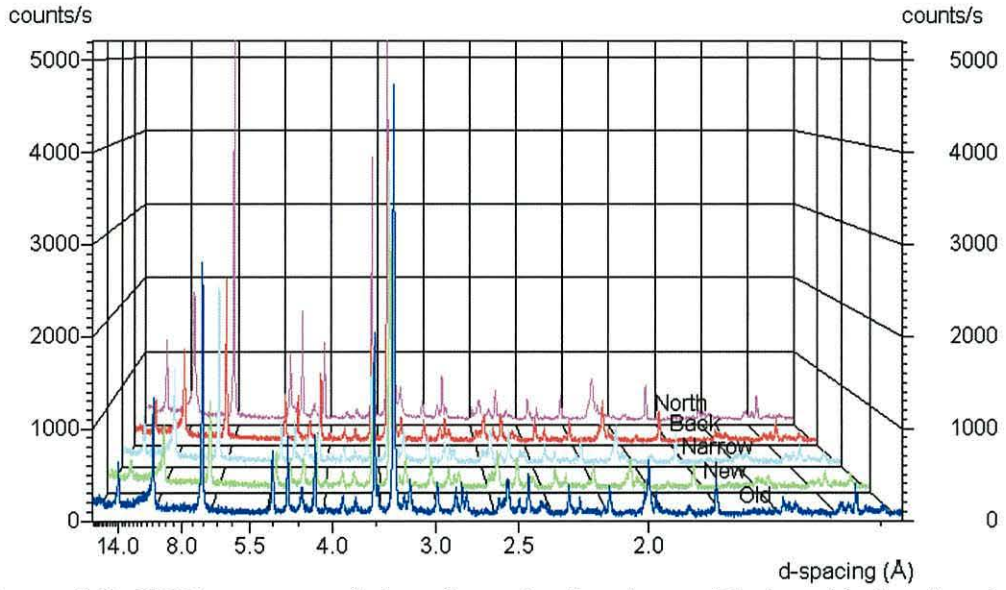

Figure 2.3. XRD patterns of slate from the 5 veins at Llechwedd showing the close similarity between the samples from each vein.

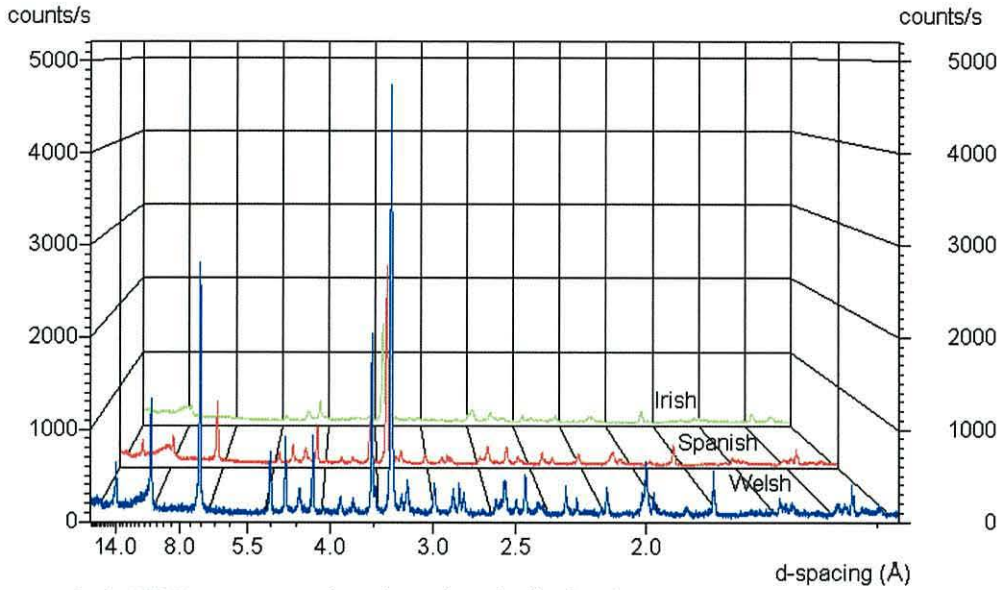

Figure 2.4. XRD patterns showing the similarity between Welsh and Spanish slate and the differences with the Irish slate.

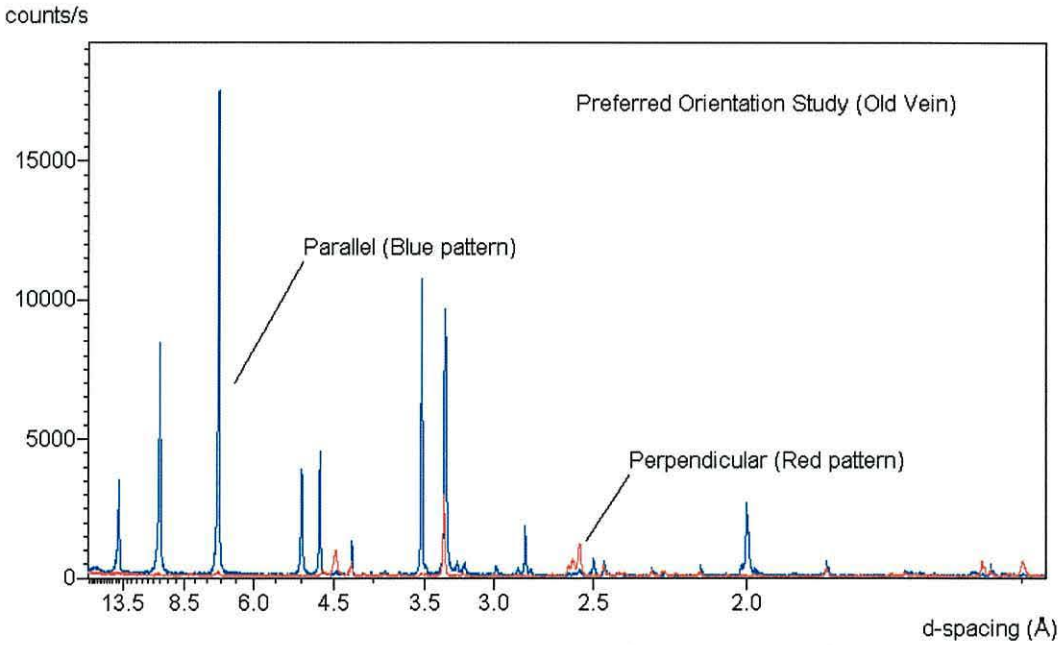

Figure 2.5. Typical XRD patterns of slate cut parallel and perpendicular to the cleavage plane.

2.1.2. Infrared Spectroscopy

Following XRD analysis of slate from the 5 Llechwedd veins IR analysis was also carried out in order to determine the functional groups present in the samples. Very similar spectra IR spectra were produced during analysis of Old, New, Narrow, Back and North slate veins. The characteristic IR peaks typically found for all 5 veins are listed in Table 2.3 below.

Table 2.3. Data obtained from the IR spectra of the six slate veins. The relative peak positions are given in wavenumbers (cm^{-1}).

Old	New	Narrow	Back	North	Inference
3650	3650	3650	3650	3650	Chlorite and muscovite O-H vibration.
3448	3422	3421	3422	3422	H-OH stretch of interlayer water.
1016	1028	1024	1032	1023	Si-O vibration of muscovite, chlorite + quartz silicate lattice.
798 778	799 780	798 780	797 785	799 800	Characteristic strong doublet corresponding to quartz

It was apparent that a weak, sharp peak at around 3650 cm^{-1} was generally observed. This is believed to result from the vibration of the hydroxyl groups in muscovite and chlorite *i.e.* M-OH. The detection of this peak is in agreement with the data given in the literature.[160] A strong, broad peak at *ca.*3400cm^{-1} was also produced. This peak exists in the characteristic O-H vibration region and is therefore believed to correspond to hydrogen bonded O-H present as a result of adsorbed or interlayer water in muscovite and chlorite. A much weaker peak characteristic of the δO-H bending mode was also found in the region of 1630cm^{-1} which may be due to water, this peak was however often overlapped by 'noise' on the spectrum as a result of free water vapour due to unpurged optics. The presence of peaks at 3400 and 1630cm^{-1} was also found to be in accordance with IR data on slate previously studied.[25] The strongest intensity peak was consistently seen at *ca.*1000cm^{-1}. This is believed to correspond to the silicate lattice vibration of

muscovite and chlorite. It is reported that the quartz, Si-O, vibration would also appear here and the silicate lattice stretch of muscovite and chlorite overlaps it. However, analysis of the fingerprint region of the IR spectra generally showed a characteristic doublet at around 800 and 780cm^{-1}, which indicates the presence of quartz in accordance with Rubio *et al.*[25]

2.1.4. X-Ray Fluorescence (XRF)

A portable XRF instrument was used to gain more information on selected "trace" elements but ignoring Al and Si as they were present in all samples (see EDS later). This technique was non-destructive and sample preparation did not require any extraction or dissolution. This technique was used to provide an insight to the accessory minerals present in the slate samples. The most significant elements detected were potassium and iron. These elements are often found in both muscovite and chlorite. Manganese was also found believed to be from chlorite. Another element found to be present in relatively high concentrations was titanium which indicates the presence of rutile or ilmenorutile in agreement with XRD data of samples cut parallel to the cleavage plane. Small amounts of calcium were also detected. This is believed to be a result of atomic substitution in muscovite *i.e.* Ca^{2+} substituting some of the interlayer K^{+} ions. However it is also possible that the calcium appeared as a result of the presence of other accessory minerals in slate such as calcite ($CaCO_3$) or gypsum ($CaSO_4.H_2O$). Supporting evidence for the existence of either of these minerals has not been confirmed by XRD. Small amounts of barium, rubidium, strontium were also detected. This is believed to result from ion-exchange within the slate. In addition, zirconium was found which suggests the presence of small amounts of zirconia (ZrO_4) in the slate samples (see Table 2.4).

Table 2.4. Data obtained from the XRF analysis of slate samples from the 5 Llechwedd slate veins with (a) denoting the relative concentrations of the elements found in slate and (b) showing the corresponding standard deviation from the mean concentration. (All units are mg/kg).

Element	Old	New	Narrow	Back	North
K	49028 [a]	48443 [a]	52733 [a]	45011 [a]	36582 [a]
	739 [b]	733 [b]	764 [b]	708 [b]	641 [b]
Fe	51844 [a]	63564 [a]	51406 [a]	56703 [a]	55160 [a]
	1210 [b]	1348 [b]	1211 [b]	1258 [b]	1227 [b]
Ti	6540 [a]	6359 [a]	6850 [a]	6861 [a]	6227 [a]
	218 [b]	223 [b]	229 [b]	226 [b]	212 [b]
Ca	2382 [a]	2992 [a]	3087 [a]	3091 [a]	3359 [a]
	207 [b]	213 [b]	222 [b]	226 [b]	199 [b]
Mn	3779 [a]	5515 [a]	3481 [a]	1876 [a]	1775 [a]
	590 [b]	685 [b]	579 [b]	489 [b]	480 [b]
Ba	750 [a]	619 [a]	819 [a]	653 [a]	552 [a]
	23 [b]	21 [b]	24 [b]	22 [b]	20 [b]
Rb	218 [a]	193 [a]	230 [a]	197 [a]	217 [a]
	25 [b]	24 [b]	25 [b]	24 [b]	24 [b]
Zr	168 [a]	196 [a]	183 [a]	202 [a]	181 [a]
	10 [b]	11 [b]	10 [b]	10 [b]	10 [b]
Sr	82 [a]	76 [a]	96 [a]	85 [a]	151 [a]
	11 [b]	11 [b]	12 [b]	11 [b]	14 [b]

2.1.5. Differential Thermal Analysis

Thermal transformation of layer silicates generally consists of dehydroxylation, oxidation of octahedral Fe^{2+}, destruction of the network and formation of new phases.[161] When the slate samples from Llechwedd were heated to1273K the resultant DTA showed a strong endothermic peak between 823 and 1023K (see Table 2.5). This peak is believed to

result from the dehydroxylation of the chlorite and muscovite phases. This is in accordance with data in the literature.[162,163] Oxidation of any ferrous iron present in the sample to ferric iron is also believed to occur during this dehydroxylation process. Furthermore inversion of the quartz structure can also occur within this temperature range.[11] An additional weak broad peak can sometimes be seen at around 473-673K, which can be attributed to the loss of adsorbed surface water and may therefore be associated with the observed weight loss.[39,40] The observed total weight loss was generally between 5-7%. During the heating process (up to 1273K), the samples had changed colour from blue-grey to an orange-brown. This colour change is believed to be due to the oxidation of Fe^{2+} to Fe^{3+} during the decomposition of chlorite.

Table 2.5. Results showing the temperatures of the key features of the differential thermal analysis associated with slate decomposition during heating to 1273K (temperatures given in K).

Old	New	Back	North	Inference
~250	300	--	~250	Weak, very broad endotherm corresponding to loss of surface water.
690	500	670	660	Intense endotherm over 100K. Muscovite and chlorite dehydroxylation. Quartz inversion. Oxidation $Fe^{2+} \rightarrow Fe^{3+}$
>800	700	900	850	Broad endotherm over ~150K. OH retained in structure, lost at a higher temperature resulting in lattice destruction.
7%	6%	5%	5%	Total percentage weight loss.

2.1.6. Scanning Electron Microscopy (SEM) and Energy Dispersive Spectroscopy (EDS)

The morphology of slate samples from the 5 different veins was investigated by SEM so that the bulk structure of the solids could be determined. The samples all looked identical under the electron microscope. Imaging of slate showed that it is made up of extremely thin sheets tightly compressed together. The similarity in the morphology of slate from the five veins is such that only two examples are shown in Figures 2.6 and 2.7. The high magnification possible with SEM allows clear imaging of the cleavage plane that enables slate to be split into thin sheets. This shows the correlation between the structure of slate and the observed differences in the XRD patterns of slate cut parallel and perpendicular to the cleavage plane *i.e.* the composition of slate (muscovite and chlorite) is directly responsible for the layered structure seen by SEM.

Energy dispersive spectroscopic (EDS) studies of the slate samples was also carried out in association with SEM. Intense peaks corresponding to Si and Al were observed which were ascribed to the aluminosilicate lattice of the component minerals. There were also less intense peaks corresponding to Fe and Mg believed to be from chlorite and K from the muscovite phase. These three elements act as counter ions in the muscovite and chlorite structure. The detection of these elements is therefore in agreement with the mineralogical composition determined by XRD. Titanium was also detected. This indicates that rutile is indeed present within the slate structure. The presence of Ti therefore correlates with the weak diffraction pattern detected by XRD of slate samples cut perpendicular to the cleavage plane. The technique as used here is basically qualitative, but an indication of the concentration of the elements can be inferred from the relative peak heights of the elements.

Figure 2.5: SEMs of Llechwedd slate (back vein)

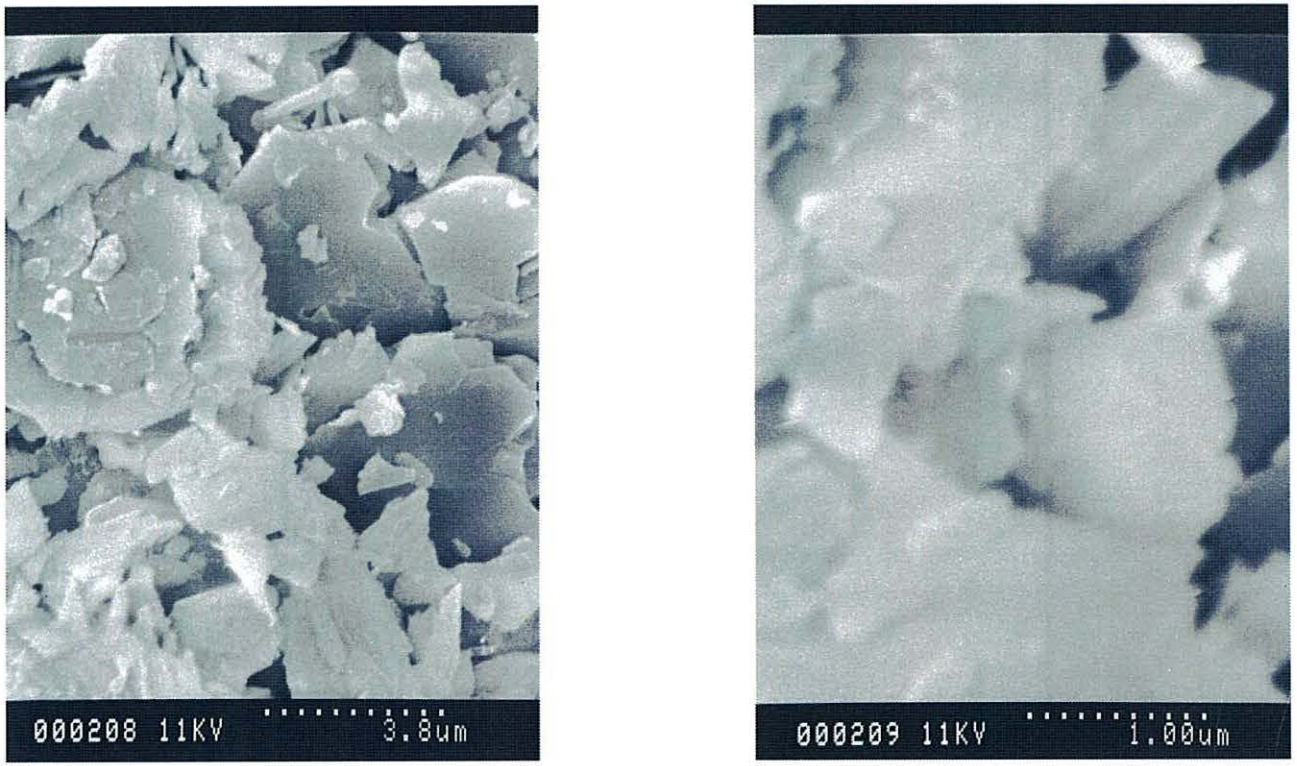

Figure 2.6: SEMs of Llechwedd slate (north vein)

2.2. Expanded Slate

In parallel to small scale experiments which form the main focus of the work in this thesis, bulk slate expansion was also carried out using a microwave-assisted gas fired (MAGF) furnace at EA Technology, Capenhurst. The best expanded products were produced when heating programme 3 and 12 had been followed which entailed heating the slate samples to 1443 and 1473K respectively (Table 2.6). From this work it was apparent that a temperature greater than 1403K was necessary to instigate good slate expansion. This information formed the basis from which to start the expansion work at University of Wales, Bangor, since the temperature limits for expansion had been determined.

IR analysis of the slate samples expanded at EA Technology *e.g.* X12-N_3 and X3-O_2, showed the disappearance of the characteristic M-OH stretching band at *ca.*3650cm^{-1} normally found in the IR spectra of unheated slate. This suggests that the hydroxyl groups present in the structure of chlorite and muscovite have been lost during heating. This is supported by XRD analysis of the expanded material which produced diffraction patterns that were completely different to those of unheated slate, clearly illustrating changes in the mineralogical composition of slate after heating (Figure 2.8). The most apparent difference, seen in all samples, was the absence of peaks corresponding to chlorite and muscovite which reflects their complete decomposition during the heating of slate above 1403K. The diffraction pattern of the expanded material produced peaks with much lower intensities than previously seen in unheated slate. Furthermore, a more uneven baseline was also produced which is consistent with expanded slate having more amorphous character than unheated slate. This correlates with the outer surface of the expanded material, in particular X12-N_3, visibly having a 'glassy' lustre and a sintered appearance. The major components of expanded slate were found to be quartz, unchanged during heating, and new phases hercynite ($FeAl_2O_4$) and mullite ($2SiO_2.3Al_2O_3$) (Figure 2.9).

Hercynite has a spinel type structure based on a cubic close packed array of oxide ions, with Fe^{2+} ions occupying tetrahedral holes and Al^{3+} ions occupying octahedral holes.[24] The formation of hercynite is in agreement with the literature which reports that the thermal decomposition of minerals belonging to the mica family, such as muscovite, commonly produce spinels as end phases.[162] Furthermore the nature of the spinel formed was reported as being dependent on the chemical composition of the mica. By comparison, mullite has a structure consisting of chains of aluminium octahedra, cross-linked by tetrahedra containing both silicon and aluminium.[26] In nature mullite is often found in localities where aluminium rich minerals have been subjected to high temperatures[26] thus illustrating its stability to elevated temperatures. Furthermore, aluminosilicate minerals are reported to often decompose to mullite.[29] Its presence in expanded slate, which originated from a material composed of the aluminosilicate minerals chlorite and muscovite, and has been subjected to high temperatures, is therefore unsurprising. Indeed XRD analysis of the inner core of a large fused piece of expanded slate from the batch labelled as X12-N_3 produced a diffraction pattern corresponding to only mullite (Figure 2.10). No peaks corresponding to quartz or hercynite was found. This material contained a network of relatively large pores, was black in colour with a 'glassy' lustre and appeared to have become much more sintered after heating than the usual product formed during expansion. Furthermore, this product had been located near the microwave inlet and is therefore believed to have been exposed to higher temperatures than that typically present in the furnace *i.e.* 1443K. It is therefore inferred that complete rearrangement of the lattice atoms has occurred to yield a single phase product as a result of reduced heat dissipation. The dark colour of this material is indicative of this process, as intense charge transfer would be expected for such a material across the visible spectrum.

Table 2.6. Summary of expanded slate samples provided by EA Technology. Slate from Old (O) and New (N) veins from Llechwedd Slate Quarry.

Sample	Size (mm)	Heating Prog.	Heating Rate (K/hr)	Max Temp (K)	Dwell Time (min)	Description
X1–O_1	2.36-5	1	500	1373	10	Dark brown/orange. No expansion.
X1–O_2	10-14	1	500	1373	10	V.dark brown/orange. No expansion.
X3–O_1	2.36-5	3	700	1473	10	Brown/black. Slight expansion.
X3–O_2	10-14	3	700	1473	10	Brown/black, 'glassy' outer surface. Highly expanded.
X6–O_1	2.36-5	6	700	1403	15	Brown/orange. Layers splitting, expansion not complete.
X6–O_2	10-14	6	700	1403	15	Brown/orange. Layers splitting, expansion not complete.
X1–N_1	2.36-5	1	500	1373	10	Brown/orange – dull surface. No expansion.
X3–N_1	2.36-5	3	700	1473	10	Dark brown/black – 'glassy' surface. Expanded.
X3–N_2	10-14	3	700	1473	10	Dark brown/black – glassy surface. Highly expanded.
X7–N_2	10-14	7	700	1408	15	Dark brown/orange. Slight expansion
X12– N_3	20-50	12	700	1443	21	Dark brown/black, glassy outer surface. Purple inner surface. Highly expanded

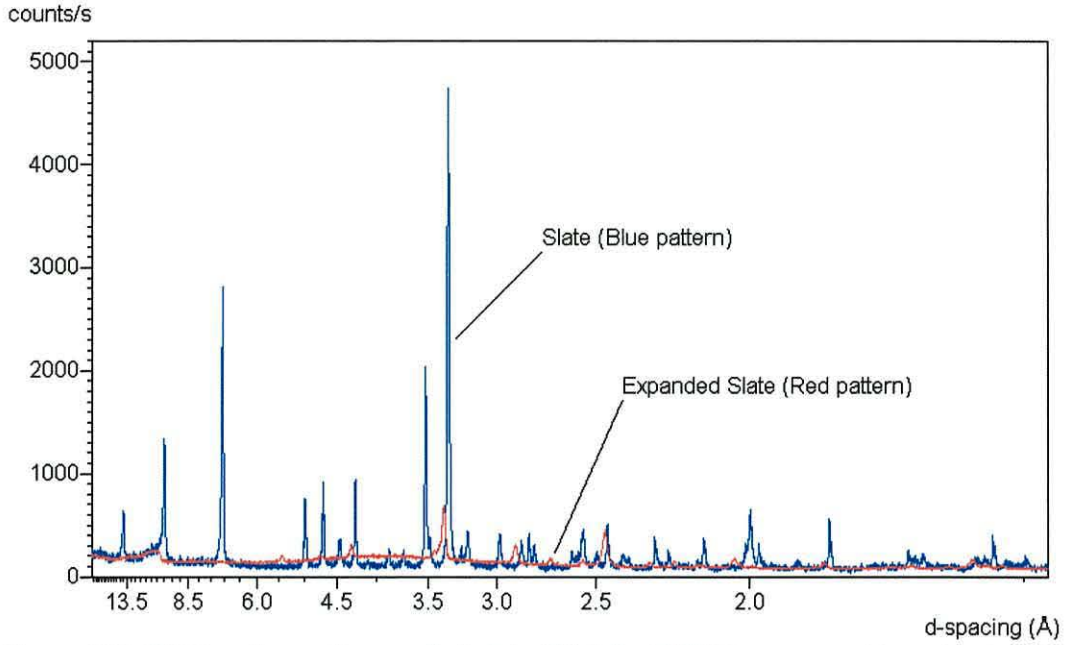

Figure 2.8. XRD pattern of expanded slate (Welsh, 1443K) compared to unheated slate.

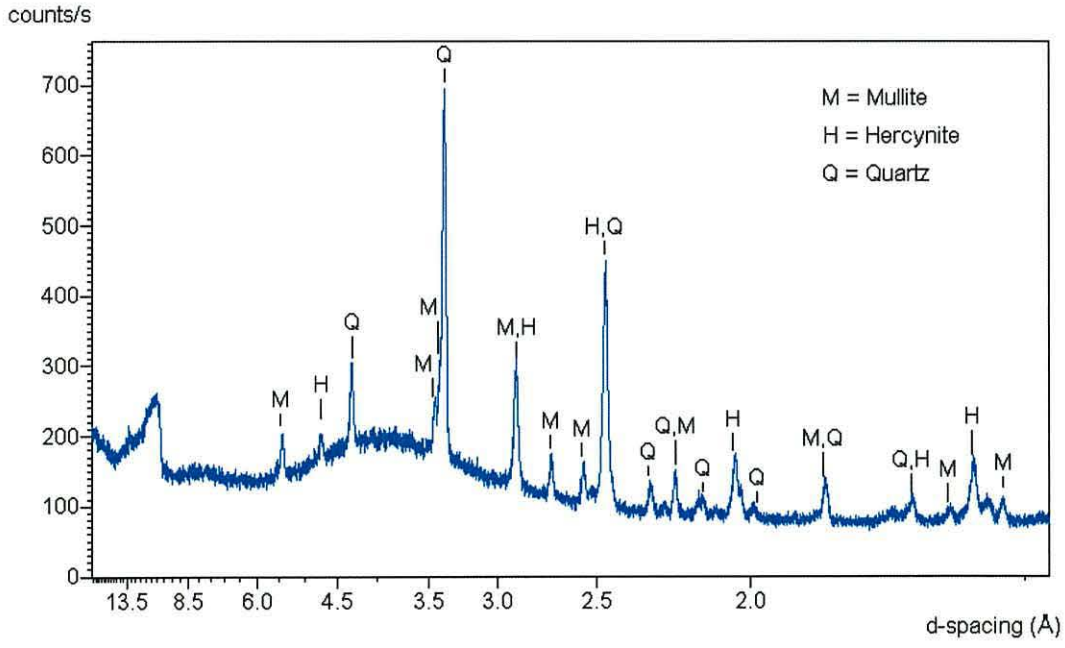

Figure 2.9. XRD pattern of expanded slate (X12, 1443K) showing the major phases; quartz (Q), mullite (M) and hercynite (H).

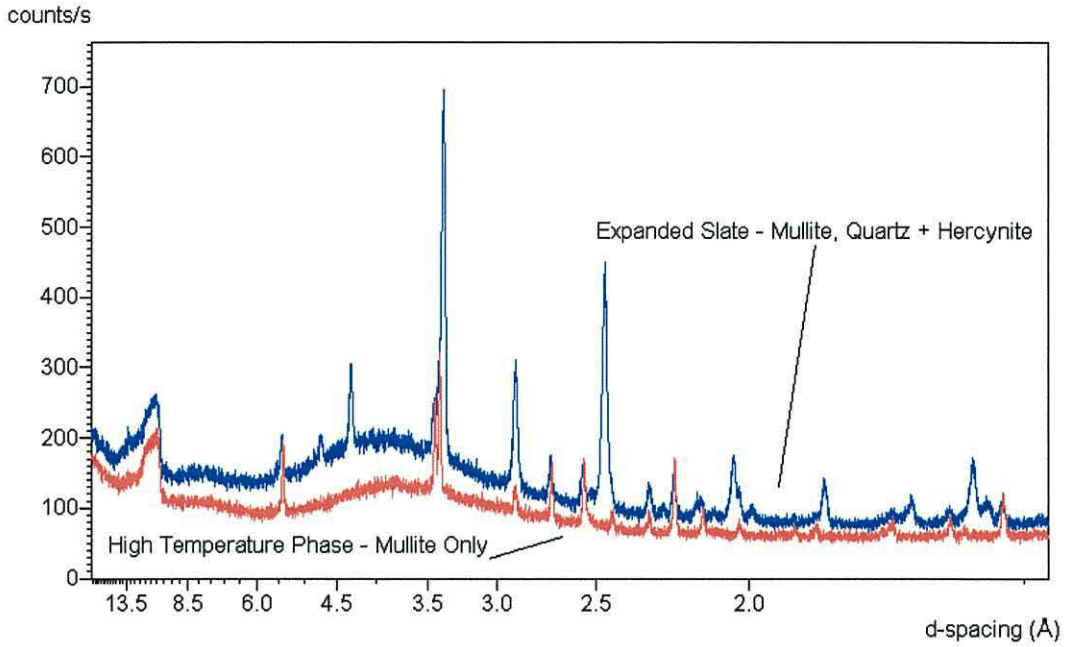

Figure 2.10. XRD patterns showing the formation of a single phase product (mullite) during slate expansion.

Microscopic analysis of unheated slate, partially expanded slate and highly expanded slate was carried out by studying thin-sections of the samples (Figure 2.11). Clear differences in the structure of the three samples could be seen. The cleavage plane of slate was clearly visible in the thin-section of unheated slate. However the sample appeared solid in nature with no apparent pores or voids. By comparison the thin-section of partially expanded slate showed numerous pores and voids closely packed together. This illustrates the differences between the degree of expansion since the thin-section of highly expanded slate showed a greater distribution of larger pores and cavities which appears to have opened up the internal structure of the sample hence giving rise to greater expansion. SEM studies also showed differences in morphology of expanded slate compared to unheated slate. A small piece of expanded slate from batch X12-N_3 was split and mounted on an aluminium stub ensuring that both the internal structure and the outer surface of the sample was visible (Figure 2.12). It was apparent that the tightly packed layers characteristic of slate was no longer present, instead the expanded slate was seen to be made up of a network of voids and cavities <1 to >200μm in size. Surface area analysis of the expanded slate however showed that these cavities did not give rise to a higher surface area material *i.e.* SA expanded slate 0.4m^2/kg compared to slate 1m^2/kg.

(a)

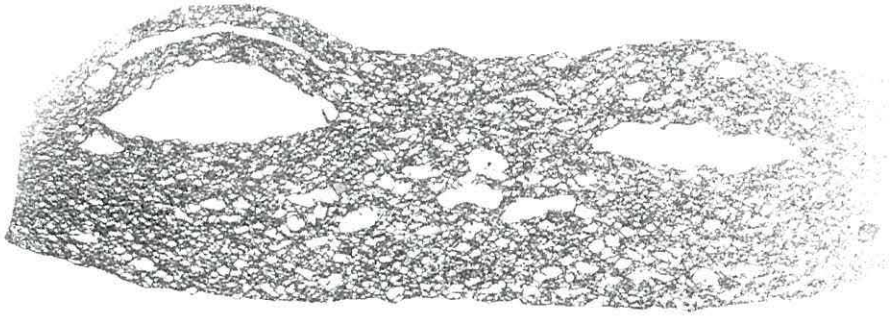

(b)

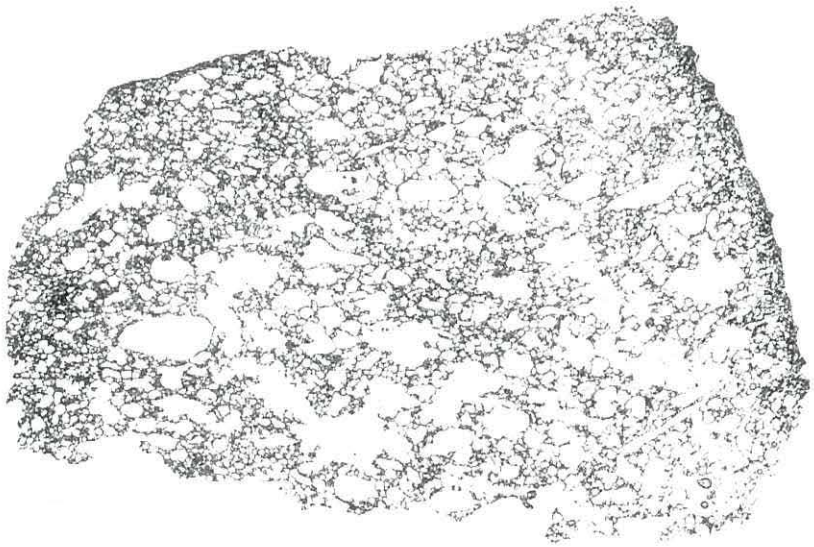

(c)

5mm

Figure 2.12. Thin sections of (a) unheated slate (Bwlch Gwyn, Blaenau Ffestiniog), (b) partially expanded slate and (c) highly expanded slate.

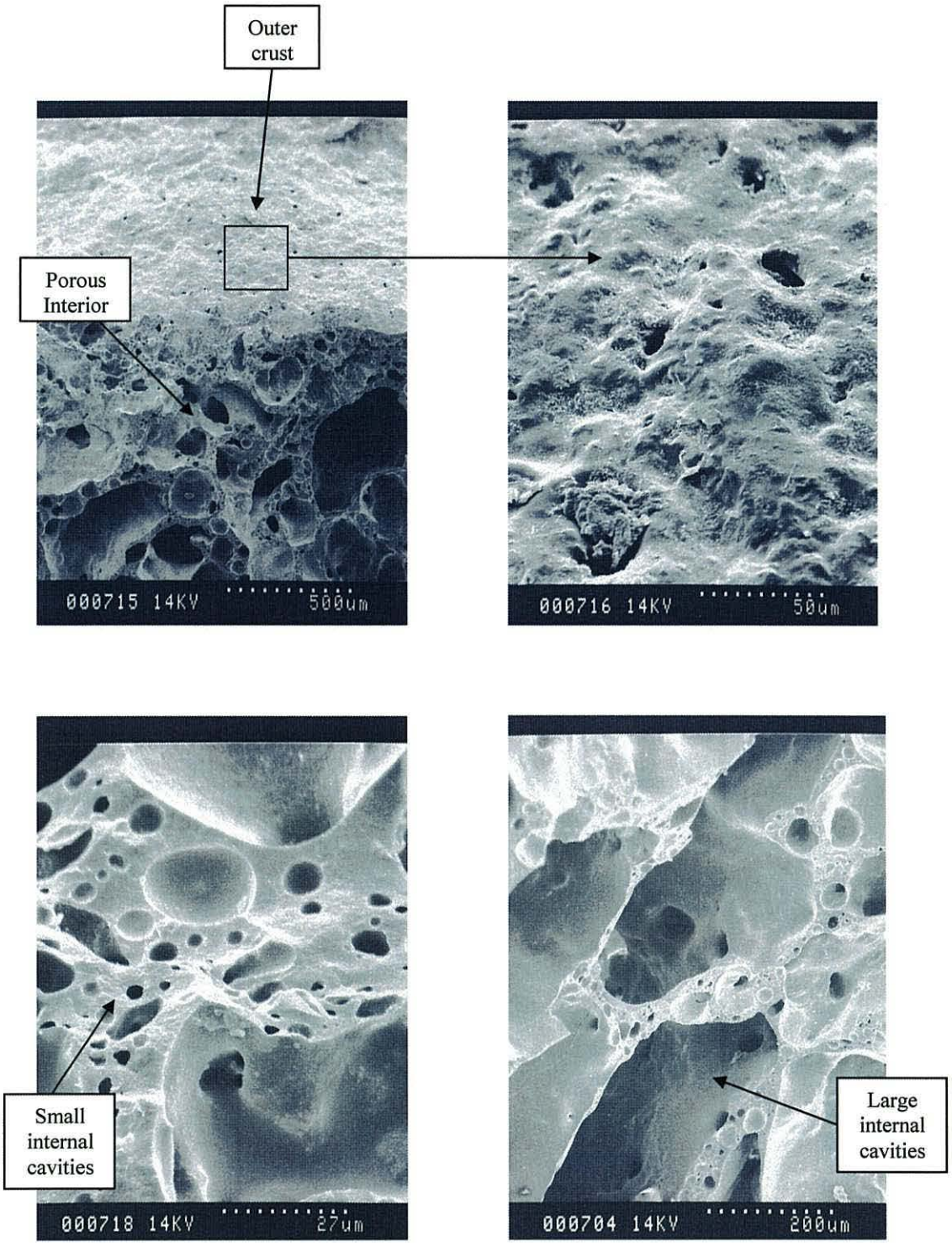

Figure 2.11: SEM images of expanded slate heated to 1453K at EA Technology.

2.4. Investigation of Expansion Process

2.4.1. Powdered Slate

Laboratory scale experiments at University of Wales, Bangor, were carried out using a Carbolite tube furnace allowing accurate temperature control to be achieved since heating rates and final temperatures could be selected as appropriate. Initial experiments were undertaken to determine the effect of heat on slate powder. Static, closed vessel experiments were firstly carried out *i.e.* experiments DWE1-4 (see Table 2.7). After some slate powder was placed inside, the stainless steel reaction vessel was evacuated to remove all air from the system. The reaction vessel was then heated and any pressure increase was monitored. No increase in pressure was noted in any of the experiments. At first this was an unexpected result since it was believed that the release of an expansion gas would result in an increase in pressure. The absence of a pressure change was however believed to be due to the small mass of slate powder used in the experiments. This is believed to account for not enough gas being released to increase the pressure sufficiently so that a change in the pressure gauge reading could be recorded. Furthermore the role of condensation had not been contemplated prior to carrying out the experiments *i.e.* as a result of the evacuated vessel any small volume of water vapour released would be condensed inside the reactor.

Table 2.7. Static closed vessel experiments.

Expt.	Heating Rate (K/min)	Final Temp. (K)	IR Inference
DWE-1	20	923	As untreated slate
DWE-2	20	943	As untreated slate
DWE-3	20	953	As untreated slate
DWE-4	20	1423	As expanded slate. No metal hydroxide str. at 3650cm^{-1}.

IR analysis of samples DWE-1, -2 and -3 produced spectra that were very similar to that previously obtained for untreated slate *i.e.* metal hydroxide stretch still present. Initial inspection of sample DWE-4 heated to 1423K showed no evidence of any expansion having occurred. However IR analysis did produce a spectrum that appeared to be different to the IR spectra of samples DWE 1-3 *i.e.* the strong peak at ~3650cm^{-1} corresponding to the characteristic metal hydroxide stretching mode ascribed to muscovite and chlorite had disappeared. The O-H group is particularly sensitive to detection by IR spectroscopy therefore its loss during analysis of sample DWE-4 clearly indicates that the complete removal of hydroxide has occurred (equation 2.1).

$$n[M(OH)] + \Delta \rightarrow n[MO] + n[H_2O] \qquad [2.1]$$

An SEM study of sample DWE-4 was carried out in order to see if any expansion had occurred. The sample generally consisted of slate particles (100-250μm) that appeared to have the layered structure of untreated slate. However some particles did appear as if expansion had been initiated since the layered structure normally associated with slate could not be seen and a number of pores could be seen in the structure (Figure 2.13). It is therefore evident that under electron microscopic analysis the expansion of slate is observed even though no increase in the relative volume of the sample was apparent. Heat treatment of slate powder under vacuum is thus believed to give rise to some expansion in small slate particles.

Following the experiments carried out in an evacuated closed-vessel system, flow-experiments have been carried out (Table 2.8). These experiments involved placing a sample of slate powder inside a quartz reactor tube and then heating the sample in a tube furnace with a flow of air passing over the sample rather than the system being in a vacuum. This was believed to more closely resemble heating conditions in a commercial furnace than the closed-vessel experiments.

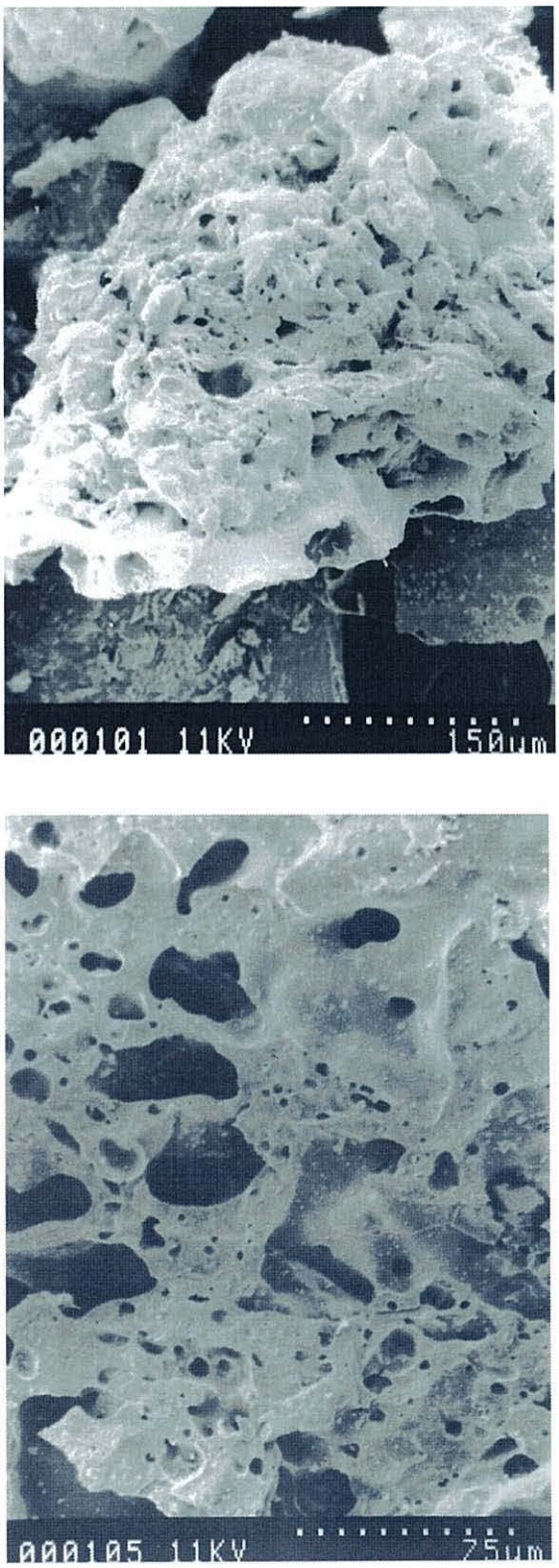

Figure 2.12. SEM images of slate powder heated to 1423K in an evacuated closed system. Morphology seen to be consistent with expansion having occurred.

Table 2.8. Summary of flow-experiments.

Expt.	Heating Rate (K/min)	Final Temp. (K)	Air Flow (ml/min)	IR Inference	XRPD Inference
DWE-6	20	923	50	As untreated slate	Chlorite {002}peak lost (7Å) Reduced muscovite {001} peak intensity (10Å).
DWE-7	20	943	50	As untreated slate	Chlorite {002} + {003}lost (7Å + 4.7 Å). Weak muscovite {001} peak intensity (10Å).
DWE-8	20	953	50	As untreated slate	Chlorite {002} + {003}lost (7Å + 4.7 Å). Weak muscovite {001} peak intensity (10Å).
DWE-9	15	1373	50	Metal hydroxide stretch lost	Chlorite and muscovite peaks lost.
DWE-10	20	1423	50	Metal hydroxide stretch lost	Chlorite and muscovite peaks lost.

IR analysis of samples DWE-6 to DWE-10 was found to be in agreement with the data obtained during analysis of the closed vessel experiments *i.e.* DWE-6, -7 and -8 heated to 923, 943 and 953K correlated well with the IR spectrum of unheated slate thus indicating that complete destruction of the lattice has not occurred by 953K. Indeed heating slate powder to 1373K is required to show the loss of M-OH from the structure of slate. By comparison, XRPD analysis of sample DWE-6 heated to 923K clearly showed that the peak at ~7Å corresponding to the {002} crystal plane of chlorite had disappeared. Furthermore the intensity of the 3 major muscovite peaks was slightly lower than normally found in untreated slate thus indicating that decomposition of chlorite, in particular, has been instigated by 923K. The loss of subsequent chlorite peaks was further illustrated in samples DWE-7 and DWE-8 which sustained heating to 943K and 953K respectively. By this temperature the {003}-chlorite peak at ~4.7Å had also disappeared and the intensity of the {001}-chlorite peak was lower thus suggesting significant chlorite decomposition by 943K. The apparent decomposition of chlorite by 943K correlates well with the large endothermic peak recorded around 923-973K during DTA analysis of slate from the Old, New, Back and North veins of Llechwedd Slate

Quarry (see Table 2.5). However, muscovite peaks were still apparent in DWE-8 (953K) thus suggesting that muscovite requires higher temperatures to decompose completely. The presence of muscovite is therefore believed to correspond to the observed M-OH band at ~3650cm^{-1} in the IR spectra of DWE-7 and DWE-8. XRPD analysis of the DWE-9 and DWE-10 heated to 1373K and 1423K also showed that greater decomposition of the minerals constituting slate had occurred. The total loss of peaks corresponding to chlorite and muscovite was apparent. Indeed the diffraction patterns of DWE-9 and DWE-10 closely resembled that previously determined for expanded slate since peaks corresponding to quartz, hercynite and mullite were present. The peaks corresponding to mullite becoming more resolved as the final temperature of the experiment increased *i.e.* in DWE-10.

SEM studies of DWE-9 did not show any evidence that expansion had occurred. By comparison it was apparent that partial expansion had taken place in DWE-10 since 'slate' particles could be found which appeared to have partially lost the layered nature of unheated slate (Figure 2.14). However no voids or pores were apparent in comparison to the expanded sample produced in the closed-vessel experiment DWE-4 thus suggesting that the expansion of slate powder occurs more readily when under vacuum. This is believed to be due to evacuating the system allowing the released expansion gas diffusing through the slate lattice to open up the slate structure to a greater degree due to the reduced external pressure surrounding the slate sample.

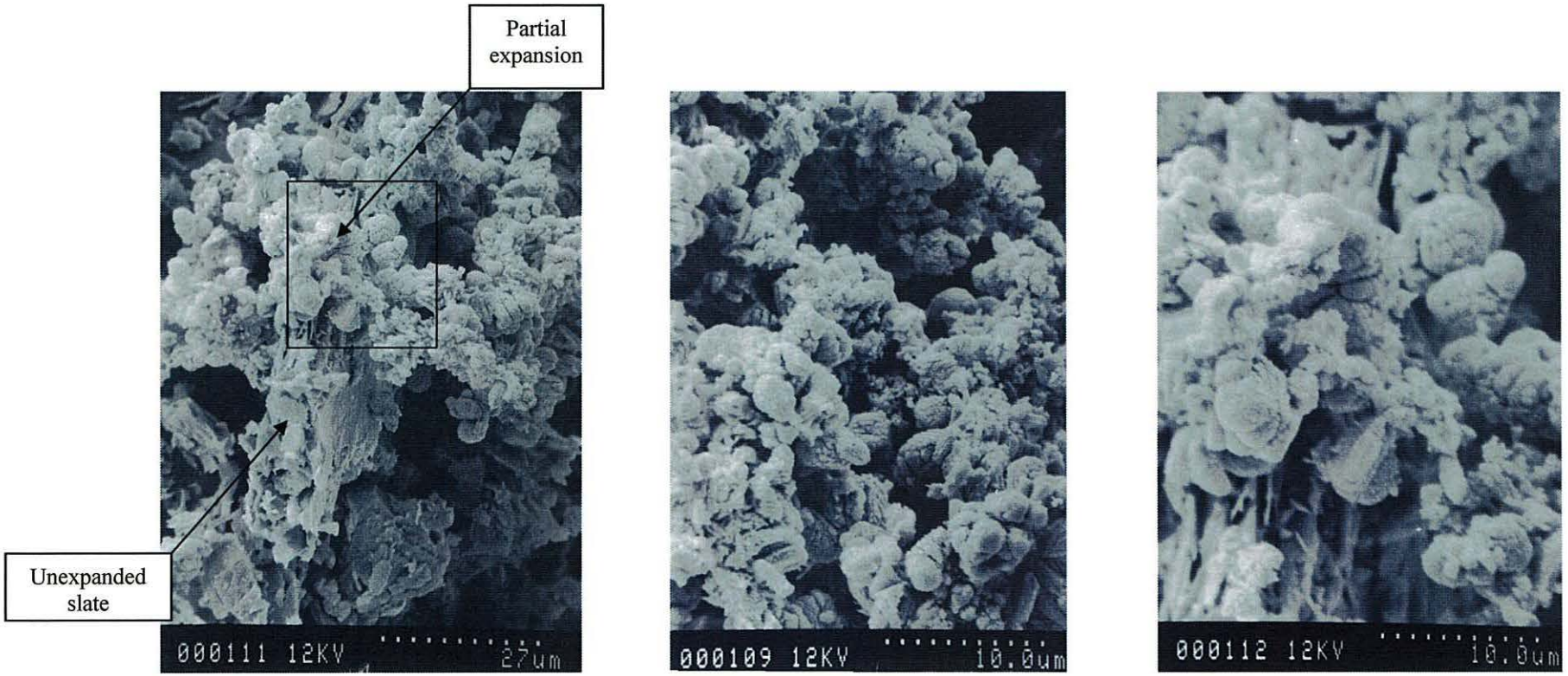

Figure 2.13. SEM images showing partial expansion of slate powder (DWE10) heated to 1423K in air.

2.4.2. Slate Tablets

2.4.2.1. Expansion Gas Determination

Analysis of the expansion gas has been undertaken by heating slate tablets (2-5x15x30mm) in a tube furnace in a nitrogen atmosphere (100-150ml/min) and condensing the exhaust gases in a glass U-tube partially immersed in a bath containing dry-ice/acetone. The aim of these two experiments was to compare the volume of water collected at various temperature ranges and to ultimately correlate the amount of water collected with the decrease in weight of the slate samples.

The first experiment ST-DWE15 involved heating a slate tablet up to 1453K in three stages (Table 2.9). During each stage the vapour, if any, that was released was collected in a U-tube and its identity confirmed as water by IR and ^{1}H NMR (single peak at δ1.65ppm). In addition, after each heating stage had been completed the slate sample was allowed to cool down, was weighed and then analysed by XRD. An initial XRD analysis of the slate tablet before heating showed the presence of muscovite, chlorite and quartz consistent with unheated slate (Figure 2.2). The first stage involved heating the sample to 873K at 20K/min. A small amount of liquid, equivalent to a single drop, had been collected inside U-tube. This water collection corresponded to a 0.5% weight loss in the slate sample. The XRD pattern of the sample after this initial heating revealed a substantial decrease in the peak heights corresponding to chlorite, especially the peaks due to the {002} and {003} planes. This therefore suggests that the water vapour released up to 873K correlates to the initial decomposition of chlorite. No expansion had taken place. The sample was then heated to 1173K whereby liquid was condensed in the U-tube between 873 and 1173K. A substantial volume of liquid was collected between these temperatures (approx. 0.5ml) which coincided with a 4.2% decrease in mass. The XRD pattern of the sample shows complete decomposition of chlorite since the peaks corresponding to chlorite have completely disappeared. There is also a decrease in the intensity of the major muscovite peaks relative to their intensity in unheated slate. However there appears to be no change in the quartz content of the sample. Again no

expansion had taken place. Finally the slate tablet was heated to 1453K at 20K/min and a 15min dwell at the critical expansion temperature was also incurred. Any vapour released between 1173 and 1453K was condensed inside the U-tube. In this instance a thin film of condensed liquid at the dry ice/acetone bath level was collected. It was evident that the slate tablet had expanded three-fold and upon weighing a further 0.5% decrease in mass was discovered. The XRD pattern of this expanded sample showed no evidence of chlorite or muscovite. Although the intensity of the peaks are lower than that normally observed for powdered expanded slate samples the major peaks do however corresponded to quartz, hercynite and mullite.

Table 2.9. Summary of experimental results for sample ST-DWE15.

Temp. (K)	Weight Loss (%)	Experimental Obs.	XRD inference
873	0.5	1-2 drops of H_2O	Reduced peak intensities of major chlorite and muscovite peaks.
1173	4.2	Approx. 0.5ml H_2O	No chlorite. Weak muscovite {001}-10Å peak.
1453	0.5	Thin film H_2O	Quartz, hercynite and mullite.

Therefore after expansion the slate tablet had lost a total of 5.2% of its original mass. This is in good agreement with the mass of water condensed in the U-tube. However it must be noted that the accuracy of the balances used for weighing the U-tube cannot be considered totally reliable when weighing out small differences in the weight of a relatively heavy object like the glass U-tube. Nevertheless it cannot be disputed that the greatest weight loss corresponds to the temperature where there is a complete destruction of the chlorite structure. However traces of muscovite still remain in the XRD pattern of the sample heated to 1173K.

In order to ascertain the point at which muscovite was no longer evident in the XRD of heated slate a second experiment, ST-DWE16, was carried out. This experiment

followed the same pattern as ST-DWE15 however additional analysis of the slate was undertaken at 1273 and 1373K (see Table 2.10).

Table 2.10. Summary of experimental results for sample ST-DWE16.

Temp. (K)	Weight Loss (%)	Experimental Obs.	XRD inference
873	0.4	1-2 drops of H_2O	Reduced peak intensities of major chlorite and muscovite peaks.
1173	4.5	Approx. 0.5ml H_2O	No chlorite. Weak muscovite {001}-10Å peak.
1273	0.2	1-2 drops of H_2O	No chlorite. Weak muscovite {001}-10Å peak.
1373	0.2	Thin film of H_2O	Only peaks corresponding to quartz resolved.
1453	0.1	Small amount of H_2O ~1drop	Quartz, hercynite and mullite.

XRD analysis of ST-DWE16 after each heating stage again demonstrated the sequence of chlorite and muscovite decay during the heating of slate up to the expansion temperature of 1453K (Figure 2.15). In agreement with ST-DWE15, it is apparent that chlorite decomposition has been initiated by 873K since the intensity of the peak at 7Å corresponding to {002}-plane has significantly reduced compared to unheated slate. After heating to 1173K it is clear that all the major chlorite peaks have disappeared *i.e.* peaks at 14, 7 and 4.7Å and ascribed to {001}, {002} and {003}-planes respectively. By comparison the major peaks corresponding to muscovite *i.e.* at ~10, 5 and 3.3Å corresponding to {001}, {002} and {003}-planes respectively, remain in the XRD pattern of ST-DWE16 heated to 1273K thus illustrating the greater stability of muscovite to elevated temperatures compared to chlorite. Upon further heating to 1373K no evidence for either muscovite or chlorite can be seen in the diffraction pattern of ST-DWE16 thus indicating complete decomposition of these minerals prior to expansion. Only peaks corresponding to quartz could be resolved in this case in contrast to the powder sample

DWE-9 heated to 1373K which showed evidence for the formation of new phases mullite and hercynite. Indeed the identification of mullite and hercynite could not be resolved until a temperature of 1453K had been reached by ST-DWE16.

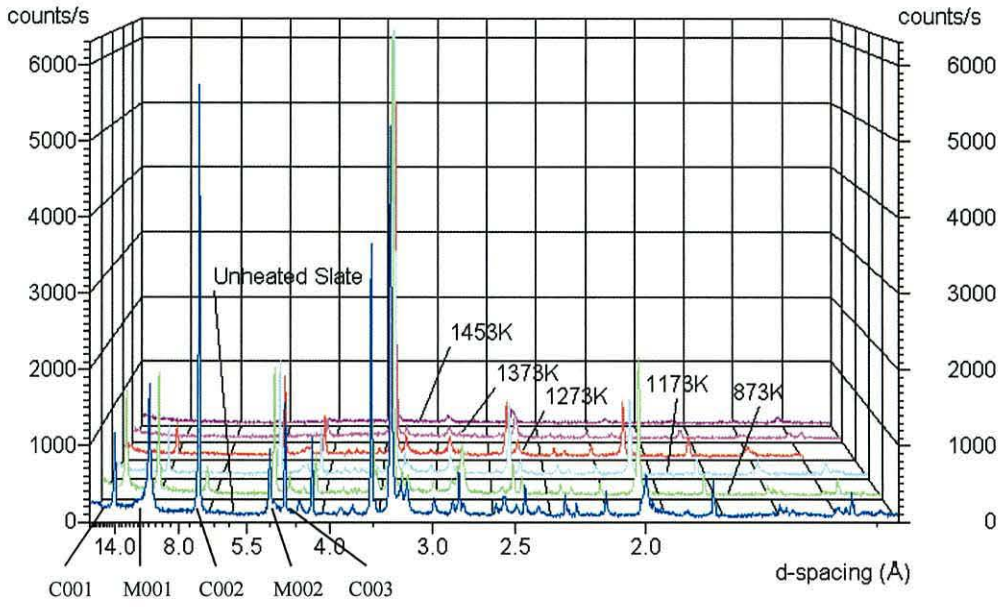

Figure 2.15. XRD patterns showing the loss of chlorite and muscovite peaks during the heating of ST-DWE16 to 873, 1173, 1273, 1373 and 1453K.

Analysis of the condensed liquid by IR and ^{1}H NMR again confirmed H_2O. The same pattern of condensation was evident in experiment ST-DWE16 as ST-DWE15 *i.e.* the greatest mass of water was condensed between 873 and 1173K in accordance with the strong endothermic peak observed in the DTA trace of slate ascribed to the dehydroxylation of chlorite (and muscovite to a lesser degree). However in ST-DWE16 a small amount of water was also condensed between 1373 and 1453K. This clearly shows that some water is released at the expansion temperature even though the decomposition of both chlorite and muscovite was confirmed by XRD by 1373K. This is believed to reflect the containment of water vapour within the slate structure upon the complete

decomposition of muscovite after 1273K. The diffusion of this vapour, held deep in the sample, at a temperature (1453K) when the slate has become pyroplastic and sufficiently mobile is therefore believed to be the key factor in slate expansion.

2.4.2.2. Expansion Control

To determine the difference in expansion between slate powder and solid slate pieces the effect of various heating programmes on the expansion of slate tablets has also been investigated. Slate tablets of the appropriate size to fit into the quartz reactor, 2-5x15x30mm, were cut from roofing tiles obtained from the Llechwedd Slate Quarry. For this series of tests slate from the Old vein was normally used. The experiments have been split into two broad groups. The first group of samples was heated following a slow heating rate. A slow heating rate was defined as being between 2-10K/min these samples have been denoted by a SH-prefix. Samples in the second group followed a more rapid heating rate between 15-30K/min. Expanded slate samples produced in this group have been denoted by a RH- prefix. In both cases heating experiments have been carried out in nitrogen and in air to ascertain whether differences in the degree of slate expansion occurs in the different atmospheres.

Experiments carried out following a slow heating rate have shown that the degree of expansion tended to decrease with decreasing heating rate. This trend was evident for samples SH-N1, SH-N3 and SH-N2 which followed a 2, 5 and 10K/min rate respectively up to a final temperature of 1453K (see Table 2.11). Initial inspection of sample SH-N1 showed that only slight expansion had occurred. This expansion gave rise to a less than two-fold increase in sample height *i.e.* from 2.5mm to 4mm (figure 2.16). The small expansion is also believed to be due to the long dwell (18hrs) incurred at 973K prior to heating to 1453K. By comparison, SH-N3, which sustained a dwell at 1273K for 48hrs exhibited non-uniform expansion across the sample. It was apparent that the middle of the sample had expanded to a much greater extent than the outer edges (Figure 2.16). The increased dwell incurred by SH-N1 is believed to have given rise to a greater loss of expansion gas as a result of increased extent of diffusion through the slate structure in a

non-pyroplastic state. Furthermore SH-N3 had incurred a long dwell (48hrs) at a temperature lower than the actual expansion temperature, in contrast to SH-N1 a faster heating rate had been followed, 5K/min compared to 2K/min. This difference in heating rate is believed to account for the difference in the degree of expansion between the two samples. The slightly faster rate appears to have ensured a 3-4 fold expansion in the middle of the sample. In contrast the outer edges expanded less than 2 fold, which is in agreement with the expansion exhibited by SH-N1. This variation clearly illustrates the importance of diffusion of the expansion gas through the internal structure of the slate tablet. This pattern of expansion is believed to show that gas held in the middle of the sample is trapped to a greater degree than the gas released at the outer edges. This trapped vapour can presumably only move in two dimensions within the slate due to the layered nature of the constituent minerals. The limited movement of the gaseous molecules is therefore believed to result in vapour produced close to the outer edges being able to escape more quickly than vapour produced deep within the slate sample hence resulting in the observed expansion taking place when the lattice was in a sufficiently mobile state at 1453K. Furthermore, sintering of the outer edges during expansion also appears to confirm that the rate of gas loss is the key to slate expansion.

By comparison sample SH-N2 showed a 3-fold volume increase (Figure 2.16). A relatively long dwell (24hrs) at 1273K was again incurred prior to heating to 1453K. However a faster rate of 10K/min was followed compared to SH-N1 and SH-N3. The apparent increased expansion is therefore believed to support the trend that increasing the heating rate favours greater expansion. A visible inspection of the internal structure of SH-N1 however showed that three relatively large cavities were present surrounded by a smaller network of pores towards the outer edges. This interior therefore shows that homogeneous expansion has not occurred after all thus suggesting that optimum conditions for expansion had not been achieved by following this heating program.

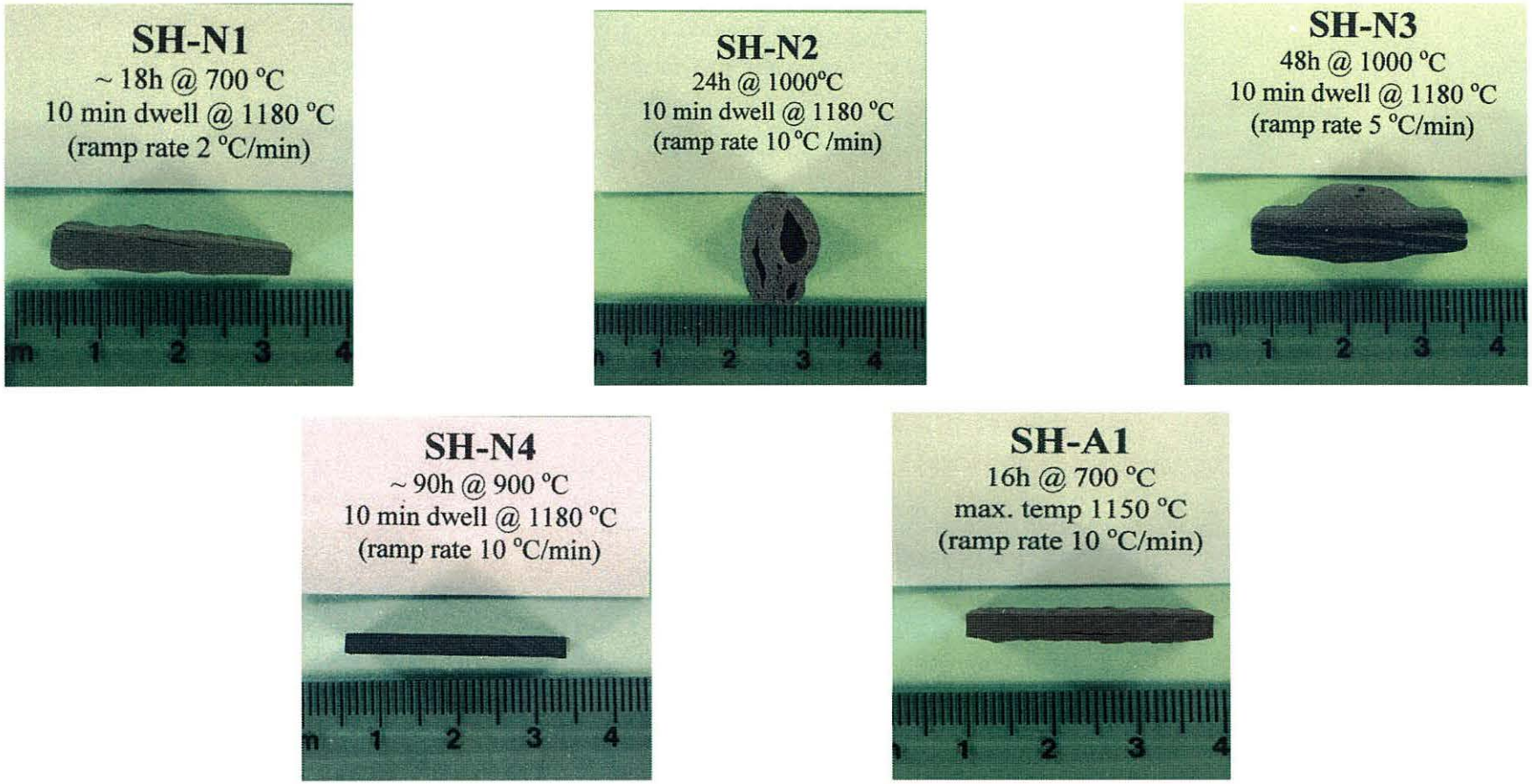

Figure 2.15. Pictures showing the difference in expansin of slate tablets obtained from slow heating (SH-) rate experiments.

Table 2.11. Summary of slow heating experiments.

Sample	Atmos.	Heating Rate (K/min)	Dwell at intermediate and max. temp (K).	Description
SH-N1	N_2	2	18h @ 973 10min @1453	< 2 fold expansion. Uneven surface topography. Blue/grey coloration. 5.1% wt loss.
SH-N2	N_2	10	24h @ 1273 10min@ 1453	3 fold expansion. Black lustrous outer surface, blue/purple inner surface. Large cavities present within structure. 5% wt loss.
SH-N3	N_2	5	48h @ 1273 10min @ 1453	2 fold expansion at edges, ~4 fold in centre. Black lustrous surface. 4.8% wt loss.
SH-N4	N_2	10	90h @ 1173 10min @ 1453	No expansion. Matt black surface colouration. 5.5% wt loss.
SH-N5	N_2	5	15min @ 1453	2 fold expansion. Purple/grey surface colouration. Irregular surface topography 5.3% wt loss.
SH-A1	Air	10	16h @ 973 10min@1423	No expansion. Some splitting along cleavage planes. Blistering appearance on upper surface. Dark brown/orange.
SH-A2	Air	10	70h @ 1173 15min @ 1453	No expansion. Dark brown surface coloration. 4.4% wt loss.

The dwell time at a temperature lower than 1453K is also believed to influence slate expansion. In order to determine the effect of a dwell longer than that sustained by SH-N1, SH-N2 or SH-N3, slate tablet SH-N4 was heated to 1173K and this temperature was held for 90 hours. The temperature was then increased to 1453K and a dwell of 10 minutes at this final temperature was incurred. This sample was found to be an exception to the trend that increasing the heating rate resulted in greater expansion since even though a rate of 10K/min had been followed in contrast to SH-N2 no expansion had occurred (Figure 2.16). Sample SH-N4 has shown that maintaining 1173K for a substantial length of time essentially ensures sufficient time for of all the vapour trapped within the slate structure to diffuse through the lattice. As a result of this dwell at 1173K when the sample was subsequently heated to 1453K *i.e.* a temperature that is usually

sufficient to ensure expansion, no gas was available to give rise to expansion. Furthermore this test has also confirmed that the presence of an accessory mineral which might decompose to release a gas at the appropriate temperature (*ca.* 1403K) is not responsible for slate expansion. The prolonged dwell at the lower temperature would not have affected this high-temperature mineral which would in theory still be present in the slate, even after a dwell at 1173K, to decompose at the expansion temperature. Since no expansion had occurred the importance of such a mineral can be dismissed.

Following the slow heating tests carried out in nitrogen two experiments were carried in air to see whether the same dependence on dwell time at 973 and 1173K was apparent for samples SH-A1 and SH-A2 respectively. Both samples followed a 10K/min heating rate. The first sample, SH-A1, was initially held at 973K for 16 hours before been heated further to 1423K. An approximate 2-fold expansion was measured for this first sample heated in air (Figure 2.16). By comparison SH-N1, which was heated in nitrogen at 2K/min and held at 973K for 18 hours prior to heating to 1453K, exhibited less expansion than SH-A1 even though a higher final temperature had been reached. This is again believed to reflect the importance of heating rate since the trend that a faster rate resulting in greater expansion had again been demonstrated independent of calcination atmosphere. By comparison SH-A1 showed less expansion than SH-N2 even though the same heating rate had been followed *i.e.* 10K/min. The decreased expansion in this case is however believed to reflect the influence of atmosphere *i.e.* better expansion apparent when slate tablets are heated nitrogen rather than air. The second sample heated in air, namely SH-A2 sustained a very long dwell of 70 hours at 1173K before subsequent heating to 1453K. In accordance with SH-N4 heated in N_2 (90hrs at 1173K) no expansion had taken place upon inspection of SH-A2. It is again apparent that prolonged heating of a slate tablet at a temperature lower than expansion ensures the loss of any vapour from the slate lattice irrespective of whether heating had occurred in air or nitrogen. This again supports the supposition that diffusion is the most important factor controlling the expansion mechanism. Furthermore SH-A2 was found to be extremely hard to cut even with a diamond saw and thus was believed to be a much stronger material. Expanded slate is also a relatively strong material but as a result of its internal structure containing

large pores and voids a much lower density is generally recorded. However since XRPD analysis of sample SH-A2 has shown that it has the same mineralogical composition expected of expanded slate it is therefore reasonable to assume that a denser material would be produced when no expansion occurs.

To form a comparison between the extent of expansion seen by following a relatively slow heating rate, experiments have also been carried out following more rapid heating rates between 15 an 30K/min (see Table 2.12). The first experiment involved heating a slate tablet at a rate of 20K/min up to a temperature of 1423K in air (RH-A1). No dwell at a lower temperature was incurred in this case. Only a slight expansion was observed, approx. <2 fold, which was less than expected (Figure 2.17). This is believed to reflect the importance of the final temperature since RH-A1 had only been heated to 1423K. This lower temperature is believed to be responsible for the slate tablet splitting rather than expanding homogeneously. In a subsequent experiment, RH-A2, the temperature was increased to 1453K and a faster heating rate of 30K/min was followed. Only a two-fold expansion was observed and upon inspection of the internal structure of the heated tablet two relatively large voids were apparent surrounded by a network of tiny pores. The degree of expansion observed in RH-A2 was again less than expected since it had been suggested that by increasing the heating rate the extent of expansion would also increase. It is therefore apparent that heating slate too rapidly reduces the degree of expansion as does following a heating rate that is too slow. The negative effect of a heating rate that is believed to be too rapid was demonstrated further in experiment RH-A4. Here a 30K/min heating rate was again followed however 1173K was maintained for 24 hours prior to heating to 1453K. The cooled sample revealed that no expansion had taken place. By comparison, sample SH-A1 (10K/min) resulted in an approximate 2-fold expansion after a 16hr dwell at 973K had been sustained(see Figure 2.17). This clearly demonstrates that the combined effect of a long dwell at 973K followed by a very rapid heating rate can result in a reduced degree of expansion to zero, as seen in RH-A4. Furthermore in comparison with samples SH-N4 and SH-A2, these samples required a 90 and 70 hour dwell at 1173K respectively to produce slate tablets that had not expanded. The increased heating rate has therefore clearly shown that a

shorter period of time is required to ensure that absolutely no expansion takes place *i.e.* the energy input into the system is effectively the same but much faster. It is therefore believed that very rapid heating *i.e.* 30K/min, gives rise to an increase in the rate of vapour dissipation through the internal structure of the slate tablet which has been shown to lead to splitting along the cleavage plane instead of good expansion. By extrapolation, it may be possible that if slate could be heated from room temperature to 1323-1473K in a matter of seconds the increased vapour diffusion through the lattice could result in the slate exploding. It is therefore evident that varying the ramp rate can control the nature of the final material.

Slate tablets were then heated in nitrogen to establish whether the same trend resulting from rapid heating was also apparent during heating under this relatively inert atmosphere. Firstly sample RH-N1 was heated to 1443K at a rate of 25K/min. A 2-3 fold expansion was recorded (Figure 2.17). This expansion is slightly less than that recorded by SH-N2 (10K/min with a 24hr dwell at 1273K). Thus illustrating that a 25K/min rate is still too fast to ensure the optimum expansion. Following this experiment RH-N2 was heated in nitrogen to 1453K by following a 15K/min heating rate. A shorter dwell at the final temperature was incurred in this case *i.e.* 5 minutes compared to the normal 10 minutes incurred by all the previous samples. The sample expanded much better (3-4 fold) compared to RH-N1 (2-3 fold). This is believed to be mostly due to the reduced heating rate *i.e.* 15K/min compared to 25K/min respectively. Furthermore the slightly higher final temperature experienced by RH-N2 is also believed to have benefitted the extent of expansion observed in this sample. However the best expanded product was achieved during experiment RH-N3. In this case a 20K/min heating rate was followed up to the final temperature of 1453K and a 15min dwell at this temperature was sustained. The slate tablet expanded to around 5 times its original volume. In fact the slate had expanded to such a degree that it had become stuck inside the quartz reaction tube. Consequently, the length of dwell at the final temperature is also believed to influence the degree of expansion. Indeed experiment RH-N4, which followed an identical heating program to RH-N3 except that a 10 min dwell at 1453K was incurred instead of 15 min, produced a final sample that was not stuck inside the

reaction tube since it had expanded to a lesser degree than RH-N3 *i.e.* 4 fold instead of a 5 fold expansion. It has therefore been demonstrated that the dwell time at 1453K is also a key factor in controlling the expansion. It is believed that a longer dwell at this temperature, when the slate is in a sufficiently pyroplastic state for the structure to become mobile, allows expansion gas from deep within the slate tablet to diffuse through the slate structure causing greater expansion.

As a result of this series, it has clearly been demonstrated that slate expansion depends on heating rate, dwell time below the expansion temperature, final temperature and dwell time at the expansion temperature. This work has enabled an optimum heating program to be developed for the expansion of slate on a laboratory scale suitable for repeated production of expanded slate samples in the Carbolite tube furnace. A heating rate of 15-20K/min is required to produce a homogeneous expanded product i.e. too slow (2-5K/min) little expansion occurs, 10K/min produces a sample with large internal voids and too rapid (30K/min) poor expansion occurs with considerable splitting. The optimum temperature has been shown to be 1453K since lower temperatures 1423 and 1443K have consistently produced products that have not shown the highest degree of expansion. Furthermore a longer dwell period at the expansion temperature tended to increase the expansion so a dwell time in the region of 10-15 mins is essential to produce the best-expanded product.

Table 2.11. Summary of rapid heating experiments.

Sample	Atmos.	Heating Rate (K/min)	Dwell at intermediate and max. Temp (K).	Description
RH-A1	Air	20	Max temp 1423	Slight expansion with considerable splitting. Very dark brown/black surface colouration. 4.7% wt loss.
RH-A2	Air	30	10min @ 1453	2 fold expansion. Very dark surface coloration. Internal structure made up of small pores, blue/grey. 4.8% wt loss.
RH-A4	Air	30	24h @ 1173 15min @ 1453	No expansion. Slight separation along cleavage planes. Very dark black/brown surface colouration. 5.5% wt loss.
RH-N2	N_2	15	5min @1453	3-4 fold expansion. Uneven topography on upper and lower surfaces. Slight separation along cleavage planes. Light blue/grey colouration. 5% wt loss.
RH-N3	N_2	20	15min@1453	5 fold expansion. Good homogeneous expansion. Uneven surface topography. Internal structure made up of network of tiny pores. Light blue/grey surface colouration. 5.1% wt loss.
RH-N4	N_2	20	10min @1453	4 fold expansion. Slight splitting. Internal structure containing network of small pores, blue/purple in colour. Darker blue/grey surface colouration. 5.3% wt loss.

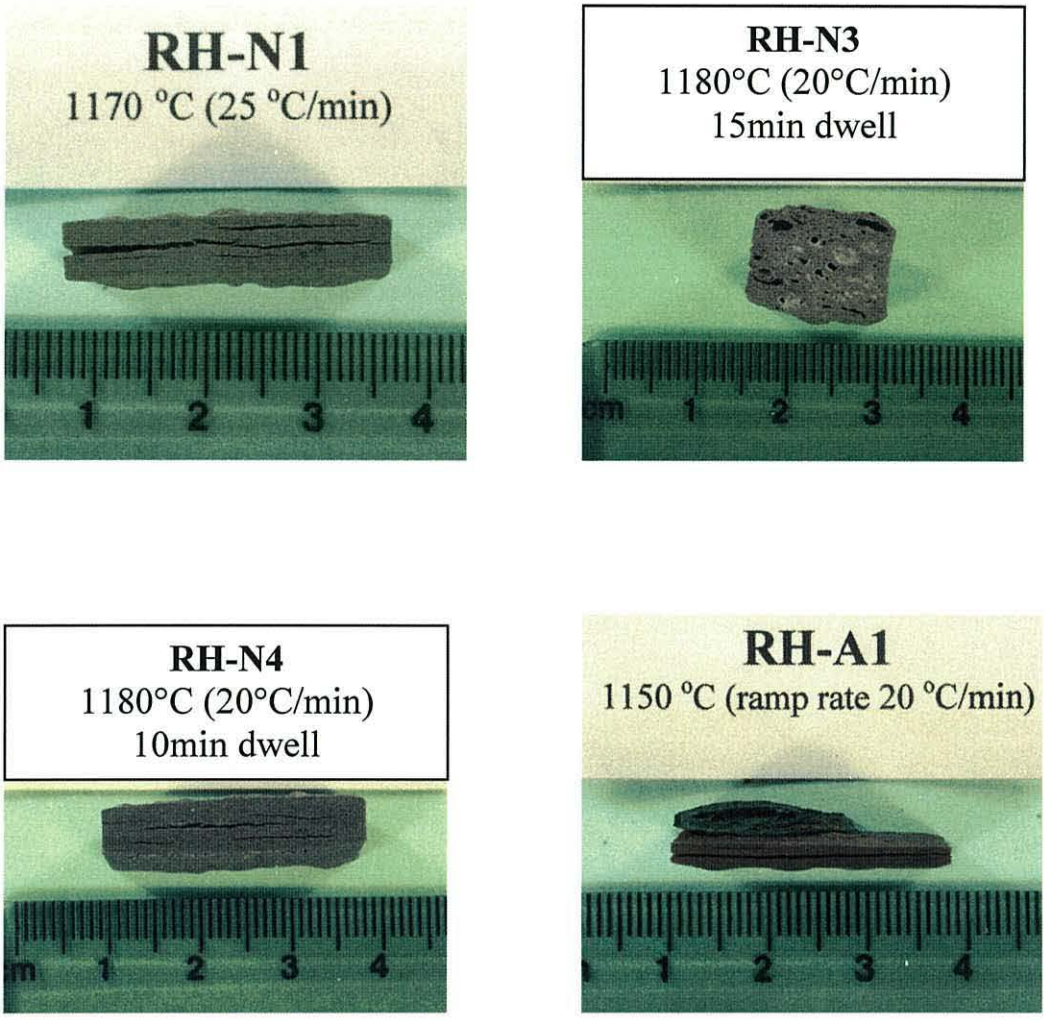

Figure 2.16. Pictures showing different expansion experienced by slate tablets heated following rapid heating (RH-) experiments.

The degree of expansion in the laboratory scale experiments has been limited by the diameter of the reaction tube. Indeed when a large slate block (15x100x100mm) underwent heat treatment at EA Technology a 7-fold expansion was measured. The results obtained from heating experiments carried out at University of Wales, Bangor, have however showed that expansion can be controlled when necessary. The optimum heating programme for the Carbolite tube furnace therefore involves a heating rate of 20K/min to 1453K with a dwell of 10 minutes at the final temperature.

XRD analysis of all the treated samples produced a diffraction pattern that correlated with those of expanded slate previously analysed in section 2.2.1. Samples denoted by SH- and RH- therefore generally consisted of quartz, hercynite and mullite. The slate tablets also consistently lost between 4-5 % of their original mass. It is therefore clear that the process of expanding slate result in the formation of a product with the same chemical composition irrespective of atmosphere *i.e.* air or N_2. However the appearance of the final materials has been found to be significantly different. The outer surface of expanded slate heated in air often appeared to be much more shiny and "glassy" than samples heated in nitrogen. Indeed the nature of expanded products formed in air was also different since more splitting and a lower volume increase was generally observed compared to N_2 samples. This is believed to reflect the close relationship between producing an expanded product from slate or producing a material more closely resembling a sintered/amorphous glass. Indeed the production of commercial glass products is highly dependant on temperature, heating rate, atmosphere and component composition to such a degree that slight variations in these parameters can result in a completely different glass being produced. The complexity seen in the production of glass is therefore expected to be just as significant in the production of expanded slate hence the different type of material produced in air compared to N_2 even though they have been shown to have the same chemical composition.

2.6 Conclusions

The major phases typically present in both Welsh and Spanish slate have been identified as chlorite, muscovite and quartz. The presence of accessory minerals such as pyrite and calcite, which have been reported as being responsible for releasing the necessary gas to instigate slate expansion have not been detected in the slate samples analysed. Their role in the expansion of slate from Llechwedd, North Wales and Villar del Rey, Spain has subsequently been shown to be negligible. The composition of expanded slate has been identified as quartz, mullite and hercynite thus illustrating the comlete rearrangement of the lattice atoms during expansion. The expanded material also has significantly more amorphous material than unheated slate.

The absence of pyrite and calcite has lead to the conclusion that SO_2 and CO_2 are not the gases that result in slate expansion. Small amounts of carbon has been reported to be present in Welsh (Blaenau Ffestiniog, 0.19% Total Organic Carbon) and Spanish (Sobrano Campo, 0.52%C) slate[159] in the form of carbonatious material such as graphite. CHN elemental analysis of Welsh and Spanish samples in this study has shown 1% and 1.5% ∀0.6%C respectively. The decomposition of this carbon may also give rise to CO_2 however elemental analysis has shown that this carbon is lost at a temperature below the expansion temperature since the instrument only reached a temperature of 1273K. The gas responsible for expansion is therefore believed to be H_2O vapour, released during the decomposition of slate's constituent minerals. Water is inherently present in the structures of both chlorite and muscovite.[26] The decomposition of chlorite has been shown to be complete by ~1173K whereas muscovite remains until >1273K. The presence of muscovite at this temperature is believed to be key in ensuring that H_2O vapour is present within the slate structure at the crucial stage (1453K) when slate is in a pyroplastic state and the lattice is sufficiently mobile to give rise to expansion. Indeed a small mass of H_2O has been condensed at the expansion temperature. The rate of diffusion of this water vapour from within the slate structure is therefore believed to be key to achieving good expansion.

The heating rate, dwell times and final temperature have all been shown to affect the degree of expansion. A heating rate that is too slow (5K/min) or too rapid (30K/min) has been shown to give rise to poor expansion believed to result from increased vapour dissipation from the samples when either heating rates are followed *i.e.* slow heating allows greater time for the vapour to escape and rapid heating allows the vapour to be lost more quickly. Indeed it is suggested that a sufficiently high heating rate could result in slate samples exploding rather than expanding. Long dwell times (~70hrs) at temperatures lower than the expansion temperature (1173-1273K) have resulted in samples that have not expanded. This also supports the supposition that the rate of vapour diffusion during the decay of chlorite and muscovite is the key to the expansion mechanism since a sufficient dwell is believed to allow sufficient time to give rise to the loss of the all the expansion gas *i.e.* H_2O vapour. The final temperature is also important to ensure that the slate is in the proper pyroplastic state to allow good expansion to take place. Varying these parameters has clearly shown that slate expansion can be controlled. Indeed in the course of this project the optimum heating programme for the expansion of Welsh and Spanish slate has been determined *i.e.* heating rate 20K/min up to the final temperature 1453K and incurring a dwell of 10mins at this temperature.

As a result of this study the differences in the extent of expansion exhibited by slates from different areas[32] is believed to be directly related to the ease of vapour diffusion through the lattice of the different slates. It has been reported that the older, Cambrian slate from Penrhyn and Dinorwic slate quarries in Gwynedd (see Figure 1.2. in Chapter One) exibit very poor expansion. By comparison the younger Ordovician slate from Blaenau Ffestiniog expand much better. Indeed the trend of younger slates showing greater expansion has also been seen in the course of this study since the Devonian slate from Spain tended to expand slightly better than the Ordovician slate of Llechwedd Slate Quarry, Blaenau Ffestiniog. The difference in expansion is believed to relate to the different degree of compression experienced by the slates during their formation over millions of years. It is inferred that older slates tend to have undergone greater compression, for a longer period of time, than younger slate thus tending to give rise to a more compressed or hard rock. Indeed slate from the Penrhyn quarry tends to be a harder

material than slate from Llechwedd. Consequently, older slates are believed to restrict the diffusion of expansion gas through their structure as a result of the material not becoming pyroplastic at the appropriate temperature to trap the released vapour within its structure. It is therefore believed that the release of water vapour and the transformation of slate's physical state form solid to pyroplastic need to coincide at around *ca.*1453K to ensure that expansion takes place.

Chapter Three - Pyrite

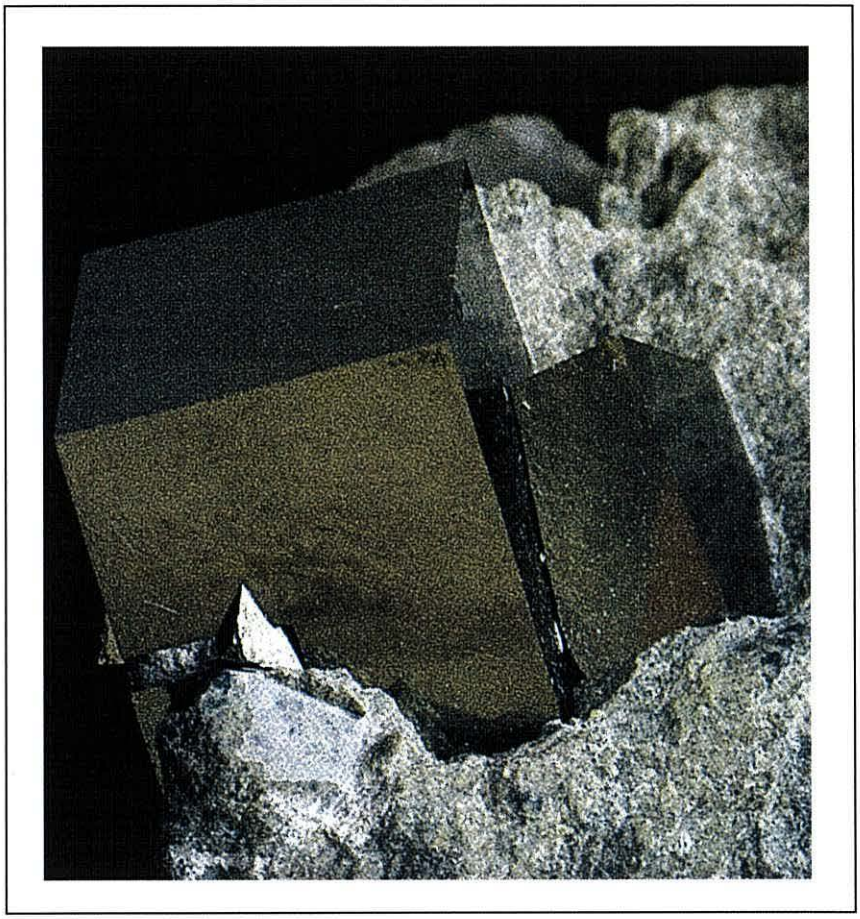

(J. Kouřimsky, *The Illustrated Encyclopedia of Minerals and Rocks*, 1995)

Chapter Three - Pyrite

3.1. Pyrite Decomposition

Pyrite is often found as an accessory mineral in slate. Pyrite has been shown to be susceptible to natural weathering processes when present in untreated slate used as a building material *e.g.* roofing slates. The problems associated with its presence in slate have previously been reported in more detail in the introduction (Section 1.3). The work in this thesis is mainly focussed on gaining a greater understanding and enhancing the development of expanded slate rather than just slate as a commercial product. It is therefore important that a fundamental understanding of the decomposition of pyrite within slate is also obtained as the slate is heated to its expansion temperature compared to pyrite alone or in coal (discussed in the Introduction). Furthermore a comparison of the extent of pyrite decay in nitrogen and air is also an important area of study since in a commercial expansion process the kiln is likely to have zones of varying O_2 concentration. A study into the differences arising from the decomposition of pyrite in relatively inert environments compared to relatively oxidising environments will therefore provide a simulation of the pyrite decomposition that will be expected if slates with pyrite incorporated into their structure undergo expansion in a commercial furnace.

This study therefore aims to ascertain if pyrite decomposition takes place during slate expansion and if so at what temperature does this occur. In order to do this, the study will initially focus on the decay of pyrite alone *i.e.* analysis of pyrite fragments obtained from a larger cubic pyrite crystal (*ca.*25x25x25mm). This work will form the basis in order to be able to compare and determine the products formed and the extent of decay of pyrite crystals situated within slate and to see if the pyrite in slate behaves differently than pyrite on its own. Furthermore any differences between surface (external) pyrite and pyrite within slate (internal) will also be studied. Oxygen content in the environment is believed to be important in pyrite decomposition therefore by carrying out experiments both in air and in nitrogen the effect of atmosphere on decomposition temperature, extent of decay and product will be determined. Experiments have therefore been carried out in

both gases up to slate the expansion temperature (1453K). Experiments at lower temperatures, 923K and 1223K, have also been undertaken. These temperatures have been chosen since work carried out investigating the expansion of slate (Chapter Two) has shown that 873-1273K is a key temperature region for the decomposition of chlorite and muscovite. The effect of heating pyrite to temperatures within this range is therefore also believed to be key to understand pyrite's decay in slate.

A review of the information gained from experiments on pyrite-only samples heated in nitrogen and air respectively will initially be discussed in this chapter. The gases released and the visible observations of the resultant material will firstly be reported on. Subsequent discussion on the weight loss suffered by the samples and the effects of temperature, heating rate and dwell times will be provided. The analysis and characterisation by XRPD, SEM and EDS of the heated material will also be discussed. Visible observation showed that differences existed between the outer and inner surfaces of the pyrite samples. In this context the outer surface has been defined as that surface present on the outside of the sample which has been exposed to the atmosphere (also referred to as exterior or external surface). By comparison, for pyrite-only samples the inner surface lies underneath this outer surface and has not been exposed to the atmosphere until the sample was broken apart after heating (also referred to as interior and internal surface). Outer and inner surface determination was carried out on a sample to sample basis. SEM in association with EDS has been found to be extremely useful in providing detailed information on the variations between the outer and inner surfaces of the heated pyrite.

3.2. Untreated Pyrite

Before the investigation into pyrite decomposition was undertaken unheated pyrite was firstly analysed by XRD, SEM and EDS in order to be able to form a comparison with the degree of decomposition in the two atmospheres (N_2 and air). The XRD pattern of the sample was found to match the pyrite reference pattern (FINK Index 06-0710) (Figure 3.1).

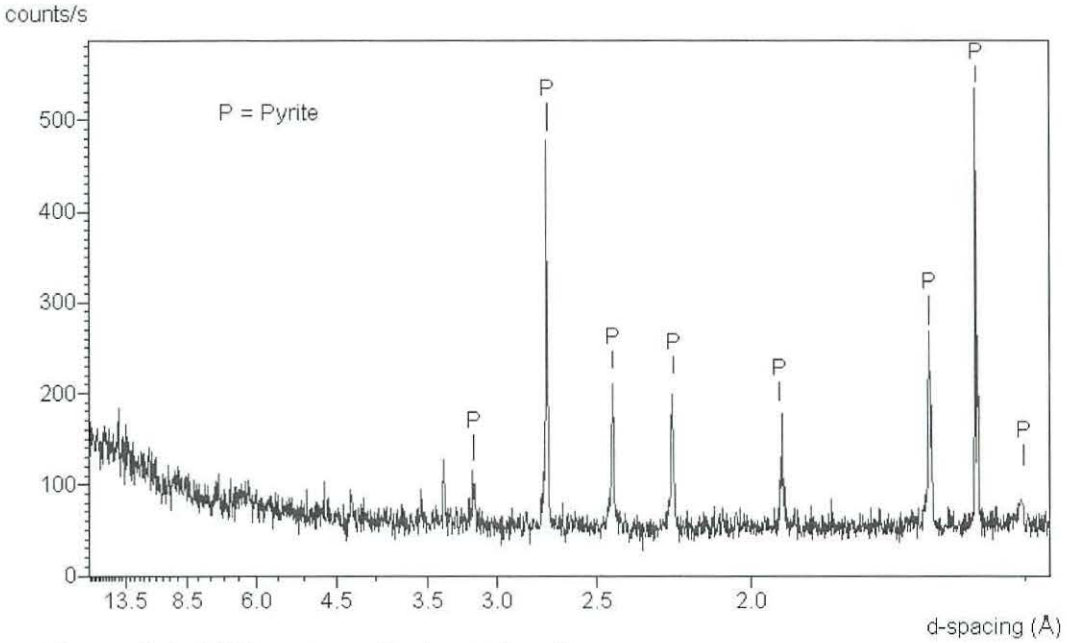

Figure 3.1. XRD pattern of unheated pyrite.

SEM studies showed that the untreated sample had a relatively featureless morphology with little topographical differences with no apparent pores or cavities. EDS analysis produced a pattern with strong sulfur and iron peaks. A Fe:S peak height ratio of 1:2 had been expected for FeS_2 however a ratio in the region of 1:3.5 was normally found. This is believed to reflect the differences in the peak area for S and Fe since it is apparent that the top half of the sulfur peak is much thinner than the Fe peak. It is therefore believed that the associated peak area would give a better correlation with the expected 1:2 Fe:S ratio. A quantitative determination of the amount of S and Fe present in the sample is therefore not possible by using EDS. However the pattern obtained during the analysis of unheated pyrite will therefore form the basis to compare peak heights of subsequent heated samples in order to gain some indication of the extent of decomposition (Figure 3.2(a)). Figure 3.2 also shows reference EDS patterns used to illustrate the loss of S from pyrite *i.e.* pattern (b) and (c). Pattern (b) corresponds to the removal of 1 equivalence of S (based on mass loss), the shape of the Fe and S peaks are very similar producing a peak height ratio ~1:1. Pattern (c) shows the total loss of S *i.e.* Fe:S ratio 1:0.

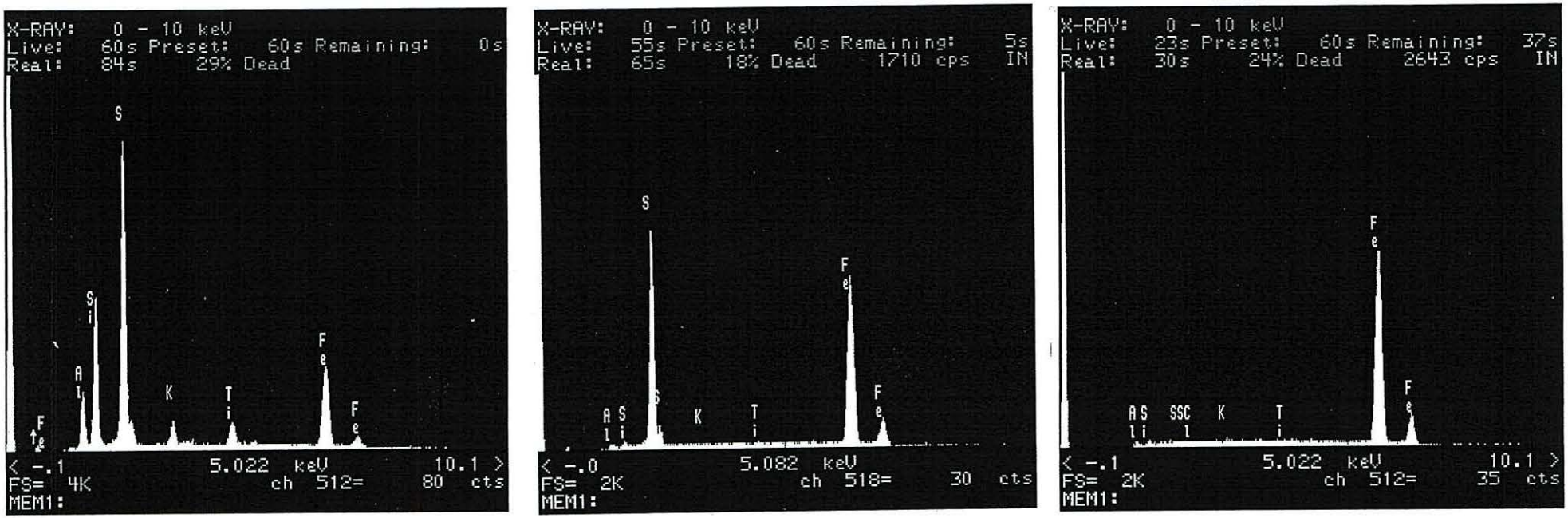

(a) (b) (c)

Figure 3.2. EDS patterns of a) unheated pyrite in slate (approx Fe:S ratio 1:3.6)

b) pyrite heated in N_2 with weight loss corresponding to loss of 1 equivalence of S (approx Fe:S ratio 1:1).

c) pyrite heated in air with weight loss corresponding to total loss of S (approx Fe:S ratio 1:0)

3.1. Pyrite Decomposition in Nitrogen

During heating of the pyrite in N_2, it was noticed that a colourless vapour was released at *ca.* 823K. This vapour condensed in the cooler parts of the reaction tube to produce a yellow precipitate. Areas of darker yellow and black particles could also be seen within the precipitated solid thus producing a colour that did not appear to be homogeneous throughout the sample collected. Melting point determination of the precipitate showed that initial decomposition occurred at 107°C, however the solid did not melt completely until a temperature of 210°C was reached. The literature value for the melting point of pure sulfur is 114-117°C.[165] Sulfur can be very sensitive to low levels of impurities which in turn effect its melting point and colour. The wide temperature range observed for the decomposition of the precipitated solid is therefore believed to show the presence of a ssecond phase within the precipitate. X-ray powder diffraction and EDS data confirmed that this precipitate was indeed sulfur. No data has been obtained relating to the identity of the second phase. Yperman *et al.* has also reported the loss of sulfur however this inference was based on TGA studies which showed a weight loss corresponding to the removal of one equivalence of sulfur from FeS_2 under Ar at 550°C.[77]

The exhaust gas was also passed through an iodate solution to determine whether any S^{2-} was present. A very slight discolouration of the iodate solution was seen (light yellow/orange) with the formation of small amounts of iodine (see equation 3.1). This is believed to be due to some sulfide being released during the decoposition of pyrite in nitrogen . Furthermore the exhaust gas was tested with lead acetate indicator paper. The indicator paper turned grey due to the formation PbS. This further reflects the presence of a sulfide species in the exhaust gas. The precise nature of this sulfide species has not been determined however it may correspond to H_2S.

$$2I^{5+} + 5S^{2-} + 12H^{+} \rightarrow I_2 + 5S + 6H_2O \qquad [3.1]$$

Following the apparent reaction at 823K it was decided to heat subsequent samples to 923, 1223 and 1453K for *ex situ* XRPD and electron microscopic analysis. Differences were found between samples heated at 923k for different periods of time (Table 3.1). For instance, a sample that incurred a dwell of 5 min at 650°C (P-22) suffered a 12.4% weight loss compared to a 24.0% weight loss for a sample heated for 24 hours (P-38). The theoretical weight loss for the conversion of pyrite (FeS_2) to troilite (FeS) is 26.7% thus indicating approximately 45% and 90% conversions respectively.

Theoretical Weight loss calculation:

$$2FeS_2 \rightarrow 2FeS + S_2$$
$$2(120) \quad 2(88)$$

Therefore % weight difference = (176 / 240)*100 = 73.3%

Corresponding to a theoretical weight loss = 26.7%

The decomposition of pyrite to synthetic troilite, FeS, (FINK index 01-1247) was confirmed by XRPD for both P-22 and P-38 (Figure 3.3). The major phases detected by XRD are given in Table 3.2. However, for the sample heated for 5min (P-22) visible observations showed that a gold lustre remained beneath the surface of the crystallites suggesting unreacted pyrite. A sample of this core material was carefully collected by physically separating it from the outer material (black) and crushed to a fine powder with pestle and mortar. XRPD analysis of this crushed material produced a diffraction pattern that was consistent with that of pyrite. In the case of P-38, which incurred a long dwell of 1440 minutes (24hrs) at 650°C, no visible evidence for an inner unreacted pyrite core existed. This was subsequently confirmed by XRPD of a fragment of the heated sample. This is consistent with a greater loss of sulfur associated with the increased weight loss observed for P-38.

Table 3.1. Decomposition of pyrite-only samples.

Sample	Gas Used	Dwell Temp (K)	Heating Rate (K/min)	Dwell Time (min)	Weight Loss (wt.%)	Conversion (%)	Experimental Observations
Pyrite	N/a	n/a	n/a	n/a	n/a	n/a	Cubic crystal with golden lustre
P-22	N_2	923	5	10	12.4	46.4[a]	Black, soft exterior (easily crushed). Golden hard internal core.
P-38	N_2	923	10	1440	24.0	89.8[a]	Black soft material throughout (easily crushed by hand).
P-52	N_2	1223	20	1-2	24.7	92.5[a]	Black soft material throughout (easily crushed by hand).
P-53	N_2	1453	20	1-2	26.8	100.4[a]	Black soft material throughout (easily crushed by hand).
P-31	Air	823	5	1-2	22.0	65.9[b]	Red/black, brittle exterior. Golden hard internal core.
P-23	Air	923	10	1-2	30.9	92.5[b]	Red/black, brittle material. Smooth external crust.
P-24	Air	1223	10	1-2	32.6	97.6[b]	Red/black, brittle material (more difficult to crush by hand).
P-27	Air	1453	20	1-2	32.0	96.0[b]	Red/black, brittle material (more difficult to crush by hand).

Conversion calculations based on theoretical weight loss values; [a] 26.7% in N_2 and [b] 33.3% in air.

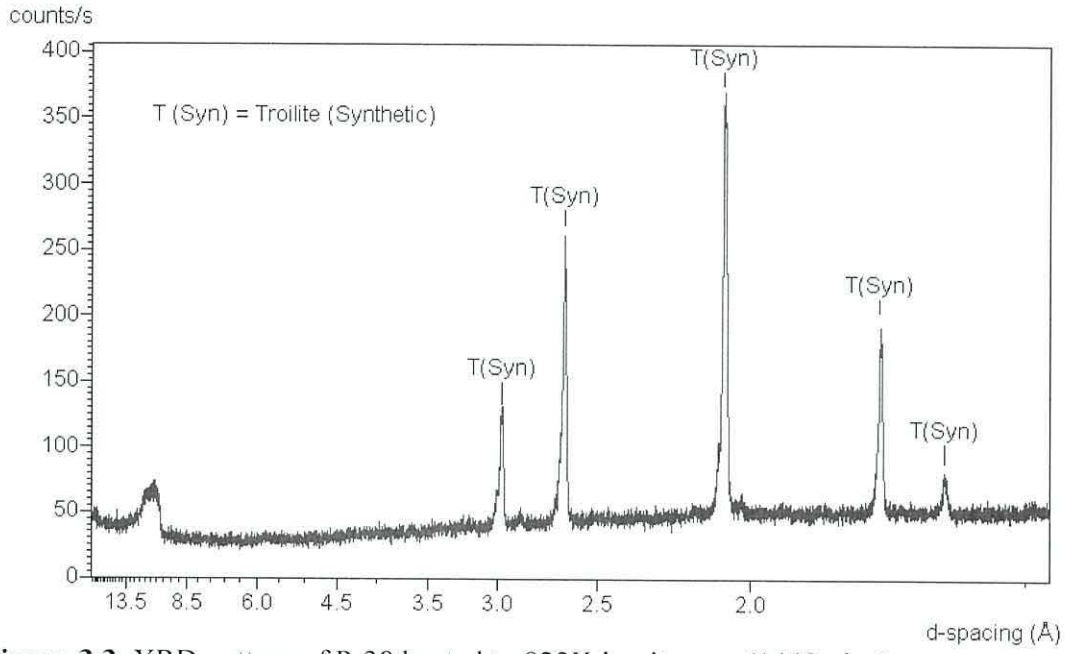

Figure 3.3. XRD pattern of P-38 heated to 923K in nitrogen (1440mins).

Table 3.2. XRPD data of pyrite-only samples heated in nitrogen.

Temp. (K)	**N_2**	
	Sample	**XRD data (major phase)**
923	P-22 (10min)	outer - Troilite (Syn) (FeS) inner - Pyrite (FeS_2)
	P-38 (1440min)	Troilite Syn (FeS)
1223	P-52	Troilite (Pyrrhotite) (FeS)
1453	P-53	Troilite (Pyrrhotite) (FeS)

Although no pyrite was detected in sample P-38 the actual weight loss was measured slightly lower than that expected for the removal of one sulfur equivalence from the original pyrite, which would in turn correspond to the complete conversion to FeS. This is believed to be due to an intermediate product being produced *i.e.* pyrrhotite ($Fe_{1-x}S$). Additional pyrite samples were therefore analysed after undergoing heating to elevated temperatures, namely to 1223 and 1453K (P-52 and P-53 respectively). Even though a relatively short dwell of 1-2min was incurred by both samples a weight loss of 24.7 and

26.8% respectively corresponding to the loss of 1 equivalence of S based on the theoretical value of 26.7%. In contrast to P-22 and P-38 the XRPD patterns of the samples heated to >1223K produced a diffraction pattern that was slightly different to synthetic troilite (01-1247). The XRPD of P-53 was found to closely match the reference pattern corresponding to troilite (pyrrhotite) (FINK Index 11-0151) (Figure 3.4). However as for synthetic troilite the chemical formula for the reference pyrrhotite (troilite) is also given as FeS therefore the difference between the two references is unclear. It is apparent that exposing pyrite to temperatures higher than 1223K ensures that the maximum amount of sulfur is lost in a nitrogen atmosphere. The apparent resistance against complete sulfur loss from the system therefore reflects the relative stability of FeS to thermal treatment in nitrogen. This has also been reported by previous workers.[84] Schaulaub reported that the maximum rate of weight loss for pyrite heated in nitrogen was observed between 600 and 660°C. He also reported that heating pyrite to 1000°C in nitrogen was not sufficient to remove 1 equivalence of S since a weight loss between 23.5 and 24.8% was generally recorded which is lower than the theoretical value of 26.7%.

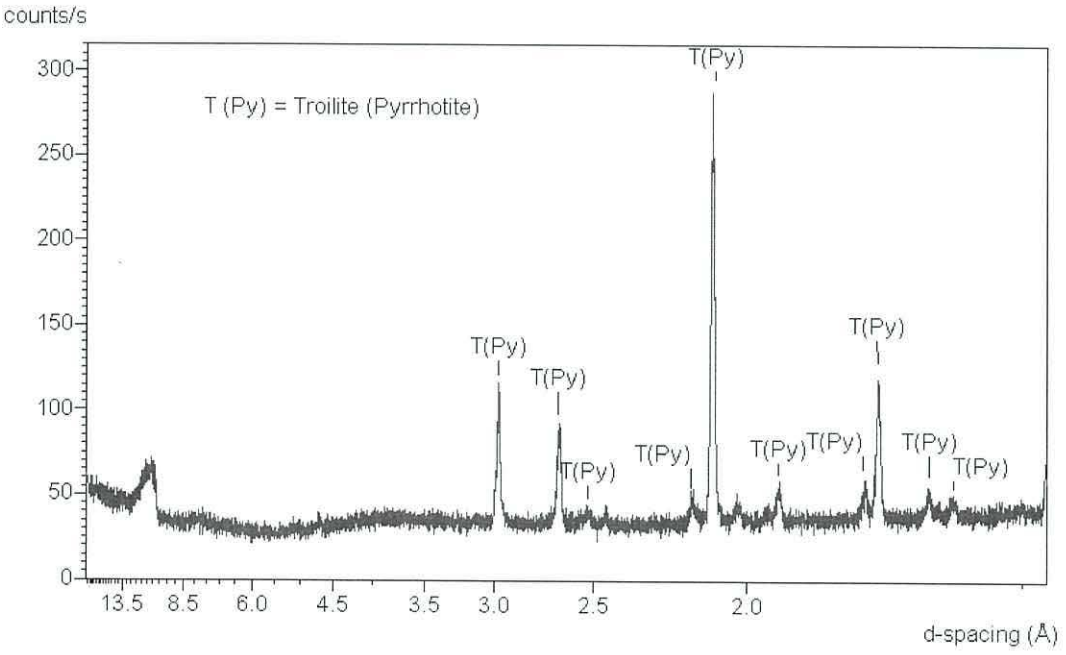

Figure 3.4. XRD pattern of P-53 heated to 1453K in nitrogen.

SEM studies of samples P-22 and P-38 heated at 923K with different dwell times, 5 min and 24 hours respectively showed significant morphological differences between the inner and outer surfaces of the samples. The inner material showed a very regular morphology giving the appearance of a very crystalline structure (Figure 3.5) whilst the outside of the samples were much more irregular containing a number of non-uniform cavities (Figure 3.6.). Energy dispersive spectroscopic analysis of the inner and outer surfaces of the samples showed a clear correlation between the approximate Fe:S intensities and the changing morphologies. Inside the sample the Fe:S ratio (based on EDS peak heights) was around 1:1 however areas with more sulfur (1:2) was also found thus indicating that a $Fe_{1-x}S$ having a greater S content than FeS is also present. On the outer surface the Fe:S ratio was closer to 1:0.25 *i.e.* only a trace amount of S was detected. The concentration differences between the two surfaces therefore reflect the non-homogeneous distribution of S through the sample. An indication of the mechanism involved in the decomposition of pyrite in nitrogen is therefore provided since it is apparent that sulfur is preferentially lost from the outside surface inwards.

It is therefore believed that the loss of S as a reaction by-product is key to the decomposition of the pyrite. The presence of sulfur atoms within the crystallites which are unable to diffuse away must either result in recombination of FeS and S to FeS_2 or to inhibit the initial FeS_2 decomposition. Certainly, kinetic studies by Lambert and co-workers has shown that the desorption of S from the surface of pyrite is the rate-controlling step.[88] However this study does not report on the effects of mass transfer or diffusion on the extent of pyrite decay. More recent work by Gibbs *et al.* has also shown the importance of the removal of sulfur from the system and have reported that pyrite decomposition is not entirely dependant on the heat transfer through the solid particle.[95] Here our evidence suggests that the rate of diffusion of S through the lattice as it decomposes is also important in limiting the extent of reaction. This has implications to pyrite situated within slate since the released sulfur here would essentially be contained within the slate structure thus inhibiting its diffusion away from the pyrite.

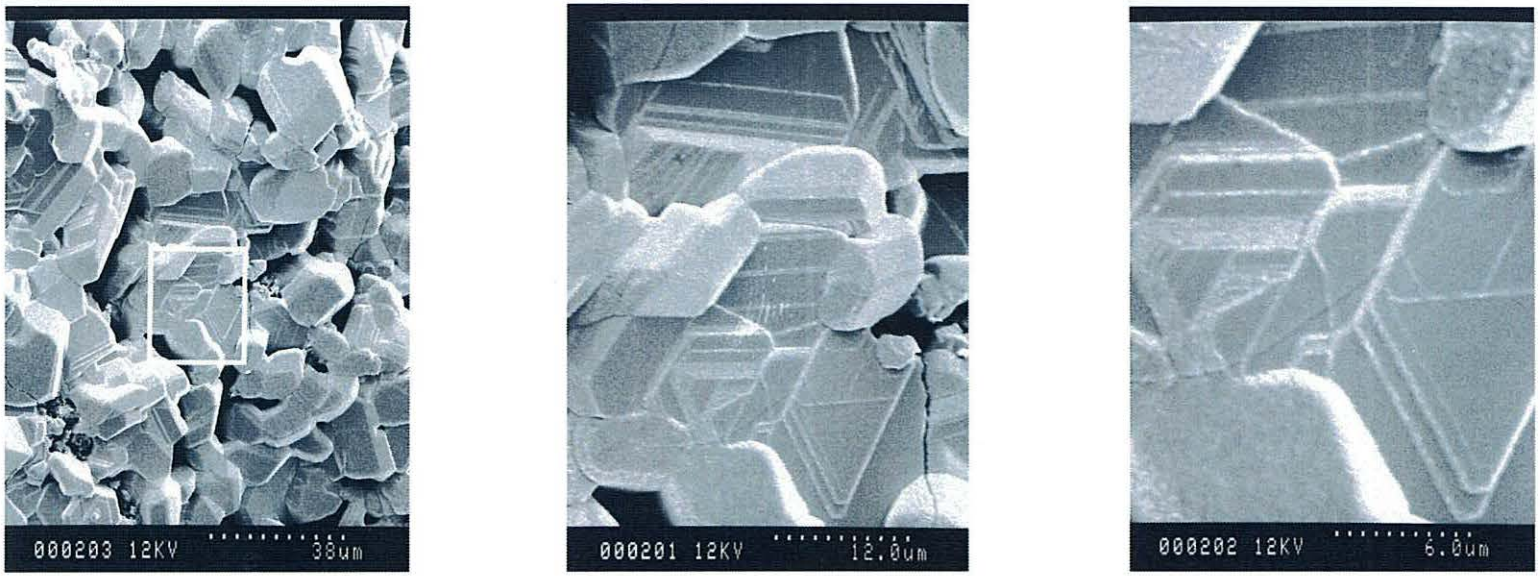

Figure 3.5: SEMs of pyrite in slate (interior, P-38) heated to 923K in nitrogen for 24 hours

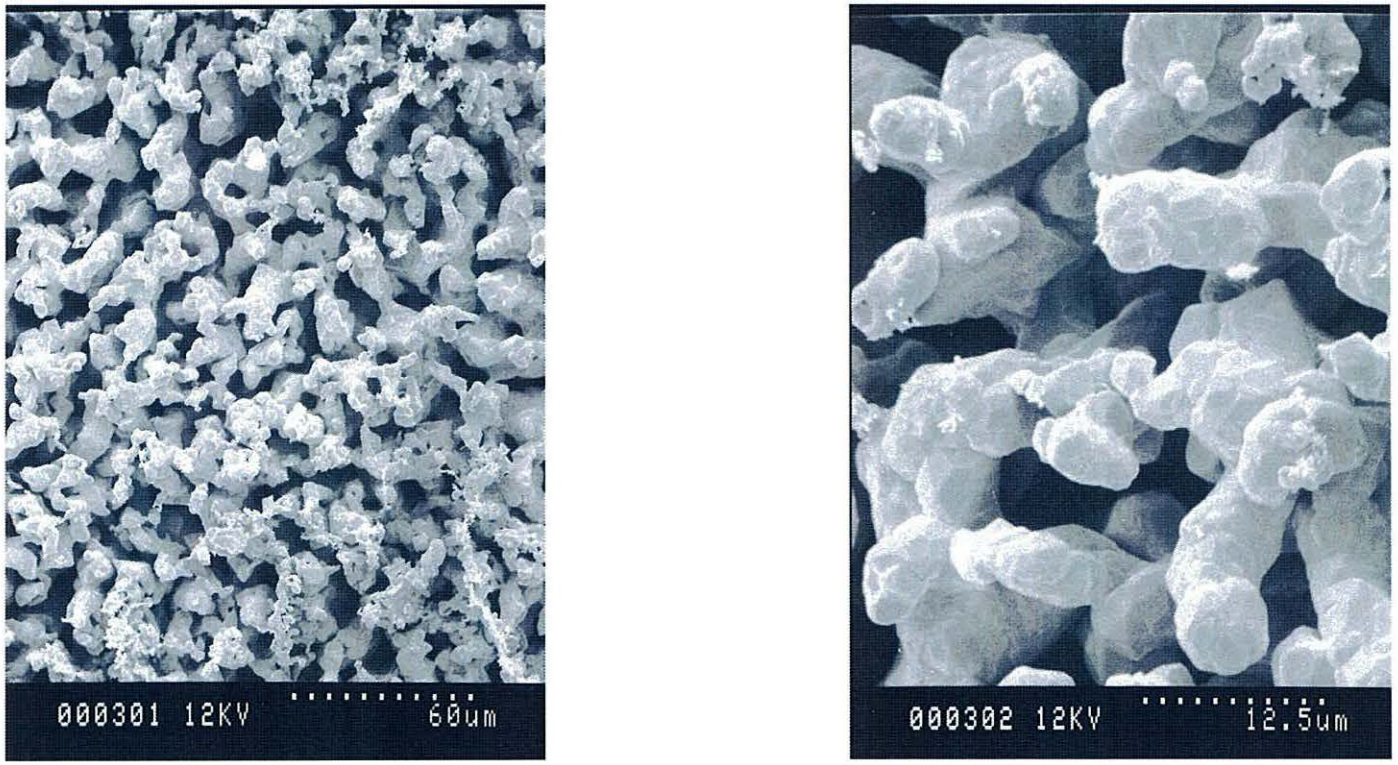

Figure 3.6: SEMs of pyrite in slate (exterior, P-38) heated to 923K in nitrogen for 24 hours

3.4. Pyrite Decomposition under Air

A series of experiments have been carried out to compare the decomposition of pyrite with increasing temperature, namely at 823, 923, 1223 and 1453K (Table 3.1). During heat treatment no sulfur was condensed during these tests in air. Instead, the release of a colourless gas was observed at $\geq$ 823K which was identified as SO_2 by chemical analysis (iodate assay) as expected (see equation 3.2).[69] By comparison to pyrite heated in N_2 the iodate solution turned a deep orange/brown. In addition I_2 was also precipitated (brown solid) thus demonstrating that much more SO_2 is released during the air experiments than S^{2-} in the N_2 experiments. The additional test at 823K has therefore been included here in an attempt to ascertain the degree of pyrite decomposition at a temperature close to the temperature at which vapour was initially released. This test was therefore intended to give an indication of the reactivity of pyrite in air compared to nitrogen.

$$2IO^{3-} + 5SO_2 \rightarrow I_2 + 5SO_3 \qquad [3.2]$$

X-ray powder diffraction of the red/black product of P-31, P-23, P-24 and P-27 consistently gave patterns corresponding to haematite (Fe_2O_3) (Figure 3.7) (see Table 3.3). However upon inspection of P-31, heated to the lower temperature of 550°C, it became apparent that the sample contained a core material of similar appearance to that previously seen in the partially converted sample P-22 heated to 650°C for 5min in nitrogen. Subsequent analysis by XRPD indeed confirmed this core material as pyrite. The weight loss of 22.0% observed by P-31 also reflects that only partial decomposition of the initial pyrite fragment took place. This value was much lower than the theoretical 33.3% weight loss calculated for the conversion of FeS_2 to Fe_2O_3 and therefore corresponds to the decomposition of approximately 66% of the original sample. By comparison a lower percentage of pyrite had been converted when a sample was heated in nitrogen (P-22, 45%) even though a higher temperature of 923K had been reached and a longer dwell of 5 minutes had been incurred thus illustrating the increased decomposition of pyrite in air. The detection of sulfur by EDS analysis of P-31 is believed to be due to the presence of pyrrhotite ($Fe_{1-x}S$) minerals or troilite (FeS). No

peaks corresponding to these sulfide minerals was detected by XRD however this may be due to low concentrations or amorphous FeS being present. The formation of pyrrhotite has previously been reported as an intermediate product during pyrite oxidation.[84,89,90] It is therefore suggested that only a small proportion of the final solids actually contain the intermediate iron sulfide compounds

Theoretical Weight loss calculation:

$$2FeS_2 + {}^3/_2O_2 \rightarrow Fe_2O_3 + 4S$$
$$2(120) \qquad\qquad (160)$$

Therefore % weight difference = (160 / 240)*100 = 66.7%

Corresponding to a theoretical weight loss = 33.3%

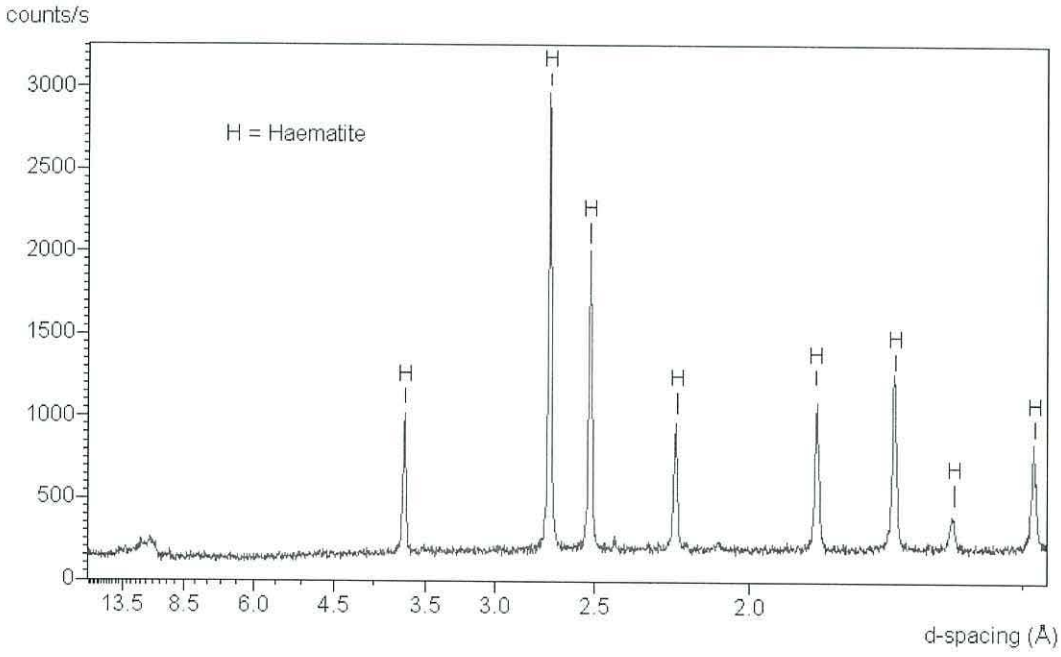

Figure 3.7. XRD pattern of P-23 heated in air to 923K.

Table 3.3. XRPD data of pyrite-only samples heated in air.

Temp. (K)	Air	
	Sample	**XRD data (major phase)**
823	P-31	Haematite (outer) Pyrite (inner)
923	P-23	Haematite
1223	P-24	Haematite
1453	P-27	Haematite

As a direct result of the apparent increased reactivity of pyrite in air compared to nitrogen the experiment design was changed so that a relatively short dwell of 1-2 minutes was incurred by all samples. It became apparent that with increasing temperature the extent of pyrite decomposition also increased. Indeed P-23 heated to 923K suffered a 30.9% weight loss corresponding to around 93% conversion, which is more than double the conversion suffered by P-22 heated to 923K in nitrogen. The highest conversion percentage (98%) was recorded as a result of the 32.6% weight loss sustained by P-24 after being heated to 1223K. This loss correlates well with the theoretical weight loss value of 33.3% thus suggesting that near complete oxidation had in fact been achieved by following a heating program that involved a rate of 10K/min and a short dwell (1-2min) at 1223K. An exception to the trend was sample P-27 since it suffered a slightly lower weight loss (32.0% loss) than P-24 even though it was heated to a higher temperature. This reduced conversion (96%) was unexpected since it was believed that exposure of the pyrite sample to 1453K would have ensured the maximum conversion of FeS_2 to Fe_2O_3. This discrepancy in the conversion trend is however attributed to the increased heating rate followed by P-27 *i.e.* 20K/min compared to 5K/min (P-31) or 10K/min (P-23 and P-24). It seems likely that the faster rate of heating essentially results in the pyrite sample being exposed to temperatures above the initial reaction temperature of *ca.*823K for a shorter period of time. Indeed, when considering P-27 a period of 31.5 minutes was incurred between 823K and reaching 1453K. By comparison, to reach 1223K at a rate of

10K/min, P-24 was exposed to temperatures higher than 823K for 40 minutes. It is apparent that effective dwell time at temperature >823K is key to ensure the optimum loss of S. More time at a sufficiently high temperature has been shown to result in more conversion thus illustrating the dependence of pyrite decay on the rate of mass transfer (S species) through the sample. These findings therefore illustrate the importance of ramp rate and not just final reaction temperature for pyrite decomposition in air. This is in agreement with the work of Schoenlaub where pyrite oxidation was found to be dependant on the length of time of exposure to the oxidising environment and not only on the oxygen concentration within the furnace.[84]

SEM studies have shown that heating the samples in air produces a material that consistently has a morphology significantly different to that previously seen for samples heated in nitrogen. Morphological differences between the inner and outer surfaces of air-samples are also apparent as for N_2 samples. In contrast to samples heated in N_2, the inner material of P-31, P-23, P-24 and P-27 does not appear to have a regular morphology and therefore a highly crystalline structure is not reflected (Figure 3.8). Indeed this inner material is made up of numerous non-uniform cavities providing the appearance of a highly corroded surface. By comparison, the external surface also appears to be very porous but the solid material surrounding these pores is very smooth and rounded (Figure 3.9). Indeed the porosity of pyrite heated in air tended to increase with increasing temperature thus indicating greater decomposition (Figure 3.10). EDS analysis of the samples again reflect the differences in the morphology of the inner and outer surfaces. As for N_2 samples the external surface generally had a much lower S intensity than the inner surface. Indeed sulfur often could not be detected at all on the outer surface. However, in contrast to the other samples heated in air (even P-31, 823K), a slightly higher sulfur concentration was detected on the outside surface of P-23 heated to 923K. This observation is however believed to result from migrated sulfur atoms present on the surface which have not been desorbed. In general, a negligible amount of sulfur was detected on the interior of air-samples compared to those heated in N_2. The approximate Fe:S ratio was normally between 1:0 and 1:0.2. It was observed that with increasing reaction temperature the amount of sulfur tended to decrease. Indeed no sulfur

was detected in sample P-24 which had been heated to 1223K. However, a trace of sulfur was found in sample P-27 (1453K) which had experienced a more rapid heating rate. This observation can be correlated with the slightly lower weight loss suffered by P-27 compared to P-24 and therefore shows a clear correlation between the extent of conversion of FeS_2 to Fe_2O_3 and the amount of sulfur remaining in the resulting material. The increased loss of sulfur from the outer surface and its subsequent removal inwards towards the core of the pyrite sample has also been demonstrated in this series of air-experiments demonstrating the removal of S from the outer surface inwards in a similar manner as that seen in nitrogen.

However entirely different products are generated when pyrite is heated in air rather than N_2 *i.e.* Fe_2O_3 compared to FeS. The morphology of these products are also completely different with N_2 samples being highly structured and air samples being very disordered and highly porous. These factors therefore illustrate the difference in the mechanism of pyrite decay in the various atmospheres. In N_2 a purely thermal process is taking place with heat inputting energy into the pyrite lattice destabilising the structure which in turn gives rise to the release of S. This S species then needs to diffuse to the surface where it can combine with other S atoms to form S_2 before being removed from the system. By comparison in air, the destabilisation of the pyrite lattice again occurs but this time a reaction occurs with the highly reactive O_2. It is therefore suggested that the reaction of $S + O_2$ to form SO_2 is much more rapid than the formation of S_2, indeed the formation of SO_2 is an exothermic process ($\Delta_r H = -296.8$kJ/mol) and will therefore provide more energy to the system. The loss of SO_2 is therefore believed to be faster than S_2 which is consistent with the increased decomposition of pyrite in air compared to nitrogen. Furthermore differences in the rate of SO_2 and S_2 removal are believed to account for the associated morphological differences in the samples. It is suggested that the reduced rate of pyrite decomposition in N_2 allows sufficient time for recrystallisation to occur to produce the highly ordered structure whereas in air this recrystallisation is not apparent.

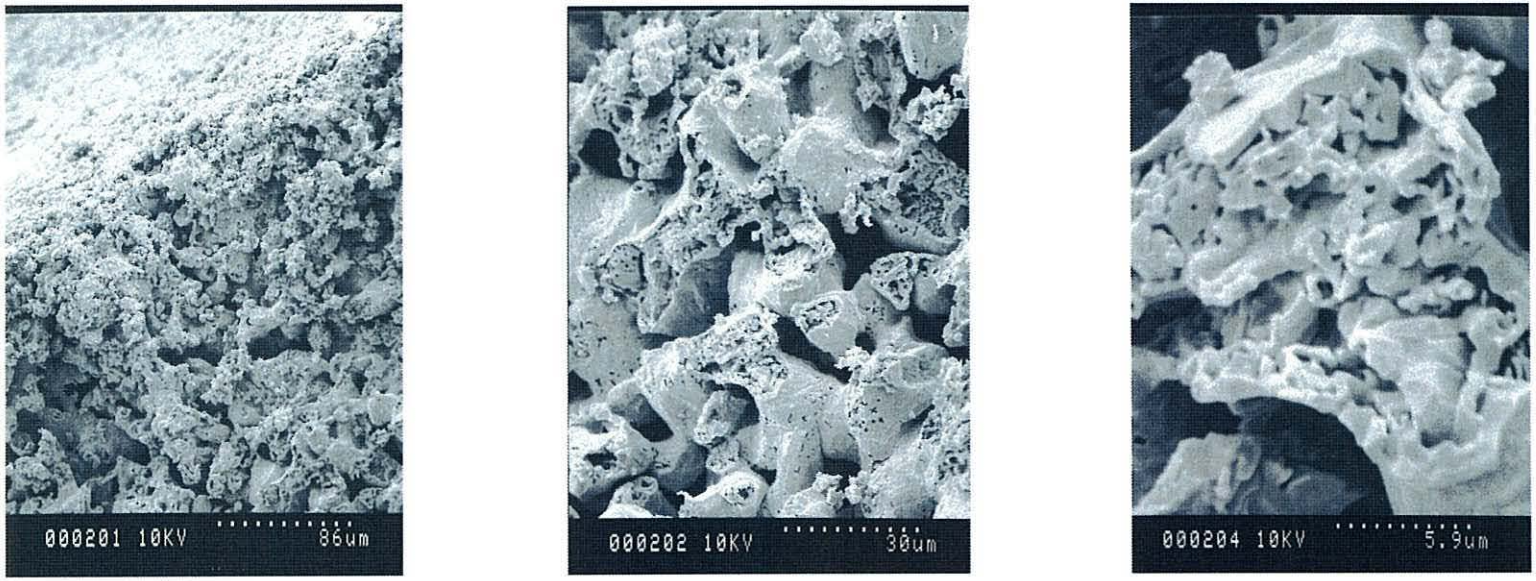

Figure 3.8: SEMs of pyrite in slate (interior, P-24) heated to 1223K in air

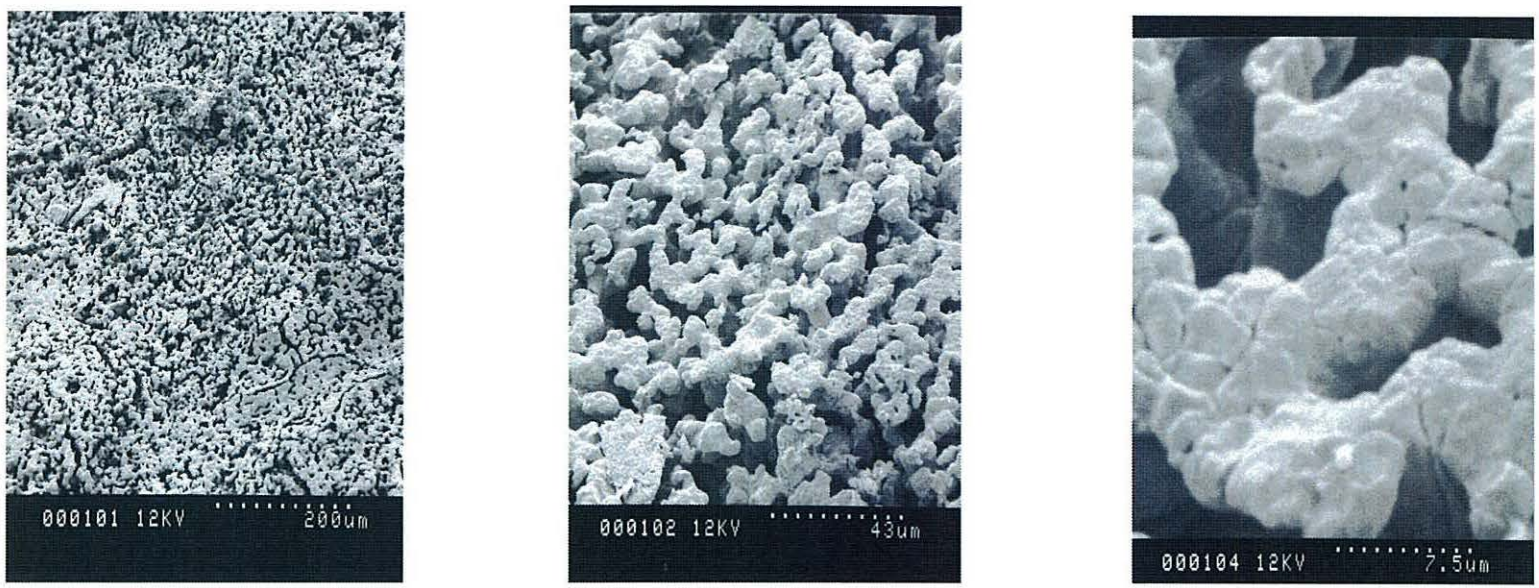

Figure 3.9: SEMs of pyrite in slate (exterior, P-24) heated to 1223K in air

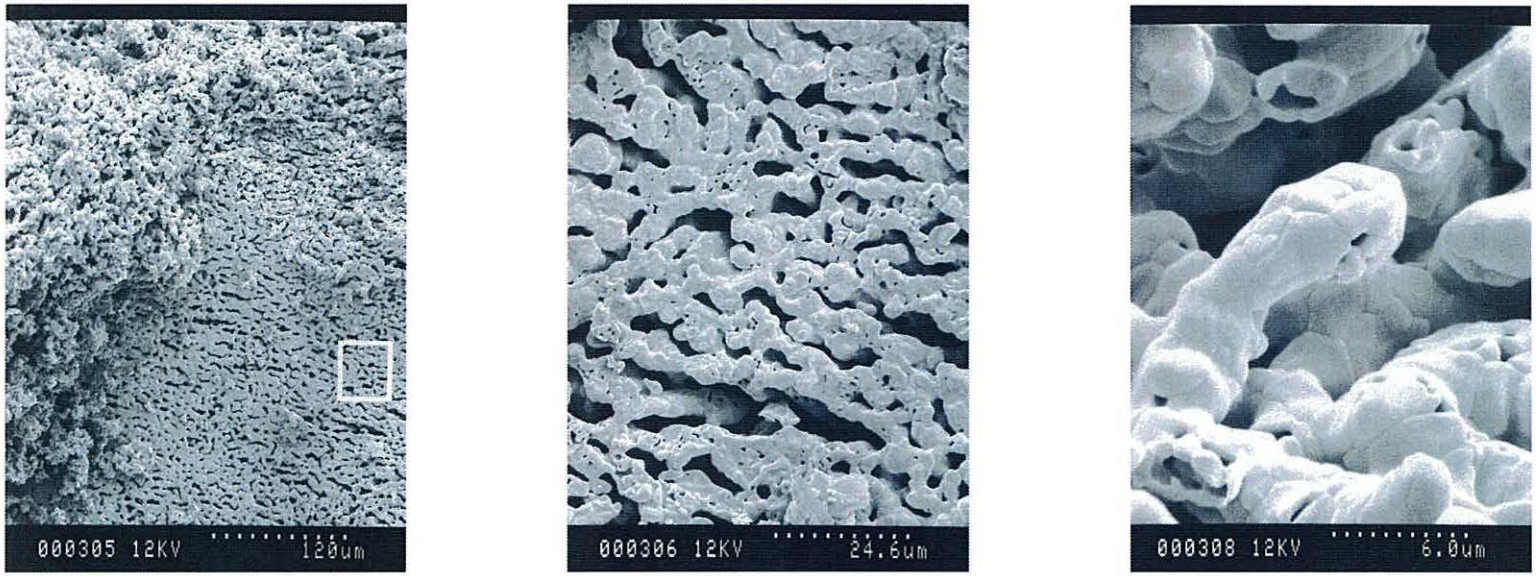

Figure 3.10: SEMs of pyrite in slate (exterior, P-27) heated to 1453K in air

3.5. Pyrite in Slate

The thermal decomposition of pyrite in various atmospheres and even in different host materials such as in coal or in gold ore has been investigated by previous workers and was reviewed in the introduction. The behaviour of this sulfide mineral in slate as it is being heated towards its expansion temperature has not been studied previously.

Slate containing pyrite from both Llechwedd, North Wales (North Vein) and Villar del Rey, Spain has been investigated by comparing the thermal decomposition of various samples in nitrogen and in air. The aim of this study was to gain an understanding of the decomposition of pyrite in slate in various atmospheric conditions to simulate the potential high and low oxygen content regions that might exist in a commercial furnace. Work in this section therefore mainly concentrates on the changes that occur in the pyrite rather than in the slate itself because detailed characterisation of the slate at the various temperatures has been discussed in detail in the slate expansion work in Chapter Two.

Samples from North Wales were chosen which contained a high dispersion of very small pyrite crystals (<1x1x1mm) throughout the slate matrix. These samples are denoted by an SPNW- prefix. Although pyrite crystals within the internal matrix of the slate could not be seen initially, it was assumed due to the high number of crystals on the surface that pyrite would also be present within the interior of the slate sample (Figure 3.11). It was believed and subsequently shown that cutting the slate tablet open after heating would expose the inner crystals. The definition of an inner pyrite surface in the case of pyrite in slate is therefore the pyrite surface present within the interior of the slate structure that has not been exposed to the atmosphere. The crystals present on the surface of the slate are therefore referred to as the outer/exterior pyrite. Spanish slate was found to contain much larger crystals (1-5mm in length), or clusters of crystals, but these crystals generally were fewer in number. The Spanish samples are denoted by an SPS- prefix. The use of Spanish slate with larger pyrite crystals was intended to provide insight into the effect of particle size on the extent of pyrite decay and to aid XRPD identification. The pyrite present in Spanish slate tended to have surfaces protruding out of the slate

structure due to the increased particle size. These surfaces were therefore often exposed to the heating atmosphere and not completely enclosed within the slate structure as in the case of the inner pyrite crystals in Welsh slate. A picture of the large pyrite crystals present in Spanish slate before and after heating in N_2 and in air is given in Figure 3.12.

In this section the work carried out in nitrogen will be discussed first followed by the work in air. For each of the different atmospheres, experimental results obtained from the heating of small pyrite crystals in slate from North Wales will initially be discussed. A comparison with the data gained from the decomposition of larger pyrite crystals in Spanish slate will then be given.

3.5.1. Pyrite in Slate - Decomposition in Nitrogen

A series of experiments have been carried out over 923, 1223 and 1453K as for pyrite. The effects of dwell times at various temperatures and heating rate have also been investigated (see Table 3.4). During the experiments involving slate containing pyrite from North Wales a colourless vapour was again observed from around 823K thus indicating that a reaction had been initiated. As in the case of pyrite-only samples heated in nitrogen this vapour condensed in the cooler parts of the reaction tube forming a pale yellow precipitate consistent with the formation of sulfur. Less yellow precipitate was solidified during the heating of Welsh slate containing pyrite compared to the amount produced during the decomposition of pyrite-only samples. This is believed to reflect the lower levels of pyrite present in the original slate samples. The exhaust gases in the nitrogen experiment were also passed through an iodate solution in order to test for the presence of SO_2 as in pyrite-only experiments in N_2. Slight discoloration was typically observed (very pale yellow) indicating some SO_2. The slate host material had changed upon heating from pale grey to dark charcoal, consistent with the heating of slate in nitrogen. The remains of the small pyrite crystals originally visible on the surface of the slate tablet had also changed in appearance from having a golden colour to becoming completely black. This colour change of the pyrite from gold to black had been previously been seen in pyrite-only samples heated in nitrogen.

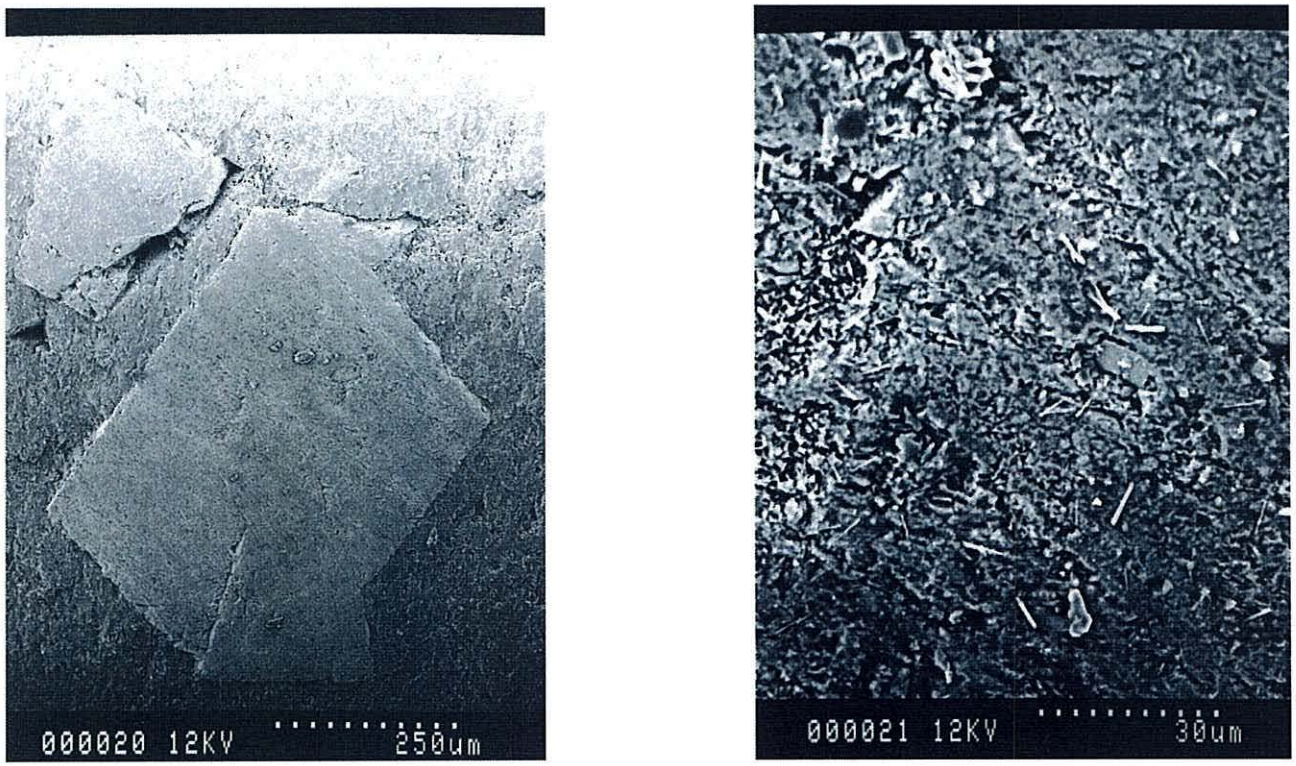

Figure 3.11: SEMs of untreated pyrite

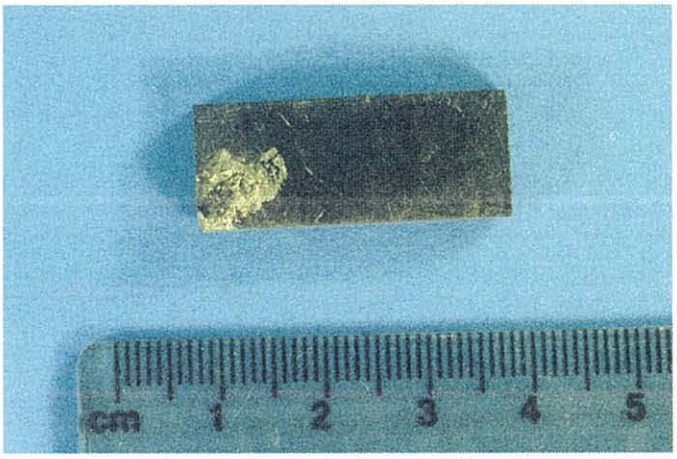

(a)

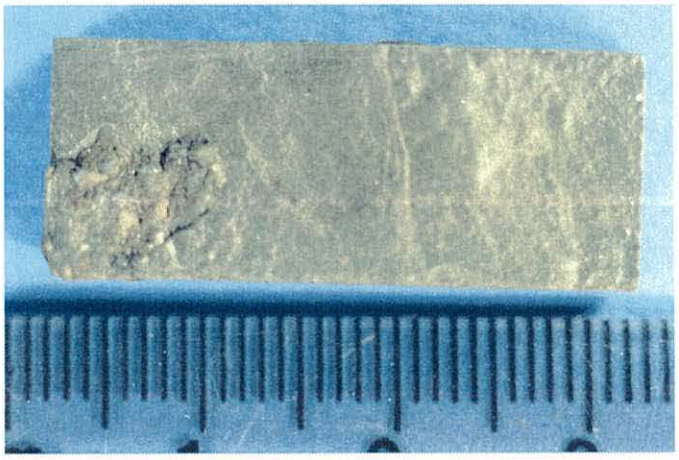

(b)

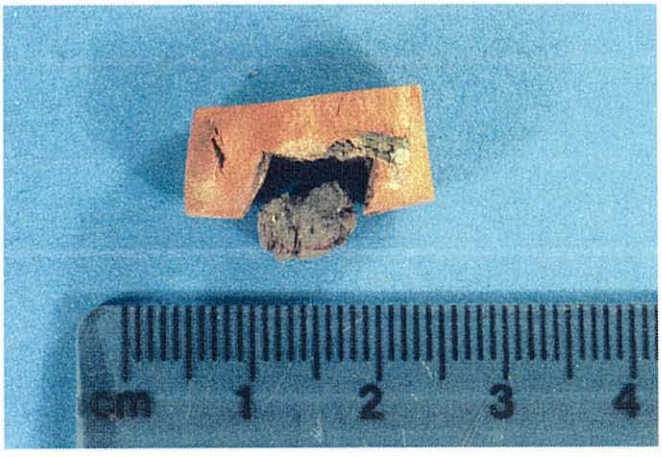

(c)

Figure 3.12: Photograph of Spanish slate tablet containing pyrite (a) before treatment, (b) after heating to 1223K in nitrogen and (c) after heating to 1453 in air.

Table 3.4. Decomposition of pyrite in Welsh and Spanish slate heated in nitrogen.

SAMPLE NAME	GAS USED	DWELL TEMP (K)	HEATING RATE (K/MIN)	DWELL TIME (MIN)	WEIGHT LOSS (WT%)	SAMPLE APPEARANCE
SPNW-DWE45	N_2	923	20	10	2.3	**Slate**: dark grey/charcoal. No expansion **Pyrite**: black external crystal. Internal crystals retain a golden lustre.
SPNW-DWE46	N_2	1223	20	10	6.1	**Slate**: dark grey/charcoal. No expansion. **Pyrite**: black crystals on outer surface. No crystals within sample observed.
SPNW-DWE18	N_2	923 1453[a]	10	1-2 1	1.2 7.2	**Slate**: dark grey/charcoal. **Pyrite**: external crystals black and decomposed, internal crystals remain pyrite colour (923K).
SPS - DWE41	N_2	923	20	10	3.4	**Slate**: dark grey/charcoal. **Pyrite**: black, soft (easily cut).
SPS - DWE42	N_2	1223	20	10-15	8.3	**Slate**: dark grey/charcoal. Slight splitting, no expansion. **Pyrite**: external material black, soft. Large internal cluster retains golden colour.
SPS - DWE40	N_2	1453	20	10-15	8.5	**Slate**: dark grey/charcoal. Approx. 2 fold expansion. **Pyrite**: black, soft (easily cut).

Note: [a]denotes sample analysed after being heated to 923K, cooled overnight then reheated to1453K.

A sample was initially heated to 923K (SPNW-45). As expected no expansion of the slate sample had occurred by this temperature however a weight loss of 2.3% was recorded. It is believed that this loss is mainly due to the initial dehydration of the surface water from the slate. However the release of white vapour, believed to be sulfur due to its precipitation as a light yellow precipitate, during heating also inevitably contributes to the overall loss in mass. The X-ray diffraction analysis of pyrite in slate heated in N_2 is summarsied in Table 3.5. SPNW-45 produced peaks consistent with the partial decomposition of chlorite and muscovite *i.e.* only the peaks corresponding to the {001} plane of both minerals had disappeared. Quartz was also detected as one of the major phases (see slate expansion work in Chapter 2). The presence of these peaks was consistent with the data obtained during analysis of the expansion process. Weak peaks corresponding to pyrite were also resolved thus indicating that complete decomposition of pyrite within the slate had not occurred. A small peak, d-spacing 2.1Å, corresponding to the major peak of the reference pattern for troilite (pyrrhotite) (11-0151).[164] However due to a complex series of peaks corresponding to the minerals present in partially decomposed slate it has been extremely difficult to conclusively determine by XRPD that FeS is indeed present in the heated sample. Furthermore, XRPD analysis of the black residue found where the original external pyrite crystals had been located prior to heating was not possible due to its low concentration on the surface of the sample. However following the findings of pyrite-only experiments it was believed that this black material was likely to be pyrrhotite or troilite.

Energy dispersive spectrometry has been found to be more useful than XRPD in the characterisation of decomposed pyrite in slate samples since small areas of the sample can be focussed on for analysis thus eliminating the problems associated with low mineral concentration. EDS analysis of the outer surface of SPNW-45 generally recorded a higher S intensity than Fe (Fe:S ratio ~1:1.5) which is consistent with pyrrhotite minerals ($Fe_{1-x}S$) rather than FeS (troilite) being present. This is consistent with XRPD data obtained for the pyrite-only samples P-22 and P-38 which had also been heated to 650°C in nitrogen. Once the sample (SPNW-45) was cut to reveal the interior, initial observations of the pyrite crystals located within the interior of the slate tablet

showed that these crystals had retained some of the golden coloration of unheated pyrite. Analysis by EDS focussing on the inner crystals confirmed that pyrite remained within the slate since a Fe:S ratio in the order of 1:3 was detected producing a pattern very similar to the reference EDS pattern of unheated pyrite in Figure 3.1(a). The presence of pyrite correlates with the weak pyrite peaks present in the X-ray diffraction pattern. It is therefore apparent that heating slate to 923K is not sufficient to ensure complete pyrite decomposition in slate in N_2. Morphological differences in the inner and outer pyrite crystals observed by SEM analysis of SPNW-45 also correlates with the supposition that pyrite remains relatively unchanged within slate's core. Pyrite exposed on the exterior of the slate had become more porous upon heating and retained a structured appearance which is more consistent with that seen in the inner surface of pyrite-only samples (Figure 3.13). Crystals in the interior of the slate appear to have retained the shape of typical undecomposed pyrite with no visible corrosion (Figure 3.14).

Table 3.5. Summary of XRPD data of pyrite in slate from Wales and Spain heated in N_2.

Temp (K)	Atmos	Welsh Slate		Spanish Slate	
		Sample	XRD Inference	Sample	XRD Inference
923	N_2	SPNW-45	Quartz, muscovite and chlorite peaks. FeS_2 detected. Trace FeS detected No Fe_2O_3 detected	SPS-41	Quartz, muscovite and chlorite peaks. No FeS_2 detected No FeS detected No Fe_2O_3 detected
1223	N_2	SPNW-46	Quartz and muscovite peaks. No chlorite No FeS_2 detected Trace FeS detected No Fe_2O_3 detected	SPS-42	Quartz and muscovite peaks. No chlorite No FeS_2 detected No FeS detected No Fe_2O_3 detected.
1453	N_2	SPNW-18	Quartz, mullite and hercynite peaks. No FeS_2 detected No FeS detected No Fe_2O_3 detected	SPS-40	(Crystal only) Peaks corresponding to FeS detected.

Figure 3.13: SEMs of pyrite in slate (exterior, SPNW-45) heated to 923K in nitrogen

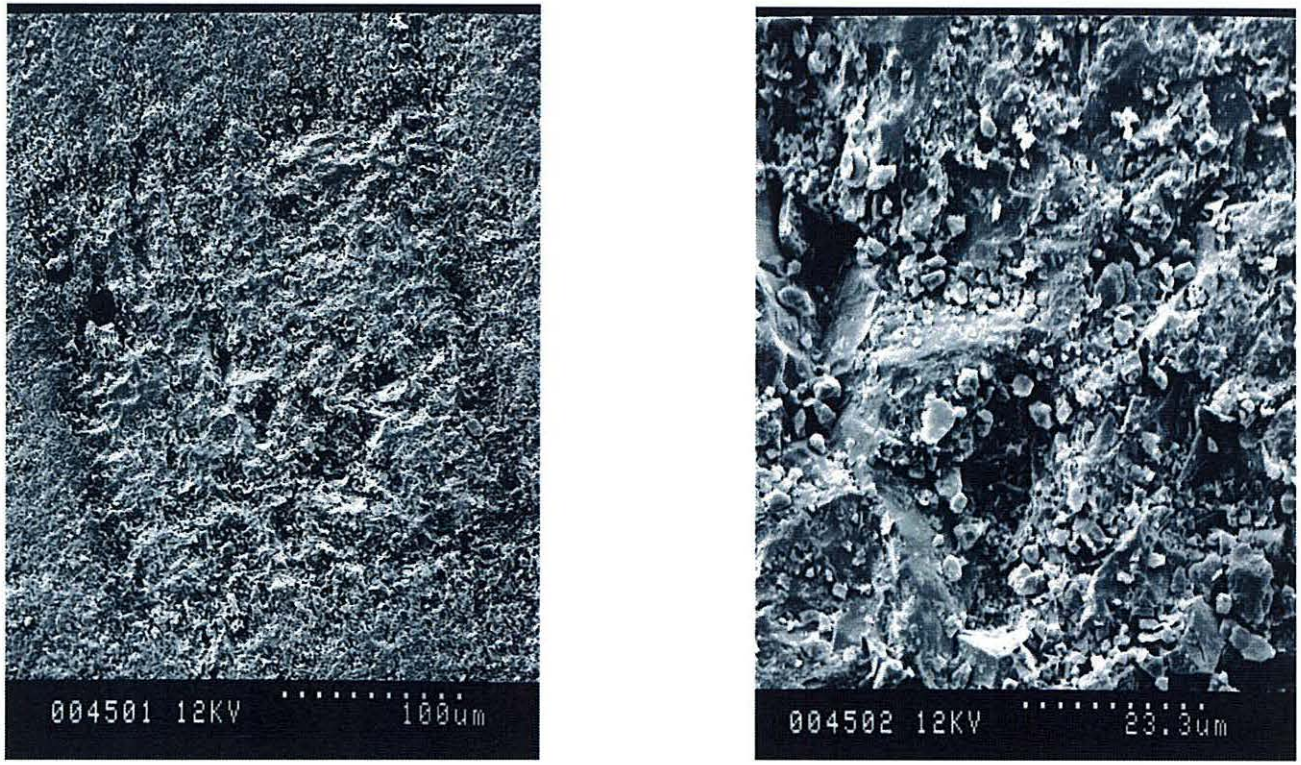

Figure 3.14: SEMs of pyrite in slate (interior, SPNW-45) heated to 923K in nitrogen

Subsequent samples, SPNW-46 and SPNW-18, were heated to higher temperatures namely to 1223 and 1453K respectively. XRPD analysis of SPNW-46 did not show any evidence for the presence of pyrite (Table 3.4). However in contrast to SPNW-45 heated to 923K, peaks corresponding to troilite instead of pyrrhotite are believed to be present in the diffraction pattern of SPNW-46 (1223K). However, as discussed for XRPD characterisation of SPNW-45 (923K), the conclusive identification of troilite in SPNW-46 is difficult due to the complexity of the diffraction pattern and the relative weak concentration of the sulfide mineral within the treated slate. Energy dispersive spectroscopy of sample SPNW-46 again detected sulfur on both the outer and inner "pyrite" surfaces. The inner surface consistently produced spectra that had a stronger S peak than that of the outer surface. The Fe:S ratio of the inner surface was generally around 1:1.5. This ratio normally reduced to 1:1 on the outer surface, as had previously been seen for SPNW-45. The inner crystals of SPNW-46 appeared by SEM to be more porous than the original pyrite crystal with a regular, structured morphology (Figure 3.15). Furthermore, almost spherical cavities could be seen that may have indicated the entrapment of a gas within the pyrite crystal during heating. Scanning electron micrographs therefore indicate a greater decomposition in the inner pyrite crystals of SPNW-46 compared to SPNW-45 since a more porous material was apparent in SPNW-46. The exterior surface appears to be significantly more porous with a wide distribution of non-uniform cavities. Here again some order within the material is visible as illustrated by the pseudo-hexagonal layered arrangement shown in Figure 3.16.

SPNW-18 initially underwent a pre-heating stage up to a temperature of 923K. Upon cooling, analysis of the resultant material correlated well with that previously observed for SPNW-45. Subsequently SPNW-18 was heated to 1453K with a relatively slow heating rate (10K/min). XRPD analysis of the sample did not provide any information on the presence of pyrite, pyrrhotite nor troilite within the treated slate (Table 3.4). SEM studies however show that both the external and internal pyrite crystals have undergone substantial atomic rearrangement during heating. The interior appeared to have an ordered structure with pseudo-hexagonal crystals similar to SPNW-46 (Figure 3.17). These crystals were larger than previously seen in Figure 3.15 and is believed to reflect

the higher temperature sustained by SPNW-45 which has enabled greater recrytallisation to take place *i.e.* more time to allow greater crystal growth. S could not be easily resolved from the EDS pattern produced during analysis of SPNW-45 due to being coated with gold to form a conducting surface. The gold peak often overlaps S. However on occasion a shoulder (S peak) was visible producing Fe:S ratio ~1:1. The outer surface appears to contain material that is highly ordered over a macroscopic scale (Figure 3.18). This material can also be seen as raised "bubbles" above the plane of the slate itself. One reason is believed to be the release of S vapour during the decomposition of pyrite becoming trapped underneath the outer FeS crust hence bloating the material out of its original cavity. Indeed, where these "bubbles" have burst or broken the approximately cubic cavity of the original pyrite can be seen thus illustrating the complete loss of FeS_2 since only craters remain. The relatively slow heating rate incurred by SPNW-18 therefore appears to effectively control the loss of sulfur which in turn allows sufficient time for atomic rearrangement to take place in order to produce the apparent ordered structure. Decomposition of small FeS_2 crystals within slate tablets requires temperatures *ca.* 1453K in order to ensure the maximum amount of pyrite decay.

The effect of heat on larger pyrite crystals within slate has also been investigated. Spanish slate was used in these tests since pyrite crystals in slate from North Wales tended to be around 1x1x1mm in size. The first experiment involved the heating of sample SPS-41 to 923K. The inner surface of SPS-41 appeared to be more porous (Figure 3.19) than the inner pyrite crystals of SPNW-45. By comparison the outer surface was made up of a relatively featureless material that appeared to have been recrystallised from a molten state. This outer material appears to produce a skin or crust around the interior of the treated pyrite crystal. However EDS study of the interior of the sample showed areas of very high sulfur concentration. Indeed the Fe:S ratio ranged from 1:2 to 1:4. This is believed to reflect the increased diffusion limitations of the larger pyrite crystal. The relatively smooth outer crust however generally had a much lower sulfur intensity (Fe:S ~1:1.5) consistent with SPNW-45.

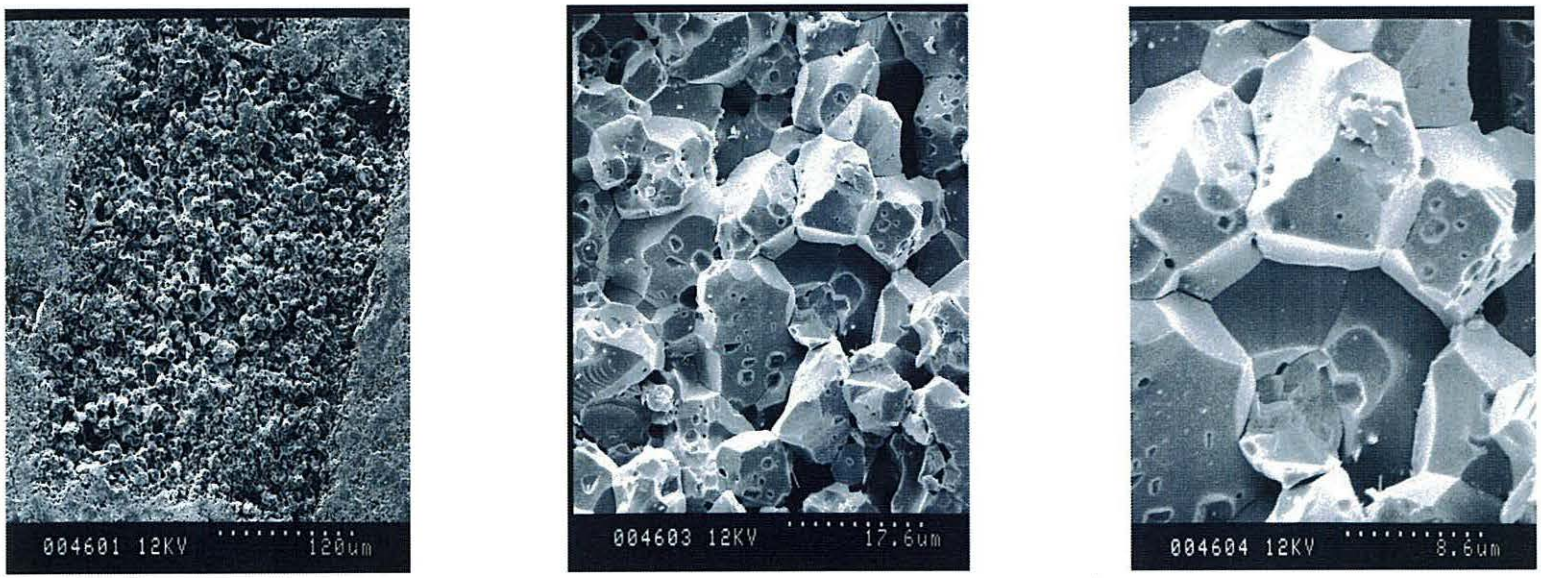

Figure 3.15: SEMs of pyrite in slate (interior,SPNW-46) heated to 1223K in nitrogen

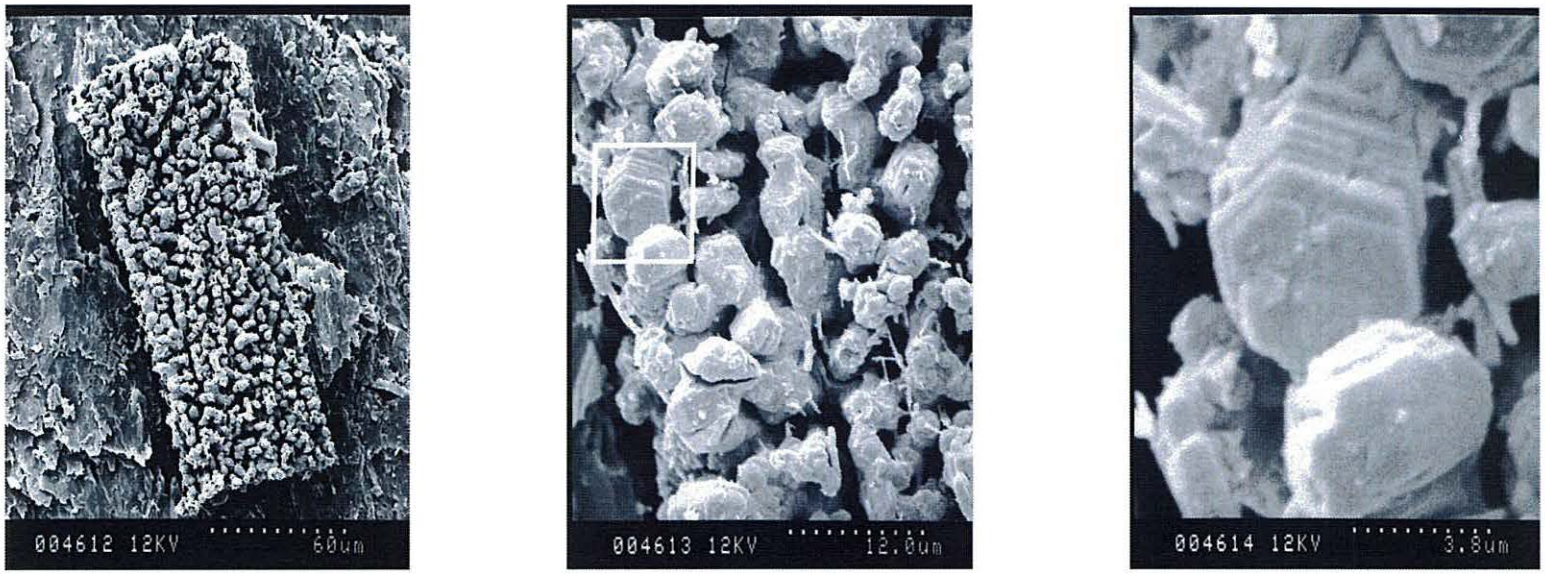

Figure 3.16: SEMs of pyrite in slate (exterior, SPNW-46) heated to 1223K in nitrogen

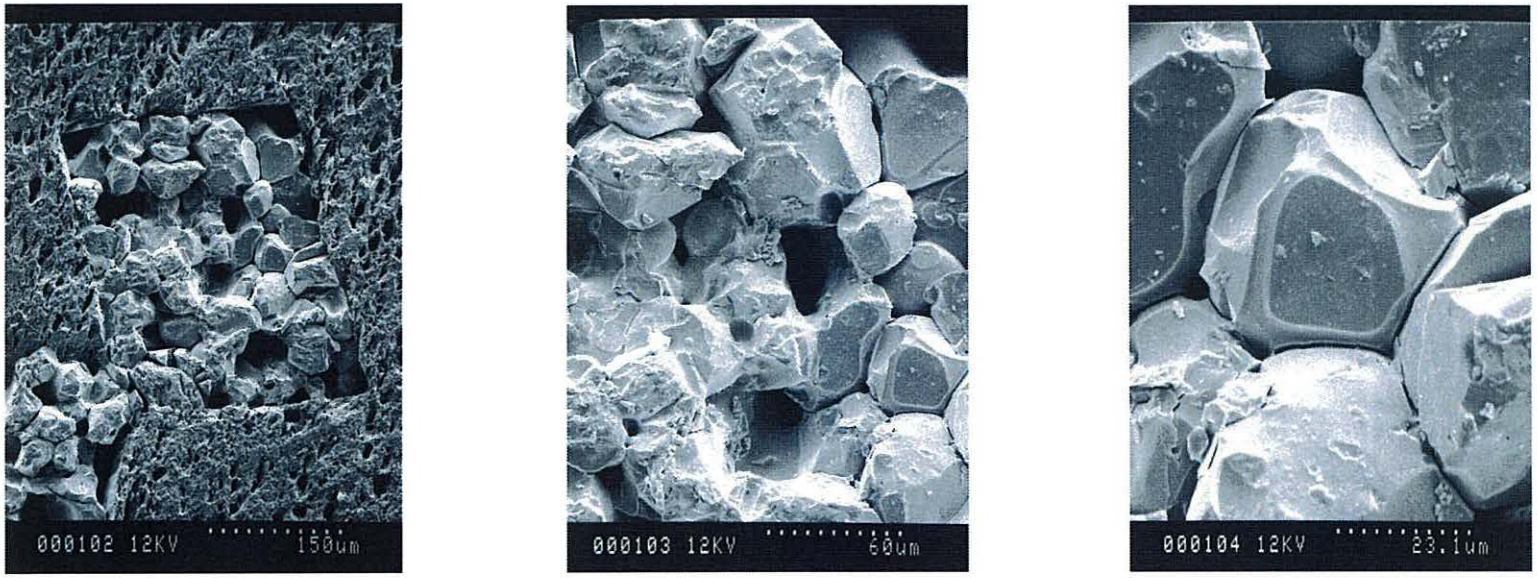

Figure 3.17: SEMs of pyrite in slate (interior, SPNW-18) heated to 1453K in nitrogen

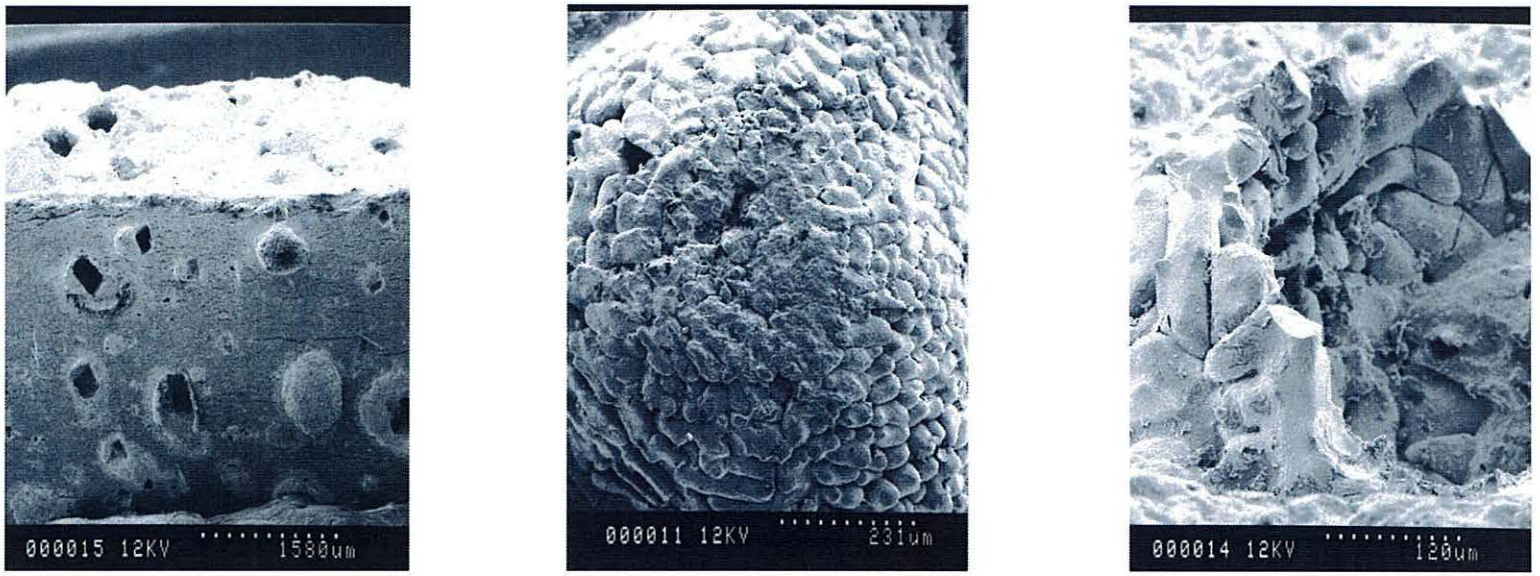

Figure 3.18: SEMs of pyrite in slate (exterior, SPNW-18) heated to 1453K in nitrogen

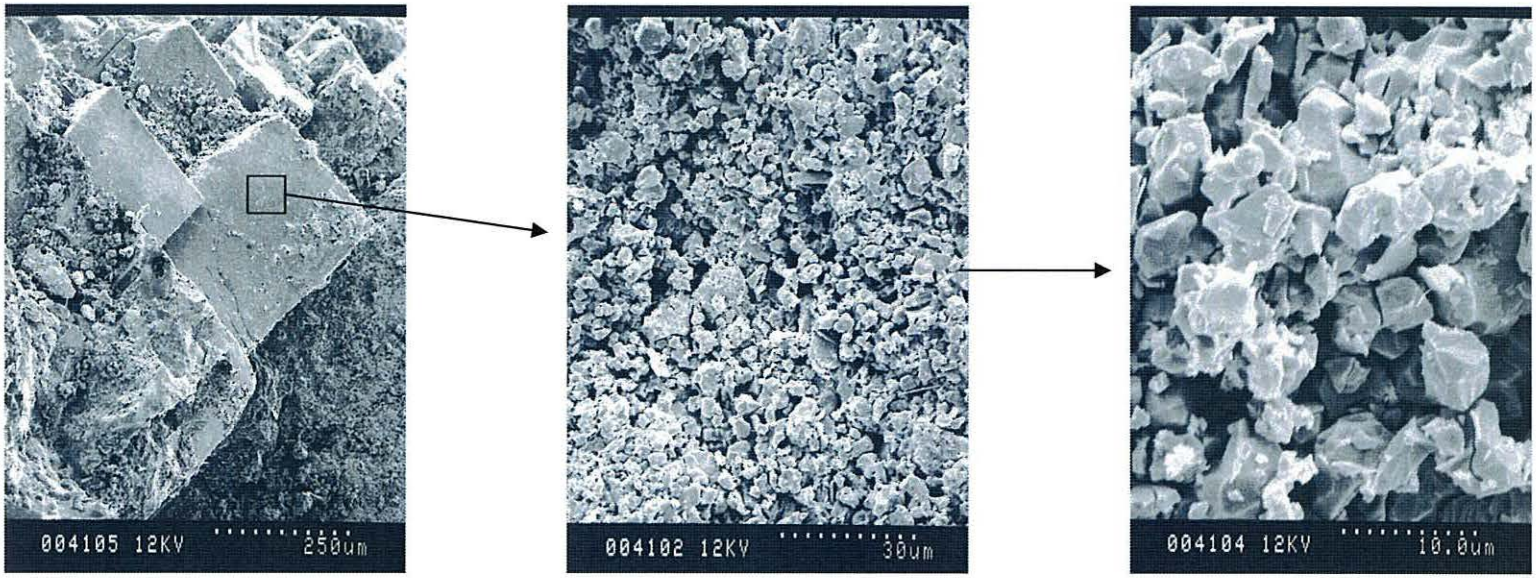

Figure 3.19: SEMs of Spanish pyrite in slate (interior, SPS-41) heated to 923K in nitrogen

Heating samples, SPS-42 and SPS-40, to higher temperatures 1223 and 1453K respectively, resulted in a reduced level of sulfur being detected by EDS compared to SPS-41. Indeed analysis of the heated pyrite crystal in SPS-42 (1223K) consistently had a much lower S concentration than SPS-41 (923K) in both the inner and outer surfaces. In the interior of the sample the Fe:S ratio was found to be around 1:1.5. The increased S intensity reflects the presence of some $Fe_{1-x}S$ within the crystal. However since the Fe:S ratio is close to 1:1 the major phase is believed to be troilite (FeS) in accordance with that found in P-52 heated to 1223K in nitrogen. The exterior however produced an energy dispersive spectrum having a much more even Fe:S ratio that was indeed closer to 1:1 than observed in the interior of the sample again reflecting increased pyrite decomposition on this outer surface thus illustrating the loss of S from the outer surface first. SEM also correlated with the S difference between the outer and inner surface since the outer surface appeared more porous and less ordered (Figure 3.20). By comparison a rounded pseudo-hexagonal shape could be seen in the inner crystals (Figure 3.21).

By comparison S in the interior of SPS-40 (1453K) was higher than that in the interior of SPS-42 (1223K), even though a higher temperature was reached. Two different morphologies could be seen in SPS-40. The first had a relatively featureless appearance with very little pores (Figure 3.22(a)). This generally produced EDS patterns with high S. The Fe:S ratio here was found to approximate 1:2.5 which is closer to that found in untreated pyrite (Figure 3.1(a)) than FeS (Figure 3.1(b)). It is therefore believed that only a small proportion of S had infact been lost from this area. This believed to reflect the larger size of the pyrite cluster reducing the rate of S diffusion through the sample resulting in less decomposition. By comparison, surrounding this apparent featureless material, a more corroded surface could be seen (Figure 3.22(b)). A Fe:S ratio ~1:0.25 was detected here. The reduced S is believed to be due to the fact that this area had been exposed to the atmosphere during heating thus had been able to lose more S *i.e.* mass transfer though the slate was not as much of a limiting factor to its decomposition. XRPD analysis of the decomposed pyrite crystal showed peaks corresponding to FeS (11-0151),[164] however no peaks corresponding to pyrite were found (see Table 3.5). The S intensity on the outer surface was found to be much lower than both SPS-41 (923K)

and SPS-42 (1223K). This shows that the increased size of the pyrite crystal does not effect the loss of S from the outer surface *i.e.* S is continually lost from the outer surface as temperature increases irrespective of particle size. It is therefore clear that particle size is an important factor when considering the extent of pyrite decomposition. Work by Montano[86] and Yperman[77] also reported on the influence of particle size on pyrite decomposition. Yperman carried out tests on pyrite in a reducing atmosphere, he believed that smaller grains were more accessible to attack by H_2 due to their increased relative external surface area and therefore were more susceptible to decay. Indeed it was reported that the maximum reduction temperature decreased as the particle size decreased. In this present study tests were carried out in nitrogen therefore attack by a reactive species (H_2) did not occur. In this case the accessibility of the interior of large pyrite crystals to thermal attack is believed to be the important factor to ensure maximum decomposition.

3.5.2. Pyrite in Slate - Decomposition in Air

The behaviour of pyrite in slate when heated in air has also been studied in order to compare the extent of pyrite decomposition with that previously studied in section 3.2.1. As for the nitrogen experiments, the effect of temperatures between 923-1453K on small pyrite crystals in Welsh slate will be discussed first before moving on to Spanish slate which tended to have much larger crystals incorporated into the slate structure (Table 3.6). As a result of the larger crystal size of pyrite in Spanish slate these crystals often had surfaces exposed to the atmosphere during heating and therefore were generally not completely encased within the slate structure.

During this series of experiments a yellow precipitate was not produced. This suggested that elemental sulfur was not generated. To confirm the identity of the exhaust gas, it was passed through an iodate solution. In accordance with the heating of pyrite-only samples the release of SO_2 is again believed to occur during the treatment of pyrite-containing slate samples. Furthermore in all cases the slate became a burnt orange/brown colour consistent with heating in this oxidising atmosphere.

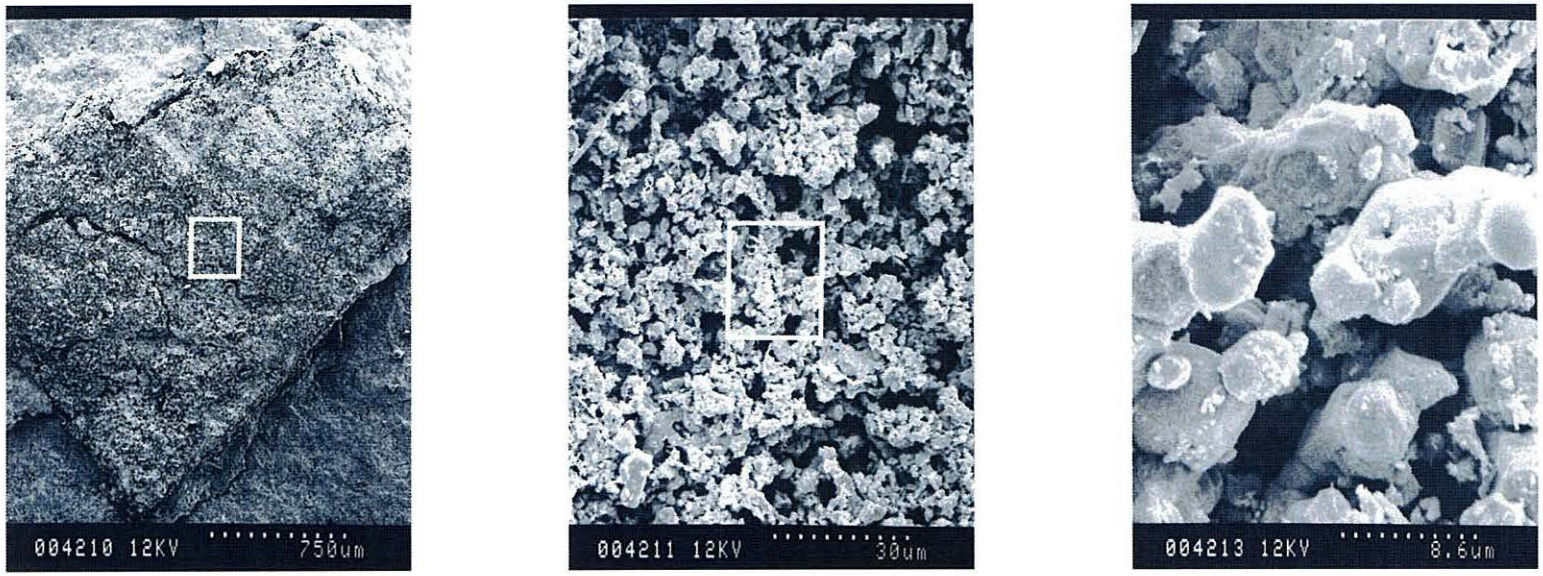

Figure 3.20: SEMs of Spanish pyrite in slate (exterior, SPS-42) heated to 1223K in nitrogen

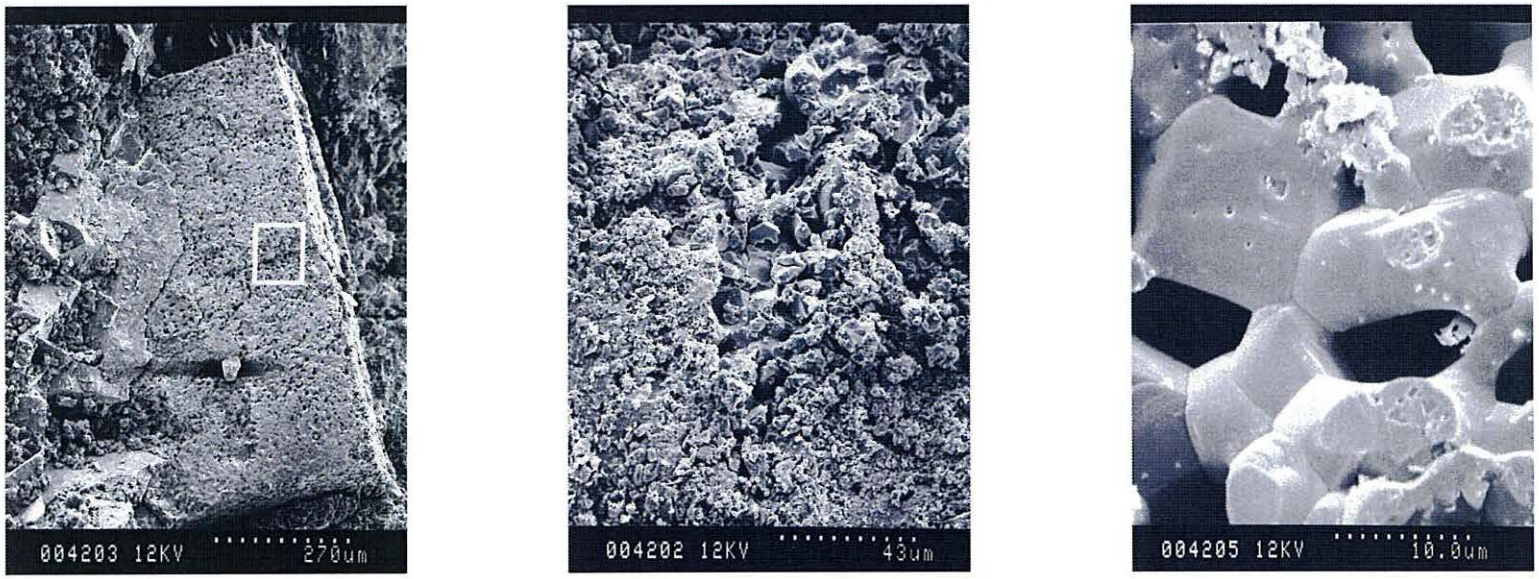

Figure 3.21: SEMs of Spanish pyrite in slate (interior, SPS-42) heated to 1223K in nitrogen

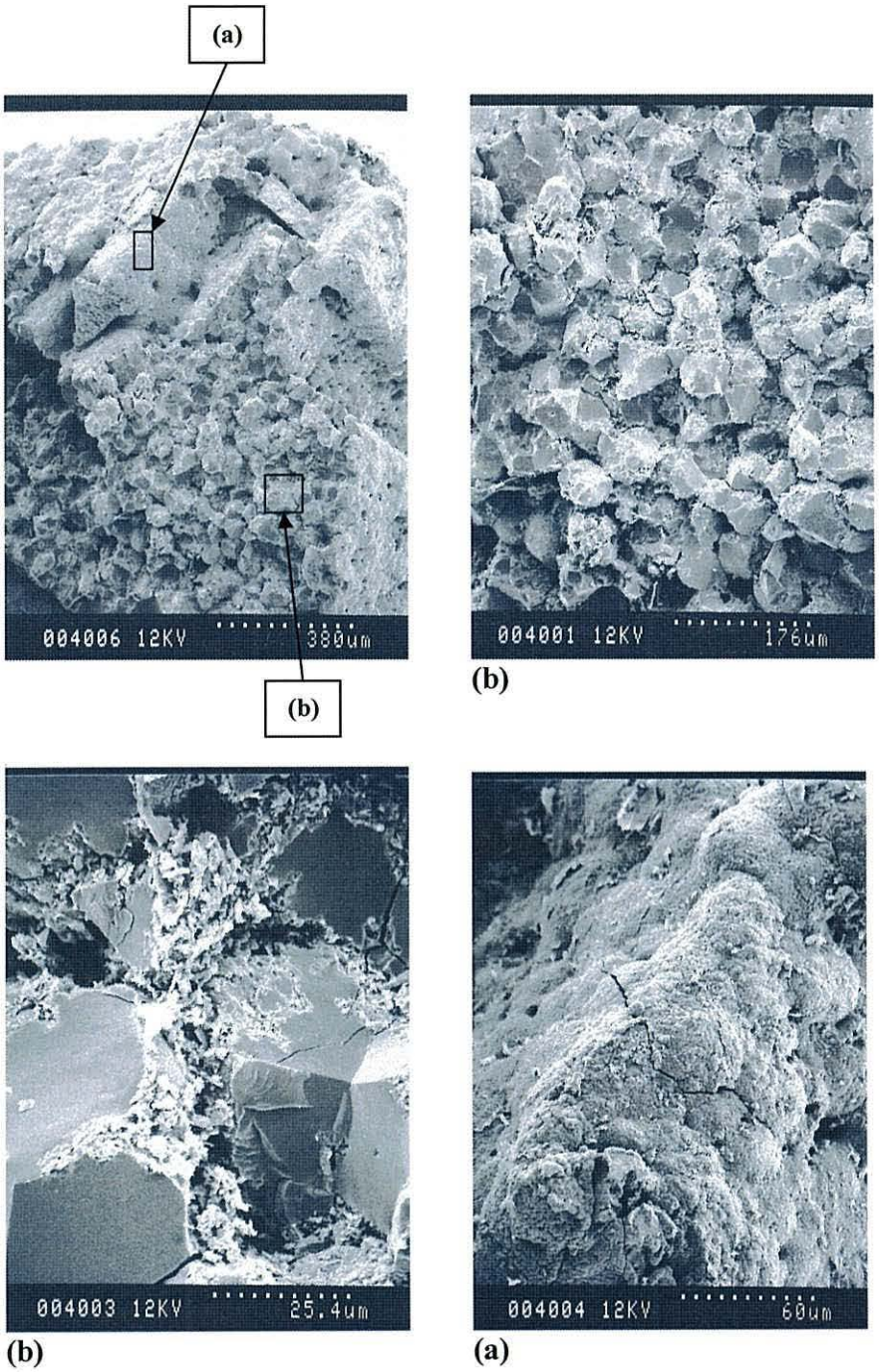

Figure 3.22: SEMs of Spanish pyrite in slate (interior, SPS-40) heated to 1453K in nitrogen

Table 3.6. Decomposition of pyrite in Welsh and Spanish slate heated in air.

SAMPLE NAME	GAS USED	DWELL TEMP (K)	HEATING RATE (K/MIN)	DWELL TIME (MIN)	WEIGHT LOSS (WT%)	EXPERIMENTAL OBSERVATIONS
SPNW-DWE47	Air	923	20	10-15	2.1	**Slate**: burnt orange/brown. **Pyrite**: bright red/orange external crystals, slight lustre.
SPNW-DWE48	Air	1223	20	10	4.8	**Slate**: burnt orange/brown. **Pyrite**: dark red/black crystals.
SPNW-DWE19	Air	1453	10	1	6.4	**Slate**: burnt orange/brown. Slight expansion <2 fold. **Pyrite**: black residue on slate surface.
SPNW-DWE26	Air	1453	20	15	7.3	**Slate**: burnt orange/brown. 2fold expansion **Pyrite**: black crystals, slight lustre.
SPNW-DWE30	Air	923 1453	20	900 15	14.0	**Slate**: burnt orange/brown. Good expansion 3-4 fold. **Pyrite**: black crystals on outer surface. No visible pyrite in core.
SPNW-DWE32	Air	923 1453	20	1200 15	11.9	**Slate**: burnt orange/brown. Good expansion 3-4 fold. **Pyrite**: external crystals blackened. No apparent internal crystals.
SPS - DWE29	Air	923 1453	20	1440 10	6.5	**Slate**: burnt orange/brown. Pyrite: bright red crystal, exterior darker red.
SPS - DWE33	Air	923 1453	20	1080 1-2	8.5	**Slate**: burnt orange/brown. **Pyrite:** dark red/black crystal.
SPS - DWE34	Air	923 1453	20	120 10	4.7	**Slate**: burnt orange/brown. Slight expansion. **Pyrite:** black crystal
SPS - DWE20	Air	1453	10	1-2	17.7	**Slate**: burnt orange/brown. 2 fold expansion **Pyrite:** black crystal, slight glassy lustre.
SPS - DWE28	Air	1453	20	15	5.1	**Slate**: burnt orange/brown. 3 fold expansion. **Pyrite:** black crystal, slight glassy lustre.

Heating Welsh slate to 923K (SPNW-47) produced a material that appeared to have small dark red crystals on the outside surface where the pyrite crystals had originally been located. The colour of this material was consistent with the pyrite samples studied in section 3.4 that were heated in air. In accordance with the initial study the dark red material found on the surface of heated slate samples was therefore also believed to be haematite *i.e.* oxidised Fe. However, XRPD analysis did not show any evidence of Fe_2O_3 or any other Fe containing mineral (see Table 3.7). Analysis by EDS did show a high Fe concentration with generally no sulfur peaks (trace S detected on random areas only). SEM studies of this external dark red material showed that a porous, irregular morphology consistent with the oxidation of pyrite-only samples at 923K providing confirmation that pyrite decomposition had in fact occurred on the external surface of the slate sample (Figure 3.23). Differences in the morphology of the pyrite crystals located within the internal structure of the slate were apparent. Little decomposition was evident by SEM analysis, as the inner crystals appeared intact and had retained a structure that correlated well with that of unheated pyrite (Figure 3.24). Indeed energy dispersive spectroscopy of the inner crystals did produce relatively strong sulfur peaks that in areas produced a Fe:S ratio between 1:3 and 1:3.5 consistent with pyrite (see Figure 3.1(a)).

Table 3.7. Summary of XRPD data of pyrite in slate from Wales and Spain heated in Air.

Temp (K)	Atmos	Welsh Slate		Spanish Slate	
		Sample	XRD Inference	Sample	XRD Inference
923	Air	SPNW-47	Quartz, muscovite and chlorite peaks. No FeS_2 detected No Fe_2O_3 detected No FeS detected	SPS-43	Quartz, muscovite and chlorite peaks. No FeS_2 Fe_2O_3 detected.
1223	Air	SPNW-48	Quartz and muscovite peaks. No chlorite No FeS_2 detected No Fe_2O_3 detected No FeS detected	SPS-44	Quartz and muscovite peaks. No chlorite No FeS_2 detected Fe_2O_3 detected.
1453	Air	SPNW-19	Quartz, mullite and hercynite peaks. No FeS_2 detected No Fe_2O_3 detected No FeS detected	SPS-20	(Crystal only) Peaks corresponding to Fe_2O_3 and Fe_3O_4 detected.

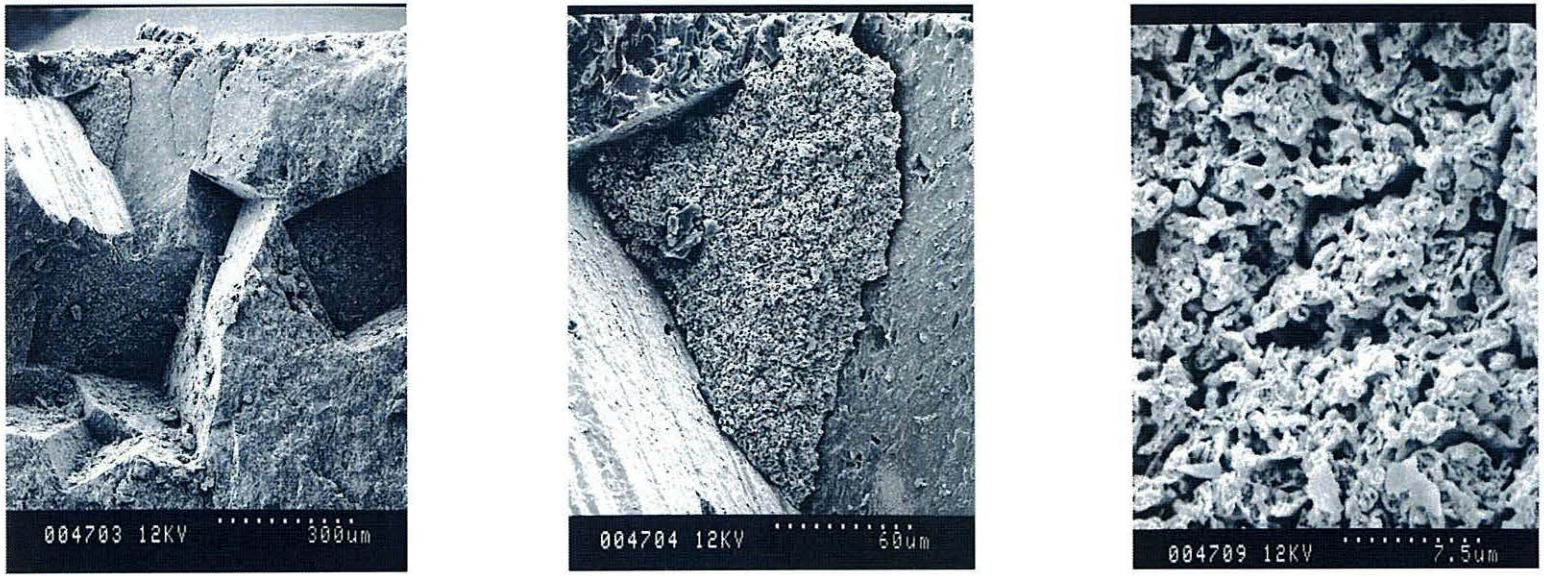

Figure 3.23: SEMs of pyrite in slate (exterior, SPNW-47) heated to 923K in air

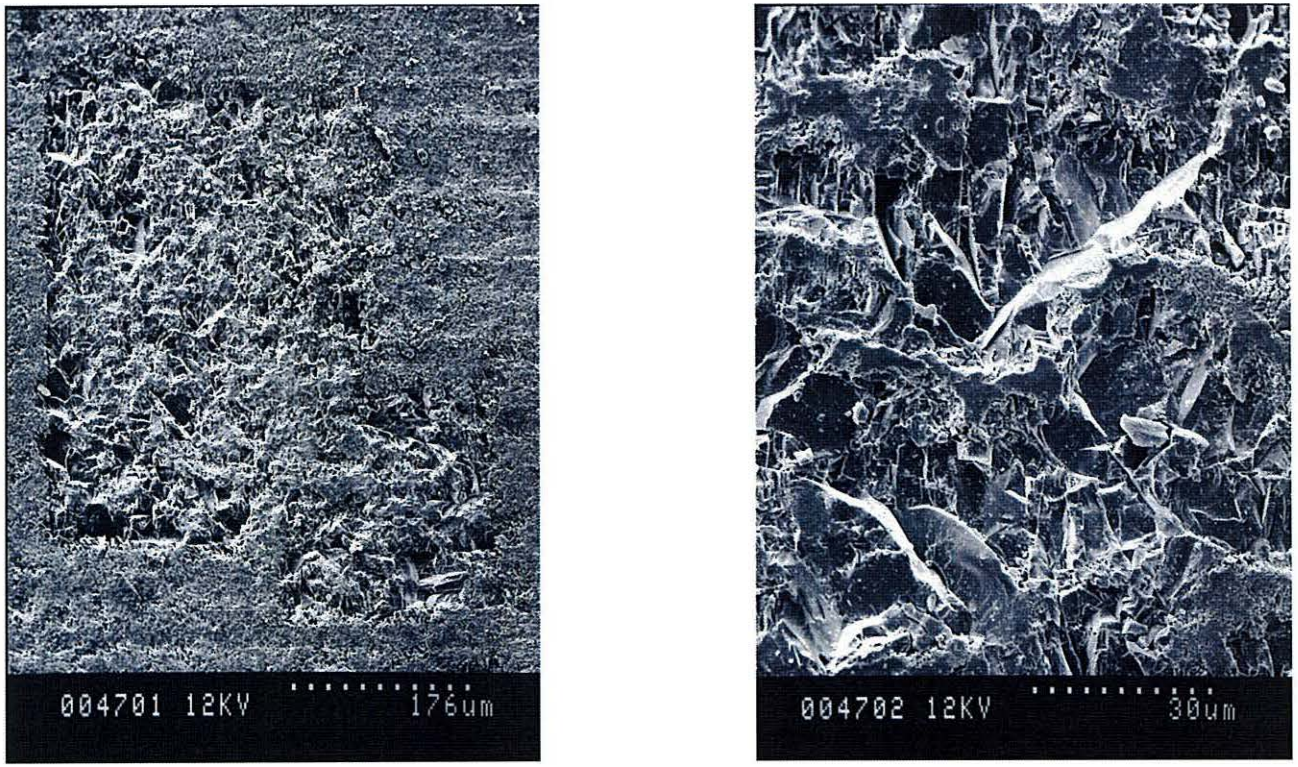

Figure 3.24: SEMs of pyrite in slate (interior, SPNW-47) heated to 923K in air

Evidently decomposition of the inner pyrite crystals had not been established by heating SPNW-47 to 923K in air since very little S had been lost. This is clearly in contrast to the decomposition observed in pyrite-only samples heated to 923K in air since no evidence was obtained for pyrite could be found and weight loss calculations determined that a 92.5% conversion to troilite had occurred in sample P-23. The enclosure of pyrite crystals within the slate structure of sample SPNW-47 therefore appears to inhibit the rate of pyrite decay. Thus illustrates that slate acts as a barrier reducing S diffusion to the exterior of the sample. Furthermore slate is a good thermal insulator may reduce heat transfer within the slate thus potentially reducing the thermal effect of the external heat source on the inner pyrite crystals. In order to investigate this hypothesis and the effect of increasing temperature on the decay of pyrite within slate subsequent samples were heated to 1223 and 1453K respectively.

The X-ray diffraction pattern of SPNW-48 (1223K) did not provide any information on whether the sample contained any pyrite or haematite. Electron microscopic analysis of samples SPNW-48 clearly showed that decomposition of the pyrite crystals within slate had been initiated this time since more cavities could be seen in the "pyrite" crystal. This internal material appeared to be more ordered than that normally found in pyrite-only samples heated in air. Indeed a morphology similar to SPNW-46 (1223K, N_2) was identified (see Figure 3.14). This suggests that pyrite crystals located within slate decompose in a similar manner irrespective of atmosphere. This shows that crystals held in slate are effectively isolated from the external atmosphere and therefore not affected by it to a great extent. EDS analysis showed that the sulfur intensity of pyrite within SPNW-48 (1223K) was significantly lower than previously detected in SPNW-47 (923K). Although the sulfur concentration remained higher than iron, a Fe:S ratio of less than 1:2 was generally recorded thus indicating that pyrite is no longer the species present inside the slate tablet.

XRPD analysis of SPNW-19 (1453K) did however have weak intensity peaks that correlate well the diffraction pattern of haematite. SEM analysis of inner pyrite again showed a porous material which appeared to have some order to its structure more

closely related to slate samples heated in N_2 than pyrite-only samples in air (Figure 3.25). A Fe:S ratio ranging from 1:1.5 to 1:0.5 was seen in the interior of SPNW-19 which suggests that total pyrite conversion to haematite has not occurred within slate even at 1453K. Indeed the relative S intensity was found to be similar to that found in SPNW-18 heated to 1453K in N_2 thus suggesting that $Fe_{1-x}S$ (or FeS) is also produced when pyrite in slate is heated in air. The overall sulfur content of SPNW-19 however did appear to be lower than that of SPNW-48 (1223K) supporting the trend that increasing the reaction temperature increases the extent of pyrite decay within the interior of slate samples. Virtually no sulfur was detected on the outer pyrite crystals of both SPNW-48 (1223K) and SPNW-19 (1453K) however these crystals did appear to have a smoother texture compared to those found on SPNW-41 (923K) and may therefore reflect the higher temperatures sustained which is believed to effectively melt the outermost surface of the crystals thus illustrating the greater decomposition of external pyrite (Figure 3.26).

The effect of longer dwell times on the decomposition of pyrite within the interior of slate has also been investigated. A heating experiment reaching a temperature of 1453K and incurring a dwell of 15min. instead of <1min (SPNW-19) has therefore been carried out. "Pyrite" crystals within SPNW-26 (15min. dwell) after heating were found to have a lower S content by EDS than SPNW-19. Subsequently a study into the effect of maintaining a dwell at 923K prior to heating to 1453K was undertaken (SPNW-30and SPNW-32). Substantially lower intensity sulfur peaks were detected by EDS when SPNW-30 (900min at 923K) and SPNW-32 (1200min at 923K) were analysed compared to SPNW-19. This dwell at the lower temperature effectively resulted the greatest degree of pyrite decomposition within slate samples observed during these experiments. SEM studies showed the presence of a highly porous material within the slate of both samples that consistently produced energy dispersive spectra with a strong peak corresponding to iron. Only trace amounts of sulfur were detected after such a long heating program had been followed. This long heating program has also affected the nature of the external pyrite crystals since SEM images show a residue that appears to have recrystallised after being molten thus producing an unstructured material that has escaped the confines of the cubic cavity of the original pyrite. In agreement with pyrite-only samples, effective

dwell time has been shown to increase the loss of S from pyrite present in slate. The increased time at a temperature high enough to initiate reaction results in sufficient time for diffusion of the S species through the slate to occur thus giving rise to greater decomposition of both the internal and external pyrite.

It was very difficult to obtain well-resolved XRPD data on the composition of the decomposed pyrite at the various temperatures due to the relatively small amount of pyrite present in the unheated slate tablets of North Wales. In order to gain a better picture of pyrite oxidation Spanish slate has also been investigated in a similar manner.

Upon heating to 923K in air the pyrite crystal present in SPS-43 became bright red, rust-like, in colour. EDS analysis of the outer "pyrite" surface of the treated crystal showed that the material essentially consisted of iron with only a trace amount of sulfur. The interior of the crystal was found to contain only a trace amount of S in comparison to the small crystals found within the slate of SPNW-47 heated to 923K. Indeed the Fe:S ratio was found to be in agreement with P-23 (923K, air) *i.e.* generally 1:0. SEM studies showed a clear correlation between this lower S intensity and the degree of decomposition within the sample since the inner surface of SPS-43 appeared to be much more porous than SPNW-47. A non-uniform distribution of cavities and pores throughout the interior of the sample SPS-43 effectively produced a material that appeared to have a completely random structure. This type of material had previously been seen in the inner surface of pyrite samples heated in air (see Figure 3.8). Heating a sample of Spanish slate to an elevated temperature of 1223K (SPS-44) changed the colour of the pyrite crystal to a deep red that appeared to be much darker than the red previously seen in sample SPS-43. EDS analysis showed only Fe on the inner and outer surfaces of the sample. This apparent complete sulfur removal was further reflected by SEM studies that showed a highly porous, unstructured material encased by an outer shell made up of a smoother material, more molten in appearance.

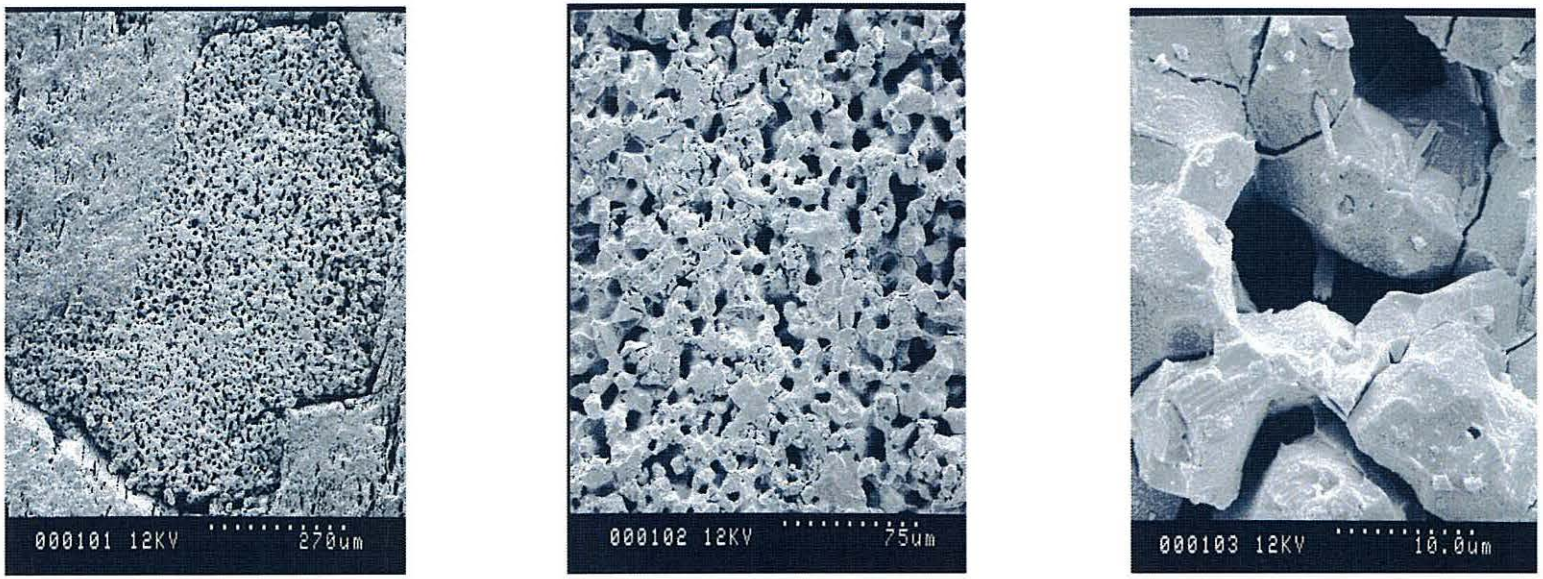

Figure 3.25: SEMs of pyrite in slate (interior, SPNW-19) heated to 1453K in air

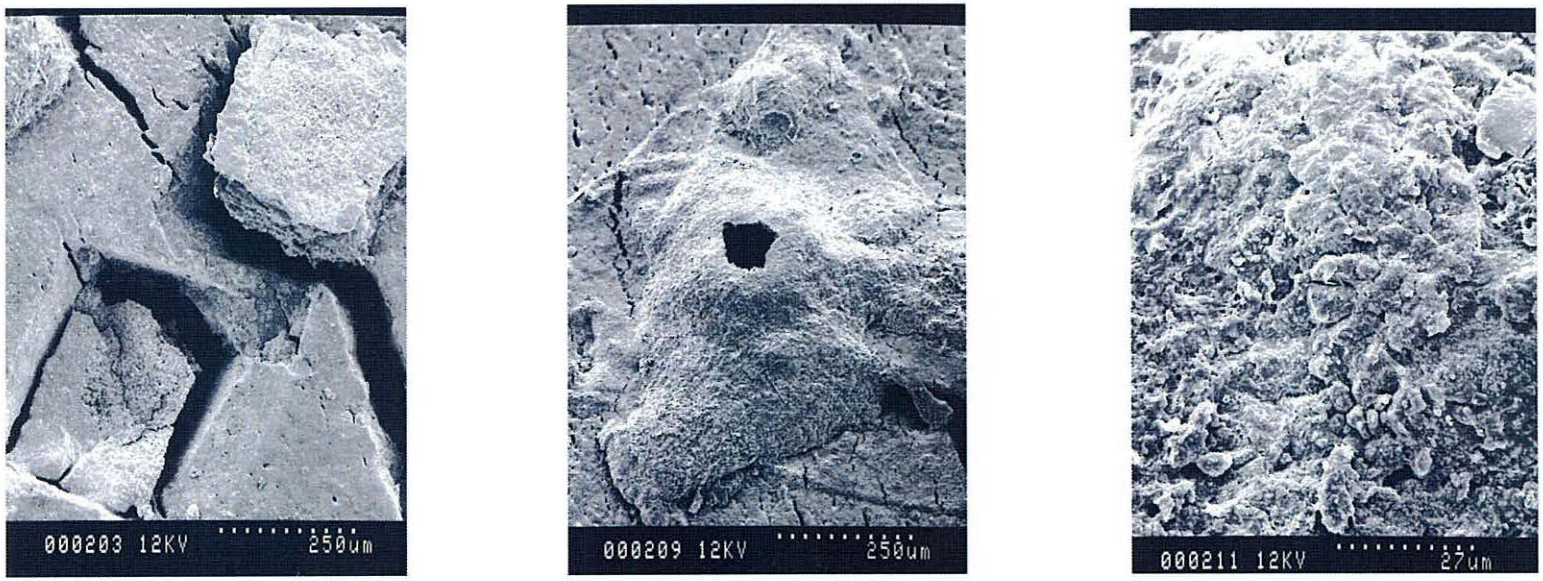

Figure 3.26: SEMs of pyrite in slate (exterior, SPNW-19) heated to 1453K in air

Samples subsequently heated to 1453K, namely SPS-20 and SPS-33, also illustrated the decay of pyrite in air. The remaining "pyrite" material at this temperature however appeared black in colour. It is therefore apparent that the degree of red colour present in the oxidised product decreases with increasing temperature. The EDS studies of these samples heated to 1453K are in agreement with that recorded for sample SPS-44 heated to 1223K *i.e.* no sulfur was detected. The presence of haematite has been confirmed here by XRPD. In addition, the diffraction pattern of SPS-20 had peaks corresponding to magnetite (Fe_3O_4). The preferential formation of magnetite over haematite at temperatures above 800°C is reported to be favoured by a reduced oxygen partial pressure within the furnace.[89] This is believed to reflect the reduced accessibility of O_2 to areas of the pyrite crystal in slate thus giving rise to the formation of both Fe_2O_3 and Fe_3O_4. SEM images obtained from SPS-20 appeared to show bloating of the pyrite crystal during the heating process.

3.6. Conclusions

In N_2 experiments heating pyrite-only, S_2 was found to be the major reaction by-product. FeS has been identified by XRD as being formed when pyrite was heated in N_2. However EDS analysis suggested that $Fe_{1-x}S$ was also present since Fe:S ratios ranging from 1:1 to 1:3 was detected. Increasing the temperature from 923 to 1453K tended to decrease the S intensity compared to Fe. Thus indicating increased loss of S corresponding to greater conversion of $FeS_2 \rightarrow FeS$. Lower levels of S were generally detected on the outer surface compared to the inner thus illustrating the mechanism of pyrite decomposition involving the loss of S from the outer surface inwards. Indeed insufficient decomposition has been shown to lead to a sample (P-22) containing a core of undecomposed pyrite. The morphology of pyrite samples heated in N_2 appeared to be porous but highly ordered producing a material that appeared to have a very crystalline structure.

By comparison pyrite heated in air produced SO_2 as the major reaction by-product. XRD analysis showed the formation of Fe_2O_3. Trace S was however detected by EDS but the

levels of S tended to decrease with increasing temperature. The S content of the outer surface was again found to be lower than the interior, in agreement with N_2 samples, thus showing that pyrite decomposition starts from the outside and moves inwards. The presence of S is however believed to suggest the generation of iron sulfide minerals as intermediate products in the decomposition of pyrite in air. The extent of pyrite decay has been found to be dependent on dwell time. Effective dwell at temperatures above 923K has resulted in greater loss of S thus suggesting that the mechanism of pyrite decay is diffusion controlled *i.e.* more time above reaction temperature ensures greater mass transport of the S species through the pyrite lattice to give rise to greater decomposition. The morphology of pyrite heated in air was found to be completely different to pyrite heated in N_2. A very porous material was again produced however this time a very disordered structure was apparent.

The differences in the morphology of N_2 and air samples is believed to reflect the differences in the decomposition mechanism in the different atmospheres. In N_2 a purely thermal process is taking place. Heat increases the energy of the pyrite lattice, destabilising the structure enough to result in the loss of S and the formation of FeS (equation 3.2). This S species then needs to diffuse through the lattice to the outer surface so that it can combine with other S to produce S_2 (equation 3.3). The loss of S in this way is believed to be the rate-controlling step and in N_2 it appears to occur slowly enough to allow sufficient time for recrystallisation to occur.

$$FeS_2 + \Delta \rightarrow FeS + S \qquad [3.2]$$

$$S + S \rightarrow S_2 \qquad [3.3]$$

In air, in addition to a thermal process taking place, O_2 is also present which can react with FeS_2 to produce Fe_2O_3 and SO_2 (equation 3.4) and any released S to produce SO_2 (exothermic process) (equation 3.5). The combined effect of thermal decomposition and reaction with O_2 is therefore believed to increase the efficiency of the pyrite decomposition in air which effectively results in a more rapid process. It is therefore

suggested that the increased rate does not allow sufficient time for recrystallisation of the lattice to take place hence the apparent disordered structure.

$$2FeS_2 + 5½O_2 \rightarrow Fe_2O_3 + 4SO_2 \quad [3.4]$$

$$S + O_2 \rightarrow SO_2 \quad [3.5]$$

The effect of diffusion on the mechanism of pyrite decomposition has clearly demonstrated by studying the effects of heating on FeS_2 crystals within slate. Here Welsh slate with small FeS_2 crystals within the slate matrix showed that the decomposition of pyrite in both N_2 and air was reduced compared to pyrite only samples heated to the same temperature *i.e.* more S was generally detected. This is believed to reflect the greater mass transfer limitation exhibited by slate, slowing down the loss of S thus reducing the decay of the internal FeS_2. The resulting morphology of these internal crystals also appeared to reflect the reduced rate of decomposition since an ordered structure could be seen. As expected, this was clearly evident in N_2 samples which showed that pseudo-hexagonal crystallites had been produced. By comparison, pyrite in slate heated in air also produced an inner material that appeared to be more structured than previously seen in pyrite-only samples heated in air. Indeed the internal pyrite in slate appeared to have a similar structure to that observed in slate samples heated in N_2, although not as well defined.

The work carried out on Spanish slate containing large pyrite crystals illustrated the effect of particle size on pyrite decay. It was clear that as particle size increased a reduction in the overall extent of decomposition was observed. This is believed to correlate with the greater diffusion necessary to ensure the loss of S species from the large pyrite crystal. Furthermore the formation of magnetite (SPS-20) suggests differences in O_2 exposure experienced by different areas of the FeS_2 crystal.

The conditions required to ensure the maximum decomposition of pyrite in slate in a commercial furnace is therefore believed to include an air atmosphere, a dwell at a temperature at or above 923K and a heating rate that is not too rapid so that the maximum

exposure to heat can be obtained. The optimium heating parameters determined for slate expansion *i.e.* rate of 20K/min and a dwell at the final temperature of 1453K has been shown to instigate pyrite decomposition within slate samples however a pre-heating stage at 923K prior to expansion is expected to give rise to greater pyrite loss.

Chapter Four - Catalysis

Chapter Four – Catalysis

4.0. Development of Novel Catalysts

In this chapter the novel use of expanded slate powder as a support material for catalytic metals will be explored. The application of expanded slate in catalysis has never been reported before; one rationale for this work being the re-use of waste slate since alumina and silica are widely used as a catalyst supports and expanded slate is an aluminosilicate. Calcination can often give rise to a high surface area material however analysis by BET isotherm of expanded slate has shown that a low surface area material is produced upon heating. Even though a low surface area has been reported (*ca.*0.4m^2/g) the fact that slate has undergone significant structural changes and compositional transformations during the heating process necessary to cause the expansion, the resultant material is therefore very stable to subsequent heating up to temperatures *ca.*1473K *i.e.* around the expansion temperature. Expanded slate also has a relatively high mechanical strength (Ten Percent Fines Value (TVF) of 60kN) and is composed of material that is chemically very inert.[101] These factors therefore contribute to expanded slate's potential to act as a good catalyst support which is believed to be comparable to other low surface area supports currently available such as mullite[1] *i.e.* a support which is used in high temperature and high pressure catalytic reactions.

The overall structure of this chapter is intended to demonstrate the cycle of stages involved in the development of a new catalyst. This cycle starts with the preparation of a new catalyst, this catalyst is then activated and its catalytic activity is tested, in this case for hydrogenation reactions. Modifications required to optimise the catalyst performance are carried out at this point after which the cycle starts all over again. In the course of the work for this thesis two main methods of catalyst preparation have been investigated. These include impregnation techniques and electroless plating. Impregnation is an established technique for the production of commercial supported metal catalysts and its application in the development of expanded slate catalysts will therefore initially be discussed in this thesis. Characterisation details of the resultant impregnated catalysts

will then be given. This section is intended, in part, to establish the characterisation methodology involving IR, XRPD, SEM and EDS suitable for the analysis of all subsequent catalysts produced during this study. A discussion of the catalyst activation and testing procedures, involving hydrogenation experiments, and modifications required in the catalyst preparation stage as a result of the recorded activity of the novel catalysts will then be discussed. The second method of catalyst preparation *i.e.* electroless plating, is relatively new to catalyst preparation and is not currently used in a commercial catalytic process. More information on the reported use of electroless plating in catalysis has been given in the Introduction (Section 1.4.2.). In the course of this study electroless plating methods described in the literature have been adapted and developed for the production of expanded slate catalysts. The development of two types of catalysts has been carried out namely the production of copper- and palladium-supported expanded slate. For both catalyst types the discussion of results will follow a similar structure to that previously mentioned for impregnated expanded slate catalysts. A discussion on the method of catalyst production will firstly be given followed by a review of the information gained from the characterisation of the resultant materials. Activation and subsequent testing of the electroless plated catalysts will then be discussed including a comparison with the data obtained from catalysis work using the impregnated expanded slate catalysts.

4.1. Impregnation Methods

The development of copper expanded slate catalysts *via* impregnation was initially attempted. Copper was chosen as the catalytic element since in the past it generally has been found to have good activity towards hydrogenation reactions (see Section 1.4.1). Two methods based on impregnation were followed. The first method, described as wet impregnation, has often been used to produce supported metal catalysts such as Cu/Al_2O_3 or Cu/SiO_2 catalysts.[122,129,130] This method involved adding an aqueous solution of copper nitrate to a sample of expanded slate powder. The mixture was then stirred 1 hour to allow the copper salt in solution to sorb to the surface of the expanded slate. The "impregnated" expanded slate was then separated from solution, allowed to dry and then

finally calcined in either air at 623K to covert any adsorbed copper nitrate to copper oxide on the expanded slate surface. The calcined material was initially analysed by IR to determine the extent of decomposition of the copper salt after heating. No peak at $1384cm^{-1}$ was detected which infers that no nitrate species is present in the sample. Nitrate is very sensitive to detection by IR producing an intense peak even if only trace amounts are present in a sample. The fact that no peak has been produced at $1384cm^{-1}$ therefore conclusively shows the absence of NO_3^-. The resulting material was then characterised by XRPD in order to ascertain whether any crystalline copper oxide or copper metal was present on the surface. No peaks in addition to those normally produced during XRPD analysis of expanded slate were seen in the diffraction pattern of samples prepared by the wet impregnation method therefore no evidence for the presence of either copper species could be obtained from using this analytical method. This suggests that sufficient copper has not been impregnated onto the surface to produce a diffraction pattern when analysed by XRD. Analysis by SEM was subsequently carried out in order to determine whether the morphology of expanded slate which had been impregnated with copper was any different to untreated expanded slate *i.e.* a search for "new" crystallites on the surface of the expanded slate was carried out. Crystallites were rarely visible by SEM but spot-analysis by EDS of those that were found did produce a pattern consistent with copper being present. Analysis of areas on the surface that did not contain any crystallites produced an energy dispersive spectrum corresponding to that normally produced by untreated expanded slate *i.e.* no copper. Following the apparent low copper loading achieved subsequent impregnation attempts were carried out stirring the expanded slate support in copper nitrate solution for up to 24 hour. No significant difference in the amount of impregnated copper was found between expanded slate kept in the impregnating solution for 1 hour or 24 hours.

Preliminary experiments were then carried out to ascertain whether the samples prepared by wet impregnation were active towards the hydrogenation of maleic acid. A standard hydrogenation experiment was carried out using maleic acid (1mole) in a Parr 3911 Hydrogenator. This reaction was initially chosen since the addition of hydrogen across the maleic acid C=C double bond was expected to give rise to the generation of a single

product *i.e.* succinic acid (equation 4.1). The equivalence of one mole of hydrogen would therefore be required to ensure complete conversion and the corresponding decrease in hydrogen pressure could then be recorded. No decrease in hydrogen pressure was observed when using copper supported expanded slate prepared *via* the wet impregnation technique. The "catalyst" was therefore deemed to be inactive under the reaction conditions of the experiment *i.e.* 60psi H_2 pressure at room temperature (*ca.*298K). The small amount of copper detected on the surface of the expanded slate by SEM is also believed to account for the inactivity of the catalyst. The apparent lack of active sites therefore also show that expanded slate itself is not catalytically active.

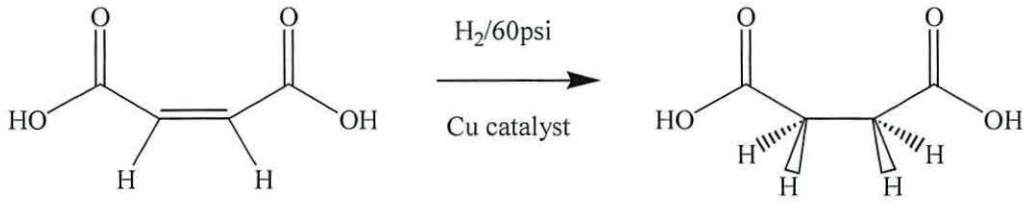

Maleic acid Succinic Acid [4.1]

Wet impregnation is a well-established preparative method for catalysts. The method relies on the success of three stages when it comes to the preparation of heterogeneous catalysts. These stages, as discussed in section 1.4.1, include the catalyst precursor being in contact with the impregnating solution for a certain period of time, then the drying of the support to remove excess solvent and finally activation of the catalyst by calcination.[5] The hydrophobic nature of the expanded slate is believed to be a key factor resulting in the small amount of copper found on the expanded slate surface since this would effectively result in the first stage of the impregnation process failing. It is essential for the solution to come into contact for sufficient time to initiate nucleation of the copper salt on the expanded slate surface. Furthermore the low surface area of the material is also believed to contribute to the low copper uptake since the lack of micropores within the structure effectively reduces the number of suitable sites available for the sorption leading to the nucleation of the copper salt to take place. Together both factors inevitably give rise to conditions on the support surface that do not favour the impregnation of the copper nitrate on the surface.

In order to overcome the problems associated with the hydrophobicity of the expanded slate a second impregnation procedure was developed. This method involved the removal of excess water from the solution through evaporation by gentle heating (~323K) of the mixture containing the expanded slate and copper nitrate solution. IR analysis of the resulting material before and after calcination in air at 673K for 4hours clearly showed the disappearance of a peak at 1384cm^{-1} corresponding to free NO_3^-. The presence of this peak in uncalcined material is strongly indicative of the presence of the copper nitrate on the surface its subsequent disappearance after heating suggests that calcination has indeed resulted in the decomposition of the salt. By comparison, analysis of the "catalysts" by XRD showed weak peaks corresponding to CuO in addition to peaks normally found in untreated expanded slate thus suggesting that some impregantion had occurred (Figure 4.1). The apparent low intensity of the CuO peaks is believed to be due to a low copper loading (*ca.* 2%). Copper metal was not detected.

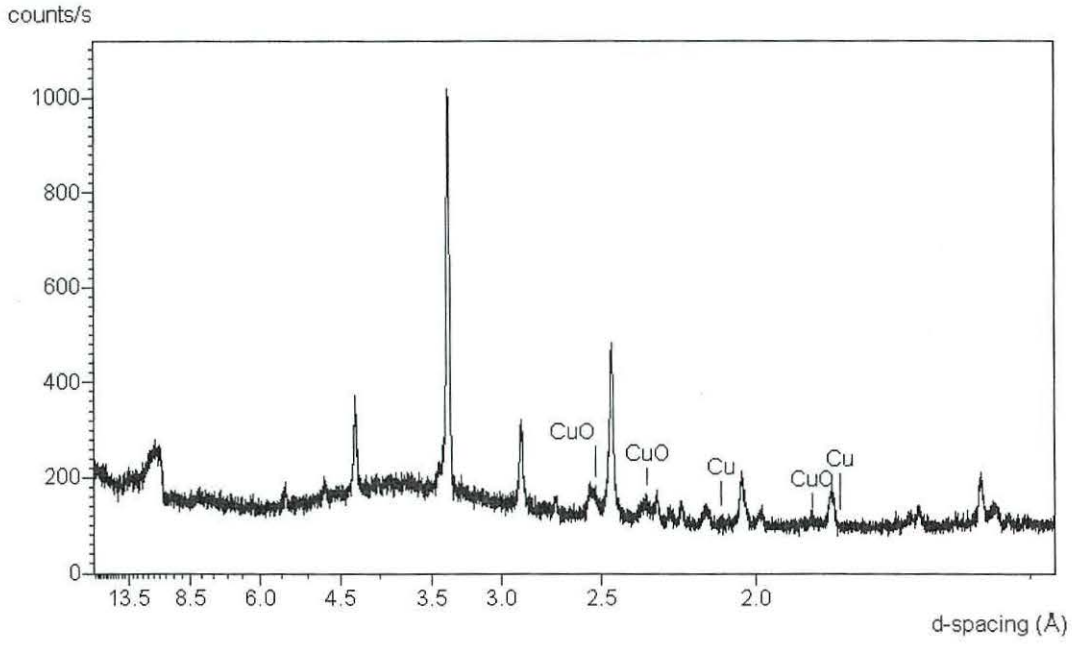

Figure 4.1. XRD pattern of copper impregnated expanded slate calcined in air for 4 hours showing expanded slate peaks; CuO and absent Cu peaks are annoted.

Analysis of the calcined material by SEM did confirm the IR and XRD data in that crystallites were again found on the surface. The SEM data however did reflect a low

copper loading since in general the morphology of the treated expanded slate powder did not appear to be significantly different to the untreated material. However more crystallites were evident in comparison to "catalysts" prepared *via* the wet impregnation technique. These crystallites were confirmed to contain copper by spot analysis using EDS. Three types of crystallites were found by SEM. These included large isolated spherical clusters, groups of clusters and small copper particles visible on the expanded slate surface (Figure 4.2). The largest clusters appeared to have a highly spherical structure with a diameter in the region of 4-6μm. Groups of spheres producing a cluster approximately up to 10μm in diameter could also be found in close proximity to each other. Islands of smaller copper crystallites (1μm) could also be seen. Energy dispersive analysis of these clusters again showed a high concentration of copper thus indicating that copper had indeed been impregnated on the surface. The formation of the large clusters, not seen previously during the analysis of wet impregnated sample, is believed to result from the evaporation of the aqueous phase during the gentle heating stage. Slow evaporation is believed to result in shrinking water droplets that effectively trap a high concentration of copper nitrate close to the expanded slate surface as a result of the surface tension of the droplet. This encourages the nucleation of the copper salt on the surface by the formation of a super-saturated solution. Subsequent calcination of the sample removes all the water and is believed to decompose the copper nitrate to copper oxide thus giving rise to the observed clusters that retain the spherical shape of the water droplet.

This second impregnation method appeared to be more successful in producing a copper supported expanded slate since SEM and EDS studies of the calcined solid did show more copper on the surface. However activity tests again did not succeed in converting maleic acid to succinic acid since no decrease in hydrogen pressure was observed during the hydrogenation experiment. No evidence for the conversion of maleic acid to succinic acid was obtained from GC analysis of the reaction solution.

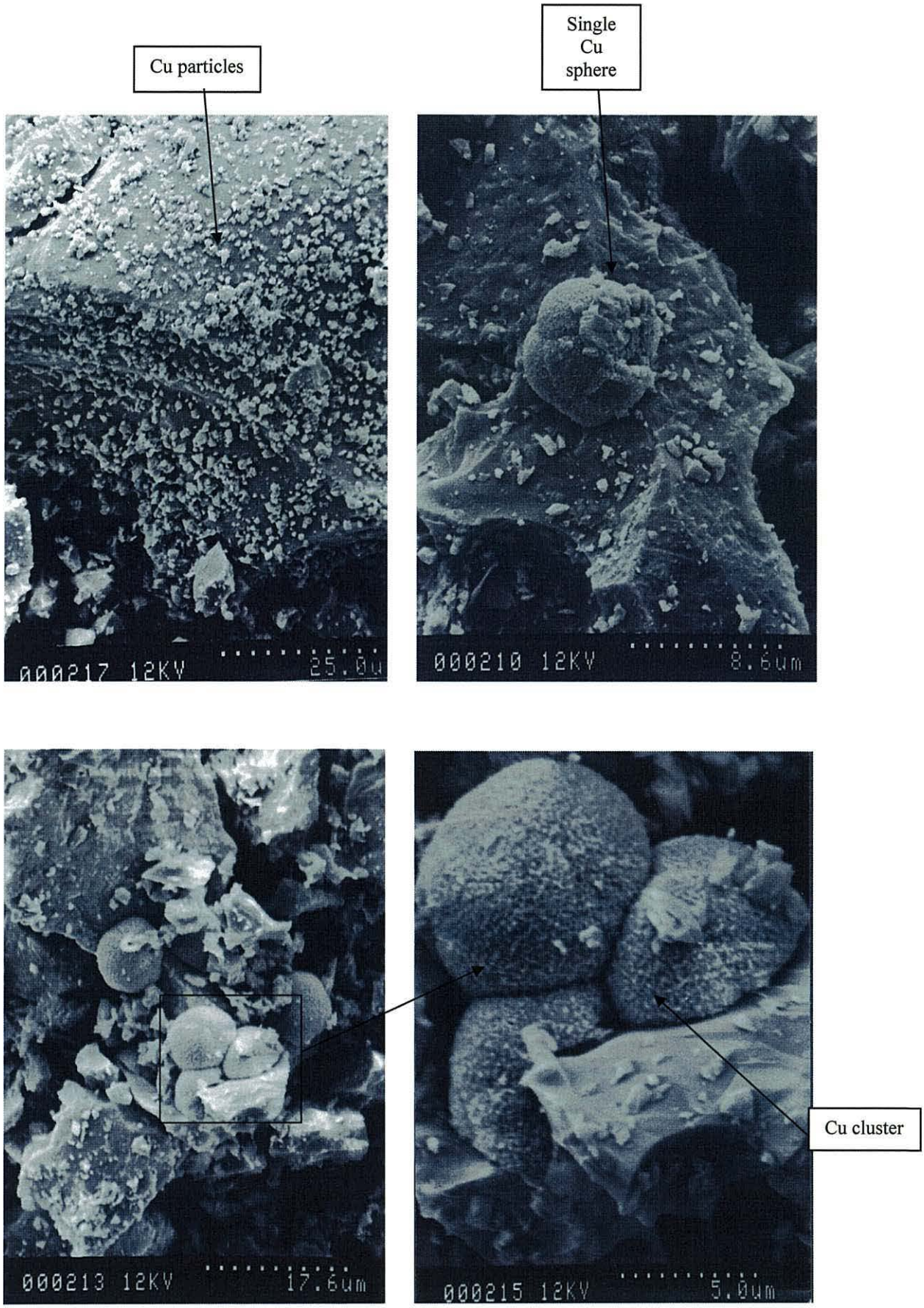

Figure 4.2. SEM images of impregnated Cu/expanded slate catalyst showing the three different types of metal deposition: small Cu particles, large, single Cu spheres and large Cu clusters.

4.2. Electroless Plating Method

4.2.1. Copper Electroless Plated Expanded Slate Catalysts

The difficulties encountered in producing an even distribution of copper on expanded slate surface led to trials of an alternative method of depositing the required active metal using electroless plating. Furthermore it was also hoped to overcome the associated inactivity of the resulting impregnated copper catalysts towards hydrogenation experiments if a sufficient metal loading could be achieved by this alternative preparation method.

Preliminary experiments were carried out to determine whether electroless plating would be appropriate for the deposition of a metal onto the surface of expanded slate. An electroless plating procedure involving the chemical reduction of nickel was carried out to test this. A plating bath was prepared which would generate a maximum loading of 10 wt.% nickel metal. SEM analysis of the material produced did show evidence for the presence of new crystallites on the surface. EDS analysis of the resulting sample confirmed that nickel was present. However spot analysis of the crystallites showed that phosphorus was also present in the same place as nickel thus indicating, in accordance with the literature,[143] that a Ni/P alloy is deposited onto the surface rather than nickel in the metallic form. No residual chlorine was detected in the crystallites by EDS therefore decomposition of the starting material, $NiCl_2$, was believed to have occurred. Following the apparent success of Ni deposition on the surface of expanded slate the preparation of copper catalysts was attempted in order to be able to compare the extent of copper dispersion with that previously seen on the impregnated copper catalysts.

Following the apparent success of depositing nickel by electroless plating on the surface of expanded slate, a method described by Chang *et al.*[152] for the preparation of copper/alumina catalysts by electroless plating was adapted for the production of copper supported expanded slate. A pre-treatment stage was found to be essential before commencing electroless plating to ensure deposition of the copper on the surface of

expanded slate. This is in accordance with the literature method for deposition of copper on alumina by Chang and co-workers. The pre-treatment initially involved washing the expanded slate in an acid bath. The sample was rinsed with water and then immersed in an alkali bath. These washing stages were reportedly carried out by Chang *et al* in order to remove contaminants such as adsorbed hydrocarbons (fats and oils) from the surface of their alumina support. The presence of adsorbed hydrocarbons was not believed to be such a problem on the surface of expanded slate nevertheless an acid and alkali wash was carried out on the expanded slate in order to be sure that a clean, contaminant free surface was achieved. The next stage in the pre-treatment involved exposing the support to a sensitising agent namely $SnCl_2$ solution. The adsorption of small amounts of tin chloride on the surface of the expanded slate was believed to sensitise the surface in a similar manner to that reported for the sensitisation of alumina by Chang *et al.* Electroless plating only takes place on a "catalytic" surface that can supply electrons to initiate the reduction of the metal salt on the surface to be plated. Once the reduction of the salt has started, the deposited metal itself then acts as a catalyst for subsequent reduction of the plating solution. It is therefore essential that a non-catalytic surface such as expanded slate be activated before electroless plating is attempted. The activating agent used in this case was palladium chloride. A fundamental understanding of the role of $SnCl_2$ and $PdCl_2$ in the pre-treatment stage has not been provided by the literature. In the case of expanded slate, it seems likely that sensitising the support material with $SnCl_2$ prior to immersing in a $PdCl_2$ increases adsorption efficiency of the $PdCl_2$ activating agent. The adsorption of Pd is then reported to provide nucleating centres on the surface of non-catalytic support materials, such as expanded slate, that effectively trigger the catalytic reaction for the electroless plating process by acting as a seeding or a catalysing agent on the substrate.[154] Activation is believed to give rise to redox reactions occurring between palladium (which can exist as either Pd^{2+}, Pd^{4+} or Pd^{6+}) and the plating salt. The reducing agent then provides the necessary electrons to initiate the reduction of the plating salt so that initial deposition occurs at the Pd nucleation sites. After pre-treatment the expanded slate was separated from the activating $PdCl_2$ solution by filtration then dried prior to immersion in the electroless plating bath.

In the case of copper electroless plating, the bath essentially contained a salt of the desired metal *i.e.* $CuSO_4$, in the presence of a chemical reducing agent, formaldehyde. The bath temperature was increased to 348K and a pH of ~9.2 was maintained by the addition of NaOH. In addition to the metal salt and reducing agent, additives such as EDTA and pyridine were also added to the bath to act as chelating agent and stabiliser respectively. EDTA binds with the Cu^{2+} in solution and prevents the precipitation of $Cu(OH)_2$ which would reduce the effectiveness of the electroless plating bath.[154] The electroless plating bath can be susceptible to spontaneous decomposition if there is an excess of catalytic surface in solution. When this occurs the metal salt is often reduced spontaneously producing metal particles in the solution rather than the metal being deposited on the surface of the substrate. To overcome this threat a catalytic poison is used to control the reaction. In the case of the copper electroless plating bath used, pyridine acted as the poison (5mg/L). Since this compound is very effective in decreasing the catalytic activity of the bath only a relatively small amount was required to ensure that the risk of spontaneous bath decomposition was reduced. During the reaction a colour change was seen from the initial dark blue of the copper sulfate solution to a final colourless solution. This was ascribed to the reduction of Cu^{2+} in the chemical plating bath. Furthermore upon drying the resulting samples had distinctly dark red/brown coloration significantly different to the original colour of the untreated expanded slate powder thus inferring that copper deposition had indeed taken place.

A series of catalysts were prepared using expanded slate by following the stages described above. These catalysts have been labelled Cu22 to Cu35 (see Table 4.1). Expanded slate powder was generally sieved prior to metal deposition and fractions with varying particle sizes ranging from <63, 63-105, 105-180, 180-250 and 250-300μm, were collected. The concentration of the plating solution was believed to be an important variable in the preparation of catalysts with consistent copper loading. Therefore in order to produce catalysts with varying copper loading, between 5-20%, the volume of the copper solution was varied during the preparation of each catalyst. A stock $CuSO_4$ solution (10M) was therefore prepared and its volume was adjusted accordingly to ensure that the required amount of metal would be precipitated from solution. Determination of

the amount of Cu deposited onto the surface was determined by re-extraction by concentrated HCl and analysis by atomic absorption spectroscopy. The solid material was then separated by filtration and the extracted copper solution diluted to within the appropriate working range (0-5mg/L). Standard copper solutions were prepared so that a calibration curve could be obtained in order to determine the actual concentration of copper in the diluted "unknown" solutions. The final concentration of the "unknown" samples was then calculated back so that a value for the actual percentage weight of copper on the surface of the expanded slate catalysts Cu22-Cu35 was obtained. The difference between the theoretical and actual copper loading achieved is illustrated in Table 4.1. The table also includes batch numbers for each of the copper catalysts. This batch number represents the pre-treatment used for each of the catalysts prior to electroless plating. All batches essentially followed the same pre-treatment stages *i.e.* washed with acid and alkali, sensitised with $SnCl_2$, activated with $PdCl_2$, filtered and then dried prior to electroless plating. An attempt was made in all cases to keep the pre-treatment process as constant as possible. However small variations are believed to have occurred from batch to batch due to differences in the amount of expanded slate that underwent pre-treatment, length of time exposed to the sensitising and activating solutions and period of drying. Samples from each batch were the taken and exposed to different electroless plating baths to produce the appropriate catalyst. For example catalysts Cu32 and Cu33 were initially taken from the same pre-treated batch (no.18) but underwent different electroless plating to produce a different copper loading on their surfaces.

Table 4.1. Electroless copper supported expanded slate catalysts.

BATCH NO.	SAMPLE	PARTICLE SIZE (μm)	Cu LOADING		EFFECTIVE DEPOSITION (%)
			Theoretical Wt.% Cu	Actual Wt.% Cu	
8	Cu22	63 – 105	10	5.42	54.2
9	Cu23	63 – 105	15	11.88	79.2
10	Cu24	105 – 180	10	1.80	18.0
11	Cu25	180 – 250	10	8.99	89.9
12	Cu26	250 – 300	15	5.78	38.5
13	Cu27	<63	10	7.33	73.3
14	Cu28	75 – 105	5	1.59	31.8
15	Cu29	105 – 180	10	9.25	92.5
16	Cu30	105 – 180	10	9.50	95.0
17	Cu31	63 – 105	10	9.50	95.0
18	Cu32	63 – 105	15	13.00	86.6
18	Cu33	63 – 105	20	15.75	78.7
19	Cu34	105 – 180	15	11.50	76.6
19	Cu35	105 – 180	20	16.75	83.7

A 100% copper uptake was not achieved however a good correlation (> 50% effective deposition) between the theoretical and actual copper loading was generally recorded. The preparation method was the same for all samples therefore the extent of copper plating should theoretically also be the same. However during plating some copper was also deposited on the inside of the reaction vessel as a metallic orange film. This is believed to account for the discrepancy in the copper loading determined for each catalyst. Furthermore the copper loading was found to be independent of expanded slate particle size since no significant differences in the copper content on catalysts with large expanded slate (250μm) particle sizes compared to small particle size (63μm) was generally detected. However three catalysts were found to have poor copper loading

(< 50%) *i.e.* Cu24, Cu26 and Cu28 with effective deposition 18.0, 38.5 and 31.8% respectively. Indeed upon termination of the electroplating process during the preparation of these three catalysts it was observed that the plating bath remained light blue in colour. This therefore suggests that complete reduction of the copper sulfate solution had not occurred hence the maximum deposition had not been achieved. This is believed to reflect variations in the initial pre-treatment stage since subtle differences may occur from batch to batch. No evidence for significant differences between batches before plating has been obtained however slight variations are believed to influence the effectiveness of the plating process. The process is believed to be sensitive to the amount of $PdCl_2$ adsorbed onto the surface during the pre-treatment stage since if no pre-treatment is carried out no copper is detected on the surface of the final material. The problems found during the development of catalysts using the impregnation technique are therefore likely to affect the extent of Pd adsorption to produce the necessary nucleation sites on the expanded slate surface.

Samples Cu22 - Cu35 were also analysed by XRPD before and after calcination. Analysis of the samples after plating shows that in addition to the peaks corresponding to the constituent minerals of expanded slate, two strong, broad peaks corresponding to copper can be observed on the diffraction patterns with d-spacings ~2.4X and 1.85X. The position of these peaks has been found to be in accordance with Cu deposited on the surface and not a salt or oxide of copper. Therefore in contrast to the XRPD data of impregnated copper catalysts the information gained from the analysis of copper electroless plated catalysts shows that copper was successfully deposited onto the surface of the expanded slate powder. This finding is consistent with the literature data that reports the deposition of copper metal on the surface of alumina.[152] Copper metal is therefore initially produced however XRD analysis of the material after calcination in air showed that CuO was generated (Figure 4.3). Calcination in nitrogen maintains the Cu(0) species however copper diffraction peaks appear to be sharper and more intense compared to those produced during analysis of uncalcined samples thus suggesting that recrystallisation has taken place (Figure 4.4).

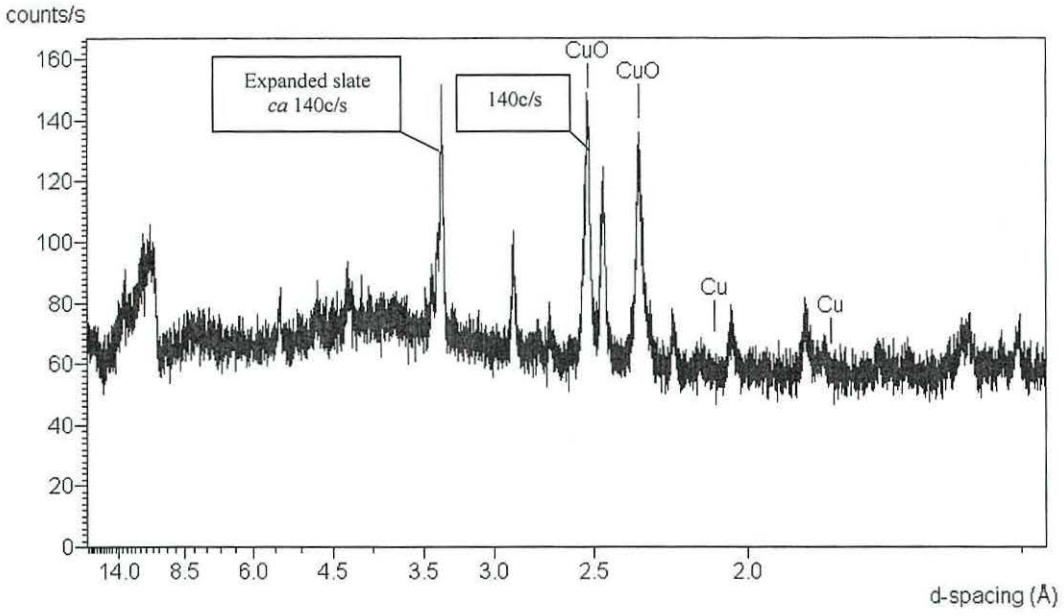

Figure 4.3. XRD pattern of Cu electroless plated expanded slate calcined in air .

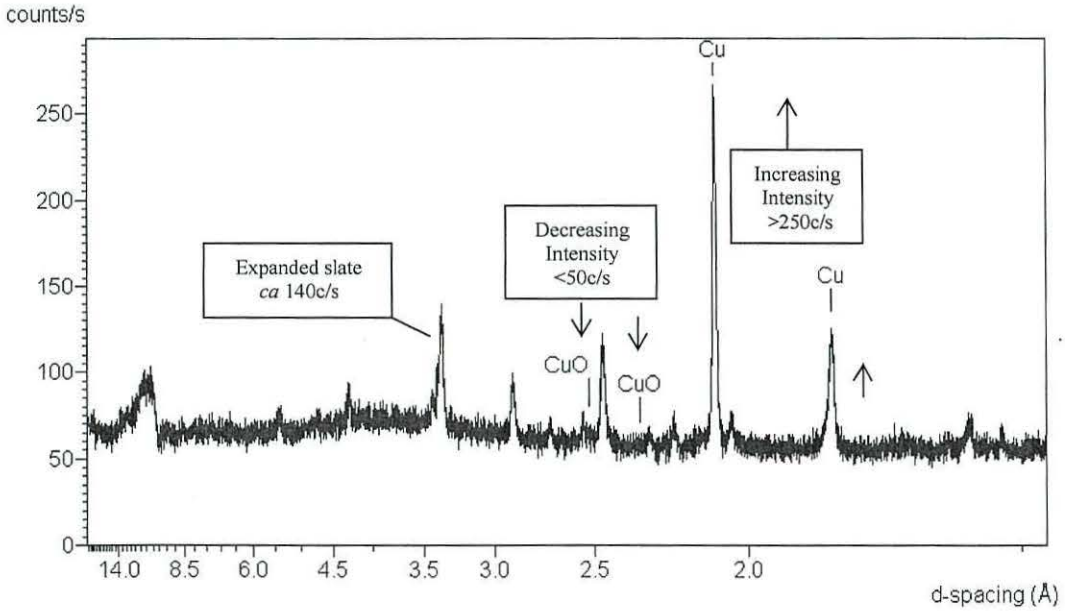

Figure 4.4. XRD pattern of Cu electroless plated expanded slate calcined in nitrogen showing increase in peak intensities of Cu and decrease in CuO intensities relative to expanded slate (*e.g.* at 3.4Å).

An investigation by SEM and EDS analysis has also been carried out in order to determine the morphological and compositional differences of electroless plated Cu/expanded slate catalysts compared to the impregnated samples. SEM studies have shown that the copper electrolessly deposited on the surface is generally well dispersed and distributed across the whole surface of the slate (Figure 4.5). The crystallite size of the adsorbed copper also appears to be relatively homogeneous (*ca.* 0.5-2μm in diameter) even when the copper loading is varied. The observed consistency therefore suggests that copper crystallite size is independent of copper loading within the range tested *i.e.* 5-20wt.%. Isolated large clusters as previously seen for "catalysts" prepared by the impregnation method are not observed. The EDS patterns were found to correlate well with the data obtained from the XRD analysis of Cu/expanded slate prepared by electroless plating since strong peaks corresponding to Cu were generally recorded when the sample was analysed. By comparison, EDS analysis of test samples that had not undergone any form of pre-treatment did not produce any Cu peaks thus clearly illustrating the importance of the pre-treatment stage. Furthermore, peaks corresponding to tin, palladium and chlorine were also generally found to be absent when catalysts Cu22-Cu35 were analysed by EDS. The absence of Pd and Sn is believed to be due to the fact that only very low concentrations of $SnCl_2$ and $PdCl_2$ were used for sensitising and activating the expanded slate powder respectively. The absence of chlorine was especially encouraging since Cl can act as a poison for copper catalysts thus reducing their catalytic activity.[101]

Electroless plating has therefore proved successful in the preparation of copper supported on expanded slate. The catalytic activity of these catalysts towards the hydrogenation of maleic acid was then tested. The reaction was carried out at 60psi and standard room temperature (298K). No decrease in hydrogen pressure was observed during the testing of any of the electroless plated copper catalysts. In order to test the effect of calcination conditions and the copper oxidation state on catalyst activity, samples that were initially calcined in air (CuO) and found to be inactive, were recalcined at 673K under nitrogen to produce Cu in the metallic form. These tests also proved unsuccessful. Further attempts to activate the catalysts were carried out which involved heating samples in hydrogen at

523-623K for between 2 and 16 hours in order to reduce the CuO normally present on the surface to Cu. The resultant samples were again found to be inactive since no pressure decrease was observed. The apparent inactivity towards maleic acid hydrogenation under the experimental conditions used was in accordance with that previously recorded for impregnated copper catalysts. Consequently, trials were carried out to investigate whether the activity of the copper catalysts increased upon heating of the maleic acid solution to 348K. In addition hydrogenation experiments involving nitrobenzene, at room temperature and 348K, and cyclohexene were attempted. No decrease in hydrogen pressure was observed in any of the reaction systems.

In contrast to the impregnated copper catalysts, adequate copper loading was believed to have been achieved by following the electroless plating method for catalyst preparation. It has been shown that hydrophobicity and the lack of interaction with other solvents *e.g.* organic solvents, is a problem during the production of expanded slate catalysts. It is therefore a possibility that the inactivity of the copper catalysts during H_2 tests arises from the fact that sufficient reactant is unable to adsorb onto the hydrophobic expanded slate surface thus preventing the initiation of the catalytic process. Furthermore diffusion limits associated with hydrogen passing through the reactant solution are believed to hinder the accessibility of the catalyst surface to the reactants thus reducing the likelihood of a reaction taking place. By comparison, Cu/alumina catalysts prepared by Chang *et al* have shown good activity and selectivity towards the dehydrogenation of alkanes such as 1,4-butane.[8] Indeed the reaction involving 1,4-butane is in the gaseous phase therefore the diffusion limits were not a factor and the problems of hydrophobicity were not present in the testing of electroless plated alumina catalysts by Chang *et al.* It is also a possibility that these copper/expanded slate catalysts require harsher reaction conditions to become effective *i.e.* higher temperature (>348K) and/or greater pressure (>60psi). Unfortunately these experimental conditions are beyond the safety limits of the Parr 3911 Hydrogenator and therefore could not be investigated by using this instrument.

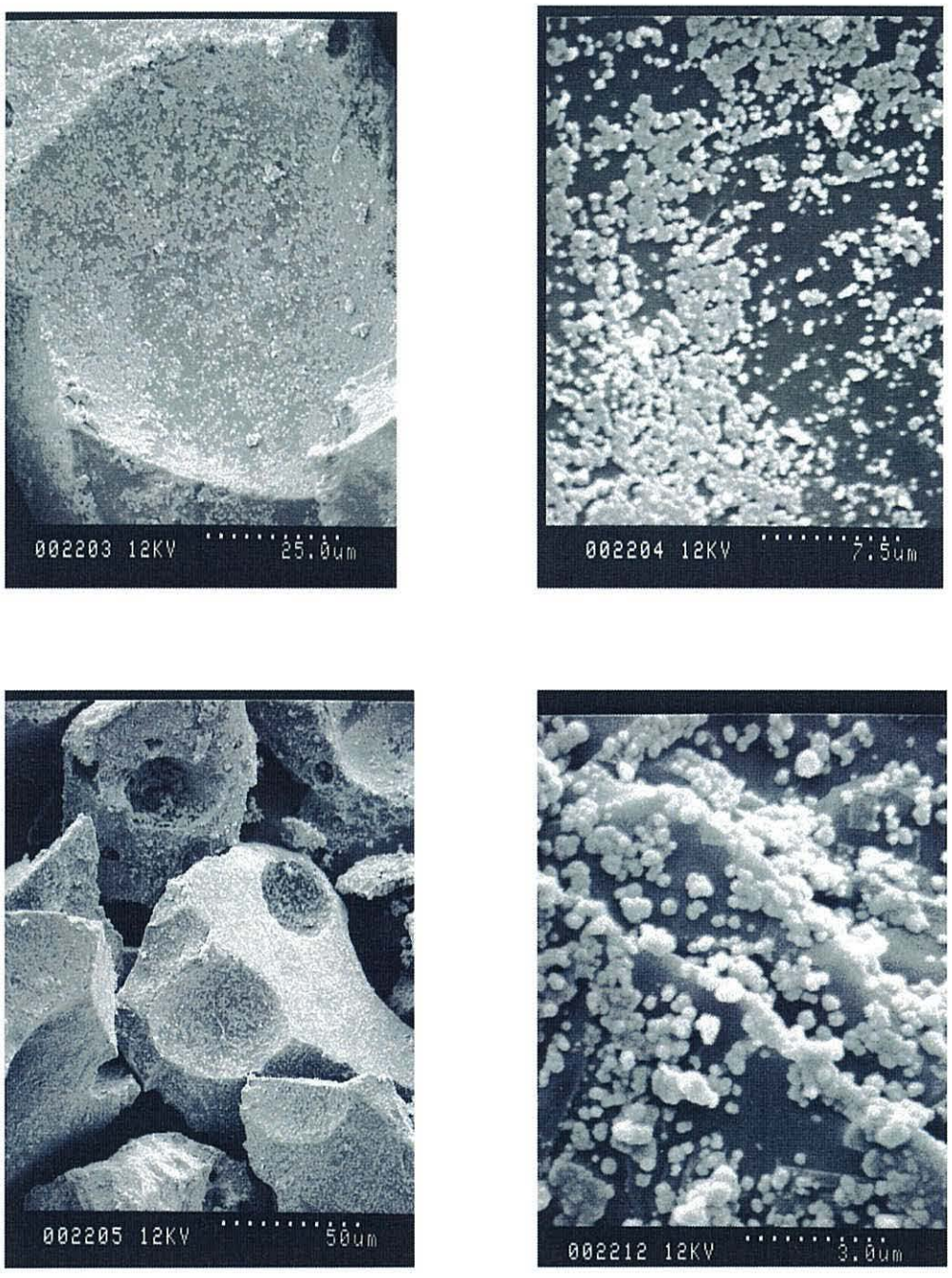

Figure 4.5: SEM images of copper deposited on expanded slate by the electroless plating method; showing wide distribution of small copper particles across the whole surface.

4.2.2. Palladium Electroless Plated Expanded Slate Catalysts

As a result of the apparent inactivity of the copper supported expanded slate catalysts under the conditions limited by the hydrogenation apparatus novel palladium based catalysts have been prepared. Palladium has been chosen as an alternative metal to copper since palladium is generally reported as having greater catalytic reactivity and was therefore expected to have higher activity with respect to hydrogenation reactions.[101] The increased activity and cost of this metallic element are therefore factors that have resulted in catalysts being prepared with Pd loadings in the range of 1-5 wt.% instead of the higher theoretical copper loadings of 5 to 20 wt.%.

The method used for depositing palladium onto the surface of expanded slate was essentially the same as that previously described for the preparation of copper electroless plated catalysts. The same pre-treatment stage was followed involving initial acid and alkali washing, $SnCl_2$ sensitisation and $PdCl_2$ activation. However in this case the plating bath was made up using palladium chloride and sodium hypophosphite as a reducing agent. Ammonium chloride and ammonium hydroxide were used as complexing agent and stabiliser respectively. The bath temperature was maintained at around 323K and pH 9.2. Upon addition of sodium hypophosphite a colour change took place from the initial dark orange/brown of the plating solution to colourless. Furthermore vigorous effervescence could be seen thus providing some evidence that reduction of Pd(II) had occurred. After reaction the dried catalysts had an almost black coloration, much darker than the original colour of the untreated expanded slate powder. In addition the samples calcined under nitrogen became distinctly silver/grey in appearance which is believed consistent with palladium in the metallic form thus providing further evidence for the reduction of Pd(II) having occurred.

A series of palladium plated expanded slate catalysts have therefore been prepared with actual palladium loading in the range of 0.9 – 4.25 wt.%. (see Table 4.2). Different palladium loading was again achieved by changing the volume of a stock palladium

solution (2g/L) to be used in the plating bath. As in copper electroless plating the concentration of the plating solution was kept constant. The mass of palladium deposited onto the surface of the expanded slate powder was determined by re-extracting the palladium back into solution then determining its concentration by ICP-AES and calculating back to obtain the Pd loading on the surface. The samples were initially digested in nitric acid (concentrated acid: water ratio 5:1) so that any palladium on the surface would dissolve in the acidic solution. The acidic palladium solutions were then diluted to within the appropriate concentration range in accordance with the standard solutions prepared to generate an accurate calibration curve.

Table 4.2. Electroless deposited palladium expanded slate catalysts.

Batch No.	Catalyst	Calc. Atmos	Calc. Temp (K)	Particle Size (:m)	Pd Loading		Effective Deposition (%)
					Theoretical wt.%Pd	Actual wt.%Pd	
20	Pd1(1)	N/A	-	63 – 105	2	2.39	119.5
20	Pd2(2)	Air	673	63 – 105	3	1.01	33.6
21	Pd3(2)	N_2	673	105 – 180	4	3.00	75.0
21	Pd4(1)	N/A	-	105 – 180	5	5.60	112.0
21	Pd4(2)	Air	673	105 – 180	5	1.34	26.8
21	Pd5(1)	N/A	-	105 – 180	2	1.48	74.0
21	Pd5(2)	Air	673	105 – 180	2	1.03	51.4
21	Pd6(1)	N/A	-	105 – 180	3	0.49	16.3
22	Pd7(2)	Air	673	63 – 105	1	0.43	43.0
23	Pd8(2)	N_2	673	105 – 180	2	1.93	96.5
23	Pd9(1)	N/A	-	105 – 180	3	3.50	116.6

The data obtained during analysis of extracted Pd samples shows that the Pd electroless plated catalysts that had undergone calcination in air at 313K tended to produce results indicating that a lower mass of Pd had been extracted from the expanded slate surface in comparison to uncalcined samples *e.g.* Pd4(2) calcined in air was recorded as having a

much lower Pd content than uncalcined Pd4(1). A slightly lower Pd concentration than expected was also detected for catalysts that had undergone calcination in nitrogen *e.g.* Pd3(2). Pd extractions from uncalcined samples were therefore found to be more successful with Pd concentrations generally in accordance with the theoretical concentration determined before hand. An exception to this trend appears to be Pd8(2) since although calcination in nitrogen has occurred extraction of the palladium from the surface produced a result that was consistent with the theoretical value. It is possible that these results reflect the loss of palladium during the calcination process. However it is more likely that calcination produces palladium species on the surface of expanded slate that are more difficult to extract thus resulting in less Pd being detected by ICP-AES. This clearly illustrates differences in the nature of the palladium species before and after calcination. However in some cases the effective deposition rose to over 100% c.*f.* Pd1(1), Pd4(4) and Pd9(1) with 119.5, 112.0 and 116.6% deposition respectively. This is believed to reflect discrepancies in the volume of the Pd plating bath initially used. The increased palladium content may also result from the cumulative effect associated with the extraction of $PdCl_2$ solution used as an activating agent in the pre-treatment stage in batches 20 and 21 thus reflecting the apparent success of palladium sorption during pre-treatment.

XRPD analysis of calcined and uncalcined samples also shows significant differences between the diffraction patterns of the respective samples. In addition to the peaks normally found corresponding to expanded slate *i.e.* peaks relating to quartz, mullite and hercynite, the diffraction patterns of the uncalcined palladium plated samples also exhibit a relatively weak, broad peak with d-spacing 2.24Å (Figure 4.6). This may be due to the structure of the initial electroless Pd film having some amorphous character alternatively the broad weak intensity peak may reflect small crystal size or poor crystallinity. Upon calcination at 313K in an inert atmosphere such as nitrogen the resulting material produced a diffraction pattern with much sharper peaks matching those of elemental palladium *e.g.* Pd4(2) (Figure 4.7) with major peaks at 2.24 and 1.95Å.[164] By comparison reports of electroless deposited palladium calcined in argon state the formation of two crystalline phases namely pure Pd and a phosphorous containing complex Pd_6P.[150] Peaks

corresponding to the latter have not been identified in the diffraction patterns obtained for calcined electroless palladium on an expanded slate support. However XRPD also shows that calcination in air generally gives rise to two phases (PdO and Pd) on the surface of expanded slate *e.g.* Pd2(2) (Figure 4.8). Again no evidence for the presence of Pd_6P has been observed in these samples. The differences seen by ICP-AES of the mass of palladium extracted from uncalcined compared to calcined samples is therefore believed to directly result from the apparent compositional differences of the Pd present on the surface of the samples. Indeed samples that had undergone calcination in air or nitrogen showed XRPD evidence of crystalline PdO and/or Pd remaining on the surface even after extraction in concentrated acid had taken place. The XRPD patterns of the extracted uncalcined samples also correlate with the higher Pd concentrations determined by ICP-AES since the resulting diffraction pattern was in agreement with that previously seen for untreated expanded slate with no broad peaks at around 2.24Å nor any other peaks corresponding to either Pd or PdO. This therefore suggests that recystallisation of the original amorphous Pd film through calcination resulting in the formation of crystalline phase Pd or PdO generates palladium species that are less soluble in acid.

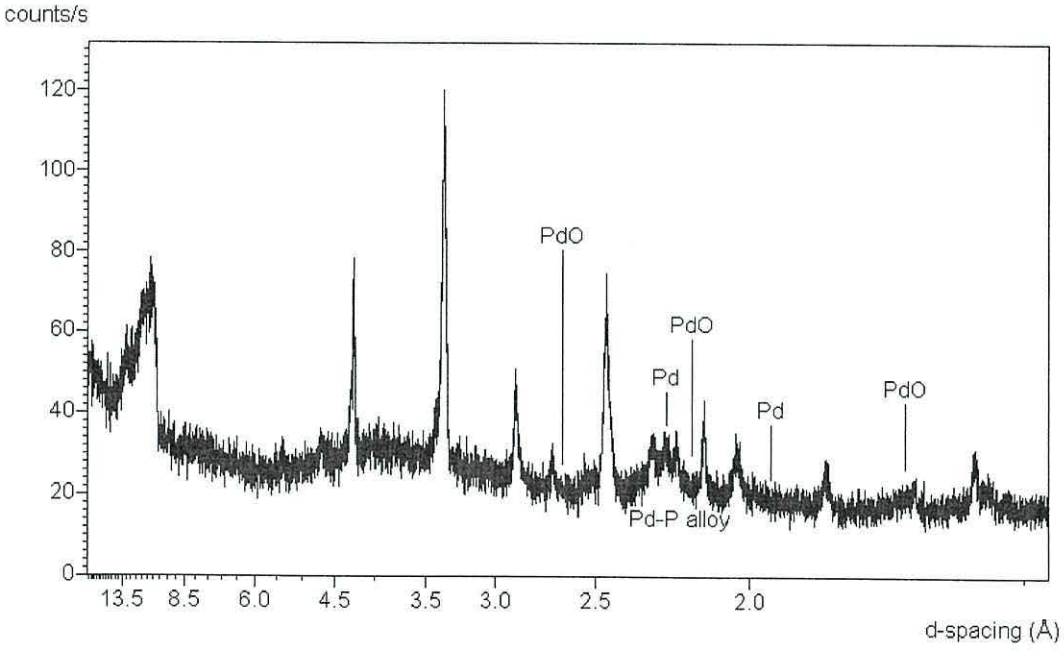

Figure 4.6. XRD pattern of electroless plated expanded slate catalyst Pd2(1)–uncalcined.

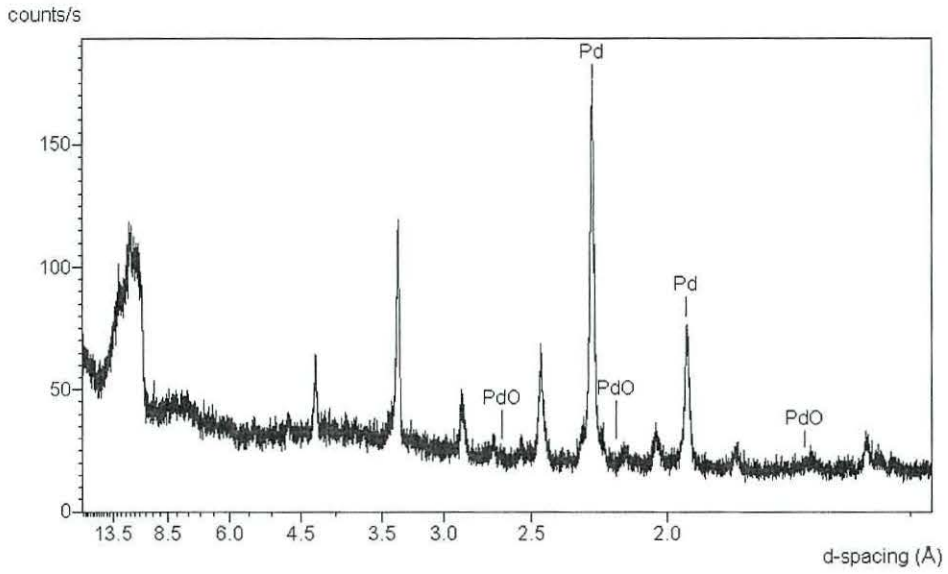

Figure 4.7. XRD pattern of Pd electroless plated expanded slate calcined in nitrogen (Pd4(2)) showing expanded slate peaks; Pd and absent PdO peaks.

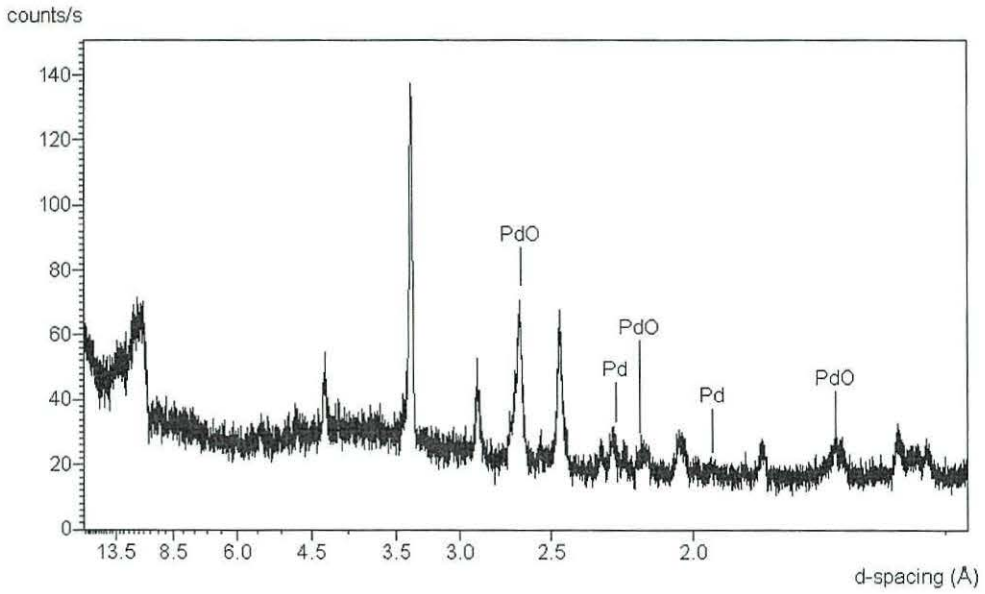

Figure 4.8. XRD pattern of Pd electroless plated expanded slate calcined in air (Pd2(2)) showing expanded slate peaks; PdO and lower intensity Pd peaks compared to calcination in nitrogen.

The length of calcination time required to convert the initial amorphous Pd film to crystalline Pd or PdO has also been investigated. Calcination in air showed that both Pd and PdO are produced. A longer calcination period in air was therefore expected to reduce the amount of Pd on the surface by generating more PdO. However XRPD analysis of calcined samples have shown that the length of heat treatment has very little effect on the ratio of Pd:PdO of samples calcined in air *i.e.* there is no significant difference between the intensity of the Pd peaks found in the diffraction patterns of samples heated for 4 hours compared to those heated overnight.

Analysis of the palladium plated samples, before and after calcination, by scanning electron microscopy shows a distribution of small crystallites extending across the whole surface of the expanded slate powder (Figure 4.9). There appeared to be no significant differences in the surface morphology of samples calcined in air, in nitrogen or in uncalcined samples. In fact the morphology of the Pd samples was consistent with that previously observed for copper electroless plated expanded slate samples. EDS analysis focussing on the crystallites visible on the surface of uncalcined samples generally produced spectra with strong peaks corresponding to palladium. Spot-analysis of areas high in palladium also recorded weak peaks corresponding to phosphorous. This is in agreement with work carried out by Djokić who stated that an amorphous Pd-P alloy was initially formed as the deposited species when electroless deposition of palladium was carried out using sodium hypophosphite as the reducing agent.[150] Calcined samples again produced a strong Pd peak when analysed by energy dispersive spectroscopy however surprisingly the intensity of the minor P peak was generally found to be very similar to that found during analysis of the uncalcined samples. In this case the Pd:P ratio based on peak height intensities was found to be approximately 15:1. This suggests that recrystallization of the initial Pd-P coating during calcination to produce either Pd or PdO does not result in the removal of phosphorous from the surface. It is not possible to distinguish between PdO and Pd by EDS since the instrument's beryllium window blocks low energy radiation such as that produced by oxygen. Similarly EDS could not confirm the identity of the phosphorus species present on the surface of calcined expanded slate so

the effect of calcination conditions on the phosphorous could not be conclusively determined.

In comparison to reactions carried out using impregnated or electroless plated copper catalysts preliminary hydrogenation experiments testing the activity of palladium electroless plated expanded slate catalysts showed promising results for the conversion of maleic acid to succinic acid. In this case a decrease from the starting hydrogen pressure of 60psi was observed. Following this initial success a more comprehensive study of the relative activity of the various palladium catalysts towards hydrogenation reactions involving maleic acid, nitrobenzene and cyclohexene has been carried out and will be discussed in detail in the next section.

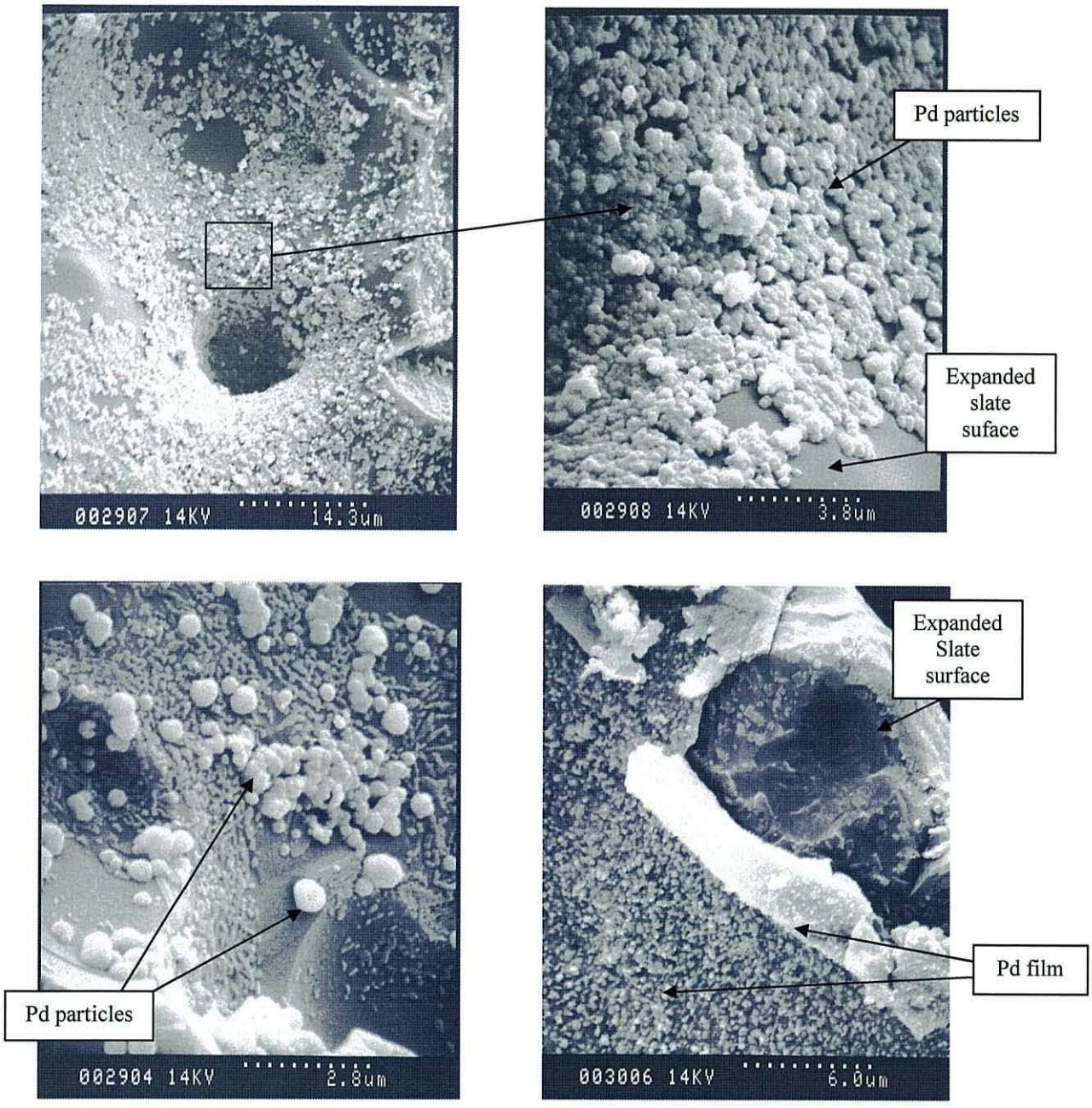

Figure 4.9. SEM images of Pd electroless plated expanded slate catalysts; showing wide distribution of metal particles on the surface.

4.3. Hydrogenation Experiments

4.3.1. Standardising the Hydrogenator

To be able to accurately record and compare the degree of hydrogen consumption observed during experiments using different Pd catalysts it was necessary to standardise the Parr 3911 Hydrogenation apparatus prior to use. This standardisation procedure involved making preliminary runs using a known concentration of reagent that reduced completely and quantitatively to produce a single product. The pressure decrease per mole of hydrogen could then be used as a basis for estimating the progress of an "unknown" reaction. The standard starting compound normally used for this process was maleic acid (equation 4.1). The standardisation process was carried out under a hydrogen pressure of 60psi at room temperature (293-298K) and a catalyst known to be active towards the hydrogenation of maleic acid was used. Standardisation was therefore carried out using a Raney nickel type catalyst (0.1g). To initiate and maintain reaction and to reduce the effects of diffusion the reaction vessel was shaken vigorously throughout the standardisation procedure. The shaking mechanism is essential since it reduces the problems associated with diffusion limits encountered in liquid phase reaction as a result of the hydrogen atoms having to pass through the reaction solution to be adsorbed onto the surface of the catalyst. A hydrogen pressure decrease of 9psi (±1psi) over a period of 2hrs was consistently seen corresponding to 0.11moles of hydrogen being consumed. This corresponds to the calculated amount of hydrogen required to convert 0.1 moles of maleic acid to succinic acid. The standardisation is clearly an important stage to carry out since information gained from the application of Raney nickel in this way can also be used to compare the rate of hydrogenation of the maleic acid catalysed by palladium electrolessly plated catalysts. Raney nickel can therefore effectively act as a reference catalyst for subsequent reactions.

4.3.2. Maleic Acid Hydrogenation

A series of tests have been carried out using Pd electroless plated expanded slate catalysts. In agreement with the hydrogen pressure decrease observed in the standardisation reactions using the Raney nickel type catalyst, a consistent maximum pressure decrease of 9psi (±1psi) was recorded by the most active palladium catalysts (see Table 4.3). However, in contrast to Raney nickel, reactions catalysed by palladium/expanded slate catalysts were left for a much longer period of time to ensure completion *i.e.* ~24hrs compared to 2hrs. For instance only a 5psi pressure fall was observed after 5 hours in the case of Pd(4) in experiment E6. The activity of the palladium catalysts for maleic acid hydrogenation is therefore believed to be lower than that of Raney nickel since a 9psi pressure fall was observed within 2 hours for this catalyst. Since 0.1 mole of hydrogen again should have been consumed in this process, it is therefore possible to use the decrease in the tank pressure (9±1psi) as a method for measuring and/or regulating the amount of hydrogen consumed in other reactions.

Table 4.3. Maleic acid hydrogenation experiments.

Expt. No.	Catalyst	Pd wt.%	Pd Species	Total Time (hrs)	Pressure Decrease (±1psi)	No. Moles H_2 Consumed
E1	Pd2(2)	3	PdO/Pd	43.00	8	0.08
E2	Pd2(3)	3	Pd	25.75	3	0.03
E3	Pd2(2)	3	PdO/Pd	23.50	9	0.10
E4	Pd1(2)	2	Pd	26.50	4	0.04
E5	Pd1(1)	2	Pd-P alloy	24.00	0	0
E6	Pd2(4)	3	PdO/Pd	23.50	9	0.10
E7	Pd3(4)	4	PdO/Pd	53.75	8	0.08
E8	Pd7(2)	1	PdO/Pd	27.50	7	0.08
E65	Pd/Al_2O_3	5	Pd	1.75	9	0.18
E66	PdO/Al_2O_3	5	PdO	2.50	8	0.08

The Pd catalysts which produced highest conversions have been found to be Pd2(2), Pd3(4), Pd2(4) and Pd7(2) in experiments E1, E7, E6, and E3 respectively (Table 4.3). These catalysts were exposed to air during calcination thus resulting in the formation of the oxidised palladium species as well as elemental palladium, which was confirmed by

XRPD. The XRPD patterns of these active catalysts generally produced an apparent PdO:Pd ratio, based on the relative intensities of the major peaks corresponding to PdO and Pd, as ≥1:1 *i.e.* the most active catalysts tended to have more intense peaks corresponding to PdO than Pd thus suggesting a higher concentration of the oxidised species on the surface. Unfortunately a quantitative determination of the amount of PdO and Pd on the surface cannot be obtained by X-ray diffraction in this case. By comparison catalysts Pd2(3) and Pd1(2), calcined in nitrogen, did not give rise to complete conversion of maleic acid in experiments E2 and E4 since only a small pressure decrease was normally recorded. It is therefore clear from these results that expanded slate supports with PdO present on the surface exhibit greater activity towards the hydrogenation of maleic acid than catalysts calcined in nitrogen containing only elemental Pd (no PdO detected by XRPD). The importance of calcination is also reflected by the apparent inactivity of the uncalcined sample Pd1(1) which did not generate any pressure decrease when tested with regards to maleic acid reduction in experiment E5. The precise nature of the uncalcined surface was not known however it is evident that recrystallization of the initial Pd-P alloy deposited on the expanded slate surface is essential for a reaction to take place.

Experiments have also been carried out using commercially available Pd/Al_2O_3. A 9psi decrease was observed within 2hrs thus it has comparable activity to Raney nickel towards the hydrogenation of maleic acid. In order to conclusively determine whether complete conversion to succinic acid had been achieved the resultant solution was analysed using High-Performance Liquid Chromatography. The chromatograms of reaction solution E65 was compared with the chromatograms of reference maleic and succinic acid solutions. It was clear that reaction systems that had consumed the equivalent of 0.1 mole of hydrogen (9psi) produced a single peak corresponding to succinic acid. E66 which gave rise to a 8psi fall in hydrogen pressure again produced a peak matching succinic acid. However a weak peak corresponding to maleic acid was also found thus indicating that some maleic acid remained.

4.3.3. Nitrobenzene Hydrogenation

The bulk of the activity work using electroless plated palladium expanded slate catalysts focussed on the hydrogenation of nitrobenzene. In this case nitrobenzene acts as both the reactant and the solvent. The aim of these experiments was to be able to compare the activity of palladium catalysts with different palladium loading (2-5 wt.%) and to investigate the effect of palladium oxidation state on nitrobenzene (NBz) reactivity. Furthermore, the effect of temperature on reaction rate and catalyst activity has also been studied in a series of experiments that were limited to 2 hours and carried out at ambient room temperature and 348K.

4.3.3.1. Room Temperature Nitrobenzene Experiments

These experiments have again been carried out in reaction conditions similar to those for the maleic acid experiments *i.e.* at room temperature with an initial hydrogen pressure of 60psi. In these cases the reactions have been maintained for a relatively long period of time, generally for longer than 24 hours, in order to analyse the extent of product formation and to gain some knowledge of the long-term activity of the various catalysts. (see Equation 4.2 below).

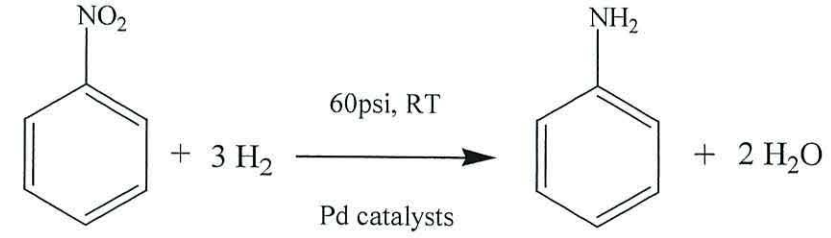

[4.2]

Unlike maleic acid hydrogenation, where only one product was formed (succinic acid), nitrobenzene hydrogenation can potentially give rise to a series of intermediate products being produced *e.g.* azobenzene and azoxybenzene. In the course of this study the selectivity of palladium expanded slate catalysts with respect to the formation of aniline has been the main focus of the investigation.

Azobenzene

Azoxybenzene

In these tests, because NBz acts as both the starting material and solvent, the theoretical maximum hydrogen consumption is potentially larger than that observed in the maleic acid experiments. From the above reaction scheme it is possible to see that the reactant to hydrogen ratio is 1:3 thus suggesting that for every one mole of nitrobenzene three moles of hydrogen should theoretically be consumed to make one mole of aniline. Since approximately one mole of nitrobenzene (100ml) was initially used, complete conversion to aniline would therefore theoretically require three moles of hydrogen, corresponding to a 270psi pressure drop (see calculation below). However in this case the potential formation of intermediate products must be taken into consideration before the volume of hydrogen consumed can be solely related to the conversion of nitrobenzene to aniline.

For example, Density nitrobenzene = 1.196g/ml

So, Mass (NBz) in 100ml = 1.196 x 100 = 119.6g

Number of moles (NBz) = mass in g / molecular weight

= 119.6/123 = 0.972 moles (approx. 1 mole)

The greatest observed pressure drop was recorded by catalyst Pd2(2) in experiment E9. A 110psi drop was seen after a total reaction time of 47.5 hours, corresponding to 1.22 moles of hydrogen (see Table 4.4). This is much lower than the amount of hydrogen required for complete conversion to aniline. In fact the information gained from the calculated hydrogen consumption indicates that an approximate 40% conversion has been achieved. By comparison, previous work studying Raney nickel type catalysts has shown that the activity of this type of catalyst decreases substantially with time for nitrobenzene hydrogenation.[166] A drop in hydrogen pressure in the order of 48psi was generally not

exceeded. As a result of theoretical study it was inferred that the build-up of polymerisation products deposited on the catalyst surface during reaction deactivated the Raney nickel catalyst sufficiently thus ensuring that the NBz reaction did not proceed after around 3hrs *i.e.* the high activity was often lost. The apparent life-time of electrolessly plated palladium supported expanded slate catalysts is therefore much greater than Raney nickel type catalysts. This provides very promising results for the possible future developments of Pd electroless deposited catalysts.

Table 4.4. Nitrobenzene Hydrogenation Results.

Expt.	Catalyst	Pd wt.%	Pd Species	Total Time (hrs)	Pressure Decrease (±1psi)	No. Moles H_2 Consumed
E9	Pd2(2)	3	PdO/Pd	47.50	110	1.222
E10	Pd7(2)	1	PdO/Pd	26.25	31	0.344
E11	Pd2(2)	3	PdO/Pd	74.30	69	0.767
E12	Pd5(3)	2	PdO/Pd	75.00	63	0.700
E13	Pd8(2)	2	Pd	17.00	0	0
E15	Pd9(2)	3	PdO/Pd	50.00	80	0.889
E16	Pd2(2)*	3	PdO/Pd	2.25	11	0.122

One of the most active catalysts was again found to be Pd2(2). This catalyst was taken from the same batch as that used in maleic acid experiment E3 (see Table 4.3). As for maleic acid hydrogenation the greatest catalytic activity was again observed when palladium plated expanded slate catalysts were calcined in air prior to testing *i.e.* PdO was present on the surface. However, by comparison, in NBz experiment E13 the use of catalyst Pd8(2), calcined in nitrogen, did not result in any decrease in hydrogen pressure being observed. The presence of Pd alone on the surface of expanded slate is therefore believed to produce inactive catalysts with respect to the reduction of nitrobenzene. This is in contrast to maleic acid hydrogenation where slight hydrogen consumption was noted when catalysts calcined in nitrogen were tested.

Catalysts before and after testing have been analysed by XRPD. The nature of the palladium on the surface of expanded slate was shown to be dependent on calcination conditions and has previously been discussed in section 4.3.2. Diffraction patterns of used active catalysts were found to be markedly different to those of the unused catalysts. It was apparent that the peaks corresponding to PdO in the active samples had disappeared after use. In fact elemental Pd was generally detected on the surface instead of PdO. This therefore illustrates that reduction of PdO on the surface of expanded slate also takes place during the hydrogenation of nitrobenzene. This reduction is believed to be directly related to the apparent activity of the samples calcined in air. The ability to reuse a catalyst has also been investigated. Catalyst Pd2(2) used in experiment E9 was recalcined in air at 313K for 4hrs to produce Pd2(2)*. XRPD analysis of Pd2(2)* showed that PdO was reproduced on the surface. Subsequent testing of the recalcined catalyst reflected the presence of PdO since a hydrogen pressure drop was recorded thus indicating that Pd2(2)* was active towards further hydrogenation reactions.

By comparison, SEM analysis did not show any differences between the morphology of used and unused samples *i.e.* no nitrobenzene polymerisation product observed on the surface. The high dispersion of crystallites was still apparent even after the samples had been used to catalyse the reduction of nitrobenzene. Energy dispersive analysis correlated with the apparent similarity in the morphology of the samples since the relative peak heights and Pd:P ratio were consistent with that previously seen during the analysis of unused catalysts in section 4.3.2.

In addition to catalyst characterisation the reaction products from experiments E9-E16 have also been analysed by GC, GC-MS and FTIR to gain an insight into the degree of nitrobenzene conversion to aniline and the selectivity of the respective catalysts towards this product. It was apparent that complete conversion of nitrobenzene to aniline had not occurred since peaks could be found corresponding to both compounds when the reaction solutions were analysed by GC. However the calculated amount of hydrogen consumed in the experiments correlated well with the conversion ratio of nitrobenzene to aniline

detected by GC *i.e.* aniline:nitrobenzene ratio tended to increase with increasing hydrogen consumption.

In addition to greater product formation increased H_2 consumption also resulted in two layers being formed. The top layer has a much smaller volume (1-5ml, depending on hydrogen consumption) and is initially colourless but becomes a cloudy, muddy brown solution upon standing in air. The bottom layer is consistently dark orange/brown in colour compared to the initial light yellow coloration of nitrobenzene. Infrared analysis of the top layer produces a spectrum that is characteristic of water *i.e.* very strong, broad peak at ~3500cm^{-1} and a weaker peak at 1643cm^{-1}. The presence of water is in accordance with the reaction scheme given previously (Equation 4.2). Water is immiscible with nitrobenzene resulting in two the layers being observed if a sufficient volume of water is produced. GC-MS analysis of the top aqueous layer generally produces a complex pattern including relatively weak peaks, compared to the bottom layer, corresponding to aniline and nitrobenzene (water cannot be easily detected by GC-MS). Indeed aniline and nitrobenzene are soluble and sparingly soluble in water respectively, this can therefore explain the brown coloration of the resulting solution. Analysis of the bottom organic layer by GC-MS showed that in addition to nitrobenzene and aniline trace amounts of intermediate products have also been produced, namely azobenzene and azoxybenzene.

The formation of these two intermediates during NBz reduction over palladium and platinum supported glass fiber catalysts has been reported by Höller in the literature.[167] However, Höller *et al* also reported evidence for the presence of nitrosobenzene and phenylhydroxylamine, especially in experiments utilising Pt supported glass fibre catalysts. The reaction scheme proposed by these workers is illustrated in Figure 4.10. In contrast, no data has been found relating to the formation of these last two intermediate compounds in the experiments involving supported expanded slate catalysts. This therefore suggests that the mechanism involved in the hydrogenation of nitrobenzene to aniline using Pd/expanded slate catalysts follow the sequence nitrobenzene→azoxybenzene→azobenzene→aniline since the other hydrogenation

products nitrozobenzene, phenylhydroxylamine and hydrazobenzene have not been detected.

The IR analysis of the bottom layer produced spectra that have peaks characteristic of both nitrobenzene and aniline. This is in agreement with the information gained from the GC and GC-MS analysis, which clearly showed that the solution was made up of a mixture of starting material and product. No peaks corresponding to either azobenzene nor azoxybenzene have been identified in the lower layer by IR in comparison to GC and GC-MS. This is believed to be due to their relative trace concentrations and hence their IR signals being much weaker compared to that of nitrobenzene and aniline.

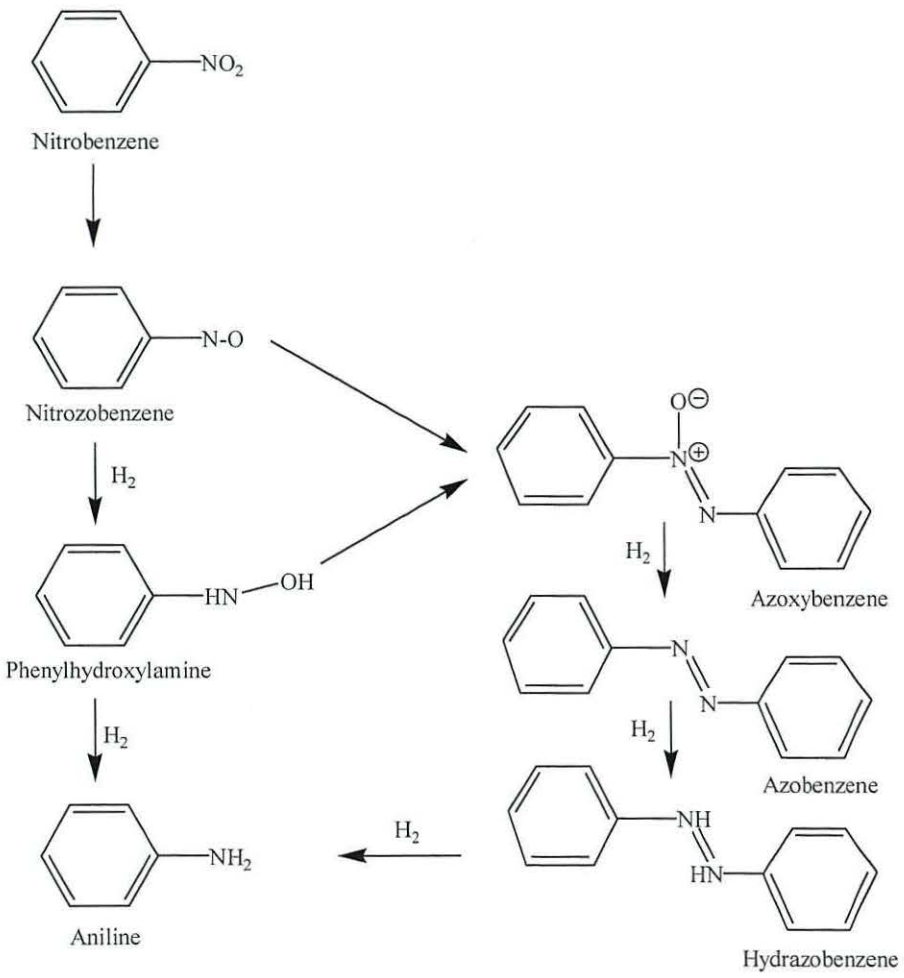

Figure 4.10. Reaction scheme for the selective hydrogenation of nitrobenzene.[167]

Analysis of the reaction solutions therefore clearly showed that Pd electroless plated expanded slate catalysts demonstrate selectivity towards $-NO_2$ group hydrogenation of nitrobenzene since no ring hydrogenation products were detected.

4.3.3.2. Effect of Temperature on Nitrobenzene Hydrogenation

A series of experiments have been carried out in order to study the effect of increasing the temperature of reaction to 343K on the rate of hydrogen consumption in nitrobenzene hydrogenation reactions. The experiments were again carried out using the 3911 Parr Hydrogenation apparatus with an initial hydrogen pressure of 60psi and 100ml nitrobenzene. Temperature control was achieved by wrapping a heating jacket around the bottle. The temperature in the reaction vessel was measured and controlled by installing a stainless steel sheathed thermocouple into the solution inside the reaction vessel and connecting it to a temperature controller. Furthermore reaction times were limited to 2 hours for all experiments so that the duration of the experiment did not play a factor in determining the relative activity of the palladium catalysts.

It was evident that reactions carried out at 348K tended to give rise to a greater pressure drop being recorded than that measured during reactions at room temperature (293-298K) (see Table 4.5). A slight increase in the volume of hydrogen consumed was found when catalyst Pd2(2), calcined in air, was tested in experiments E33 (343K) compared to E34 (RT). This trend was more apparent for catalysts Pd1(A) and Pd1(B) calcined in air for 4hours and overnight respectively. Although Pd1(B) was calcined for a longer period of time a significant difference in its activity compared to Pd1(A) was not observed neither at 343K nor RT. This supports the findings previously discussed in section 4.4.3.1 on the effect of calcination on catalyst activity in that a long calcination period has again been shown to be unnecessary to optimise the activity of palladium supported expanded slate catalysts. In addition, increasing the solution temperature did not appear to increase the activity of catalysts calcined in nitrogen. This was demonstrated in experiments E35, E37, E39 and E41, whereby a pressure decrease between 0 and 0.5psi was consistently

measured. The slight pressure drop (0.5psi) produced by Pd9(A) and Pd9(B) however is believed to be due to the detection of small amounts of PdO on the surface by XRPD.. XRPD analysis of used catalysts has shown that PdO again disappears after reaction. The reduction of PdO has previously been mentioned in section 4.4.3.1 after hydrogenation reactions had been maintained for >24hrs *e.g.* catalyst Pd2(2) in experiment E9 (Table 4.4). The apparent loss of PdO after 2hour experiments therefore suggests that reduction of this palladium species occurs during the initial stages of nitrobenzene hydrogenation.

An investigation into the activity of a commercial palladium supported catalyst was also carried out to provide a comparison with the data obtained during the application of electroless plated Pd/expanded slate catalysts in nitrobenzene hydrogenation experiments (Table 4.6). A Pd/alumina (5wt.% Pd) was obtained from Aldrich Chemicals for use as a reference catalyst. The greatest pressure drop (25psi) was observed in experiment E22, which utilised Pd/Al_2O_3 at 348K. This pressure drop at 348K was double that observed when the same reaction was carried out at RT. However, in contrast to Pd/expanded slate catalysts the oxidation of Pd/Al_2O_3 in air at 400°C (4hrs or overnight) consistently resulted in a catalyst that had lower catalytic activity towards the reduction of nitrobenzene. XRPD analysis of uncalcined Pd/Al_2O_3 produced a diffraction pattern corresponding to mainly the minerals boehmite ($\alpha Al_2(OOH)_2$) and gibbsite ($\alpha Al(OH)_3$) (Figure 4.11). An extremely weak peak corresponding to pure palladium was also visible. Analysis of the calcined material however showed that calcination gave rise to some decomposition of the alumina support. The XRPD diffraction pattern now had peaks corresponding to only boehmite and not to gibbsite (Figure 4.12). Furthermore broad peaks corresponding to PdO could also be seen. This is believed to result from sintering of the palladium during calcination. SEM studies have shown no significant differences in the morphology of PdO/Al_2O_3 compared to Pd/Al_2O_3, which appeared to have isolated crystallites (Figure 4.13). EDS analysis of both the isolated crystals on uncalcined alumina and the surface coating of calcined alumina produced patterns consistent with palladium. The decrease in catalytic activity of calcined alumina catalysts is therefore believed to result from the apparent sintering effects of the surface palladium oxide generated during exposure to air at 673K.

Table 4.5. Effect of temperature on nitrobenzene hydrogenation using electroless plated Pd/expanded slate catalysts.

Expt.	Catalyst	Mass of Catalyst (g)	Pd wt.%	Calcination Conditions	Pd Species	Total Time (mins)	Reaction Temp. (K)	Temp. Rise (K)	Pressure Decrease (±1psi)	No. Moles of H_2 Consumed
E27	Pd1(A)	1	2.4	4hr/400°C/air	PdO	2:01	348	--	13.5	0.150
E28	Pd1(A)	1	2.4	4hr/400°C/air	PdO	2:00	RT	7	8	0.089
E29	Pd1(B)	1	2.4	18h/400°C/air	PdO	2:00	348	--	14.5	0.161
E30	Pd1(B)	1	2.4	18h/400°C/air	PdO	2:00	RT	12	11	0.122
E33	Pd2(2)	1	~3	18h/400°C/air	PdO/Pd	2:18	348	--	15	0.167
E34	Pd2(2)	1	~3	18h/400°C/air	PdO/Pd	2:13	RT	9	13	0.144
E35	Pd9(A)	1	3.5	4hr/400°C/N_2	Pd	2:00	348	--	0.5	0
E37	Pd9(B)	1	3.5	18h/400°C/N_2	Pd	2:00	348	--	0.5	0
E39	Pd8(2)	1	~2	18h/400°C/N_2	Pd	2:00	348	--	0	0
E41	Pd3(2)	1	~4	18h/400°C/N_2	Pd	2:00	348	--	0	0
E43	Pd11(A)	1	~4	4hr/400°C/air	PdO	2:15	348	--	12	0.133
E44	Pd11(A)	1	~4	4hr/400°C/air	PdO	2:00	RT	7	7	0.078
E45	Pd12(A)	1	~5	4hr/400°C/air	PdO	2:00	348	--	16	0.178
E46	Pd12(A)	1	~5	4hr/400°C/air	PdO	2:40	RT	8	11	0.122

Table 4.6. Effect of temperature on nitrobenzene hydrogenation using Pd/alumina (reference catalyst).

Expt.	Catalyst	Mass of Catalyst (g)	Pd wt.%	Calcination Conditions	Pd Species	Total Time (mins)	Reaction Temp. (K)	Temp. Rise (K)	Pressure Decrease (±1psi)	No. Moles of H_2 Consumed
E22	Pd/Al_2O_3	0.4	5	As purchased	Pd	120	348	--	25	0.278
E23	Pd/Al_2O_3	0.4	5	As purchased	Pd	120	323	--	14	0.156
E24	Pd/Al_2O_3	0.4	5	As purchased	Pd	120	RT	15	12.5	0.139
E25	PdO/Al_2O_3(A)	0.4	5	4h/400°C/air	PdO	123	348	--	15	0.167
E26	PdO/Al_2O_3(A)	0.4	5	4h/400°C/air	PdO	120	RT	11	12	0.133
E31	PdO/Al_2O_3(B)	0.4	5	18h/400°C/air	PdO	120	348	--	18	0.200
E32	PdO/Al_2O_3(B)	0.4	5	15h/400°C/air	PdO	122	RT	7	8.5	0.094

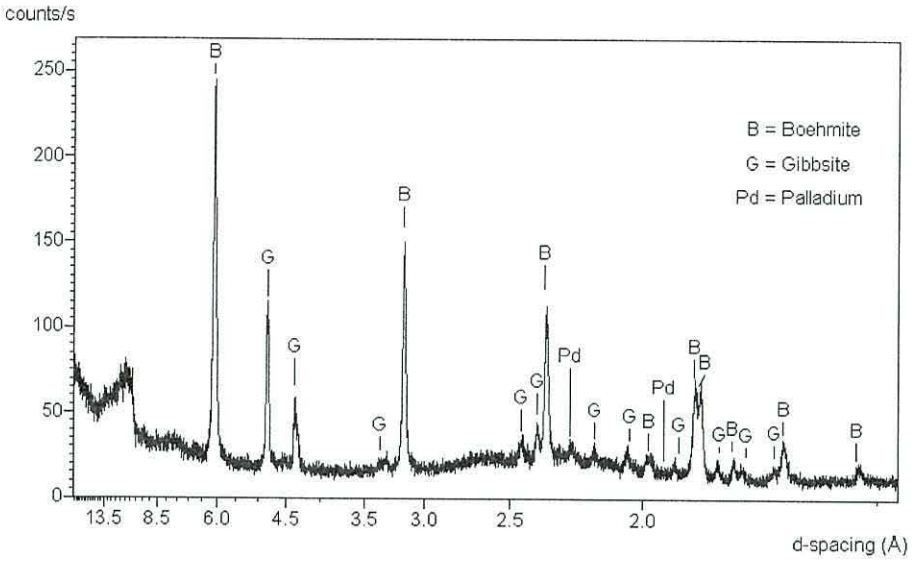

Figure 4.11. XRD pattern of untreated Pd/alumina reference catalyst.

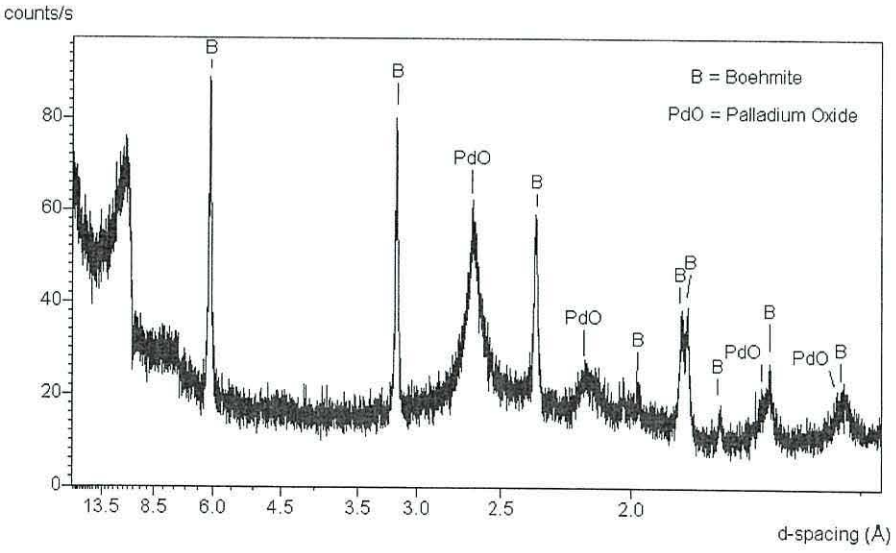

Figure 4.12. XRD pattern of palladium supported alumina reference catalyst calcined in air (PdO/alumina).

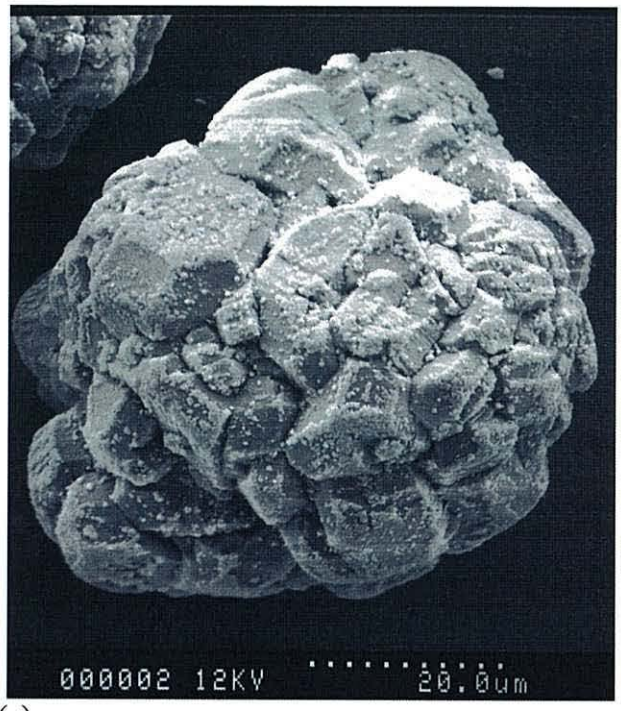

(a)

(b)

Figure 4.13. SEM micrographs of palladium supported alumina catalyst (a) untreated catalyst and (b) catalyst calcined in air at 673K.

As a result of a thermocouple being present inside the reaction vessel changes in the temperature of the reaction solution during RT experiments could be monitored. It was apparent that as nitrobenzene hydrogenation proceeded a slight increase in the solution temperature occurred during the process. A temperature rise between 7 and 12K was observed. This rise in temperature was found to coincide with the period of greatest activity since a more rapid pressure decrease was also observed at this time (Figure 4.14 and 4.15). The highest temperature was normally maintained for between 5-10 minutes, after which point it decreased slowly back to room temperature. This is believed to result from the fact that the hydrogenation of nitrobenzene is an exothermic process. Indeed the calculated enthalpy of reaction for the process based on the difference between the enthalpy of formation of products and reactants is –552.8kJ/mol at room temperature (RT). The input of external heat through the heating jacket therefore provides more energy for nitrobenzene molecules to overcome the activation energy (E_a) of the system. Consequently the rate of reaction increases giving rise to more heat (exotherm) which in turn provides more energy for more NBz molecules to overcome the E_a. Hence the greater hydrogen consumption being observed when the solution is heated.

As result of reaction times being relatively short (2hrs), the formation of a second layer was generally not observed during these experiments. The amount of nitrobenzene converted to aniline was low relative to NBz experiments maintained for >24hrs (Section 4.4.3.1). This was supported by the relatively small drop in pressure being observed in all experiments compared to reaction maintained for >24hrs (Table 4.4). The decrease in pressure directly relates to the consumption of hydrogen and thus to the amount of product formed. This therefore corresponds to *ca.*0.3 moles of hydrogen being consumed, theoretically producing 0.1 moles of aniline. GC-MS analysis of the resulting solutions indeed showed that nitrobenzene remained to be the major phase however trace amounts of aniline was also detected. The formation of aniline was further supported by GC and IR. However no evidence for the formation of the intermediate products azobenzene or azoxybenzene was obtained. This is believed to be due to the concentration of these intermediates being too low to be detected by GC, GC-MS or IR analysis.

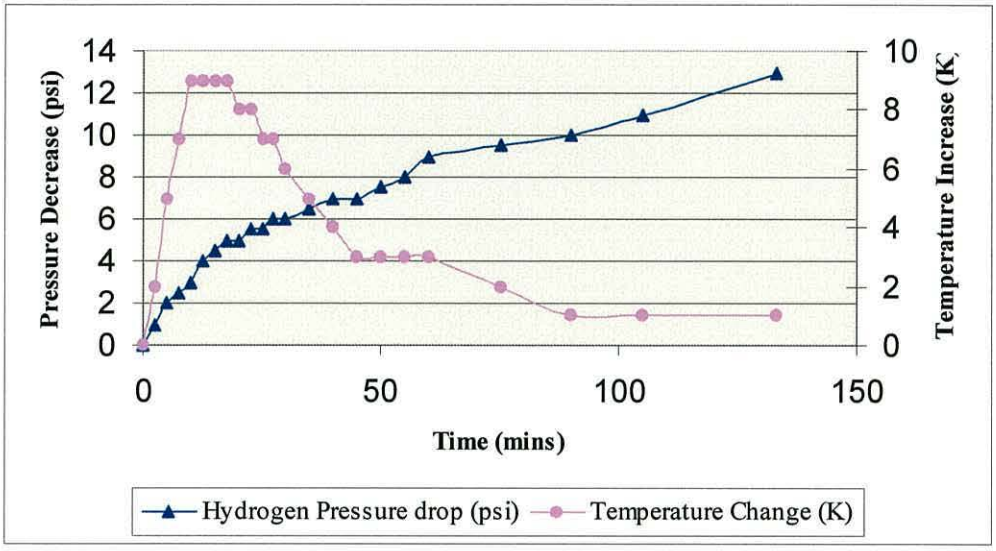

Figure 4.14. Graph illustrating the pressure decrease and associated temperature increase recorded over a 2hr period during NBz hydrogenation experiment E34 (RT) using catalyst Pd2(2).

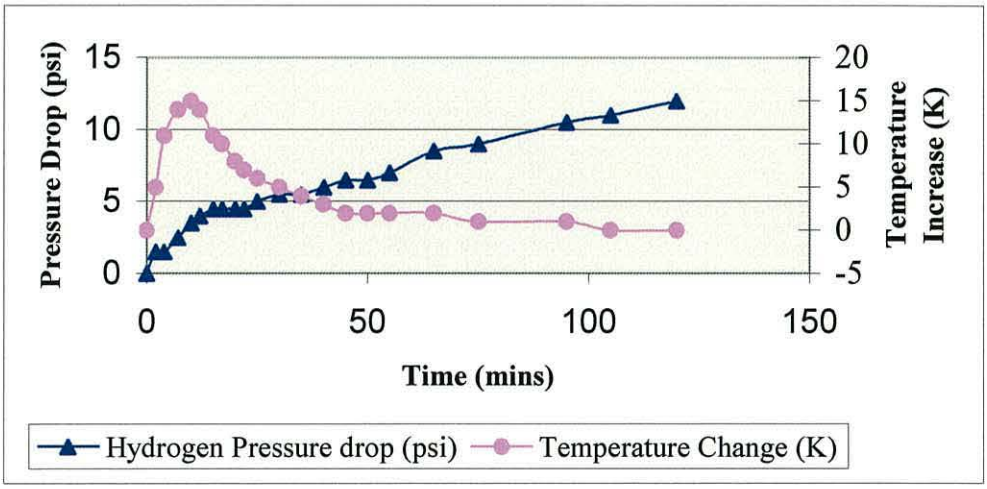

Figure 4.15. Graph illustrating the pressure decrease and associated temperature increase recorded over a 2hr period during NBz hydrogenation experiment E24 (RT) using catalyst Pd/Al_2O_3 (larger temperature correlates to increased catalytic activity).

4.3.4. Cyclohexene Hydrogenation

Hydrogenation experiments involving cyclohexene (equation 4.3) have also been carried out in order to test the ability of palladium supported expanded slate to catalyse reactions other than just maleic acid (polar molecule with C=C bond reduction) and nitrobenzene (organic molecule with $-NO_2$ group reduction). Cyclohexene is different to these two compounds in that the C=C bond to be hydrogenated is within a non-polar molecule and part of a ring structure. An insight into the range of compounds hydrogenated using the novel expanded slate catalysts will therefore be obtained following this study. The commercially available Pd/alumina catalyst was again used as a reference catalyst for this experimental series.

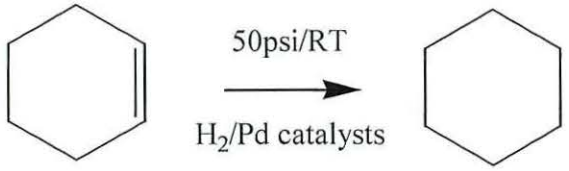

Cyclohexene Cyclohexane [4.3]

These reactions were again carried out in the standard hydrogenation apparatus. The reaction conditions were adjusted in this case since cyclohexene is a more volatile compound than nitrobenzene (boiling point 83°C compared to 210°C respectively).[13] The effect of this increased volatility on the hydrogenation apparatus was not known therefore the starting pressure and reactant volume were reduced *i.e.* starting pressure (50psi) and only 50ml of cyclohexene, in order to ensure safety during the experiments. Furthermore, heat was normally not put into the system as a result of the relatively low boiling point of cyclohexene. However if the experiments proved unsuccessful at room temperature the bottle temperature was carefully raised to 323K to try and initiate reaction. The reaction time was again generally limited to between 1-2 hours and any decrease in pressure or increase in temperature was recorded at regular intervals.

Work on cyclohexene hydrogenation has shown that palladium catalysts, which were successful in reducing nitrobenzene, have also been found to be active catalysts in these

experiments (see Table 4.7). However a greater pressure drop was consistently recorded during cyclohexene hydrogenation reaction at room temperature compared to nitrobenzene experiments *e.g.* catalyst Pd11(A) gave rise to a 17.5psi drop in E49 compared to 7psi in E44 (cyclohexene and nitrobenzene respectively). This trend was also evident for Pd12(A). The use of Pd2(2) however did not appear to give a significant increase in pressure drop compared to during cyclohexene hydrogenation (E51) compared to experiments carried out in nitrobenzene (E34) however it must be noted that only 0.5g of the catalyst was used in experiment E51 compared to the normal 1.0g and the reaction was only maintained for 1 hour. It is therefore evident that increased activity has also been shown by Pd2(2). The activity of the commercially available Pd/alumina catalyst also demonstrated this trend. It is believed that cyclohexene hydrogenation is also an exothermic since a temperature rise between 2 and 13K was recorded ()rH = - 117.8kJ/mol). The most active experiments that consumed the largest volume of hydrogen also corresponded to the highest increase in temperature. This is clear from E50 utilising catalyst Pd12(A) which recorded a 21psi pressure drop and a 13K temperature rise from RT.

Surprisingly Pd3(2) calcined in nitrogen did result in a reduction from the initial pressure therefore indicating that Pd has some catalytic activity towards cyclohexene hydrogenation. This is in contrast with data gained from nitrobenzene experiments which consistently proved unsuccessful when catalysts calcined in N_2 were used *c.f.* E41 using catalyst Pd3(2) in Table 4.5.

Due to the relatively short reaction times complete conversion of cyclohexene to cyclohexane was not expected. Analysis of the resulting solution by GC however did show the presence of two distinct peaks which are believed to correspond to cyclohexane and cyclohexene respectively. This therefore provides evidence that cyclohexene conversion has occurred.

Table 4.7. Cyclohexene hydrogenation experiments.

Expt	Catalyst	Mass of Catalyst (g)	Pd wt.%	Calcination Conditions	Pd Species	Total Time (hours:mins)	Reaction Temp. (K)	Temp. Rise (K)	Pressure Decrease (±1psi)	No. Moles of H_2 Consumed
E47	Pd/Al_2O_3	0.4	5	As purchased	Pd	1:15	-	11	20	2.22
E47*	Pd/Al_2O_3*	0.4	5	Reused	Pd	1:00	-	3	2.5	0.27
E48	Pd/Al_2O_3	0.1	5	As purchased	Pd	19:05	-	2	15.5	1.72
E49	Pd11(A)	1.0	4	4h/673K/air	PdO	2:10	-	13	17.5	1.94
E50	Pd12(A)	1.0	5	4h/673K/air	PdO	2:07	-	13	21	2.33
E50*	Pd12(A)*	1.0	5	Reused	PdO	1:00	-	6	5	0.55
E51	Pd2(2)	0.5	2	18h/673K/air	PdO/Pd	1:18	-	1	4	0.44
E52	Pd3(2)	1.0	3	18h/673K/N_2	Pd	1:07	-	2	4	0.44

4.4. Conclusions

Electroless plating was found to be a more effective preparative technique than impregnation in the production of a metal supported expanded slate catalyst. The hydrophobic nature of expanded slate is believed to reduce the interaction between the metal salt in solution and the expanded slate surface thus resulting in reduced adsorption. Evaporation of the aqueous phase during impregnation resulted in copper being deposited on the surface however large spherical clusters were normally generated. By comparison electroless plating has been found to result in deposition that appeared to be widely distributed over the whole surface of the expanded slate powder. Copper and palladium based expanded slate catalysts were successfully prepared by following this method.

Copper has consistently been found to be inactive towards the hydrogenation of maleic acid, nitrobenzene and cyclohexene under the reaction conditions *i.e.* 50-60psi hydrogen pressure and at atemperature between 298-353K. Palladium/expanded slate was found to be a more successful hydrogenation catalyst. Catalysts calcined in N_2, found to contain only elemental Pd, proved inactive. However calcination in air producing PdO species was consistently seen to result in a decrease in H_2 pressure, and was thus found to be active towards hydrogenation reactions. The activity of some Pd electroless plated expanded slate catalysts compared to the reference catalyst Pd/Al_2O_3 with respect to nitrobenzene hydrogenation at room temperature over a period of 2hrs is summarised in Table 4.7. The activity of the catalysts is illustrated by the revised pressure decrease based on 0.02g of Pd on the surface.

For example, 0.5g reference catalyst with 5wt% Pd used in the experiment has a theoretical Pd mass equal to 0.02g *i.e.* 0.5x0.05 = 0.02g Pd. Similarly, 1.0g Pd1(A) with a Pd loading in the region of 2.4wt% has a theoretical Pd mass of 1x0.024 = 0.024g. The activity of Pd1(A) based on 0.02g Pd has therefore be calculated as follows:

Actual pressure drop*0.02/0.024 = Activity of catalyst

i.e. 13.5*0.02/0.024 = 12 psi

Table 4.7. Summary of catalyst activity based on 0.02g Pd on surface of catalyst.

Catalyst	Pd Loading (wt%)	Pd species	Actual pressure drop (psi)	Activity (Revised pressure drop) (psi)
Pd1(A)	2.4	PdO	13.5	12
Pd2(2)	3	PdO/Pd	15	10
Pd9(A)	3.5	Pd	0	0
Pd11(A)	~4	PdO	12	6
Pd12(A)	~5	PdO	16	6
Pd/Al_2O_3	5	Pd	25	25
PdO/Al_2O_3	5	PdO	15	15

In contrast to Pd plated expanded slate catalysts, the reference catalyst Pd/Al_2O_3 was found to be more active than PdO/Al_2O_3. Indeed PdO/Al_2O_3 was found to have a comparable activity with PdO/expanded slate catalysts. Increasing the temperature of the reaction, nitobenzene and cyclohexene hydrogenation, tended to increase the activity of both the expanded slate and reference alumina catalysts.

It has therefore been demonstrated that expanded slate can be used as an effective support for a catalytically active metal such as palladium. However scope for further work investigating the activity of Pd/expanded slate catalysts towards cyclohexene hydrogenation and the effect of temperature and pressure on different reactions in more detail is evident. Additional surface characterisation following catalyst deactivation over time would also provide a greater understanding of the activity of the electroless plated catalysts. Furthermore catalyst testing using specific high temperature reactions such as cracking, incinerations etc would also provide an interesting area for further research.

Overall Conclusions

Overall Conclusions

Slate obtained from the Llechwedd Slate Quarry, North Wales and Villar del Rey Quarry, Spain, showed very little difference in their chemical compositions. The overall composition of the slate samples analysed in this study was muscovite, chlorite and quartz. Very little accessory minerals were generally detected; typically no pyrite or calcite was found in the Welsh samples. The decomposition of minerals, chlorite and muscovite, inherently present in slate has been shown to give rise to the release of water vapour. This water vapour is believed to be responsible for slate expansion. The optimum heating parameters for the expansion of Llechwedd slate (and Villar del Rey slate) has been determined *i.e.* heating rate of 20K/min up to a final temperature of 1453K and maintaining this temperature for 10mins. It has also been determined that the degree of expansion is dependent on the rate of vapour diffusion through the internal lattice of the slate prior to the slate becoming sufficiently pyroplastic at 1453K. Alterations in the heating rate, final expansion temperature, dwell times at or below the expansion temperature have been shown to effect the degree of expansion thus demonstrating the ability to control slate expansion.

Pyrite decomposes in nitrogen mainly losing sulfur in the form of S_2 vapour and producing troilite (FeS) as the final product. In air complete loss of S (as SO_2 gas) can be achieved with the final product typically identified as haematite (Fe_2O_3). The decomposition of FeS_2 has been shown to be favoured by heating in an air atmosphere. In air compared to N_2 the decomposition of FeS_2 occurs *via* reaction with O_2 in addition to a purely thermal effect. Pyrite heated in N_2 tended to produce a much more ordered product than pyrite heated in air *i.e.* greater recrystallisation had occurred in N_2. Reduced FeS_2 decomposition was observed when pyrite was present within slate compared to external pyrite. This was attributed to the increased diffusion effect of S having to pass through the host material thus reducing the rate of S loss. The mechanism of FeS_2 decay within slate is believed to be independent to atmosphere since the morphology of internal pyrite heated in air (although less ordered) appeared very similar to internal pyrite heated in N_2. Pyrite decay in slate is therefore believed to follow the same mechanism as pyrite-only heated in N_2 *i.e.* purely a thermal process with no reaction with O_2.

Expanded slate has been shown to be effective as a support material for a suitably active metal. Electroless plating was found to be more effective than impregnation in depositing the active phase onto the surface of the support. Copper and palladium have been successfully deposited on the surface of expanded slate powder. Copper continually proved unsuccessful under the reaction conditions as a catalyst for the hydrogenation of maleic acid, nitrobenzene and cyclohexene. By comparison, palladium supported expanded slate proved to be active hydrogenation catalysts. PdO was found to be the active species not Pd in contrast to the reference catalyst which showed greater activity when Pd was present on the surface rather than PdO.

Chapter Five - Experimental

Chapter Five - Experimental

5.1. Mineralogical Determination

Slate samples were obtained from the 5 slate veins at Llechwedd, Blaenau Ffestiniog. Analysis of the minerals orientated parallel and perpendicular to the cleavage plane were obtained by polishing the surface of the cleaved slate tablets (mean size 30x25x3-5mm) with fine-grained sandpaper to obtain a completely smooth, flat surface. In order to obtain an adequate surface area for perpendicular analysis, several tablets (3-5) were bonded together with epoxy resin and then cut along the horizontal to produce a tablet of approx. 3mm thickness. Analysis was the carried out by XRD.

5.2. Slate Expansion Experiments

5.2.1. Static "closed-vessel" experiments

Small amounts (~ 0.02-0.05g) of slate were placed in the stainless steel reaction vessel (see Figure 5.1 below). The system was then evacuated and heated either to 923, 993 or 1423K at a heating rate of 10K/min. The products obtained after heating were analysed by IR, SEM and EDAX as appropriate.

Figure 5.1. Schematic of stainless steel reaction vessel.

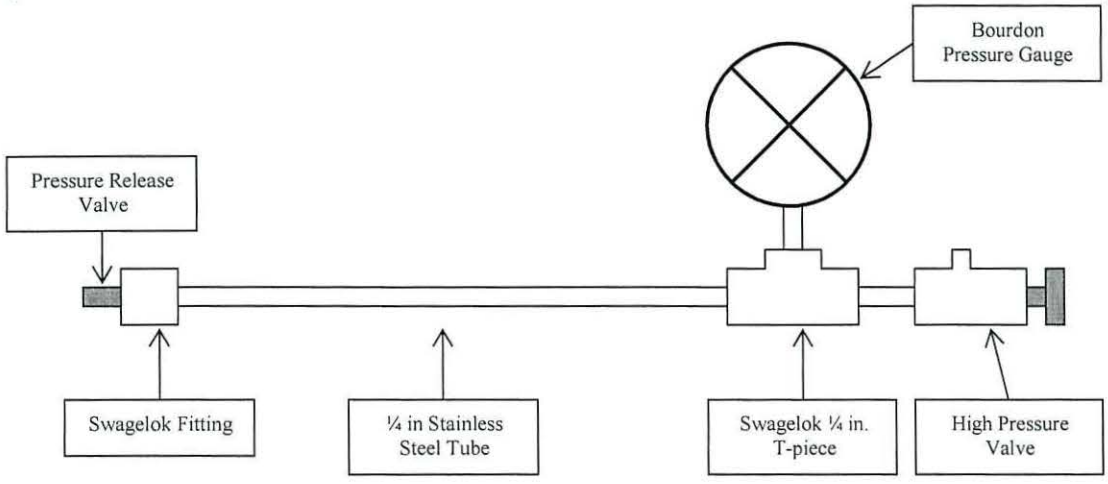

5.2.2. Flow Experiments

Powdered slate samples (~ 0.5g) were placed into quartz sample boats inside a quartz reactor tube (see Figure 5.2). The slate samples were then heated in a Carbolite tube furnace to varying temperatures (923-1423K) under a flow of nitrogen (100 cm^3/min) (Figure 5.3). The exhaust gases generated during heating were then trapped in a glass U-tube and condensed at 195K in a dry ice/acetone slush bath. The solid products were analysed by IR, XRD and SEM. Analysis of the condensed gas was carried out by IR and ^1H NMR.

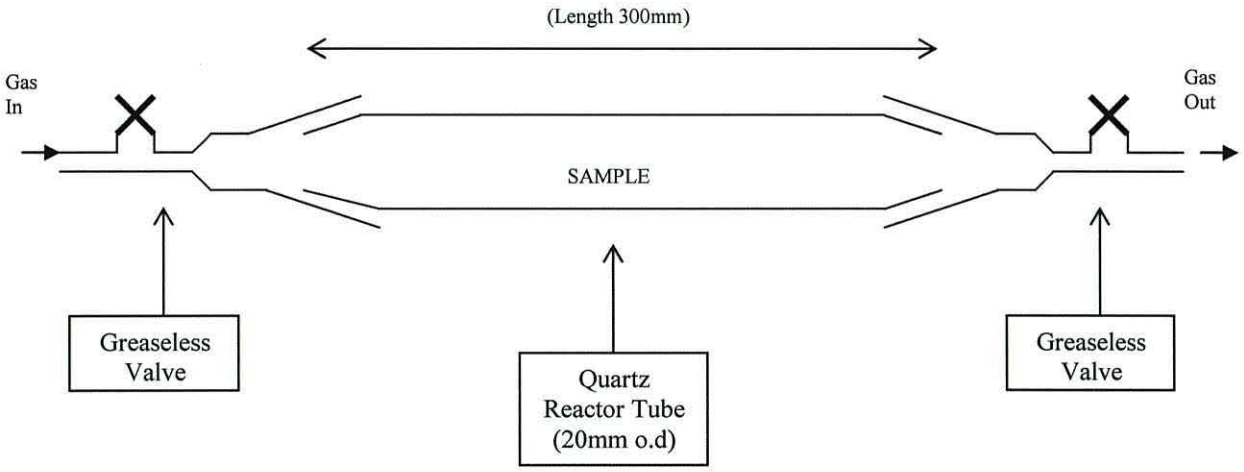

Figure 5.2. Diagram of quartz reactor.

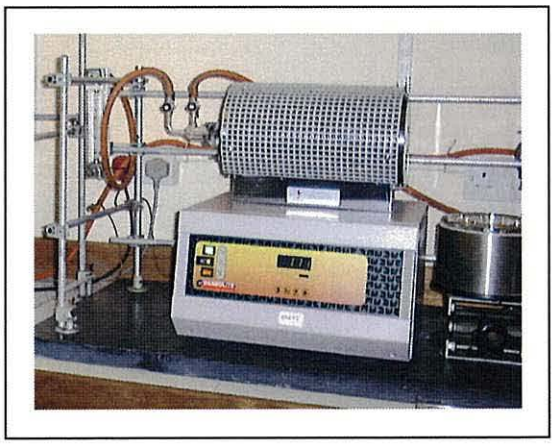

Figure 5.3. Photograph of Carbolite tube furnace.

5.2.3. Bulk Slate Expansion (EA Technology)

Slate from Llechwedd Slate Quarry (New and Old vein) was crushed (mean particle sizes 28x37.5mm) and fired in a microwave-assisted gas firing (MAGF) Stage 1 kiln (up to 10kg per batch) at EA Technology, Capenhurst, UK. Slate expansion was carried out by following a heating program consisting of a 700K/h heating rate up to a maximum temperature of 1463K (dwell time was typically 10 minutes). This work was carried out by EA Technology staff and samples were supplied to University of Wales, Bangor for subsequent investigation.

5.2.4. Expansion of Slate Tablets (University of Wales, Bangor)

Slate samples were obtained from the 5 slate veins at Llechwedd, Blaenau Ffestiniog and from the quarry at Villar del Rey, Spain. Slate tablets (mean size 20x15x4mm) were cut using a diamond saw from roofing tiles provided by the respective companies. These tablets were then placed inside the centre of a quartz reactor tube and then inserted into the tube furnace for heating (Carbolite furnace model MTF 12/25/250). The quartz tube was initially flushed with air or nitrogen gas (depending on experiment) prior to heating to ensure a stable, continuous gas flow. Heating programmes from Table 5.1 were followed depending on whether an air or nitrogen atmosphere was required, respectively. These tables are ordered in chronological order from left to right and describe the heating sequences followed by samples thus providing information from the initial starting temperature, heating rates, intermediate dwell temperatures and times, to the final maximum temperature and the dwell times incurred. Data on the atmosphere and gas flows are also provided. A comparison of the relative expansion observed in each sample has been carried out. Furthermore a series of slate tablets heated in a nitrogen environment have been used in expansion gas determination experiments whereby the gases released were trapped and condensed in a similar manner as previously described in section 5.2.2. (Figure 5.3). Expanded slate samples were subsequently analysed by IR, XRD, SEM and EDS.

Table 5.1. Heating programmes for slate expansion experiments carried out in air and nitrogen atmospheres

Program No.	Initial Temp. (K)	Heating Rate (K/min)	Intermediate Dwell Temp. (K)	Dwell Time (min)	Final Temp. (K)	Final Dwell Time (min)	Atmosphere	Gas Flow (cm^3/min)
S-A1	293	5	700	1020 (17h)	1423	0	AIR	50
S-A2	293	5	900	1080 (18h)	1453	10	AIR	50
S-A3	293	5	900	4200 (70h)	1453	15	AIR	50
S-A4	293	20	--	--	1443	5	AIR	50
S-A5	293	20	--	--	1453	1-2	AIR	100
S-A6	293	20	--	--	1453	10	AIR	100
S-A7	293	20	--	--	1453	120 (2h)	AIR	50
S-A8	298	30	900	1440 (24h)	1453	10	AIR	50
S-A9	293	30	--	--	1453	10	AIR	50
S-N1	293	25	--	--	1443	15	N_2	50
S-N2	293	2	973	1080 (18h)	1453	0	N_2	50
S-N3	293	5	1273	2880 (48h)	1453	10	N_2	50
S-N4	293	10	1273	1440 (24h)	1453	0	N_2	50
S-N5	293	10	1173	5400 (90h)	1453	10	N_2	50
S-N6	293	20	873 1173 1273 1373	30 45 50 55	1453	60	N_2	50-100
S-N7	293	20	--	--	1453	10	N_2	100

5.3. Pyrite Decomposition

Three types of sample have been studied during this work: Pyrite, slate containing pyrite from the New vein of the Llechwedd Quarry, Blaenau Ffestiniog, North Wales and slate containing pyrite from the Villar del Rey quarry, Bathajoz, Spain. These samples have been labelled as P, SPNW and SPS respectively. For pyrite experiments, a pyrite crystal (initial size *ca.*25x25x25mm) was cut into smaller pieces generally around 8x6x3mm in size. In general solid pieces were analysed. However, some experiments were also carried out on pyrite that had been crushed to a fine powder by pestle and mortar. Slate tablets, generally with dimensions in the order of 30x20x3mm, with pyrite visible on their surface obtained from Llechwedd and Villar del Rey also underwent similar heat treatment.

In a typical experiment a sample was simply placed in quartz sample boats before being placed inside the quartz reactor for subsequent heating in the tube furnace (Carbolite furnace model MTF 12/25/250) to a pre-defined temperature in the range 823-1473K depending on the type of sample and experiment. As for slate expansion experiments, the tube was firstly flushed with air or nitrogen gas as appropriate. The different samples have been heated at varying rates, to different dwell temperatures and held at these dwell temperatures for a range of times. Descriptions of the heating programmes followed are included in Table 5.2 for air and nitrogen experiments. The resultant heated samples were analysed by XRD, SEM and EDS.

Table 5.2. Heating programmes for pyrite decomposition experiments carried out in air and nitrogen atmosphere.

Program No.	Initial Temp. (K)	Heating Rate (K/min)	Intermediate Dwell Temp. (K)	Dwell Time (min)	Final Temp. (K)	Final dwell Time (min)	Atmosphere	Gas Flow (ml/min)
P-A1	293	5	--	--	823	1-2	AIR	100
P-A2	293	5	--	--	923	0	AIR	100
P-A3	293	10	--	--	923	1-2	AIR	100
P-A4	293	20	--	--	923	10-15	AIR	100
P-A5	293	5	--	--	1223	1-2	AIR	150
P-A6	293	20	--	--	1223	1-2	AIR	100
P-A7	293	20	--	--	1223	10-15	AIR	100
P-A8	333	5	650	1080 (18h)	1453	1-2	AIR	100
P-A9	293	5	--	--	1453	15	AIR	100
P-A10	293	10	--	--	1453	1-2	AIR	100
P-A11	293	10	--	--	1453	10	AIR	100
P-A12	293	20	650	2	1453	10	AIR	100
P-A13	293	20	650	900-1440 (15-24h)	1453	10-15	AIR	100
P-A14	293	20	850	120 (2h)	1453	15	AIR	100
P-N1	293	5	823	2-5	923	0	N_2	100
P-N2	293	10	--	--	923	10	N_2	100
P-N3	293	10	--	--	923	1440 (24h)	N_2	100
P-N4	293	20	--	--	923	1-2	N_2	100
P-N5	293	20	--	--	923	10	N_2	100
P-N6	293	20	--	--	1223	1-2	N_2	100
P-N7	293	20	--	--	1223	10-15	N_2	100
P-N8	293	10-15	--	--	1453	10-15	N_2	100
P-N9	293	20	--	--	1453	1-2	N_2	100

5.4. Catalyst Preparation

Slate from both the Old and New veins, Blaenau Ffestiniog, was expanded at EA Technology, Capenhurst. This material (batch slate 205) was used for catalyst preparation.

5.4.1. Impregnation Method 1

The first method used (wet impregnation) involved adding a sample of expanded slate powder to an excess of copper nitrate solution ($2Cu(NO_3)_2.5H_2O$). This mixture was then left to stir overnight (up to 24 hours) to ensure maximum adsorption of copper nitrate onto the expanded slate surface. The solution was then removed by filtration and the solid collected and then calcined at 623-673K for between 2-3 hours in order to decompose the nitrates. The resulting material was analysed by IR, XRD, SEM and EDS.

5.4.2. Impregnation Method 2

This second technique involved the removal of excess water from the solution through evaporation. The expanded slate and copper nitrate mixture was stirred vigorously whilst being heated gently (< 323K). Once most of the water had evaporated the resulting slurry was dried in a dessicator under vacuum and then calcined at 623-673K for 2-3 hours to remove all traces of nitrates from the surface. The resulting material was analysed by IR, XRD, SEM and EDS.

5.4.3. Electroless Plating

The electroless plating of copper metal on the surface of alumina has previously been reported by H. Chang *et al.*[152] The procedure reported in this paper has been followed and modified in order to optimise the process for the deposition of metals, for the first time, on the surface of expanded slate.

5.4.3.1. Copper Electroless Plating

Expanded slate powder was initially pretreated to ensure removal of any contaminants that may be present on the surface as follows. The expanded slate was firstly subjected to an alkali bath (50ml, 1M NaOH) 338-343K for 15mins, then acid washed (50ml, 25 vol.%H_2SO_4) at 303-308K for 15 mins, sensitized (20g/l $SnCl_2$ and 40ml/l HCl solution) at 298-303K for 10 mins, activated (0.25g/l $PdCl_2$ and 0.5 ml HCl solution) at 313-318K for 25mins and finally dried at 358K in a vacuum oven for a minimum of 16 hours.

The pretreated expanded slate was then placed in a copper plating bath that contained 0.04M $CuSO_4.5H_2O$ (copper(II) source), 0.08M EDTA.4Na (chelating agent), 0.08M HCHO (reducing agent) and 5mg/l pyridine (stabiliser). The bath temperature was maintained at 343-348K for 30-45mins. The pH of the solution was monitored throughout and adjusted to around 12-13 with alkali (1M NaOH). The bath was stirred continuously. The copper plated expanded slate was separated by filtration and washed thoroughly with distilled water. The final product was then dried at 358K in a vacuum oven for a minimum of 24hours.

A number of batches of the copper/expanded slate "catalysts" have been prepared with varying copper loadings (theoretical 5, 10 and 15 wt.% Cu). The variations in the copper loading were achieved by changing the volume of the copper plating solution. In addition two of the six batches (Batch 2 and 5) also incurred a pre-activation stage prior to copper deposition. This involved the heating of the unplated expanded slate under hydrogen at 523K for >12 hours.

5.4.3.2. Palladium Electroless Plating

Expanded slate powder was initially pretreated to ensure removal of any contaminants that may be present on the surface as follows. The expanded slate was firstly subjected to an alkali bath (50ml, 1M NaOH) 338-343K for 15mins, then acid washed (50ml, 25 vol.%H_2SO_4) at 30-35 °C for 15 mins, sensitized (20g/l $SnCl_2$ and 40ml/l HCl solution) at

303-308K for 10 mins, activated (0.25g/l $PdCl_2$ and 0.5 ml HCl solution) at 313-318K for 25mins and finally dried at 358K in a vacuum oven for a minimum of 16 hours. The deposition of palladium was carried out using the following solution: 2g/L palladium chloride hydrate, 27g/L ammonium chloride complexing agent, 10g/L sodium hypophosphite reducing agent and 160ml/L ammonium hydroxide as a stabiliser. Optimisation of the plating conditions involved heating the solution to 323K prior to addition of the reducing agent then maintaining an alkaline pH of approx. 9 throughout deposition. The plating conditions were kept relatively constant for 30 minutes to ensure that maximum deposition took place. However the deposition rate for this process appears to be very fast and the majority of the plating in fact occurred within the first 2-3 minutes after addition of the reducing agent. This observation is consistent with the literature data, where a plating rate of up to 2.5μm/hr has been recorded.[3] The palladium plated expanded slate was separated by filtration and washed thoroughly with distilled water. The final product was then dried prior to calcination either in the vacuum oven at 358K or in the tube furnace in air at 383K overnight.

A series of palladium plated expanded slate catalysts have been prepared with palladium loadings between 1 and 5wt.%. The variations in the palladium loadings were achieved by changing the volume of the palladium plating solution used.

5.5. Hydrogenation Experiments

A series of hydrogenation experiments have been carried out using a Parr 3911 hydrogenator. This is a purpose built apparatus designed specifically for hydrogenation activity tests of catalysts. The instrument consists of a large H_2 gas reservoir (approx. 4 litre capacity) with a separate reaction vessel (0.5 litre). There are input and output valves to allow the gases to move freely through the instrument in addition to a separate valve that can close the reaction vessel off from the main gas chamber thus isolating the reaction mixture. A vacuum/pressure manifold is used for ease of alternating between gas input and evacuation of the system. Here access to a safety release valve is available in the event of a high H_2 pressure build up. The chamber is filled with hydrogen until a

pressure of 50-60psi (depending on experiment) is attained. (See Figures 5.4). The observed decrease in pressure directly corresponds to the amount of hydrogen consumed in the reaction therefore it is possible to determine the number of moles of starting material converted to products by using the mathematical formula: -

$$PV=nRT$$

where P = pressure, V = volume, n = number of moles, R = gas constant and T = temperature

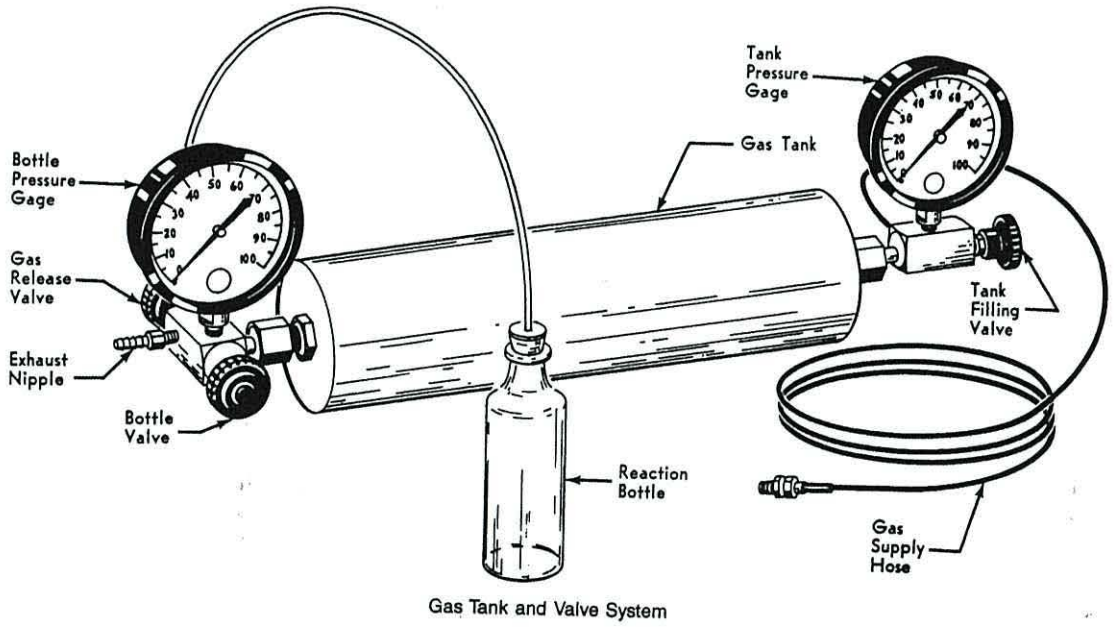

Figure 5.4. Diagram of hydrogenator.

5.5.1. Standardisation (Maleic Acid Experiments)

Standardisation of the apparatus involved the hydrogenation of pure maleic acid. Experimentally, maleic acid (11.6g, 0.1M) was initially dissolved in 95-99% ethanol (150ml) and reduced using active catalysts (1.0g). The reaction solution and catalyst were placed in the reaction vessel and securely clamped in the shaking mechanism of the Parr Hydrogenator. The air in the system was removed by evacuation and the apparatus was subsequently purged with nitrogen three times then similarly with hydrogen. Once

purged of air the system was filled with hydrogen until a predefined pressure was attained, normally 60psi. The reaction bottle was then shaken vigorously to initiate the reaction. The reaction was maintained until no more hydrogen was consumed *i.e.* until the hydrogen pressure remained constant.

The number of moles of hydrogen actually consumed can therefore be calculated by the following method: -

Ideal gas law $PV = nRT$

Pressure decrease (P) = 9psi

= 0.6atm (1 atmosphere = 14psi)

Total volume of reactor (V) = $4.5dm^3$

Gas constant (R) = $0.0820575 dm^3 atm K^{-1} mol^{-1}$

Temperature (T) = 25°C = 298K

Rearranging the equation,

Total number of moles of H_2 $n = PV / RT$

$= (0.6*4.5)/(0.0820575*298)$

= 0.11 moles

The calculated value (0.11 moles) for the maximum observed pressure drop (9psi) is therefore in accordance with the theoretical value.

A series of experiments have been carried out in order to determine the activity of various Cu and Pd/expanded slate catalysts towards maleic acid hydrogenation. Catalysts before and after use have been analysed by XRD, SEM and EDS. Reaction products have been studied by IR, GC and GC-MS.

5.5.2. Nitrobenzene Hydrogenation Activity Tests

Nitrobenzene (1mol, 100ml) and catalyst (1.0g) were placed in a reaction bottle and securely clamped in the shaking mechanism of the Parr Hydrogenator. The air in the system was again removed by evacuation and the apparatus was subsequently purged as previously discussed in the standardisation procedure (section 2.4.1.). The system was then filled with hydrogen until a pressure of 60psi was attained. The reaction bottle was then shaken vigorously to initiate the reaction. A series of experiments have been carried out where the hydrogenation reactions have been maintained generally for greater than 24hrs in order analyse the activity of various catalysts over a relatively long period of time. Catalysts before and after use have been analysed by XRD, SEM and EDS. Reaction products have been studied by IR, GC and GC-MS.

5.5.3. Nitrobenzene Heating Experiments

The effect of temperature on catalytic activity has been studied by carrying out a series of experiments following the methods described in sections 5.5.1 – 5.5.3. The reaction temperature was increased by wrapping a heating mantle around the reaction vessel prior to being secured in the shaking mechanism. The temperature in the reaction vessel was measured and controlled by installing a stainless steel sheathed thermocouple into the reaction vessel and connecting it to a temperature controller. The experiments in this series were limited to around two hours. Analysis of the reaction products was conducted by IR, GC and GC-MS. Characterisation by XRD, SEM and EDS of used catalysts were also carried out.

5.5.4. Cyclohexene Hydrogenation Activity Tests

A series of experiments have been carried out by essentially following the standard method previously discussed in section 2.4.1. However, in this case cyclohexene (50ml) was the reactant used and the experiments were initiated at a lower starting pressure of

50psi. As in previous experiments, catalysts before and after use were analysed by XRD, SEM and EDS. Reaction products have been studied by IR, GC and GC-MS.

5.6. Characterisation Techniques

5.6.1. X-ray Powder Diffraction (XRPD)

An aluminium holder was filled with the sample with the sample to be analysed. This was then placed in a Philips X-ray Diffractometer, which utilised Co-K_α radiation, 0.178897nm, with an Fe filter. The analysis was carried out with a continuous scan at varying scan rates, namely 0.04°/sec, 0.02°/sec, 0.005°/sec and 0.002°/sec, between the range of $2\theta = 5–75°$. The overnight scan, 0.002°/sec scan rate, proved to be most effective for all samples, by improving the signal to noise ratio and thus producing clearer diffraction patterns with more defined peaks. For each sample, the data was compared with the literature values held on the Philips X'pert Database and in the FINK index powder diffraction files.

5.6.2. Infra-red Spectrophotometry (IR)

A Perkin Elmer 1600 series FT-IR spectrophotometer was used. The analysis of solid samples was carried out through the preparation of KBr discs. Solutions and aqueous samples were analysed as neat liquids. The number of scans (1-16) required for a sufficient spectrum varied depending on necessity with a typical spectral resolution of $4cm^{-1}$.

5.6.3. Scanning Electron Microscope (SEM) and Energy Dispersive Spectrometer (EDS)

In general powdered samples were studied by SEM, however a solid piece of expanded slate was also analysed. The samples were mounted onto an aluminium stub using double-sided carbon tape for the powdered samples and epoxy resin for the solid pieces.

They were then coated with a thin gold film for 5 minutes at 1.2 kV. The samples were then placed in a Hitachi S-520 SEM and suitable micrographs taken of the gold plated material. Uncoated samples were also examined using a-LINK Energy Dispersive Spectrometer (EDS).

5.6.4. X-ray Fluorescence (XRF)

Slate tablets were cut to the appropriate size (*ca.* 4cm^2) and polished to obtain a relatively flat surface. The samples were then placed under the X-ray window of a portable TN Spectrace 9000 XRF spectrometer. Three X-ray sources (Cd^{109}, Fe^{55} and Am^{241}) were used to analyse the samples. Elements below Na in the periodic table could not be analysed by this instrument.

5.6.5. Differential Thermal Analysis (DTA)

A 'Stanton-Redcroft' DTA instrumentation was used to thermally analyse the slate samples. A small amount (*ca.* 0.01g) of powdered slate was placed in Pt crucibles and heated against a reference sample, alumina, to 1273K at a rate of 10K/min.

5.6.6. Inductively Coupled Plasma-Atomic Emission Spectroscopy (ICP-AES)

The actual amount of palladium deposited onto the surface of the expanded slate powder during catalyst preparation was determined by re-extracting the palladium back into solution then determining its concentration on a Jobin Yvon Emission JY138 Ultrace inductively-coupled plasma atomic emission spectrometer (ICP-AES). The samples were initially digested in nitric acid (concentrated acid: water ratio 5:1) for approximately 30 minutes at a temperature between 368-378K. Once cooled the solid was separated by filtration and washed with analytical grade water. The acidic solution and washings were then collected and diluted to make up 250ml solutions.

5.6.7. Atomic Absorption Spectroscopy (AAS)

The amount of copper loaded onto the surface of the slate samples was determined by re-extracting the copper back into solution then determining its concentration on a Varian SpectraAA-250 Plus spectrophotometer utilising acetylene gas as the flammable source. The samples (except Batch 6, 15 wt.% Cu) were initially digested in nitric acid (50ml, 8M) for 30-45 min. at a temperature around 368-378K. Once cooled the solid was separated by filtration and the solutions diluted to obtain the required concentration range for the instrument *i.e.* dilution to 40μg/ml in order to optimise the 218.2nm wavelength of the instrument's Cu lamp.

5.6.8. Gas Chromatography-Mass Spectrometry (GC-MS)

Sample analysis was carried out on a Hewett Packard 5890 Split/Splitless 30 Gas Chromatogram using helium carrier gas and following coupled to a Finnigan 4500 Mass Spectrometer. The column used was a 30m x 0.25mm (internal diameter) REX-5MS (Restek Corporation). Initial oven temperature was 323K (2mins) rising to 523K (5mins) at a rate of 15K/min.

5.6.9. Gas Chromatography (GC)

Sample analysis was carried out using a CHROMPACK CP9001, with flame ionisation detector, a splitless injector and a helium carrier gas. The column used was a 15m x 0.53mm STABILWAX (Restek Corporation). The carrier gas flow rate was 6.0ml/min with the injector temperature at 473K and detector temperature at 523K. Initial oven temperature was set to 353K for (2mins) rising to 473K (2mins) at a rate of 20K/min.

5.6.10. High-Performance Liquid Chromatography (HPLC)

Maleic acid/succinic acid analysis was performed by HPLC using a Kronton Instrument (UK) Ltd. With double beam optics, a deutirium lamp (λ=190-400nm),

spectrophotometric detector (Biotek Kontron, UK) and Kroma 2000 integration software. A 20µl injection loop was used to deliver samples to an ODS 5µm C-18 column; 4.6x200nm (Waters Ltd) guard column. Water was used as the mobile phase with a flow rate of 1.0ml/min and λ=210nm.

References

References

1. R.N. Crockett, *Slate: A Mineral Dossier*, No.12, London, HMSO, 1975.
2. *McGraw-Hill Encyclopedia of Science and Technology* (6th Ed.), McGraw and Hill Co., NY, 1987, **16**, p.462.
3. W. Gutt, W.H. Harrison, P.J. Nixon M.A. Smith and A.D. Russell, *A Survey of the Locations, Disposal and Prospective Uses of the Major Industrial By-products and Waste Materials*, Building Research Establishment Current Paper CP19/74, Department of the Environment, 1974.
4. J.L. Davies, *Segontium Roman Fort*, CADW, Welsh Historic Monuments, 1999.
5. K.L. Watson, in *Slate Waste: Engineering and Environmental Aspects*, Applied Science Publishers Ltd., 1980.
6. M.J.T. Lewis, in *Llechi: Slate*, Gwynedd Archives Services, 1976.
7. D.M. Rees, in *Amgueddfa Chwareli Gogledd Cymru* (North Wales Quarrying Museum), National Museum of Wales, 1974.
8. Richards, Moorehead & Laing Ltd., in *Slate Waste Tips and Working in Britain,* report by the Department of the Environment, HMSO, 1995.
9. B. Smith and T.N. George, in *British Regional Geology: North Wales* (3rd Ed.), British Geological Survey, HMSO, 1961.
10. I.W. Jones, in *Slate and Slatemen of Llechwedd*, Quarry Tours Ltd, Blaenau Ffestiniog, 1975.
11. M. Burn, in *The Age of Slate*, Quarry Tours Ltd., Blaenau Ffestiniog, 1976.
12. Gwynedd Chronicle, 4th July 2001.
13. E. Williams, *Daily Post* (Wales), 23rd Nov. 1998.
14. E. Williams, *Daily Post* (Wales), 25th Nov. 1998.
15. B.A. Pluijim, N. Ho, D.R. Peacor and R.J. Merriman, *Nature*, 1998, **392**, 348.
16. C. Pellent, in *Rocks and Minerals*, Dorling Kindersley, London, 1992.
17. D.A. Rothery, in *Geology, Teach Yourself*, Hoddler Headline Plc., London 1997.
18. J.L. Roberts, in *Geological Structures*, Macmillan Press, 1989.
19. R. Mason, in *Petrology of the Metamorphic Rocks*, George Allen & Unwin Ltd, London, 1978.

20. J. Challinor and D.E.B. Bates, in *Geology Explained in North Wales*, David & Charles, Newton Abbot, 1973.
21. M. Williams, in *The Slate Industry*, Shire Publ. Ltd., 1991.
22. D. Hart, *The Building Slates of the British Isles*, Building Research Establishment Report, 1991.
23. R.H O'Neill, *The Quarry Manager's Journal*, 1959, **43**(9), 345.
24. L. Smart and E. Moore, in *Solid State Chemistry, An Introduction* (2nd Ed.), Chapman & Hall, London, 1997.
25. M.A. Rodriguez, J. Rubio, F. Rubio, M.J. Liso and J.L.Oteo, *Clays and Clay Minerals*, 1997, **45**, 670.
26. W.A. Deer, R.A. Howie and J. Zussman, in *An Introduction to Rock Forming Minerals* (2nd Ed.), Longman, 1992.
27. W.J. and N. Phillips, in *An Introduction to Mineralogy for Geologists*, John Wiley & Sons Ltd, 1980.
28. S.W. Bailey (Ed.), *Mineralogical Society of America, Review in Mineralogy*, 1989, **13**.
29. L.G. Berry, B. Mason and R.V. Dietrich, in *Mineralogy* (2nd Ed.), W.H. Freeman and Co., 1983.
30. H.H. Read, in *Rutley's Mineralogy*, Thomas Murby and Co., London, 1963.
31. F.J. North, in *The Slates of Wales* (2nd Ed.), National Museum of Wales, Cardiff, 1927.
32. E.H. Coleman and P.J. Nixon, *A Survey of Possible Sources in Wales of Raw Materials for the Manufacture of a Lightweight Expanded Slate Aggregate*, Building Research Establishment Current Paper CP78/74, Department of the Environment, 1974.
33. J. Kouřimský, in *The Illustrated Encyclopedia of Minerals and Rocks*, Sunburst Books, London, 1995.
34. F. and R. Atkinson, in *Rocks and Minerals*, Penguin Books, London, 1979.
35. G. Brown (Ed.), in *The X-ray Identification and Crystal Structure of Clay Minerals*, Mineralogical Society, London, 1967.
36. C.M. Warshaw and R. Roy, *Geol. Soc. Am. Bull.*, 1961, **72**, 1455.
37. C.M. Koretsky, D.A. Sverjensky, J.W. Salisbury and D.M. D'Aria, *Geochim. et Cosmochim. Acta*, 1997, **61**, 2193.

38. P.W. Atkins, *Physical Chemistry* (6th Ed), Oxford University Press, Oxford, 1998.

39. R.E. Bevins, *A Mineralogy of Wales*, National Museum of Wales, Geological Series No.16, Cardiff, 1994.

40. A. Harker, in *Metamorphism: a study of the transformations of rock masses*, (3rd Ed) Methuen, London, 1950.

41. S.E. Manahan, in *Environmental Chemistry*, (5th Ed), Lewis Pulb., 1991.

42. J. Hinks and G. Cook, *The Technology of Building Defects*, E & FN Spon, 1992.

43. B. Velde, in *An Introduction to Clay Minerals*, Chapman & Hall, 1994.

44. A.A. Boateng, E.R. Theon and F.L, Orthlieb, *Inst. of Chem. Engineers*, 1997, **75**, 278.

45. *Rock Products*, 1970, **73**, 59.

46. Http://www.buildex.com – found by "expanded shale" keyword search using Google search engine 3rd Sept. 2001.

47. W.H. Harrison, *Concrete*, 1974, **c2**, 41.

48. P.C. Hewlett (ed.), in *LEA's Chemistry of Cement and Concrete*, 4th Ed., Butterworth Heinemann, Oxford, 1998.

49. Http://www.escsi.org – found by "expanded shale and clay" keyword search using Google search engine 3rd Sept. 2001.

50. S.J. Hayde, US 1707395, 1929.

51. E.H. Coleman, British Patent 401685, 1933.

52. E.H. Coleman, *Concrete and Constructional Eng.*, 1936, **31**, 47.

53. J.E. Conley, *Trans. Amer. Inst. Of Mining, Metall. and Petrol Engineers*, 1942, **148**, 161.

54. F.J. Cservenyak, J.A. Ruppert and D.E. Garen, *Report of Investigations – US Dept of Interior Bureau of Mines*, 1948, **RI4401**, 65.

55. E.G. Ehlers, *Ceramic Bull.*, 1958, **37**, 95.

56. G. Baudet, *Bulletin du B.R.G.M.*, 1971, **2**, 2.

57. E.H. Nichols, R.M. Beyard, assign. The Funkhouser Co., US 2463994, 1949.

58. C.G. Harford, E. L. Kreidl and J.L. Utter, assign. Arthur D. Little, Inc., US 2654136, 1953.

59. G. Carpenter, GB 6931168, 1953.

60. Southern Lightweight Aggregate, GB 820971, 1959.

61. R. Hannah, *Gazette*, Sept 16, 1969.

62. J. Griffiths, *The Leader,* June 29, 1973.

63. *The Leader,* July 13, 1973

64. S.E. Jepsen and J.C. Jansen, *Wat. Sci. Tech.*, 1993, **27**(5-6), 369.

65. Http://www.hydroponics.webcentral.com.au/info/articles/leca.htm – found by "LECA" keyword search using Google search engine 3rd Sept. 2001.

66. A.C. Day, A.P. Young and R.A. Kyffin, assign. Greaves and Sons Ltd, US 4728471, 1988.

67. R.A. Kyffin, US 5482458, 1996.

68. P.H. Ribbe (ed), *Min. Soc. Am, Sulfide Minerals: Short Course Notes*, Vol. 1, 1974.

69. C.N. Alpers and D.W. Blowes (Eds), in *Environmental Geochemistry of Sulfide Oxidation*, American Chemical Society, 1994.

70. A.B. Busbey, R.R. Coenraads, P. Willis and D. Roots, in *Rocks and Minerals: The Ultimate Guide to the Earth*, HarperCollins, London, 1996.

71. Dioscorides, "*De Materia Medica*", *ca.* 75 AD

72. Pliny The Elder, Caius Plinius Secandus, "*Historia Naturalis*", *ca.* 77 AD.

73. Theophrastus, "Περi λiθσζ", 315 BC.

74. R.T. Lowson, *Chem. Rev.*, 1982, **82**(5), 461.

75. J.W. Mellor, in *A Comprehensive Treatise on Inorganic and Theoretical Chemistry: Vol. XIV*, Longmans, Green and Co., New York, 1935.

76. D.A. Jenkins, D.B.Johnson and C. Freeman, in *Environmental Mineralogy: Microbial Interactions, Anthropogenic Influences, Contaminated Land and Waste Management*, The Mineralogical Society Series 9, (Editor) P.J. Treloar, Alden Press Ltd, UK, 2000.

77. I.I. Maes, J. Yperman, H. Van den Rul, D.V. Franco, J. Mullens and L.C. van Poucke, *Energy and Fuels*, 1995, **9**, 950.

78. C.M. Eggleston, J. Ehrhardt and W. Stumm, *Am. Min. Soc.*, 1996,**81**, 1036.

79. T.O. Pritchard, "Development of Expanded Slate for Horticultural and Aggregate Use", paper presented at Eurothen 2000 Conference, Lisbon 19-21 Jan 2000. Full paper held in conference proceedings.

80. Peter J. Holliman, Slate Weathering, unpublished results.

81. R.J. Collins, P.T. Sherwood and A.D. Russell, *Efficient Use of Aggregates and Bulk Construction Materials,* Vol. 1, BRE Report, 1993.

82. I. Casanova, A. Aguado and L.Agulló, *Cement and Concrete Res.*, 1997, **27**(11), 1627.

83. I. Casanova, A. Aguado and L.Agulló, *Cement and Concrete Res.*, 1996, **26**(2), 993.

84. R.A. Schoenlaub, *J. Am. Ceram. Soc.*,1969, **52**(1), 40.

85. P.S. Maa, C.R. Lewis and C.E. Hamrin jr., *Fuel*, 1975, **54**, 62.

86. P.A. Montano, P.P. Vaishnava, J.A. King and E.N. Eisentrout, *Fuel*, 1981,**60**, 712.

87. G.P. Curran, G.E. Goring and C.W. Zielke, *Ind. Engng. Chem.*, 1954, **46**(1),

88. J.M. Lambert jr., G. Simkovich and P.L. Walker jr., *Metall. and Mat. Trans. B*, 1998, **29B**, 385.

89. S.J. Groves, J. Williamson and A. Sanyal, *Fuel*, 1987, **66**, 461.

90. S. Musić, S. Popović and M. Ristić, *J. Radioanal. and Nucl Chem.*, Articles, 1992, **162**(2), 217.

91. H.M. ten Brink, J.P. Smart, J.M. Vleeskens and J. Williamson, *Fuel*, 1994, **73**(11), 1706.

92. G.C. Bond, in *Heterogeneous Catalysis*, (2nd Ed.), Calerendon Press, Oxford, 1987.

93. J.L.F. Monteiro, *The Can. J. of Chem. Eng.*, 1981, **59**, 511.

94. J.J. Robinson, *J. S. Afr. Inst. Min. Metall.*, 1988, **88**(4), 117.

95. M.D. Gibbs, T.N. Smith and B. Verbaan, *Trans. Instn. Min. Metall. (Sect. C: Mineral Process. Extr. Metall.)*, 1997, **106**, C69.

96. M.D. Gibbs, T.N. Smith and B. Verbaan, *Trans. Instn. Min. Metall. (Sect. C: Mineral Process. Extr. Metall.)*, 1997, **106**, C74.

97. O. Levenspiel, in *Chemical Reaction Engineering* (2nd Ed.), New York, Wiley, 1972.

98. B. Meyer, *Chem. Rev.*, 1976, **76**(3), 367.

99. P.P. Kirilov, I.N. Gruncharov and Y.G. Pelovski, *Thermochimica Acta*, 1994, **244**, 79.

100. D.M. Hausen, *Rev. of Extractive Metallurgy*, 1991, 31.

101. V. Ponec, G.C. Bond, in *Studies of Surface Science and Catalysis: Catalysis by Metals and Alloys*, Vol. 95, Elsevier Science B.V., 1995.

102. D.F. Shiver, P.W. Atkins and C.H. Langford, in *Inorganic Chemistry*, Oxford Univ. Press, Oxford, 1990.

103. P. Wells, *Chem. in Britain*, 1992, **28**, 989.

104. J.M. Thomas and W.J. Thomas, in *Principles and Practice of Heterogeneous Catalysis*, VCH.

105. M.V. Twigg (Editor), in *Catalyst Handbook*, (2nd Ed.), Manson Publishing Ltd., London, 1996.

106. M. Bowker, in *The Basis and Applications of Heterogeneous Catalysis*, Oxford University Press, Oxford, 1998.

107. P.G. Menon, *Chem. Rev,* 1994, **94**, 1021.

108. H. Adkins, in *Reactions of Hydrogen with Organic over Copper, Chromium Oxide and Nickel*, The University of Wisconsin Press, Madison Wisconsin, 1937.

109. P. Fouilloux, *Appl. Catal.*, 1993, **8**, 1.

110. P. Gallezot, P.J. Cerino, B. Blank, G. Fleche and P. Fluertes, *J. Catal.*, 1994, **146**, 93.

111. A. Corma, *Chem. Rev.*, 1997, **97**, 2373.

112. C. Perego, P. Villa, *Cat. Today*, 1997, **34**, 281.

113. A. Chauvel, B. Delmon and W.F. Hölderich, *Appl. Catal. A:General*, 1994, **115**, 173.

114. G. Hutchings, *Chem. in Britain*, 1992, **28**, 1006.

115. D. Barthomeuf, *Catal. Rev.* 1996, **38**, 584.

116. L.A. Boot, A.J. van Dillen, J.W. Gues and F.R. van Buren, *J. Catal.*, 1996, **162**, 5.

117. L.A. Boot, A.J. van Dillen, J.W. Gues and F.R. van Buren, *J. Catal.*, 1996, **163**, 186.

118. L.A. Boot, A.J. van Dillen, J.W. Gues and F.R. van Buren, *J. Catal.*, 1996, **163**, 195.

119. J.W. Hill and R.H. Petrucci, in *General Chemistry: An Integrated Approach* (2nd Ed.), Petrice Hall, London, 1999.

120. B. Mile, D. Stirling and M.A. Zammitt, *J. Mol. Catal.*, 1990, **62**, 179.

121. C.S. John, D.M. Clarkand I.E. Maxwell, in *Perspectives in Catalysis*, ed. J.M. Thomas and K.I. Zamarov, Blackwell Publ., Oxford, 1992.

122. B.R. Strohmeier, D.E. Leyden, R.S. Field and D.M. Hercules, *J. Catal.*, 1985, **94**, 514.

123. W.R.A.M. Robinson and J.C. Mol, *Appl. Catal.*, 1988, **44**, 165.

124. F. Pepe, C. Angeletti, S. De Rossi and M.L. Jacono, *J. Catal.*, 1985, **91**, 69.

125. A. Mušič, J. Batista and J. Levec, *Appl. Cat. A: General*, 1997, **165**, 115.

126. J.M. Thomas, J. Chen and A. George, *Chem. in Britain*, 1992, **28**, 991.

127. W. Zhang, H. Yahiro, N. Mizuno, J. Izui and M. Iwamoto, *Chem. Lett.*, 1992, 11, 851.

128. G. Webb, in *Comprehensive Chemical Kinetics*, ed. C.H. Bamford and C.E.H. Tipper, Elsevier, Amsterdam, 1978, vol 20.

129. S.D. Jackson and N.J. Casey, *J. Chem. Soc. Faraday Trans.*, 1995, **91**(18), 3269.

130. K. Shimazu and H. Kita, *J. Chem. Soc., Faraday Trans.*, 1985, **81**, 175.

131. C.E. Lee, P.B. Tiege, Y. Xing, J. Nagendran and S.H. Bergens, *J. Am. Chem. Soc.*, 1997, **119**, 3543.

132. T.M. Miller and G.M. Whitesides, *J. Am. Chem. Soc.*, 1988, **110**, 3164.

133. Http://www.baiker.ethz.ch/chimia.html - found by " platinum black" keyword search using Google search engine 3rd Sept. 2001.

134. A.G. Ruiz, J.D.L.Gonzáles and I.R. Ramos, *J. Chem. Soc., Chem. Commun.*, 1984, 1681.

135. S. Narayanan and K. Krishna, *Appl. Catal. A:General*, 1996, **147**, L253.

136. L.F. Liotta, A.M. Venezia, A.Martorana, A. Rossi and G. Deganello, *J. Catal.*, 1997, **171**(1), 169.

137. L.F. Liotta, A.M. Venezia, A.Martorana, and G. Deganello, *J. Catal.*, 1997, **171**(1), 177.

138. J.A. Schwarz, C. Contescu and A. Contescu, *Chem. Rev.*, 1995, **95**, 477.

139. C.H. Sivaraj and P. Kantarao, *Appl. Catal.*, 1988, **45**, 103.

140. H.H. Kung, *Catal. Rev., Sci. Eng.*, 1980, **22**(2), 235.

141. N. Mahata and V. Vishwanathan, *Catal. Today*, 1999, **49**, 65.

142. G. Leofanti, G. Tozzola, M. Padovan, G. Petrini, S. Bordiga and A. Zecchina, *Catal. Today*, 1997, **34**, 307.

143. G.O. Mallory and J.B. Hajdu, in *Electroless Plating: Fundamentals and Applications*, Electroplaters and Surface Finishers Society, Florida, 1990

144. F.A. Lowenheim, in *Electroplating*, McGraw Hill, London, 1978.

145. A. Brenner and G.E. Riddell, *Natl. Bur. Of Standards, Tech Rept.*, 1947, **1097**, 5.

146. T. Mimani ans S.M. Mayanna, *Proc. Indian Acad. Sci. (Chem. Sci.)*, 1997, **109**(3), 203.
147. L.X. Yang, W.T. Hou and Y.S. Wu, *Trans. IMF*, 1997, **75**(4), 131.
148. S. Sotiropoulos, I.J. Brown, G. Akay and E. Lester, *Mat. Lett.*, 1998, **35**, 383.
149. K. Chen and Y. Chen, *Plat. and Surf. Fin.*, 1991, **84**(9), 80.
150. S.S. Djokić, *Plat. and Surf. Fin.*, 1999, **86**(6), 104.
151. K. Kondo, N. Ishida, J. Ishikawa and M. Irie, *Bull. Chem. Soc. Jpn.*, 1992, **65**, 1313.
152. H.F. Chang, M.A. Saleque, *Appl. Catal. A:General*, 1993, **103**, 233.
153. H.F. Chang, M.A. Saleque, W.S. Hsu and W.H. Lin, *J. Mol Catal.*, 1994, 94, 233.
154. H.F. Chang, M.A. Saleque, W.S. Hsu and W.H. Lin, *J. Mol Catal. A: Chemical*, 1996, **109**, 249.
155. H.F. Chang and C.F. Yang, *Ind. Eng. Chem. Res.*, 1997, **36**, 2080.
156. H.F. Chang and W.H. Lin, *J. Chin. Inst. Chem. Engrs.*, 1999, **30**(1), 51.
157. W.H. Lin, C.Y. Hwang and H.F. Chang, *Appl. Catal. A: General*, 1997, **162**, 71.
158. W.H. Lin and H.F. Chang, *Surf. and Coatings Tech.*, 1998, **107**, 48.
159. D.A. Jenkins, unpublished report, 1998.
160. V.C. Farmer (Ed), in *Vibrational Spectroscopy in Mineral Science*, Mineralogical Society, London, 1974.
161. R.C. Mackenzie (Ed), in *Differential Thermal Analysis*, Academic Press, London, 1970.
162. I.C. Lapides, *J. Therm. Anal.*, 1994, **42**, 197.
163. W.R. Phillips, in *A DTA Study of Chlorites*, 1962.
164. Joint Committee of Powder Diffraction Standards (JCPDS).
165. D.R. Lide (Ed), in *CRC Handbook of Chemistry and Physics*, CRC Press, London, 1996.
166. E. Wilby and P.J. Holliman, unpublished results, 1997.
167. V. Höller, D. Wegricht, I. Yuranov, L. Kiwi-Minsker and A. Renken, *Chem. Eng. and Tech.*, 2000, **23**(3), 251.